PIC-SOL 209/6
December 1965

A R M Y • N A V Y • A I R F O R C E • A E C • N A S A

PROCEEDINGS OF THE FIFTH PHOTOVOLTAIC SPECIALISTS CONFERENCE

VOLUME I

(Of Three Volumes)

ADVANCED SOLAR CELLS

18 October 1965
Held at the NASA-Goddard Space Flight Center
Greenbelt, Maryland

This publication was prepared for the Interagency Advanced Power Group by the Power Information Center under Contract NASr-191. Questions concerning this publication should be directed to the following address:

Power Information Center
103 Moore School Building
200 South 33rd Street
Philadelphia, Pennsylvania 19104

Institute for Cooperative Research
University of Pennsylvania

FOREWORD

Continuing its interest in the photovoltaic area, the Interagency Advanced Power Group (IAPG) has published for the third time the proceedings of the Photovoltaic Specialists Conference. The content of these proceedings - a significant part of the information exchange activities of the IAPG - is of particular interest to members of its Solar Working Group.

This conference, the fifth of its kind, was cosponsored by IEEE, AIAA, and the NASA-Goddard Space Flight Center. Facilities for meetings and other arrangements were the responsibility of NASA-Goddard.

Presentations are included in the order in which delivered at the conference and were prepared from papers submitted to the Power Information Center (PIC) through the IEEE. Where papers have been authored by more than one person, cover sheets bear the name of the person who actually gave the presentation.

Presentations are arranged in three volumes and five sections reflecting the arrangement of the conference into three days and five sessions. Contents of the volumes are as follows:

Volume I - Advanced Solar Cells

Volume II - Thin Film Solar Cells and Radiation Damage

Volume III - Solar Power Systems Considerations

Transcriptions of the discussion periods following each presentation were prepared by Mrs. Marion Beckwith of Mr. Cherry's staff at NASA-Goddard. This effort is acknowledged as an important contribution to the proceedings.

Inclusion of a paper in these proceedings in no way precludes later publication in professional society journals.

PROCEEDINGS OF THE FIFTH PHOTOVOLTAIC SPECIALISTS CONFERENCE

Dates: 18, 19, and 20 October 1965

Place: NASA-Goddard Space Flight Center
Greenbelt, Maryland

Attendance

Based upon information available at the time of publication, the following list represents those who attended at least one of the conference sessions:

IAPG Members Present:

Brancato, E. L.	NRL
Cherry, W. R.	NASA-Goddard
Fischell, Robert	APL
Hamilton, R. C.	IDA
Kittl, Emil	USAECOM
Potter, Andrew	NASA-Lewis
Schwarz, F. C.	NASA-ERC
Shapiro, S. J.	USAECOM
Smith, A. H.	NASA-HQ
Uchiyama, A. A.	JPL
Wise, J. F.	AF-APL
Yannoni, N. F.	AFCRL

Government:

Anderson, Donald	NASA-Ames
Brandhorst, H. W., Jr.	NASA-Lewis
Bullis, W. M.	NBS
Campbell, Frank	NRL
Cunningham, B. T.	NASA-Goddard
Danchenko, Vitaly	NASA-Goddard
Dawson, J. R.	NASA-Langley
Duncan, C. H.	NASA-Goddard
Ellis, W. E.	NASA-Langley
Fang, P. H.	NASA-Goddard
Faraday, B. J.	NRL
Ferris-Prabhu, A. V. M.	NASA-Goddard
Finger, H. B.	NASA-HQ
Foster, J. V.	NASA-Ames
Gallagher, D. J.	NASA-Goddard
Gdula, William	NASA-Goddard
Geiger, F. E., Jr.	NASA-Goddard

Government: (continued)

Goldsmith, Paul	JPL
Gordon, Frederick	NASA-Goddard
Green, Milton	USNUSL
Haynes, G. A.	NASA-Langley
Haynos, J. G.	NASA-Goddard
Hirschfield, Jule	NASA-Goddard
Hobbs, A. J.	NASA-Goddard
Janda, R. J.	NASA-Goddard
Jones, W. P.	NASA-Goddard
Kautz, H. E.	NASA-Lewis
Lambert, R. J.	NRL
Lillywhite, Malcolm	NASA-Goddard
Litynski, Z.	Library of Congress
Liu, Y. M.	NASA-Goddard
MacKenzie, C. M.	NASA-Goddard
Massie, L. D.	AFAPL
McCarron, S. G.	NASA-Goddard
Meszaros, George	NASA-Goddard
Mejia, N. V.	NASA-Goddard
Moses, E. G.	NASA-Goddard
Reetz, Art	NASA-HQ
Ritchie, D. W.	JPL
Salay, J. B.	NASA-Goddard
Schach, Milton	NASA-Goddard
Shepherd, J. M., Jr.	NRL
Shumaker, H. A.	NASA-Lewis
Sizemore, K. O.	NASA-Goddard
Slifer, L. W., Jr.	NASA-Goddard
Sokoloski, M. M.	NASA-Goddard
Spakowski, A. E.	NASA-Lewis
Statler, R. C.	NRL
Sullivan, R. M.	NASA-Goddard
Swartz, C. K.	NASA-Lewis
Tauke, Regina	NRL
Tucker, W. M.	NASA-Goddard
Waddel, R. C.	NASA-Goddard
Wannemacher, H. E.	NASA-Goddard
Wappaus, W. A.	NASA-Goddard
Weitzel, R. L.	NASA-Goddard
Yasui, Robert K.	JPL
Yuen, Joseph	NRL

Nongovernment:

Abrahams, Samuel	Fairchild Hiller
Adams, J. R.	Ball Brothers
Albright, George	Grumman Aircraft Corp.

Nongovernment: (continued)

Aldrich, R. W.	G.E. - Syracuse
Alexander, S. M.	Texas Instruments
Asbed, Norig	Hittman Associates
Augustine, Frank	Clevite Corp.
Bachner, R. L.	Solar Systems, Inc.
Baicker, J. A.	Princeton R&D Co.
Baker, J. K.	G.E. - Philadelphia
Barkley, D. W.	Libby Owens Ford
Barnhart, P. W.	Booz, Allen Applied Research
Barrett, Matt	Exotech, Inc.
Berry, Edwin	Aerospace Corp.
Bickler, Don	Hoffman Electronics Corp.
Blair, John	MIT
Boer, K. W.	Univ. of Delaware
Borson, E. N.	Aerospace Corp.
Burrill, J. T.	Ion Physics Corp.
Cain, Orison	Dow Corning
Chamberlin, R. R.	National Cash Register Co.
Chidester, L. G.	Lockheed M&S Co.
Close, J. R.	Minnesota Mining & Manuf. Co.
Cole, R. L.	Texas Instruments
Colehower, E. W.	Martin Co. - Baltimore
Cooley, W. C.	Exotech, Inc.
Cusano, D. A.	G.E. - Schenectady
Davis, Robert	Fenwal, Inc.
Downing. R. G.	TRW Systems
Downs, W. R.	Ball Brothers
Ellis, S. G.	RCA - Princeton
Feagin, R. B.	Texas Instruments
Feitknecht, J.	Allen Bradley Co.
Ferguson, G. D., Jr.	G.E. - Lynchburg
Flicker, H.	TRW Systems
Goldstein, Bernard	RCA - Princeton
Gould, J. A.	Clevite Research Center
Griffin, T. A.	Harshaw Chemical Co.
Halstead, R. E.	G.E. - Schenectady
Hangen, N. R.	RCA - Princeton
Hawkins, K. D.	Ryan Aeronautical Co.
Hicks, J. M.	Westinghouse Research
Hietanen, J. R.	Clevite Corp.
Hill, E. R.	Harshaw Chemical Co.
Holmes-Siedle, A. G.	RCA Labs. - Princeton
Hui, W. L. C.	RCA - Princeton
Holloway, H.	Philco Research
Hood, John	Dow Corning Corp.
Huffman, F. N.	Martin Co. - Baltimore
Ichikawa, Y.	Westinghouse - Youngwood
Iles, P. A.	Hoffman Electronics Corp.

Nongovernment: (continued)

Jilg, E. T.	Communications Satellite Corp.
Johnson, C. E.	Bellcomm Inc.
Julius, R. F.	Keltec Industries, Inc.
Kaye, S.	EOS, Inc.
Keramidas, B. G.	Harshaw Chemical Co.
King, W. J.	Ion Physics Corp.
Kling, H. P.	Hittman Associates
Lamb, A. H.	Atlantic Instruments & Electronics, Inc.
Ling, K. S.	RCA - Mountaintop
Lisak, L. R.	General Dynamics/Convair
Loferski, J. J.	Brown University
Luft, Werner	TRW Systems
Mann, A. E.	Spectrolab
Marks, B. S.	Lockheed M&S Co.
Martin, J. H.	Johns Hopkins Univ. - APL
Maxwell, K. H.	Philco Corp.
Medved, D. B.	EOS, Inc.
Mihm, F. I.	Heliotek
Miller, W. J.	G.E. - Lynchburg
Mlavsky, A. I.	Tyco Labs., Inc.
Mott, J. L.	Fairchild Hiller Corp.
Nelms, G. E.	Honeywell, Inc.
Nichols, Donald	General Atomic
Noble, E. B.	Westinghouse - Washington
Noel, G.	RCA - Princeton
Oman, Henry	Boeing Co.
Pearson, G. L.	Stanford University
Perkins, D. M.	RCA - Princeton
Pollack, S. R.	Univ. of Pennsylvania
Prince, M. B.	EOS
Ralph, E. L.	Heliotek
Rappaport, Paul	RCA - Princeton
Ratcheson, W. I.	Boeing Co.
Ray, K. A.	Hughes Aircraft Co.
Rensin, Ernest	ITT Federal Labs.
Reynard, D. L.	Lockheed M&S Co.
Riel, R. K.	Westinghouse - Youngwood
Rubin, Irwin	Solar Systems, Inc.
Runyan, W. R.	Texas Instruments
Sachs, I. M.	Optical Coating Labs.
Schaefer, J. C.	Harshaw Chemical Co.
Schlotterbeck, R. S.	G.E. - Lynchburg
Schwarz, F. R.	RCA - Princeton
Sequeira, Edward	EOS
Shirland, F. A.	Clevite Corp.
Skarman, J. S.	National Cash Register
Stanley, A. G.	MIT Lincoln Lab.

Nongovernment: (continued)

Stein, Irving	RCA - Princeton
Stevenson, R. D.	Douglas Aircraft
Stewart, Elmer	Harshaw Chemical Co.
Stonebraker, E. R.	Westinghouse - Youngwood
Stroebel, J. D.	Dow Corning Corp.
Tada, H. Y.	TRW Systems
Tarneja, K. S.	Westinghouse - Youngwood
Teener, J. W.	Johns Hopkins Univ. APL
Thomareas, Steve	Ryan Aeronautical Co.
Timberlake, A. B.	Battelle Memorial Institute
Toole, J. M.	RCA - Mountaintop
Uhler, E. F.	RCA - Harrison
Vette, James	Aerospace Corp.
Vineyard, Ray	Texas Instruments
Vohn, Paul	RCA - Princeton
Vrablik, E. A.	MIT - Lincoln Lab.
Wiener, Paul	RCA - Princeton
Williamson, E. M., Jr.	Libby Owens Ford
Winkler, S. H.	RCA - Princeton
Wolf, Martin	RCA - Princeton
Wysocki, J. J.	RCA - Princeton
Zehner, D. W.	Westinghouse - Baltimore
Zimmerman, Elizabeth	Philco Research Labs.

IAPG Secretariat:

Ashleigh, R. F.	PIC
Williams, F. E.	PIC

Program Committee

Paul Rappaport - Chairman
Robert E. Fischell - Secretary
Arvin H. Smith - Treasurer
William R. Cherry - Arrangements
Joseph J. Loferski - Technical Papers Coordinator

Robert Hamilton	Fred A. Shirland
Andrew E. Potter	Joseph F. Wise
Bernd Ross	Martin Wolf

VOLUME I

TABLE OF CONTENTS

Introductory Remarks
John W. Townsend, Deputy Director, NASA-Goddard SFC

PART A. ADVANCED SOLAR CELLS

Wrap-Around Contact Solar Cells — A-1
J. M. Toole, Radio Corporation of America

Development of Epitaxial Structures for Radiation Resistant Silicon Solar Cells — A-2
W. R. Runyan, Texas Instruments Incorporated

Drift Field Dendritic Silicon Solar Cells — A-3
K. S. Tarneja, Westinghouse Electric Corporation

Status of Advanced Solar Cells at Electro-Optical Systems, Inc. — A-4
S. Kaye, Electro-Optical Systems, Inc.

Panel Discussion: Present Status of Silicon Solar Cells
Moderator: W. R. Cherry, NASA-Goddard SFC
Panel: Eugene L. Ralph - Heliotek — A-5
Peter Iles - Hoffman Electronics — A-5.1
K. S. Ling - RCA — A-5.2
Robert L. Cole - Texas Instruments — A-5.3
Robert K. Riel - Westinghouse — A-5.4

PART B. ADVANCED SOLAR CELLS

Ion Implantation as a Production Technique — B-1
J. T. Burrill, Ion Physics Corporation

Solar Cells from Epitaxial Gallium Arsenide on Germanium — B-2
K. H. Maxwell, Philco Applied Research Laboratory

Impurity Photovoltaic Effect in Cadmium Sulfide — B-3
John Blair, Massachusetts Institute of Technology

Integral Glass Coatings for Solar Cells — B-4
P. A. Iles, Hoffman Electronics Corporation

Solar Cell Coatings — B-5
B. S. Marks, Lockheed Missiles and Space Company

Introductory Remarks

by

John W. Townsend, Jr.
Deputy Director
NASA-Goddard Space Flight Center
Greenbelt, Maryland

I'd like to bid you welcome to the Goddard Space Flight Center on behalf of its management. Unfortunately, Dr. Clark is otherwise occupied this morning or he'd be here in person.

As many of you may be aware, Goddard is the NASA center that is primarily responsible for the unmanned earth satellites. JPL has the basic responsibility for deep space missions; Marshall for boosters; and Houston for the manned flights. Normally, I would probably end this welcoming address with a few more glorious words about our Center, but to this group I think I'd like to say a few more words because I think it's particularly appropriate that a meeting such as this is held at Goddard.

As you know, we're one of the largest customers for photovoltaic devices, particularly solar cells, and from my position, I have noted through the past several years several things that I think are of interest and directly pertinent to you. In the first place, we have a continuing problem in radiation damage to solar cells in orbit. We have gotten something of a handle on this problem and we can predict such damage better. We have also developed some cells that are most resistant to this type of damage. However, it seems to me that there's a lot of work that remains to be done in this area.

The second thing that I've noticed is something I think is of very great interest to you, since I will assume that the people in this room would be partial to photovoltaic sources of space power as opposed to batteries and nuclear energy. This is the fact that we seem to be facing a very fundamental obstacle, in at least our unmanned spacecraft, at about the one kilowatt power level. Specifically, as you know, we have solar arrays on many of our satellites that will provide approximately a thousand watts in orbit, or at least they will in the initial portion of the satellite lifetime. I think these arrays have gotten just about as unwieldy as they're likely to get for mechanical reasons and for reliability in deployment. In other words, I think we've gone just about as far as we can in creating giant arrays in space. You can always go one step further in almost any development--but I think most of us are pretty horrified now at the type of device we have to deploy. It is also true that most of the proposed nuclear power systems are very complex, involving not only the usual difficulties of handling radioactive

materials (which in certain cases may actually be a small nuclear power plant), but one must have a large radiator in space to dissipate heat and a closed-loop system of some sort involving a generator. This device itself will be frightening to deploy in space, and there are all sorts of questions concerning micrometeorite hazard as well as direct damage to components on board the spacecraft caused by radiation from the power source. So I have my own personal doubts that this type of power is going to be very feasible, particularly on unmanned missions. Now, the manned people are still getting along, as you know, with batteries and fuel cells, and for the foreseeable future their demands, which are high power for relatively short periods of time, can be taken care of. But for the unmanned missions, I'm quite concerned. If you talk about direct broadcast satellites or some of the advanced applications satellites, such as large communications repeaters, navigation satellites, things of this nature, we're going to need more power than a thousand watts, and for a much longer period of time. It seems to me that the answer here is going to be in your laps, in that we need greatly increased efficiency or new technological "break-throughs", so there is a lot of room for fruitful research. If we could get a factor of two (which doesn't seem theoretically impossible) increase in efficiency, a solar cell's going to be very reasonably competitive throughout the next decade. If, on the other hand, our efficiencies stay at the levels that they do and the power demands continue to increase, solar cells are going to be on their way out, I think. So, with that philosophizing, I'll turn you back to your chairman.

Again, welcome. We're very pleased to host you.

PIC-SOL 209/6
Section A-1

WRAP-AROUND CONTACT SOLAR CELLS

Presented by

J. M. Toole

Radio Corporation of America

Special Electronic Components and Devices

Mountaintop, Pennsylvania

18 October 1965

WRAP-AROUND CONTACT SOLAR CELLS

K. S. Ling and J. M. Toole
Radio Corporation of America
Special Electronic Components and Devices
Crestwood Road
Mountaintop, Pennsylvania

A portion of the work reported here was performed under NASA Contract NAS5-3812. The objectives of the contract were to develop a silicon solar cell with a wrap-around contact, and to develop a module by bonding wrap-around cells on a printed circuit board. A wrap-around cell is one with both N and P contacts on the inactive surface of the cell. A diagram of the cell which was finally developed is shown in Figure 1. The dimensions chosen for the cell were purely arbitrary, and can be modified as required. The N surface has six grid lines. On the back side of the cell are the two contacts; the strip at the top is the N-contact. A picture frame is used around the P-contact to eliminate the need for edge cleaning.

A brief outline of the fabrication process for conventional cells is as follows. Many of the essential but nonfundamental steps are omitted.

1. Diffuse phosphorous to produce the N-layer in the P-type silicon.
2. Acid etch the N-layer from the back of the wafer.
3. Evaporate titanium and silver for the negative and positive contacts.
4. Sinter in hydrogen.
5. Evaporate an antireflective coating of silicon monoxide.
6. Inspect for mechanical dimensions and test for electrical output.

The only deviation from the standard procedure in making a wrap-around cell is the addition of a masking operation prior to etching the back of the wafer. The N-strip along one edge of the cell is preserved by masking it with a sprayed wax layer prior to the etching operation.

A new fixture had to be designed and fabricated for the evaporation of the contacts since titanium and silver must be evaporated on both sides of the silicon wafer, and also along one edge of the wafer so the N-contact can be brought around to the back side of the cell. The fixture designed was similar to a rotisserie. It rotates inside the evaporator so that the front side, the back side, and one edge of the wafer can be evaporated continuously. The same principle can be adopted for the conventional cell

and reduce the pump down cycle from two to one. The jigs that hold the silicon wafers have one side machined away to expose the edge of the wafers for evaporation. Each cavity of the jig is individually spring loaded to accommodate the variations in wafer thickness, and to prevent the wafers from moving around in the cavity. Cells have been fabricated using wafers varying in thickness from 0.007 to 0.017 inch. The process of evaporation is identical to that of conventional cells.

Since both contacts are on the inactive surface of the cell, a special test fixture is necessary. Figure 2 illustrates the construction of such a test fixture. The usual features such as independent current and voltage measuring points and vacuum hold down are incorporated. Not shown in the diagram is a bakelite strip which divides the block into two. This is done to insulate the negative and positive contacts. The fixture is mounted on a thermoelectric cooler for temperature control.

Table I provides data on the electrical characteristics of 2 by 2 centimeter cells produced in the manner described. The test conditions for these data were one hundred milliwatts per square centimeter - tungsten illumination having a color temperature of $2800^{\circ} \pm 50^{\circ}K$, a filter of three centimeters of water, and the temperature of the cells was $25^{\circ}C$. If cell 3A is thrown out as not being typical because of a high series resistance, as exhibited by the large drop-off in current from zero volts to 0.460 volts, then the air mass one efficiencies at 0.460 volts range from 13.0% to 14.1%. This corresponds to an air mass zero spread of 10.8 to 11.7 percent greater than that available from conventional cells because of the increase in active area gained by locating the N-contact on the back side of the cell. These data are representative of what could be expected in a production run of these devices. In general, the I-V characteristics are well shaped, and the temperature coefficients of open circuit voltage, maximum power point, and short circuit current are the same as conventional cells under a tungsten source.

As with any device to be used in space application, reduced weight is a prime consideration. Wrap-around cells have been fabricated from very thin wafers - 0.006 to 0.008 inch thick silicon. These thin cells maintain good efficiencies while drastically reducing the weight. On a large solar array, a reduction in weight of thirty to forty percent as compared with conventional cells, is quite an attractive savings if it is not at the cost of reduced power.

In an effort to determine the effects of damaging radiation, several wrap-around cells with a nominal thickness of 0.007 inch were exposed to a flux of 2×10^{15} (1 Mev) electrons per square centimeter. At the same time several cells of the Nimbus variety were exposed to the same dosage of 1 Mev electrons. These cells were 2 by 2 centimeters having a base resistivity of 1.2 to 2.0 ohm centimeter; solder dipped, and a nominal thickness of 0.017 inch. The thin wrap-around cells had a base resistivity of 1.2 to 2.0 ohm centimeter; however, they were not solder dipped. Both types of cells were coated with silicon monoxide, and all cells had a uniform

coating and appeared to be of the same color. The cells were sweated on Kovar blocks, and I-V characteristics and spectral response were recorded. The I-V characteristics were measured using the RCA Space Arc and the following were the test conditions: intensity - 139.6 milliwatts per square centimeter, cell temperature - 28°C. An airplane flown standard cell was used to calibrate the intensity. Table II represents the data for this test. In the first column the prefix WA is the designation used to represent a wrap-around cell; while N is the designation for a Nimbus type cell. The second column headed "Isc" is the short circuit current prior to irradiation, and the third column headed "Isc" is the short circuit current after bombardment. The fourth column headed Δ Isc is the difference of the short circuit current before and after irradiation. The fifth column headed "% change" is the degradation in short circuit current expressed in percentage. For the carbon arc data the average percent change for the wrap-around cells was 18.9 percent compared to an average of 22.7 percent for the Nimbus cells. Thus the thin wrap-around cells offer an improvement in radiation resistance of about four percent. Table III provides data for tungsten measurements.

It would appear that cells fabricated from thin wafers are less susceptible to damage from 1 Mev electrons. Admittedly the sample size is small, but the trend is quite evident. The difference is easily explained. The base region of the solar cell is responsible for generating that part of the response which is the greatest in the red. Since it is the loss of response to the red that is caused by radiation a thin cell should offer an increase in radiation resistance. If one were to compare cells fabricated from a thin wafer and one, say, twice as thick, then the latter should have the greater response in the red. This is the case as shown in Figure 3, which is a comparison of normalized relative response between the thin wrap-around cells and the Nimbus cells. Each curve is an average of the type of cell it represents. However, the spectral response of the four wrap-around cells were nearly identical, as were the responses of each of the Nimbus cells. This being the case, Figure 3 offers a complete comparison between any one of the thin wrap-around cells with any one of the Nimbus cells. The thin wrap-around cells peak at 0.81 microns while the Nimbus cells peak at 0.88 microns. In every case then, the thicker cell has a greater response to the red wavelengths. As would be expected, any attempt to decrease the cell's thickness results in a certain loss in conversion efficiency, and a compromise must be made between increasing radiation resistance and decreasing initial efficiency. A study should be made to adjust the parameters for optimum mission requirements.

As was previously mentioned, the development of a module fabricated with wrap-around cells was also an objective of the contract. The cells were mounted on a printed circuit board the construction of which is shown in Figure 4. The board was a flexible, epoxy filled, fiber glass material with copper conductors bonded to it. Of course there are many materials and configurations which can be used for the board and the metal conductive strips.

The modules were constructed by jigging ten cells simultaneously in position over the metallic strips that were part of the board. The assembly was then placed on a hot plate and the N and P connections of each cell were sweated to the proper connection strip. Thus all connections were made at one time. Tables IV and V provide data on the electrical characteristics of modules, constructed as described, and measured under a tungsten source at 139.6 milliwatts per square centimeter and 25°C, before and after completion of twenty-five thermal cycles from -78.5°C to +60.0°C. As with the cells, I-V characteristics were well shaped and temperature characteristics were as expected.

Figures 5 through 8 show possible variations in the construction of modules and shingles. Figure 5 shows a front and rear view of a module constructed on a circuit board. Figure 6 shows a front and rear view of a series connected module constructed on a circuit board. Figure 7 shows a front and rear view of a module constructed with metallic interconnecting strips. Finally, Figure 8 shows a front and rear view of a series connected module constructed with metallic interconnecting strips.

In summary, then, wrap-around solar cells are quite feasible as are modules fabricated from them. The cost of wrap-around cells compares favorably with cells of conventional design, and on a long production run where tooling costs can be absorbed, costs are nearly equal. The benefits to be gained by using wrap-around cells are a five percent increase in output power and the possibility of using easier module fabrication techniques. Wrap-around cells have undergone environmental tests and sufficient data exists to assure any potential user of their reliability. There are, however, a few points where this configuration represents a disadvantage. Since both contacts are on one side of the cell, after they have been bonded to a circuit board, inspection of the solder joints becomes a problem. In the event replacement or rework on a panel is necessary, it is possible to remove cells without any difficulty, but resoldering and inspection may be problems. These problems are definitely not insurmountable and appear as problems since there has been no real experience in using them. The answer to these problems will have to come with increased usage.

Special acknowledgement is due Charles Onesko for the fabrication of evaporation jigs, test fixtures, and processing of all wrap-around cells.

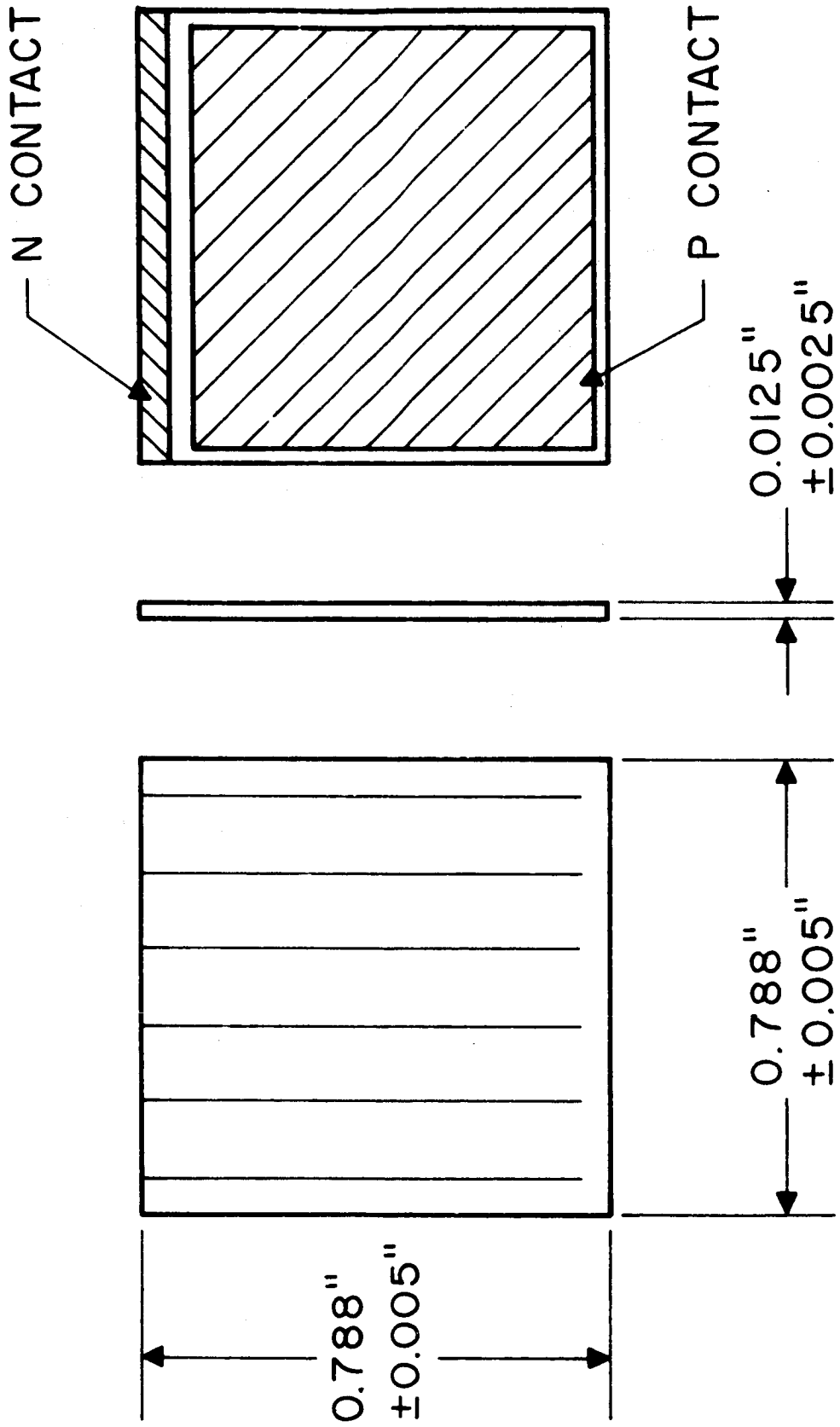

Figure 1

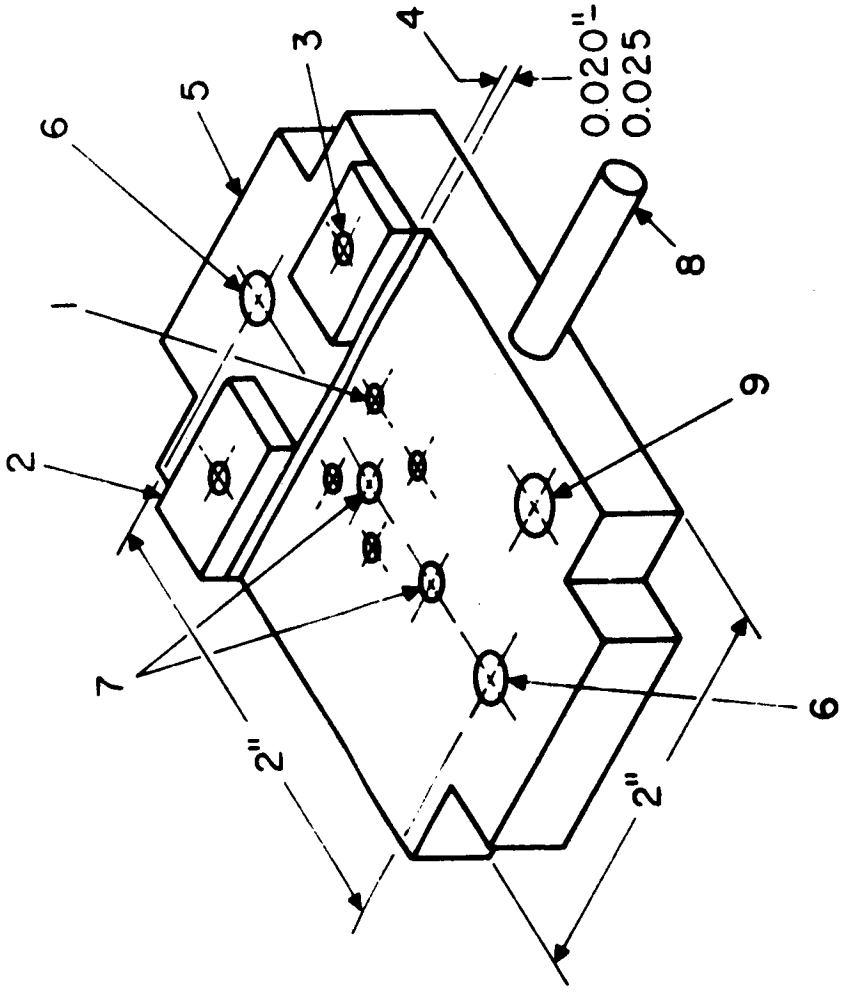
1
2
3
4
5
6
7
8
9
0.020"-
0.025
2"
2"
6

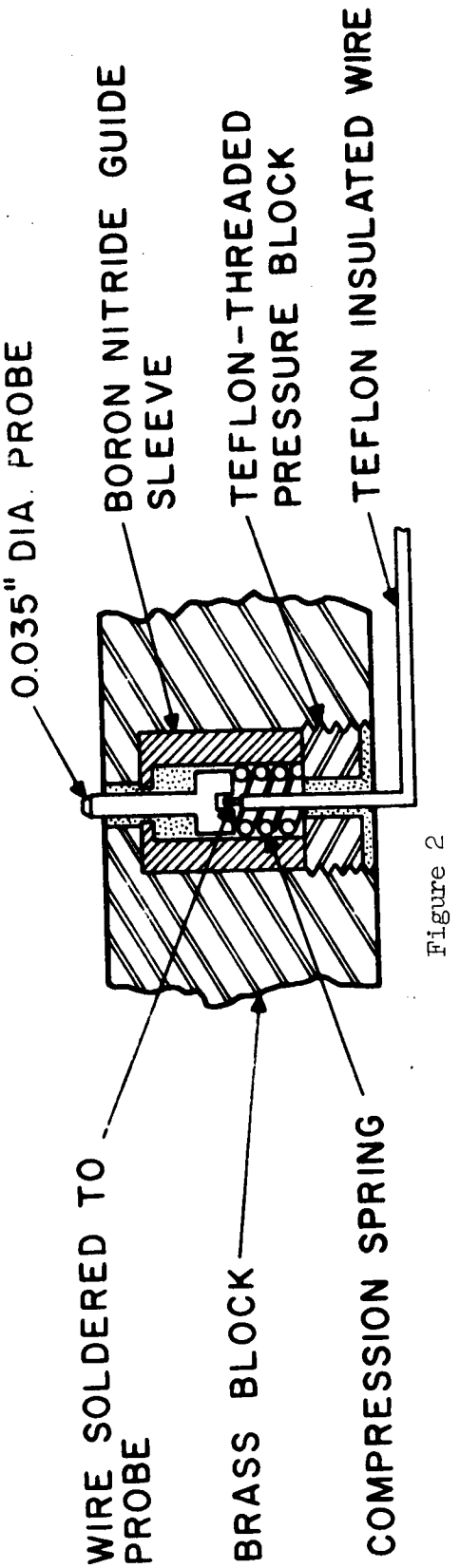
0.035" DIA. PROBE
BORON NITRIDE GUIDE SLEEVE
TEFLON-THREADED PRESSURE BLOCK
TEFLON INSULATED WIRE
WIRE SOLDERED TO PROBE
BRASS BLOCK
COMPRESSION SPRING

Figure 2

WRAP-AROUND CELL DATA

TEST CONDITIONS: TUNGSTEN ILLUMINATION = 100 mW/cm^2
COLOR TEMPERATURE = 2800°K
TEMPERATURE = 25°C
FILTER = 3-cm WATER

Cell	I_{sc}	V_{oc}	I @ 0.46 V	Power Output (mW)	Eff. @ 0.46 V (%)
1A	126	0.597	115	52.90	13.2
2A	125	0.595	113	51.98	13.0
3A	127	0.590	100	46.00	11.5
4A	125	0.597	115	52.90	13.0
5A	127	0.597	117	53.82	13.4
6A	129	0.597	116	53.36	13.3
7A	132	0.597	121	55.66	13.9
8A	133	0.598	121	55.66	13.9
9A	132	0.597	120	55.20	13.8
10A	132	0.598	123	56.58	14.1

Table I

RADIATION TEST DATA

TEST CONDITIONS: CARBON ARC SOURCE = 140 mW/cm^2
TEMPERATURE = 28°C

Cell	I_{sc}	I_{sc}	ΔI_{sc}	% Change
WA1	143.8	116.5	27.3	19.0
WA2	148.0	118.0	30.0	20.2
WA3	145.0	118.0	27.0	18.6
WA4	145.9	119.5	26.4	18.1
N5	142.0	109.5	32.5	22.9
N6	143.0	107.0	36.0	25.2
N7	140.0	112.0	28.0	20.0

Table II

RADIATION TEST DATA

TEST CONDITIONS: TUNGSTEN - 140 mW/cm^2
TEMPERATURE 28°C

Cell	I_{sc}	I_{sc}	ΔI_{sc}	% Change
WA1	130	85.2	44.8	34.4
WA2	132	84.2	47.8	36.2
WA3	128.6	83.9	44.7	34.2
WA4	131.2			
N5	132.5	78.0	54.5	41.1
N6	144.0	81.0	63.0	43.8
N7	145.6	82.9	62.7	43.1

Table III

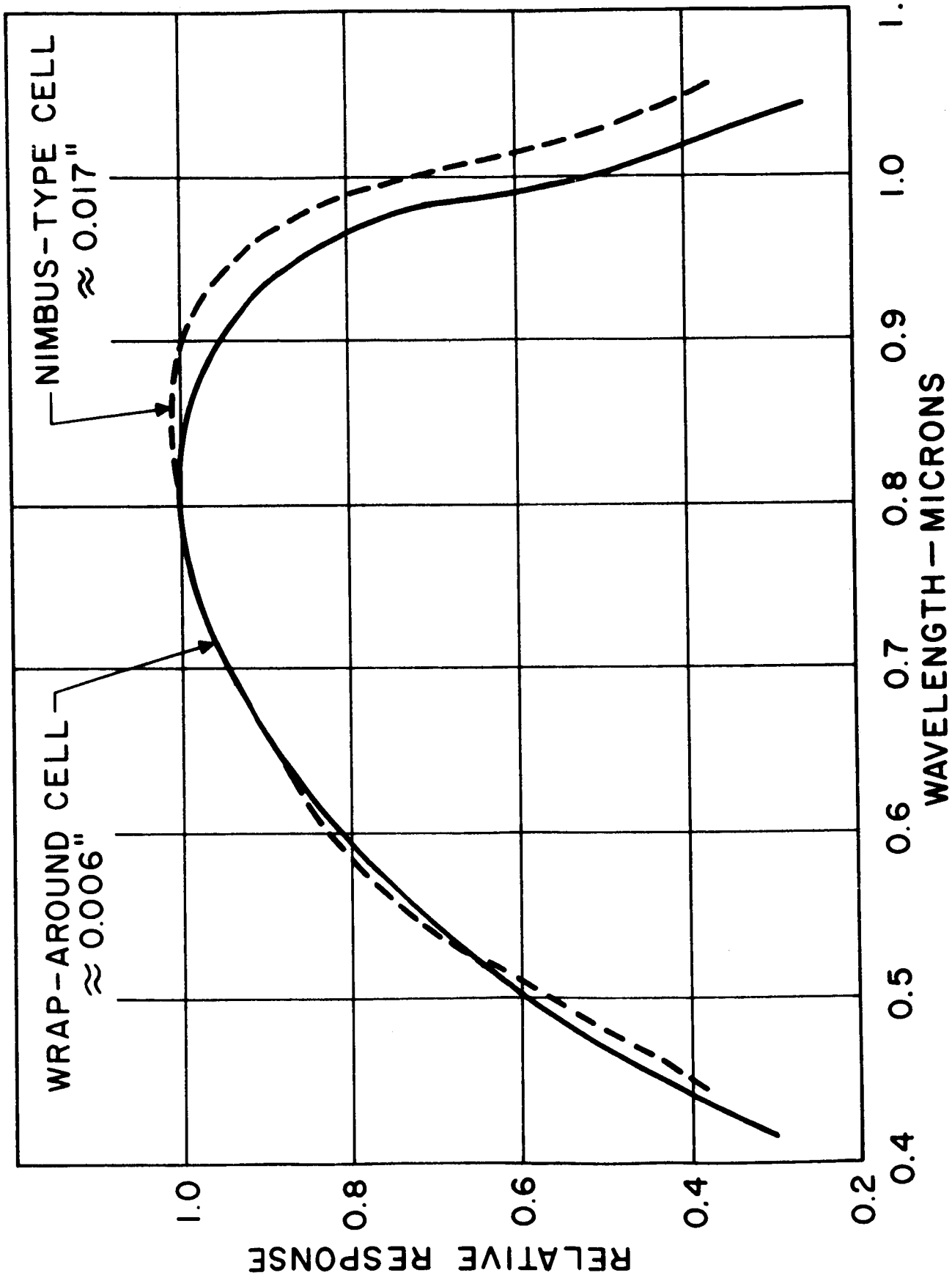
NIMBUS-TYPE CELL
≈ 0.017"
WRAP-AROUND CELL
≈ 0.006"
RELATIVE RESPONSE
1.0
0.8
0.6
0.4
0.2
0.4
0.5
0.6
0.7
0.8
0.9
1.0
1.1
WAVELENGTH—MICRONS

Figure 3

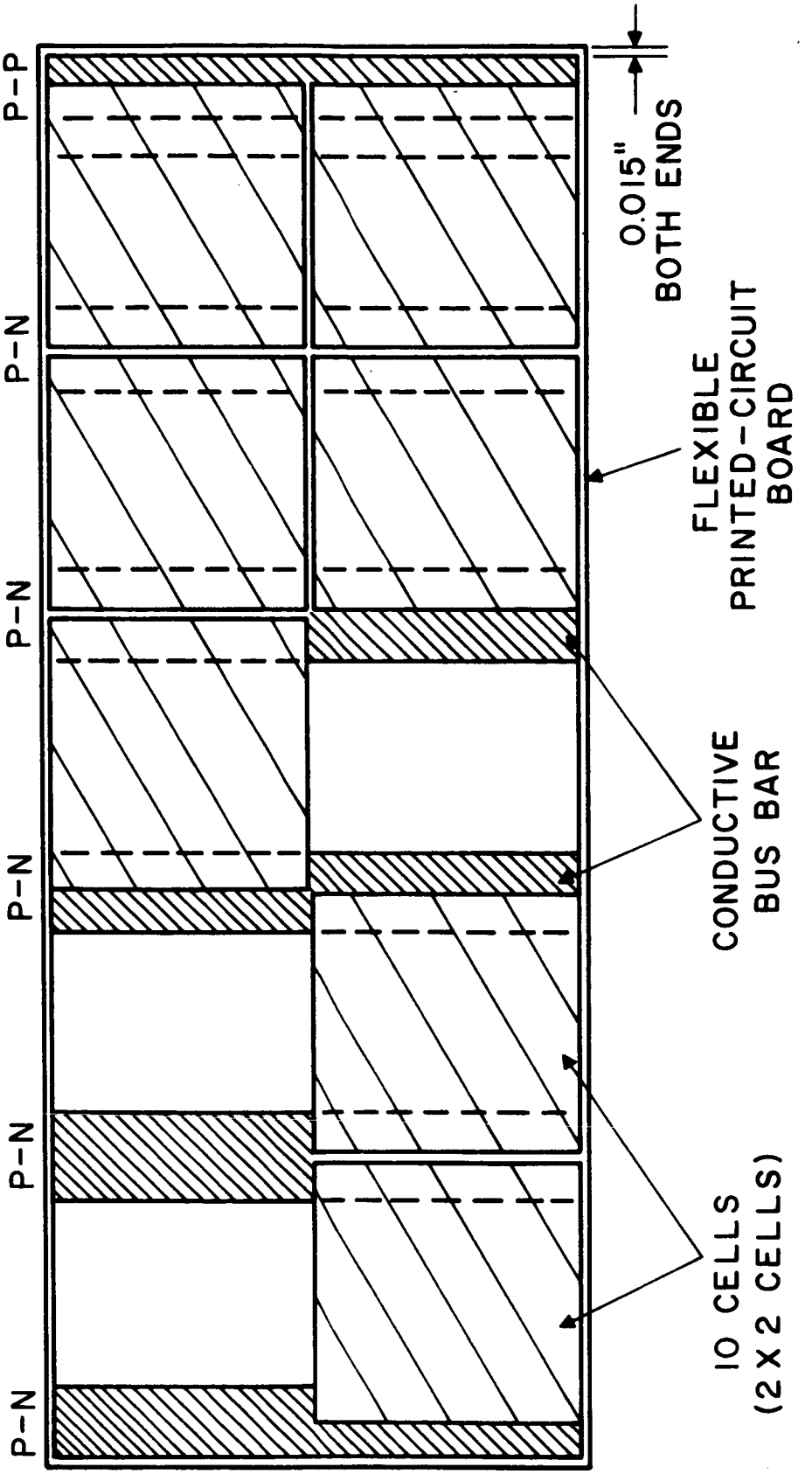
P-P
P-N
P-N
P-N
P-N
P-N
0.015"
BOTH ENDS
FLEXIBLE
PRINTED-CIRCUIT
BOARD
CONDUCTIVE
BUS BAR
10 CELLS
(2 X 2 CELLS)

Figure 4

WRAP-AROUND MODULES
INITIAL READINGS PRIOR TO THERMAL CYCLING
140 mW; AM = 0 Equivalent

Module No.	I_{sc} (mA)	V_{oc}	I_{mp}	V_{mp}	Eff. (%)	Power Output (mW)
10C	290	3.01	263	2.34	11.0	615
11C	294	2.99	263	2.32	10.9	610
12C	295	2.99	264	2.3	10.8	607
13C	302	3.01	267	2.32	11.1	619
14C	296	3.02	266	2.335	11.1	621
15C	299	3.02	268	2.34	11.2	627
16C	298	3.01	266	2.305	10.9	613
3S	290	3.00	256	2.335	10.7	598
4S	293	3.005	263	2.31	10.8	608
5S	286	3.01	256	2.335	10.7	598
Avg.	294.3	3.05	263.2	2.32	10.9	612

Table IV

WRAP-AROUND MODULES
140 mW; AM = 0 Equivalent
AFTER 25 THERMAL CYCLES OF -78.5°C to +60°C

Module No.	I_{sc} (mA)	V_{oc}	I_{mp}	V_{mp}	Eff. (%)	Power Output (mW)
10C	291	3.01	262	2.325	10.9	609
11C	296	3.05	267	2.33	11.1	622
12C	298.5	3.01	268	2.30	11.0	616
13C	304.5	3.015	270	2.315	11.2	625
14C	299.5	3.015	268.5	2.325	11.1	624
15C	300	3.015	266	2.325	11.0	618
16C	300.5	3.015	264	2.315	10.9	611
3S	294	3.10	258	2.34	10.8	604
4S	296	3.10	266	2.30	10.9	612
5S	290	3.05	259	2.33	10.8	603
Avg.	297	3.04	265	2.32	11.0	614

Table V

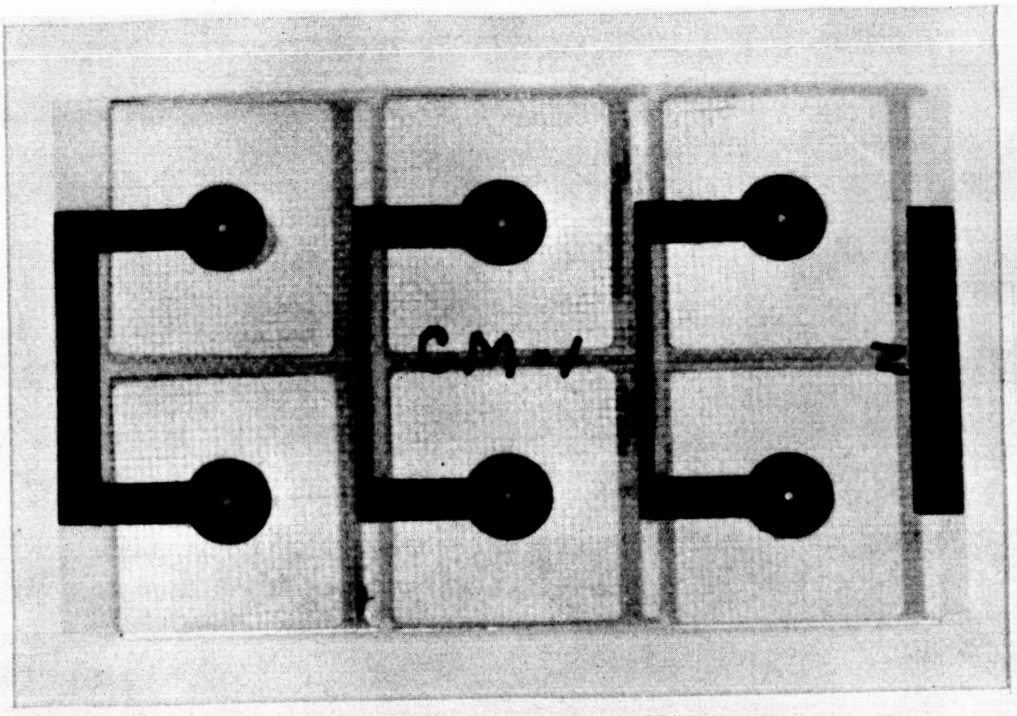

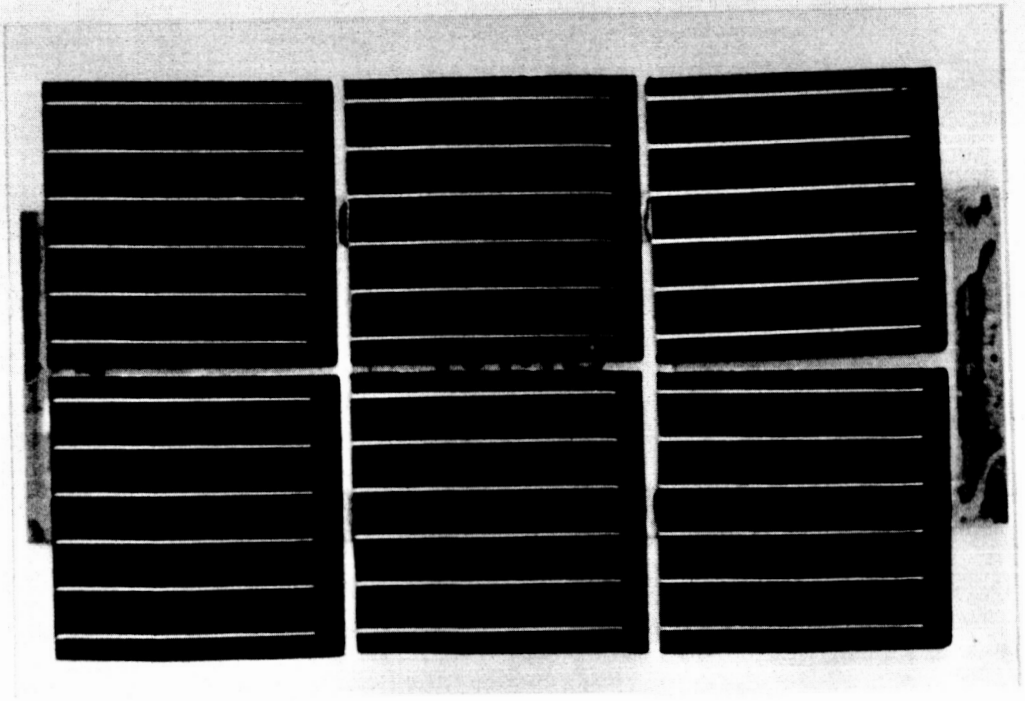

Figure 5

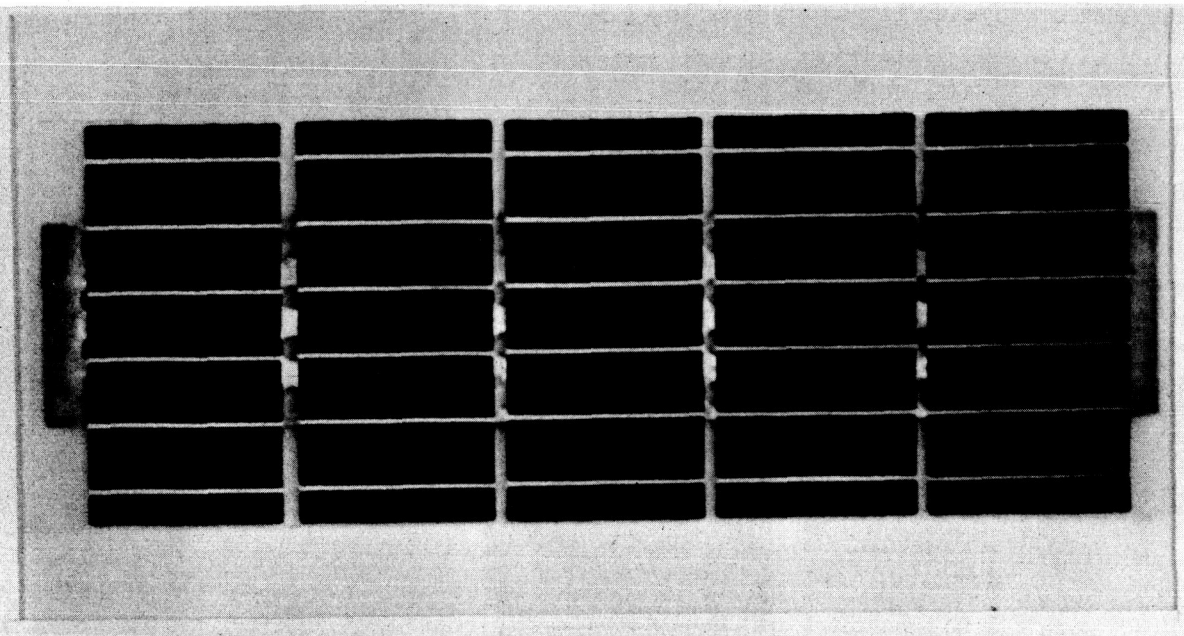

FRONT

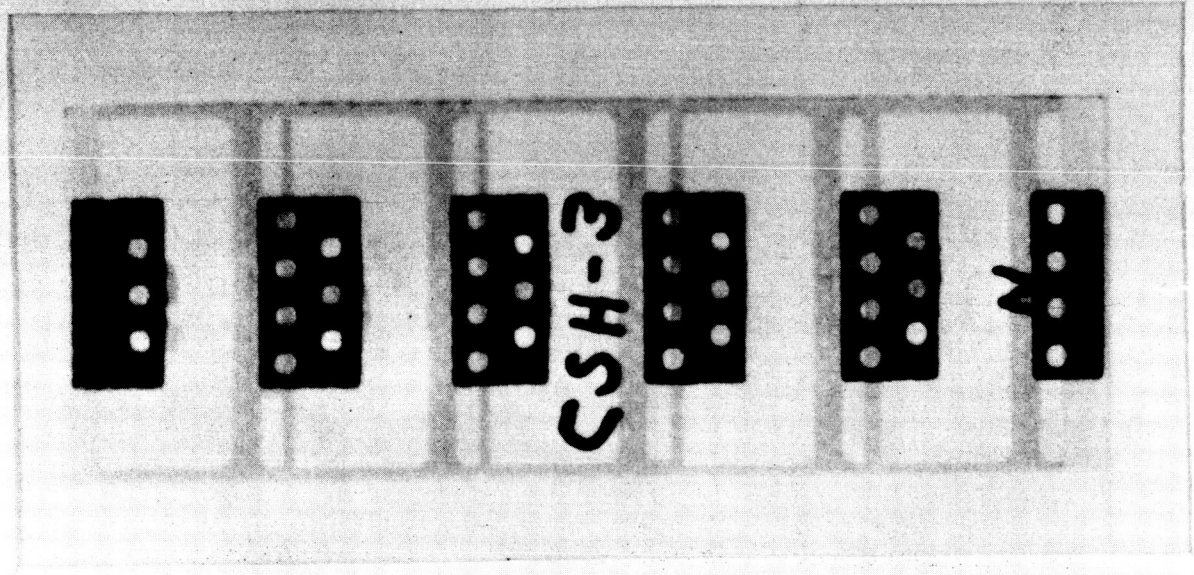

REAR

Figure 6

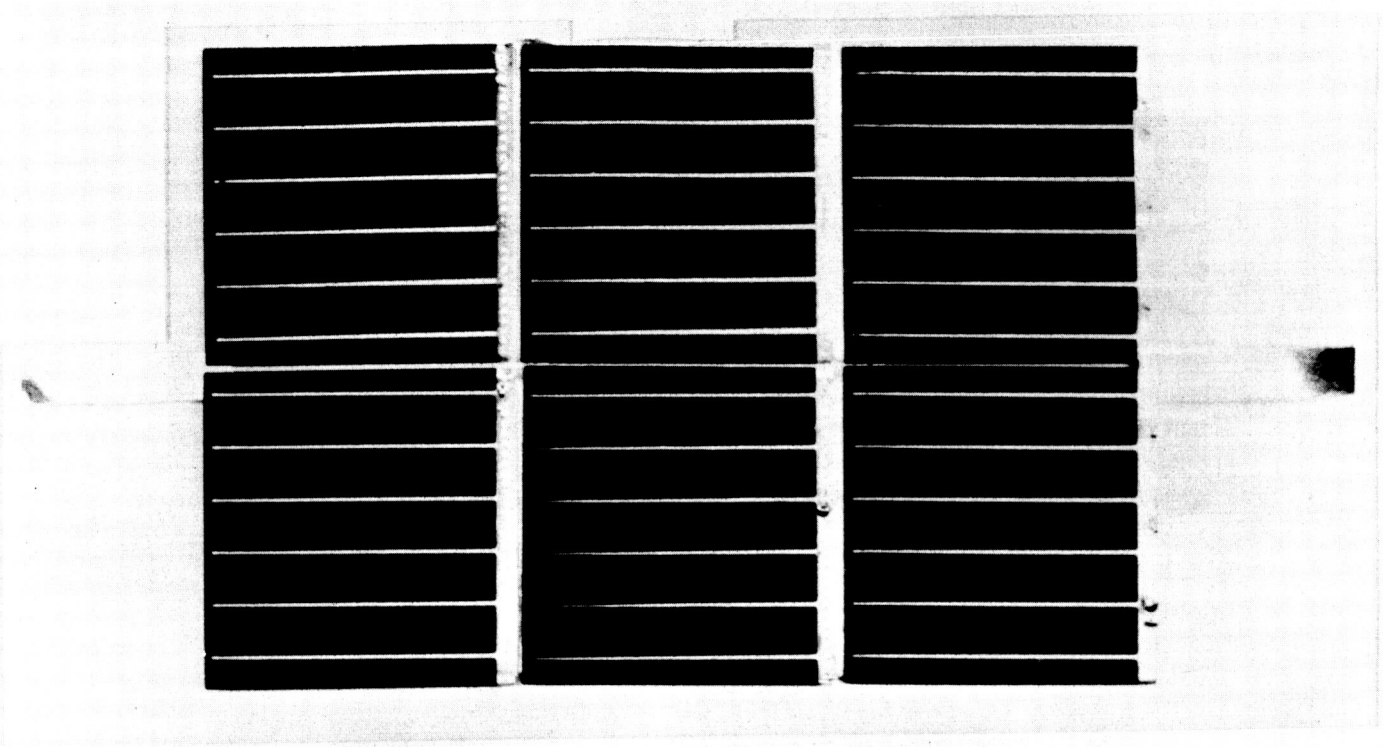

FRONT

Figure 7

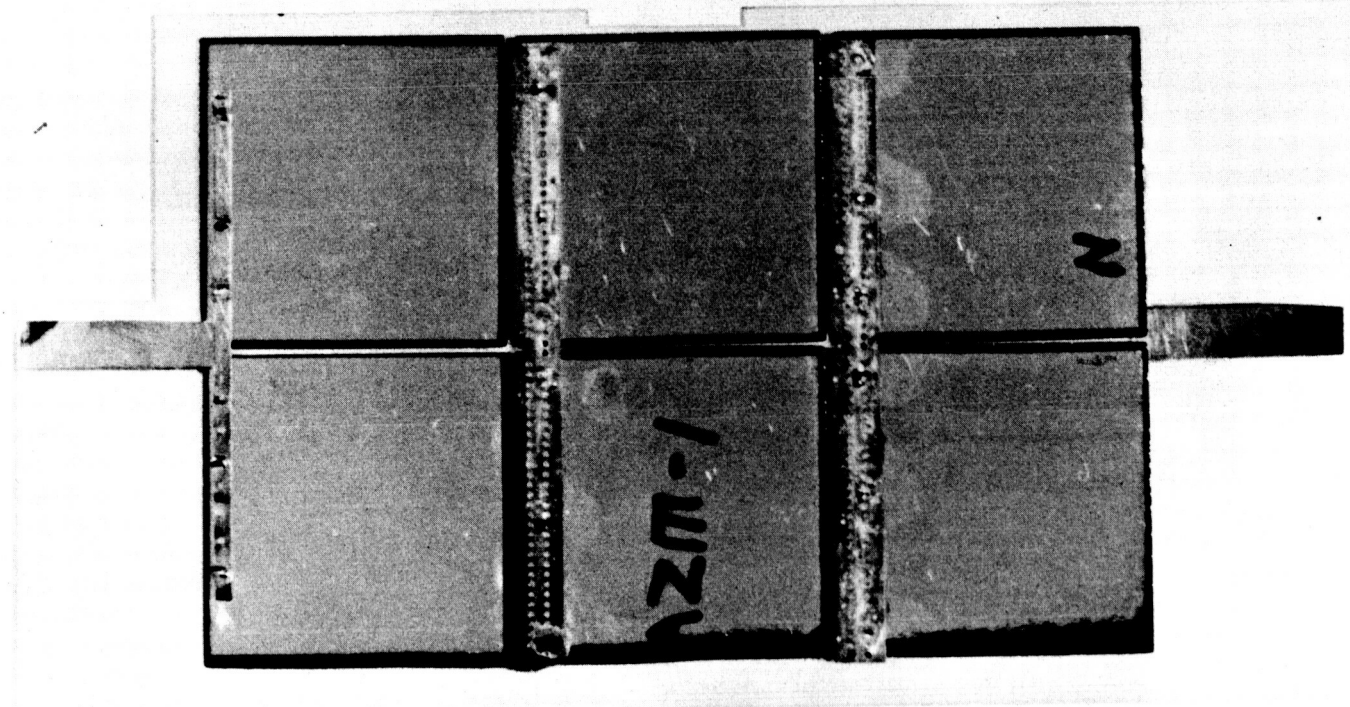

REAR

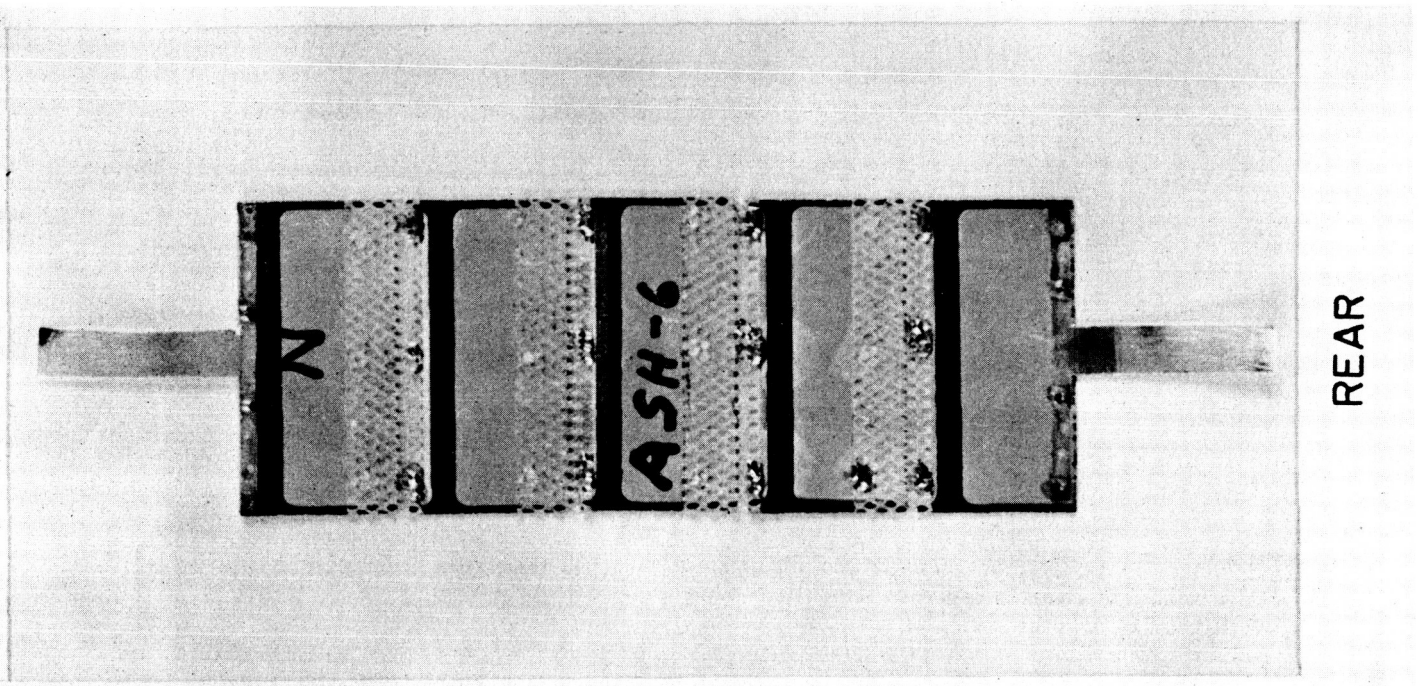

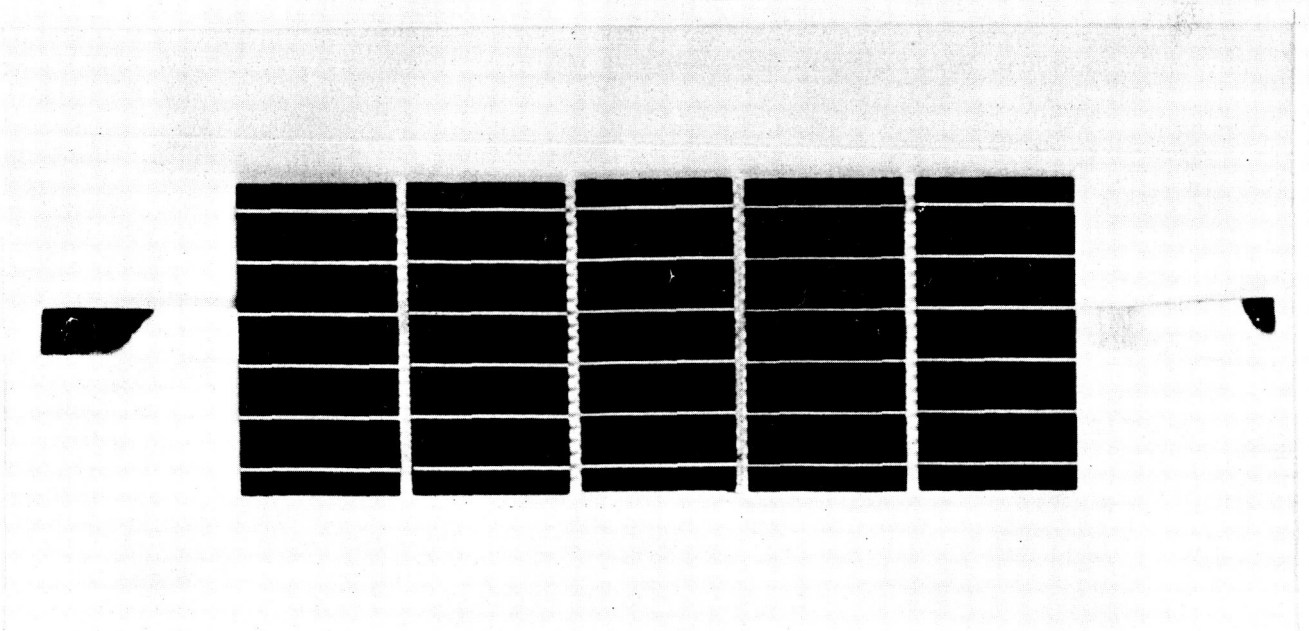

Figure 8

Discussion

Toole - RCA: If you have any questions, Mr. Ling, my associate, will be very happy to answer them.

Schach - GSFC: Did you try fabricating thicker wrap-around cells? I was curious to see the slight increase in efficiency - it's rather puzzling.

Ling - RCA: No, we haven't. We only tried thinner ones.

Schach: Do you expect that the thinner cells should show higher efficiency? Is this quite real or somewhat...

Ling: No, slightly lower. We find the thinner 2 by 2 cm cells are probably between 4 to 6 mil lower than the thicker cells.

Schach: The data you presented showed a slight increase in efficiency, didn't it, in comparison?

Ling: No.

W. Ratcheson - Boeing: Were you able to evaluate with the few numbers of samples you had what the additional handling problems might be with these thinner cells? Are they very easily broken when you attempt to form modules from them?

Ling: Not as bad as we thought. Recently we just made 200 thin cells for JPL and the breakage is quite negligible. We didn't have much breakage at all. But certainly you have to be more careful in handling them.

Ratcheson: What average efficiency air mass one did you get with the thin cells - 6 to 8 mil cells?

Ling: Six to eight mils - we were getting average about 100 milliamperes at .46 volts.

Ratcheson: Thank you.

Yuen - Naval Research Lab: Mr. Toole mentioned about the flexibility of the cell. What is the radius you could bend it to?

Ling: We never tried - we don't know. It actually bends. When we performed a peel test to evaluate the contacts, we soldered a wire to the contact, then the cell is held into a tensile fixture, then we pull on the wire. We can see the cell actually bend.

Adams - Ball Brothers: I'd like to know if you used or considered using 10 ohm cm cells for your radiation type studies since they seem to be better for radiation purposes - rather than the 1.2 ohms?

Ling: On the wrap-around cell we have not used 10 ohm cells - only 1 ohm cm cells.

Adams: Why?

Ling: Well, we made the cell under either purchase order or contract and at that time there were no specific requirements for 10 ohm cm, and we happened to have 1 ohm cm material on hand, so we used the low resistance material.

Adams: Another question: I wondered if or why the test values or the test results seem to be higher after the thermal shocks or thermal cycling on the test modules. You had 11% average instead of 10.9.

Ling: That would be due to the measurement error; since we used the tungsten light source with only one light bulb in the center, each time you scan the area over test area, there's some variation.

Adams: OK. Thank you.

*****

PIC-SOL 209/6
Section A-2

DEVELOPMENT OF EPITAXIAL STRUCTURES FOR RADIATION RESISTANT SILICON SOLAR CELLS*

Presented by

W. R. Runyan

Texas Instruments Incorporated

Dallas, Texas

18 October 1965

*This work was carried out under contract No. NAS 5-3559 from the Goddard Space Flight Center, National Aeronautics and Space Administration.

DEVELOPMENT OF EPITAXIAL STRUCTURES FOR RADIATION RESISTANT SILICON SOLAR CELLS

W. R. Runyan and Earl G. Alexander
Texas Instruments Incorporated
Dallas, Texas

Several years ago Wolf[1] suggested that the use of built-in electric fields in solar cells would lead to higher efficiencies for a given carrier lifetime, or conversely, would make cells of a given efficiency with lifetimes less than would otherwise be required. Since one of the main effects of high energy particle bombardment of solar cells is reduction of lifetime, it follows that these same built-in fields might very well be used to enhance the performance of solar cells after they have been radiated by high energy particles. Simple theory states that the optimum concentration gradient is one which gives a constant electrical field, i.e., an exponential, with the lower limit of impurity concentration being that of the intrinsic semiconductor and the higher limit being that of the solubility maximum. In actual fact, because of the decreasing mobility as the impurity concentration increases, there is an optimum field which can be generated. It also develops that the lower limit of concentration cannot be reached. This is due not only to the difficulties in obtaining very pure materials, but also because the space charge region from the junction required in a solar cell will move out until the concentration at its edge is approximately 10^{14} atoms/cc.

It further develops that although the exponential is the ideal distribution for optimum field, the same results can be very closely approximated by using a co-error distribution function. This, as will be seen later, considerably simplifies the actual construction of impurity gradients required to give these fields. The present work will be divided into the following sections:

1. A survey of calculations of the optimum concentration gradient based on optimizing cell performance by maximizing short-circuit current. (Note that this is an over-simplification since total performance also depends on cell voltage.)

2. How best to obtain these concentration gradients.

3. How to measure the concentration gradients in order to determine if they are actually as desired.

4. A brief description of cell fabrication.

5. The test results.

Since the radiation experiments are not yet completed this final section

will be comprised primarily of initial test data with only a few radiation results being given at this time.

Calculation of Optimum Concentration Gradient

As a first approximation to the solution of the optimum solar cell field, consider the requirements for minimum transit time across the base of a transistor. When minority carriers are injected on one side and collected at the other, there is a constant distance for the carriers to traverse. In the case of solar cells this, of course, is not true. The carriers are generated throughout the bulk of material, depending on the wavelength and the absorption coefficients in question. Following Varnerin[2], we may define the base transit time t as the ratio of stored charged Q_s to the emitter current I_e. Now if a one dimensional structure is considered, this can be expressed as:

$$t = -q\int_o^w \frac{n\,dx}{J} \tag{1}$$

where q is electronic charge, w is the base width, and J is the emitter current density. If the case is considered in which electrons are injected into a p-type base, the current density is given by:

$$J_n = q\mu_n nE + qD_n \frac{dn}{dx}, \tag{2}$$

where D_n is the electron diffusion coefficient, μ_n the electron mobility and E is the electric field seen by the electrons. The electric field is given by:

$$E = \frac{kT}{q} \frac{d\ \ln N_A}{dx} \tag{3}$$

If the transit time is computed from this set of relations and a constant mobility, curves 1 and 2 of Fig. 1 result. If, instead of constant mobility, the values are computed using Irvin's resistivity versus impurity concentration data[3], the other curves of Fig. 1 are obtained. From this it is seen that because of the decrease in mobility at high concentrations there is indeed an optimum field and that it can be produced by only two or three orders of magnitude change in doping level. Because exponential distributions are rather difficult to obtain experimentally and co-error function distributions often result as a natural consequence of diffusion, the differences that might occur between a co-error and exponential distribution were examined and found to be minor.

In a solar cell the conditions are somewhat more complex than those just considered. If the base region of an n on p cell is considered, the electron current is again as given before. It is, however, necessary to include both generation and recombination. In steady state for the p-type

base region the continuity equation becomes:

$$\frac{1}{q}\frac{dJ}{dx} - \frac{n}{\tau} + G = 0 \qquad (5)$$

The generation term G(x) is given by:

$$\int_0^{\lambda_g} \alpha(\lambda)\, \Phi\ (\lambda)\, e^{-\alpha(\lambda)x} d\lambda \qquad (6)$$

where $\alpha(\lambda)$ is the absorption coefficient at a given wavelength. $\Phi\ (\lambda)$ is absorbed photon density at a wavelength λ, and λ_g is the wavelength corresponding to the band gap of the solar cell material. When this more complicated case has been solved[4], it is seen that there is an optimum field width which turns out to be roughly twice the diffusion length for the shorter lifetimes. This is shown in Fig. 2. The width of the field is in all cases as significant and in some cases more important than the magnitude of the aiding drift field once a certain minimum field has been reached. The field generated by a three-order-change impurity concentration across the width w is sufficient to optimize collection efficiency if the proper width is employed. When the lifetime is related to the integrated flux density, the short-circuit current versus total flux can be computed and gives the curves of Fig. 3.

That these results are to be expected may be intuitively seen from the following reasoning. First assume that all carriers that are generated closer to the junction than a diffusion length L will be collected, while any carriers formed further away than L will recombine before reaching the junction. If a field is now superimposed between x_1 and x_2 of Fig. 4 no improvement in collection efficiency will be observed if x_1 is greater than L, since all of those carriers originating beyond L will still recombine before arriving at the junction. For x_1 and x_2 both less than L, some improvement will be observed. But even if the transit time across the distance x_1 and x_2 were 0 and if x_1 were at $x = 0$ and $x_2 = L$, the maximum number of carriers collected would be those generated between 0 and 2L from the junction. Reference back to Fig. 1 shows that a drift field can be expected to reduce the transit time by about 2.5 in optimum case. Therefore, x_2 can be removed out for a distance of 2.5L and provide enough velocity enhancement to collect everything generated within that space. Now if the same spacing of 2.5L is maintained and both x_1 and x_2 were moved a small distance ΔL away from the junction, any carriers originating between 2.5L and $2.5L + \Delta L$ would have to travel in excess of 2.5L to reach the junction, and with a portion of that distance without benefit of the built-in field. Since the greatest distance the carrier could go even with the field is 2.5L, it follows that repositioning the field to start between 0 and 2.5L will only reduce the number of carriers collected. Thus the maximum effectiveness of the field occurs when it starts at the junction and ends, for the specific case considered, 2.5L away. This result agrees well with that obtained from the rigorous derivation.

Methods of Obtaining Concentration Gradients

Having now established some guide lines as to the sort of distribution required, both with regard to the orders of magnitude at each end of the distribution and to the width of the built-in field, methods of obtaining these fields will now be examined.

Diffusion can be used to produce the required concentration gradient only if the diffusion progresses from the back side as illustrated in Fig. 5a. For normal thickness cells, such diffusions require extraordinarily long times, so thinner cells, even with their attendant difficulties, are required for this approach. A combination of compensation and diffusion from the front (see Fig. 5b) can in principle be used, but mobilities are greatly reduced and control is difficult.

Epitaxial deposition can also produce the grading and indeed seems the most suitable for this application. The dope may be programmed during deposition or a high resistivity layer may be deposited on a substrate and, by subsequent diffusion from the substrate, be converted to the proper resistivity. These two methods are illustrated in Fig. 5c and 5d. Because of difficulties in dope monitoring and control, doping variations during epitaxy usually do not directly produce the curve of Fig. 5c, but rather approximate it either by a number of jumps as shown in Fig. 6a or by a few straight line segments as shown in Fig. 6b. They are then smoothed by an additional diffusion. Note that in these two curves, the concentration, and not log concentration, is plotted as a function of distance.

After surveying these methods it appeared that deposition of constant impurity level material and subsequent diffusion offered the greatest reproducibility, and in the event that the performance of drift field cells were good enough to warrant commercial production, would lead to the least expensive process. This approach does give a co-error distribution rather than an exponential, but recall that the analysis indicated very little difference in the behavior of the two.

Measurement of Gradient

The substrate concentration levels were determined by combination of four-point probe resistivity measurements and Irvin's curves relating concentration gradient to resistivity. The concentration of the deposited layer was in general determined by three-point probe breakdown test measurement. The concentration gradient itself could only be determined by calculation from the initial conditions and the amount of diffusion in the case of cells actually fabricated and shipped. On the other hand, various destructive tests are available for measuring the concentration gradients. These will be summarized in the next few paragraphs.

If a small, abrupt-junction diode is made on the surface and the junction capacitance measured as a function as the applied voltage, the

impurity concentration can be determined. However, for the cases in question, gradients extend to such depths and the resistivities are so low that avalanche breakdown occurs before the space charge region can be moved through the graded region. This method may still be used, however, if first steps are etched into the surface as shown in Fig. 7 and diodes then made on each one. Thus if the depth of each step is no more than the width of the space region at avalanche breakdown, by profiling each diode a section of the total concentration profile may be obtained and the sections can then be combined into one continuous curve.

The measurement of sheet resistance as thin layers are incrementally removed from the surface has been long used in the determination of diffusion concentration profiles. But in this case the high concentration portion of the material is that below the surface, so that if small sections of the high resistivity material are removed, it is impossible to observe any difference in the measured resistivity. Accordingly if this scheme is to be used, lapping must proceed from the backside of the slice rather than from the front. In the standard process this would mean that up to 12 mils of material would have to be removed in a very parallel fashion before measurement could start only a half a mil or so from the front surface. This process has been modified[5] by making an angle cut as shown in Fig. 8 and then by using a close spaced four-point probe, measurements can be made down the slope. From these, resistivities are calculated in the standard fashion.

Cell Fabrication

Two processes were used in constructing the cells. In one of them the standard 1 cm by 2 cm rectangular epitaxial slice was processed in the normal way. Unfortunately, as a result of the epitaxial layer the silicon blank grew, not only in thickness, but also in lateral dimensions because of deposition on the edges. In addition, for very thick deposits, the edges became rough where the slice was separated from the epitaxial reactor susceptor after deposition. All of these slices required a rather laborious edge lapping operation to remove the roughness and decrease the lateral dimensions. In most cases slices subjected to this operation were undersized when ready for fabrication. Frequently, excess metal from the contact evaporation step would remain on the edges of the cells after fabrication and thus partially short the structure.

This method was abandoned in favor of process II in which round epitaxial slices were processed through contact application and then were trimmed to a standard size, after which a SiO coating was applied. The use of this method, similar to that used by Smith et al[6], effectively removed most of the difficulties associated with the first procedure.

Initial Electrical Data

Table I describes the various categories of cells included in this

study. In brief, drift fields from 6 to 75 microns, maximum layer resistivities from 1 to 25 ohm cm, and differences in concentration between front and back of field from 2 to 4 orders of magnitude were examined. All cells were 1 by 2 cm with maximum efficiencies (2800°K tungsten, air mass one) before irradiation between 5.5 and 12.7%. Table II lists the specific conditions used for the cells fabricated by Process II (and which are believed to be more reproducible than the remainder, which were processed by Procedure I).

Fig. 9 shows the short-circuit current distribution before irradiation for these cells. As predicted by Fig. 3, the short-circuit currents of Groups I, II and III are less than those of most of the groups with the 2 order of magnitude field. However, the two order field optimized for a much shorter lifetime (Group VII) than the others was also a poor performer.

Irradiation Data

The current degradation after irradiation was plotted as a function of initial layer resistivity (after the drift field forming diffusion, this resistivity occured only very close to the junction) and behaved similarly to nondrift cells. This is shown in Fig. 10 and shows clearly the superiority of higher resistivities.

Typical short-circuit current versus total flux data are shown in Fig. 11. In attempting to analyze and correlate these data with theory, little progress was made until the graph of Fig. 12 was made. It plots fraction of cell current remaining after a total flux of 10^{16} electrons/cm^2 versus initial current and leads to the conclusion that, while the percent degradation wildly varies with the cell, the magnitude of the final currents of the best cells is remarkably constant. This is to be expected from the following argument:

Suppose that the minority carrier lifetime τ is given by:

$$\frac{1}{\tau} = \frac{1}{\tau} + K\,\theta$$

where τ_o is the initial lifetime, K an appropriate constant and θ the integrated flux density. If the original τ_o were 10^{-5} sec, K = 3.2×10^{-9} cm^2/sec for 1 mev electrons[1] and $\theta = 10^{16}$ electrons/cm^2, τ is approximately 0.03 microseconds, a reduction of 330 from the original. On the other hand, if the cell were initially very poor and had a lifetime of only 0.1 microsecond, the final lifetime after irradiation would be $\approx$ 0.025 microseconds, or a reduction of only 4 from the original low value, and very close to the final value of the previous example. This is in agreement with the data for the best cells of Fig. 12, which showed that although the starting short-circuit currents varied widely, the final were quite close to each other. It thus becomes clear that in order to properly assess and compare cells, it is important to know something of their initial quality. One can then plot the simple curve of Fig. 13. If the cell is initially bad, there will be no noticeable degradation, but as the beginning cell quality

improves, the reduction upon irradiation becomes more pronounced, until for the very best nondrift field cell, per cent degradation, not total degradation, becomes a maximum. By the addition of a built-in field this worst condition can then be improved upon by an amount to be discussed in the next paragraph.

It is of interest to examine the theory with regard to maximum predicted improvement in short-circuit current of a drift field cell versus the total flux to which the cell is subjected. Portions of the data of Fig. 3 may be replotted to give Fig. 14, from which it can be seen that more improvement is to be expected at the higher fluxes. Furthermore, in the region where most of the present data were taken, a 20% improvement is all that is predicted. It should be remembered, however, that the open circuit voltage may very well also be improved so that the overall power output improvement of drift field cells may be considerably more than that predicted by short-circuit current alone.

In summary, it can be said that satisfactory short-circuit current theory, field incorporation techniques, and measuring methods are at hand, and that with acquisition of the remainder of the irradiation test results, a good assessment of the drift field cell capability can be made.

Acknowledgements

The authors would like to thank Mr. R. L. Cole for the cell fabrications, and Dr. Paul Fang of NASA, Goddard, for the irradiation data.

References

1. M. Wolf, "Drift Fields in Photovoltaic Solar Energy Converter Cells," Proc. IEEE 51, 674-693 (1963).

2. L. J. Varnerin, "Stored Charge Method of Transistor Base Transit Analysis," Proc. IRE 47, 523-527 (1959).

3. J. C. Irvin, "Resistivity of Bulk Silicon and of Diffused Layers in Silicon," Bell System Tech. J. 41, 387-410 (1962).

4. W. Murray Bullis and W. R. Runyan, "Influence of Mobility Variation on Drift Field Enhancement in Silicon Junction Devices", to be published.

5. S. B. Watelski, W. R. Runyan, and R. C. Wackwitz, "A Concentration Gradient Profiling Method," J. Electrochem. Soc. 112, 1051 (1965).

6. K. D. Smith, H. K. Gummel, J. D. Bode, D. B. Cuttriss, R. J. Nielsen, and W. Rosenzweig, "The Solar Cells and Their Mounting," Bell System Tech. J. 42, 1765 (1963).

Table I

Material Characteristics of Cells Studied

Substrate Resistivity (ohm-cm)	Nominal Initial Layer Resistivity (ohm-cm)	Nominal Drift Field Width (microns)
.008	8	16
.008	1.4	25
.008	3	25
.008	10	25
.008	20	25
.008	1	50
.008	2	50
.008	5	50
.008	15	50
.008	25	50
.008	10	75
.2	3	6
.2	9	14
.2	10	25
.2	14	50

Table II

Preparation Conditions for Cells Fabricated by Procedure II

Group Number	Number of Cells in Group Evaluated	Silicon Substrate Resistivity (Ω-cm)	Nominal Epitaxial Film Thickness (microns)	Nominal Epitaxial Film Resistivity (Ω-cm)	Diffusion Hours	Diffusion Temp°C
I	26	0.008	50	17	76.5	1250
II	20	0.008	25	14	18.5	1250
III	16	0.008	13	9	5.8	1250
IV	15	0.20	50	12	162	1265
V	16	0.20	25	13	51	1250
VI	14	0.20	13	9	12	1265
VII	21	0.20	6	3	3.25	1265

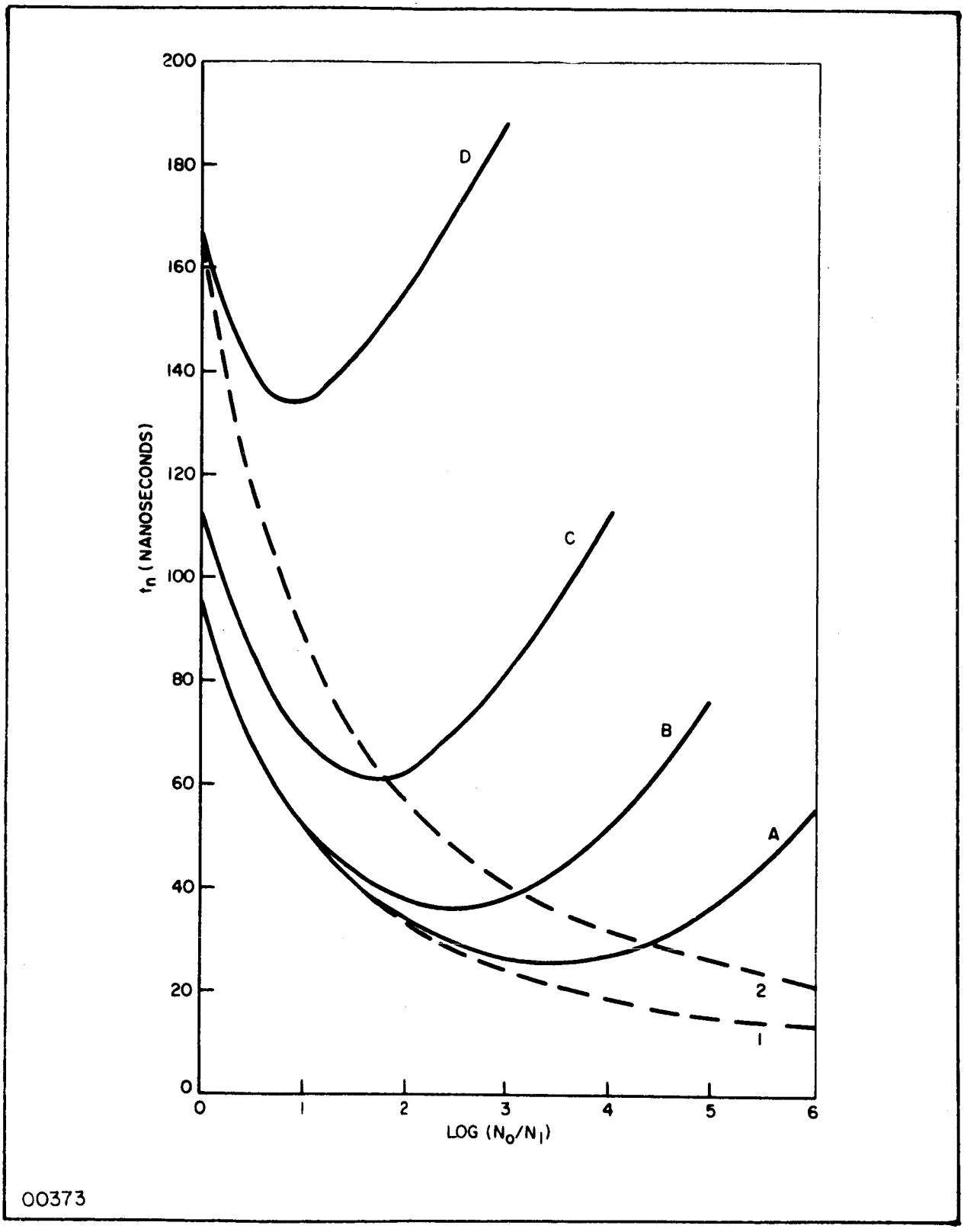

Fig. 1. Computed transit time of electrons in a p-type silicon base region 25 microns wide assuming no recombination at 300°K. The impurity concentration varies exponentially. Solid Curves: electron mobility determined from impurity concentration at each point (A, $N_1 = 10^{14}$ cm^{-3}, B, $N_1 = 10^{15}$ cm^{-3}, C, $N_1 = 10^{16}$ cm^{-3}, D, $N_1 = 10^{17}$ cm^{-3}). Dashed curves: electron mobility assumed to be independent of impurity concentration (1 $\mu_n = 1250$ cm^2 volt^{-1} sec^{-1}, 2, $\mu_n = 740$ cm^2 volt^{-1} sec^{-1}.)

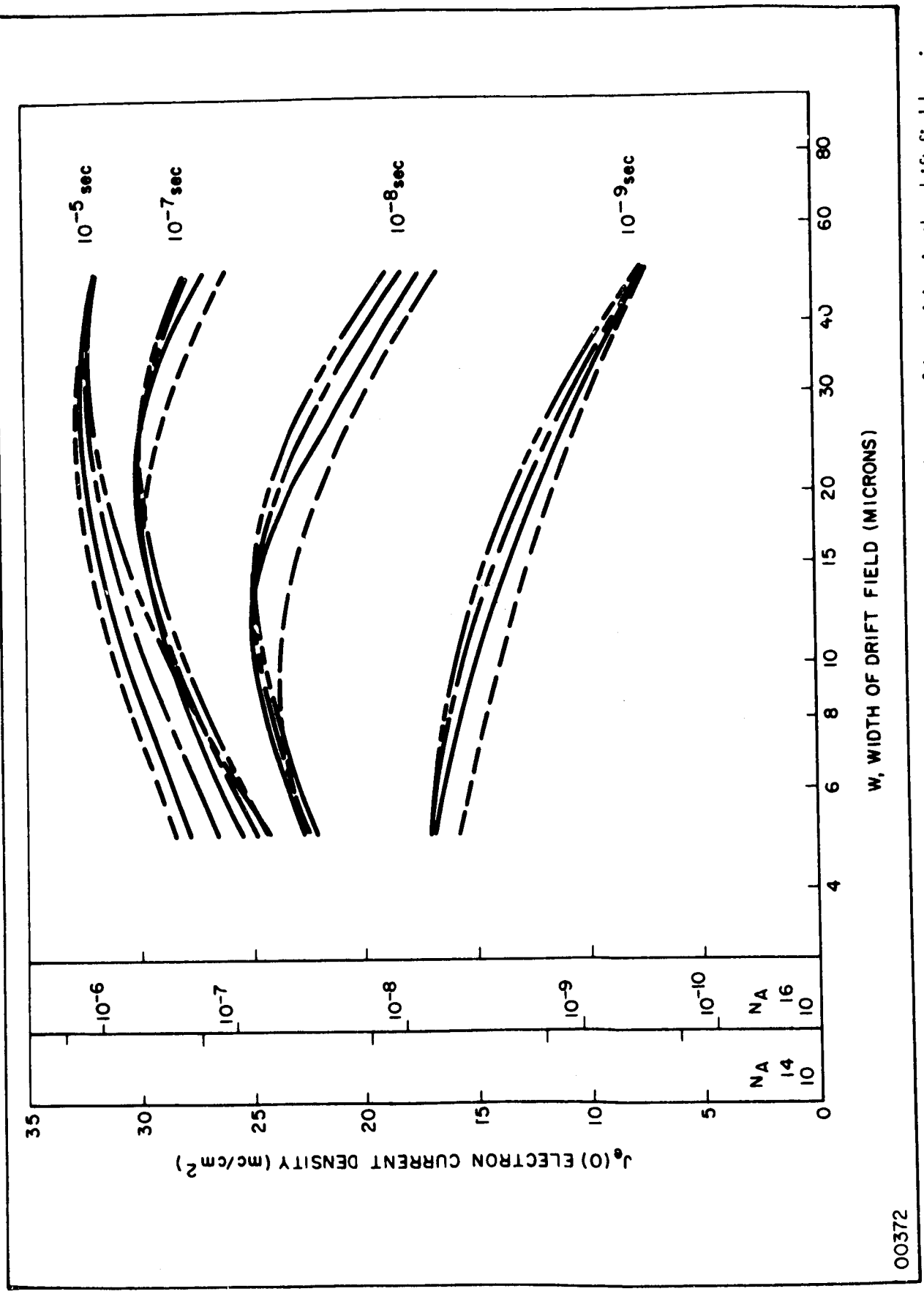

Fig. 2. Electron current density computed by assuming an exponential distribution of impurities in the drift field region. Initial acceptor concentration: 10^{17} cm^{-3} (- - - -), 10^{18} cm^{-3} (———), 10^{19} cm^{-3} (——— – ———); and 10^{20} cm^{-3} (——— – – ———). Values of electron current density for cells with $N_A = 10^{14}$ cm^{-3} and 10^{16} cm^{-3} are given at the left side for various lifetimes in the case where there is no drift field.

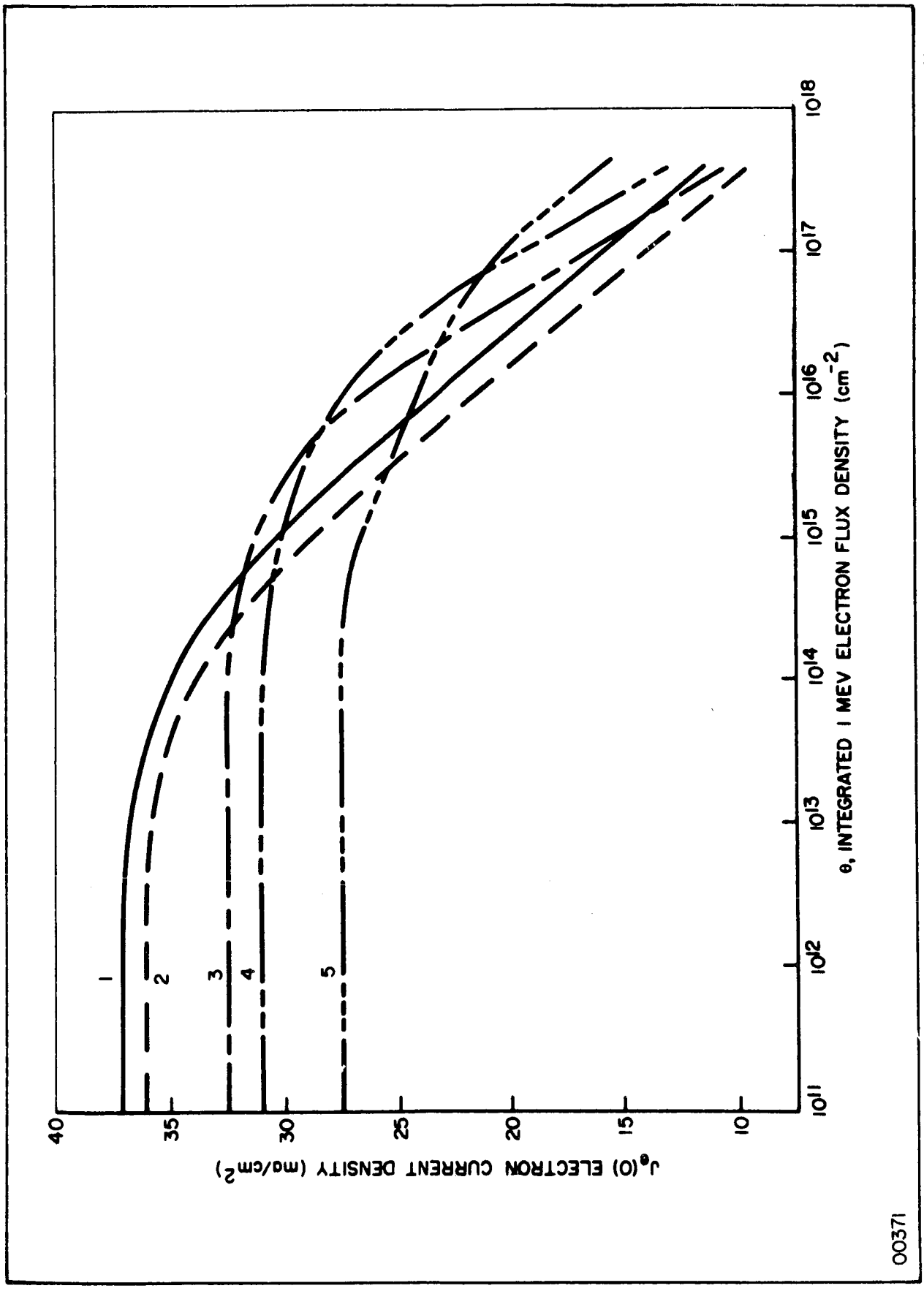

Fig. 3. Effect of irradiation by 1 Mev electrons on the short circuit electron current of an n-on-p silicon solar cell. Curve 1: no drift field, $N_A = 10^{14}$ cm^{-3}. Curve 2: no drift field, $N_A = 10^{16}$ cm^{-3}. In curves 3-5 the drift field is a result of an exponential distribution of acceptors varying from 10^{15} cm^{-3} at the junction to 10^{18} cm^{-3} in the substrate. Curve 3: 25 micron drift field. Curve 4: 12 micron drift field. Curve 5: 5 micron drift field.

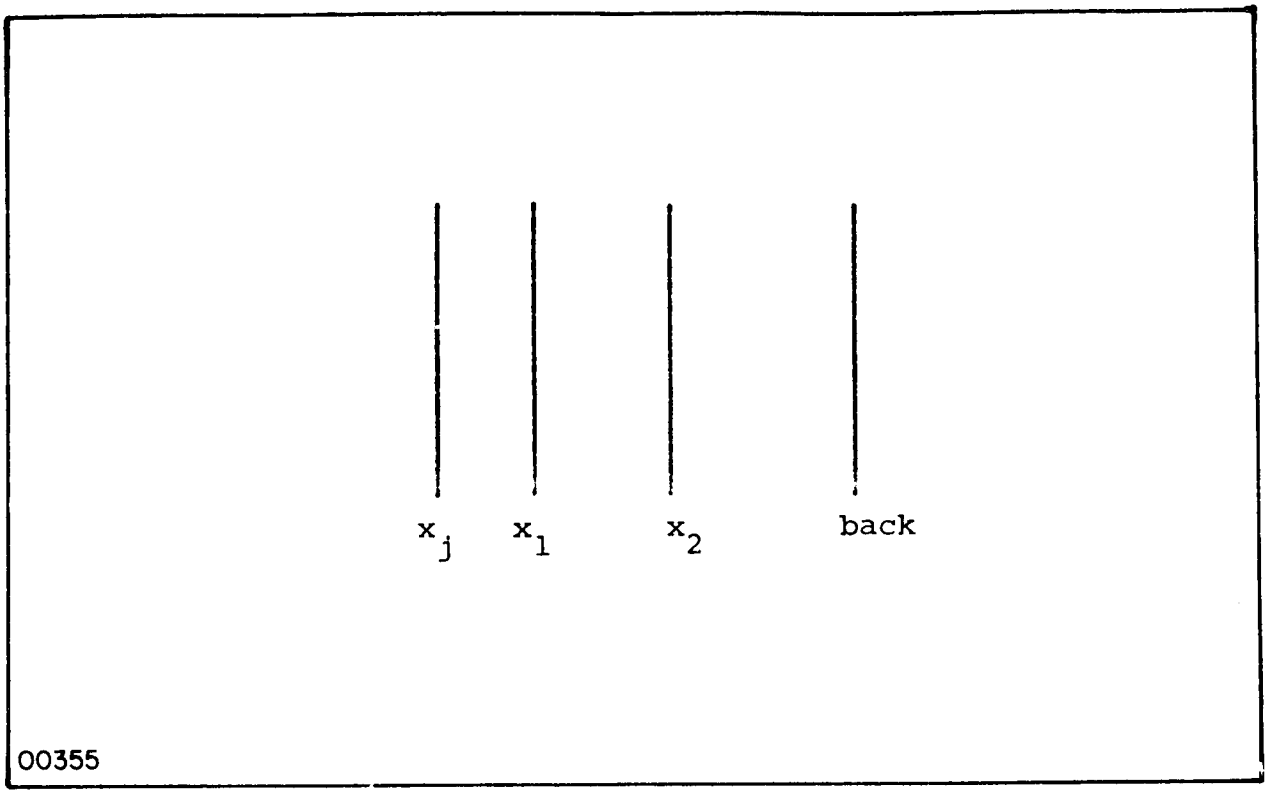

Fig. 4. Schematic View of Solar Cell Configuration

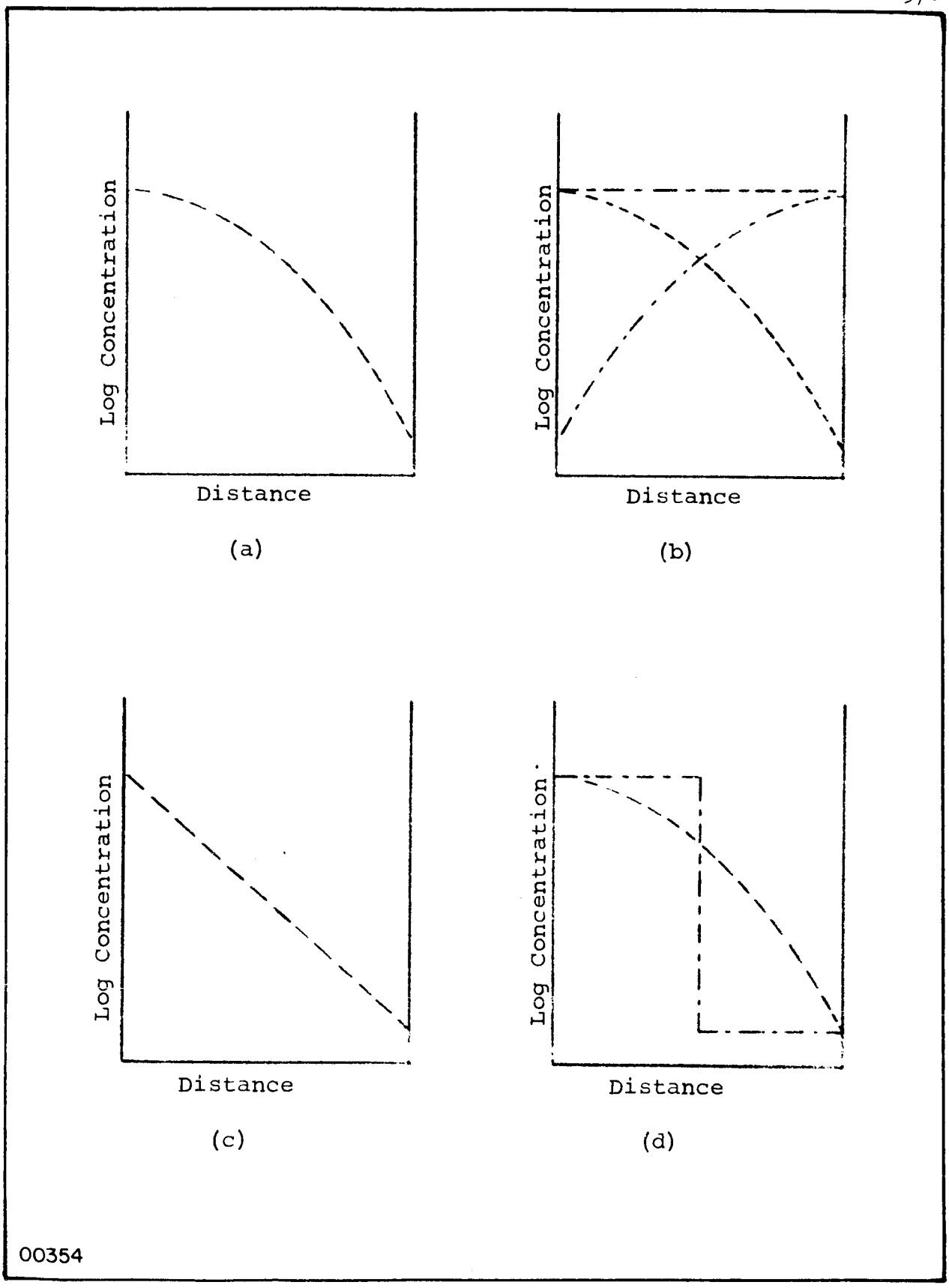

Fig. 5 Various Methods of Introducing Concentration Gradients Required in the Drift Cell

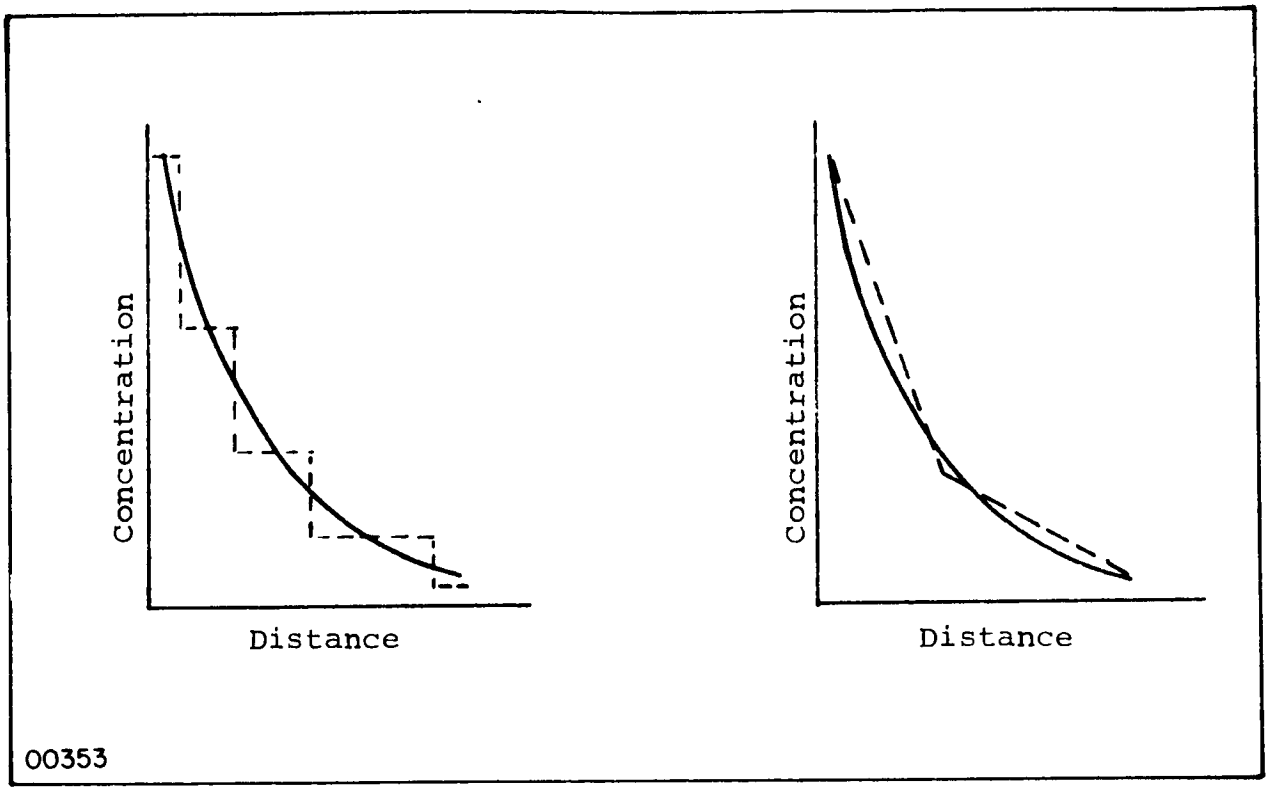

Fig. 6. Reactor Doping Approximations to an Exponential Profile

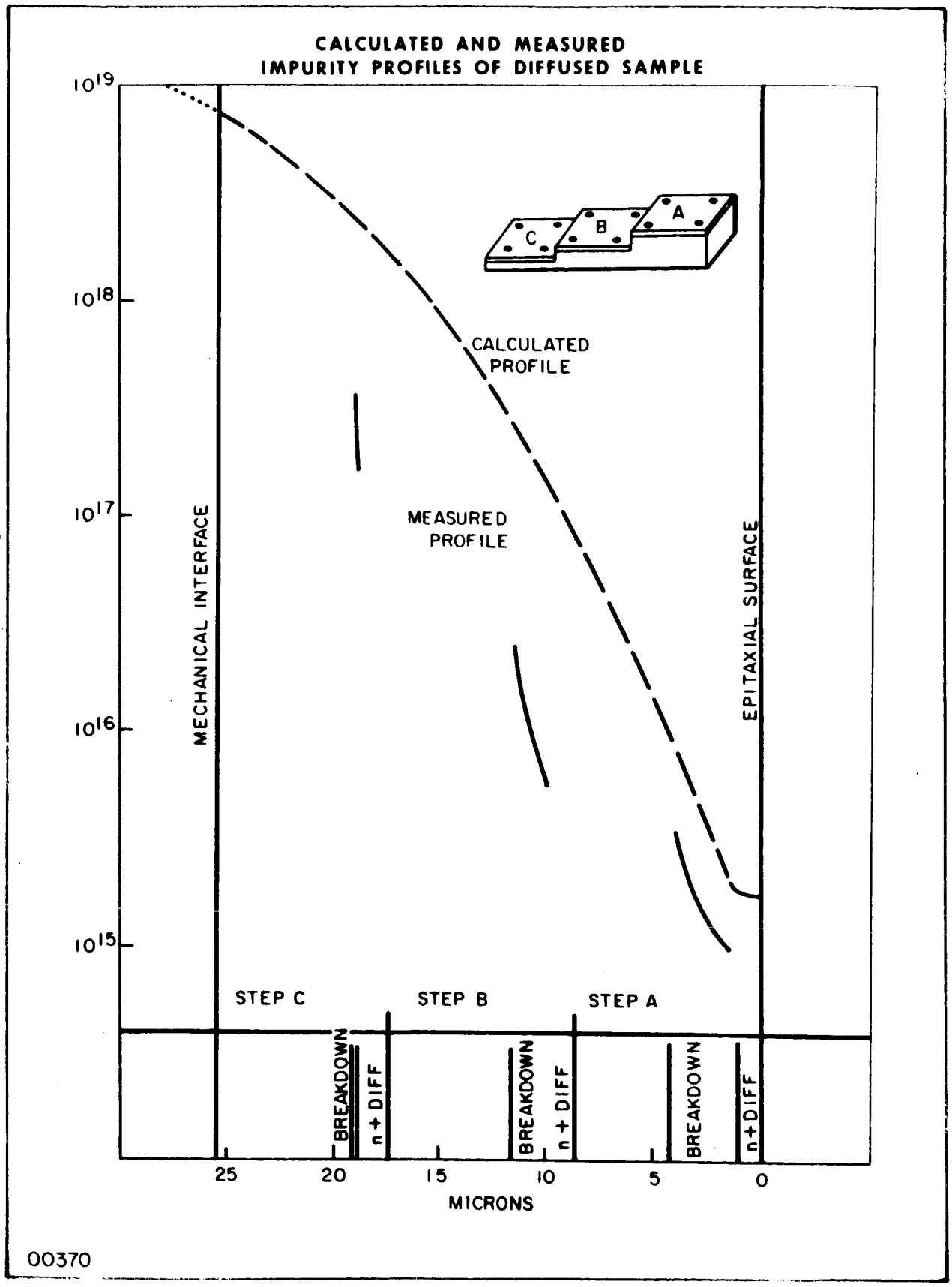

Fig. 7. Junction Capacitance Method
Applied to the Profiling of Thick Layers

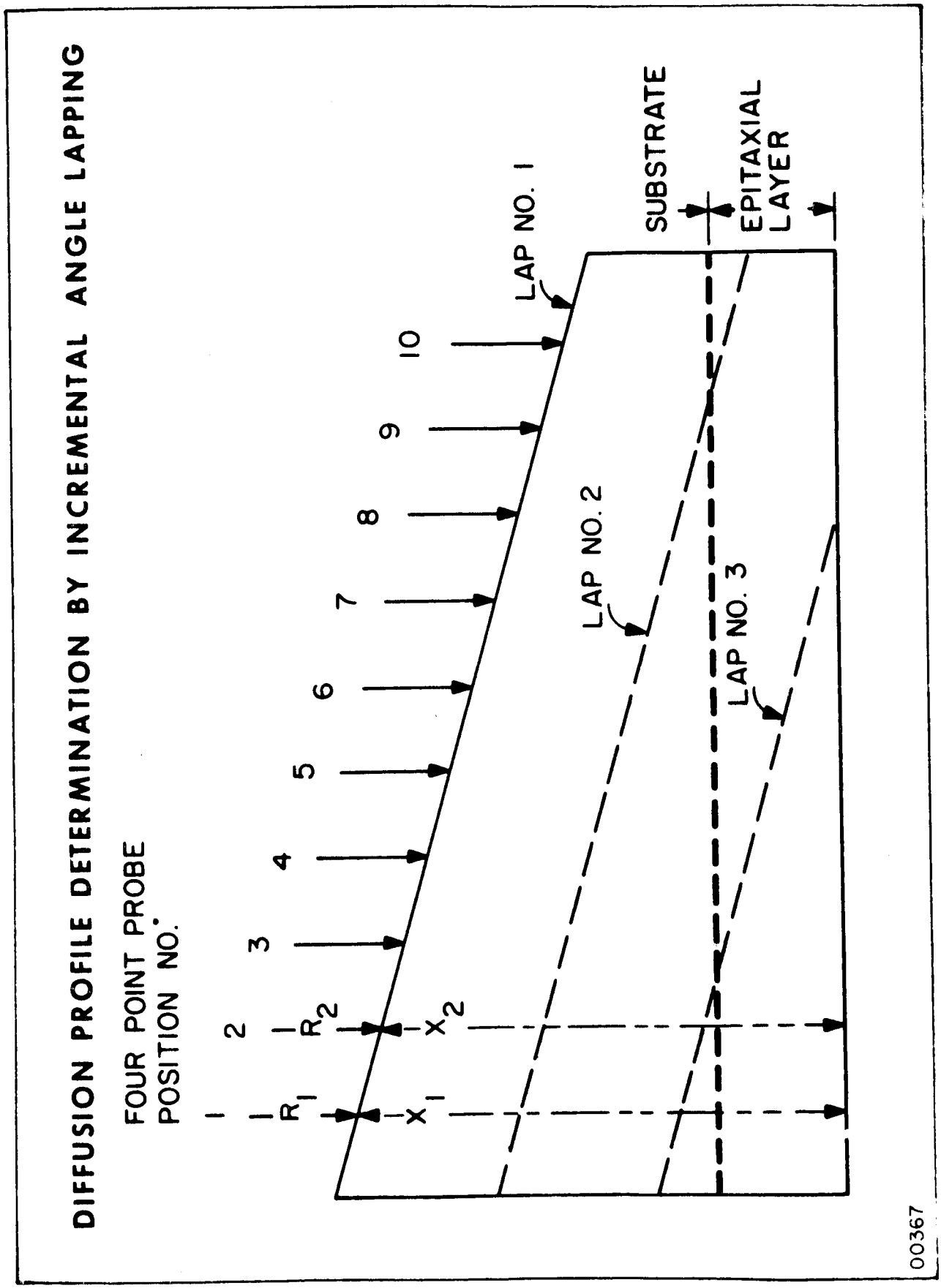

Fig. 8. Concentration Gradient Profiling Method

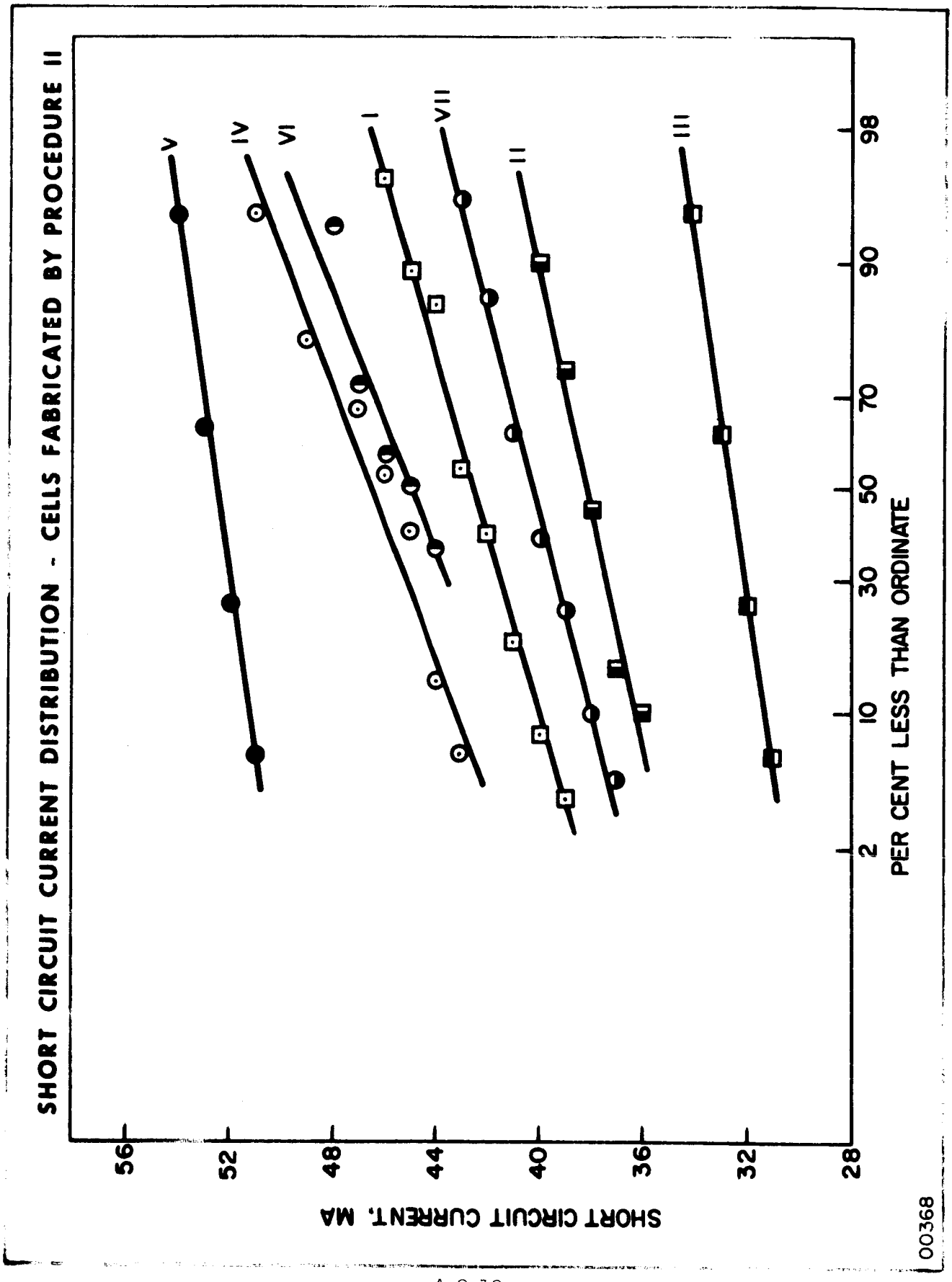

Fig. 9. Short Circuit Current Distribution for Cells Made with Various Drift Field Widths and Magnitudes

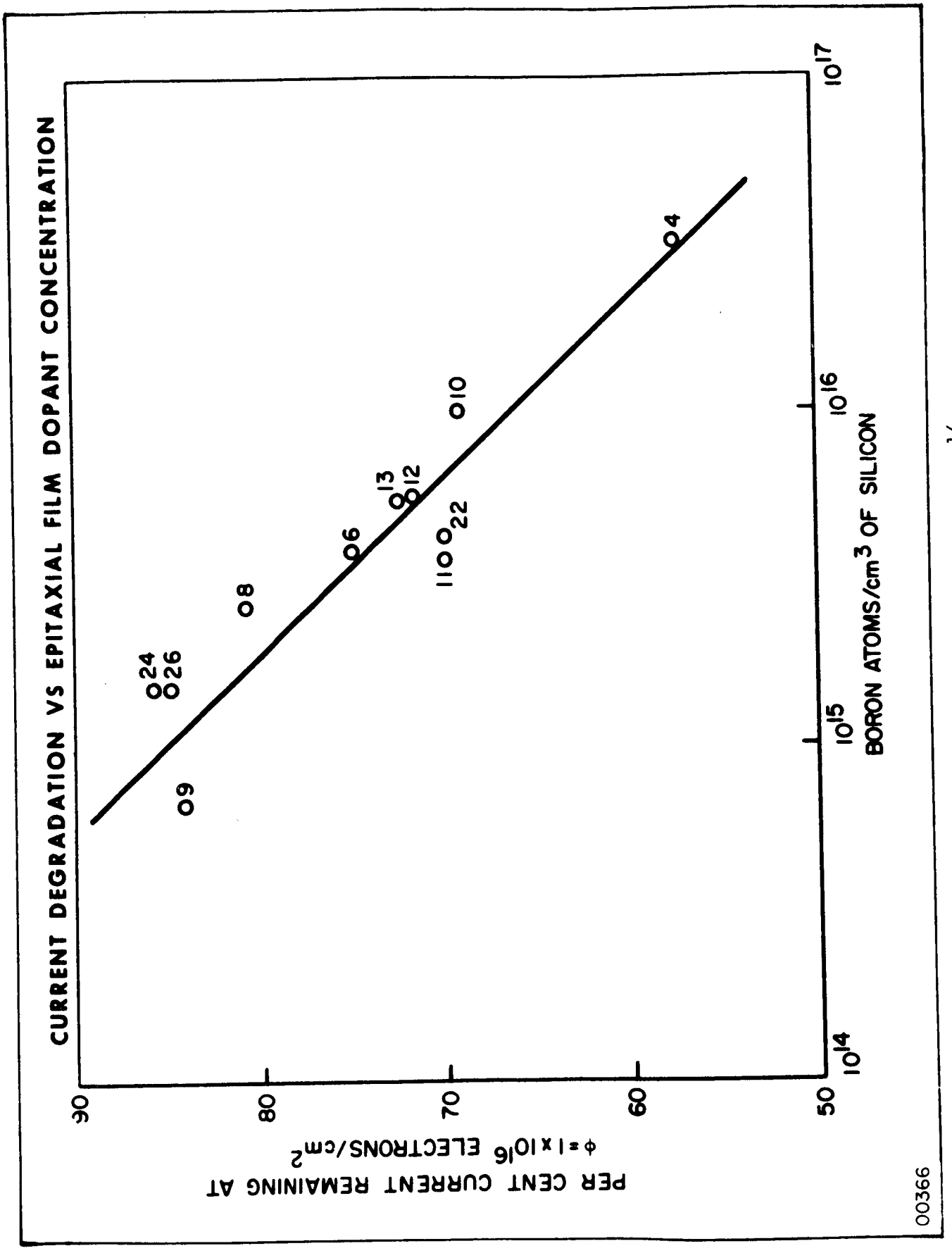

Fig. 10. Current Degradation after a Total Flux of 10^{16} One Mev Electrons

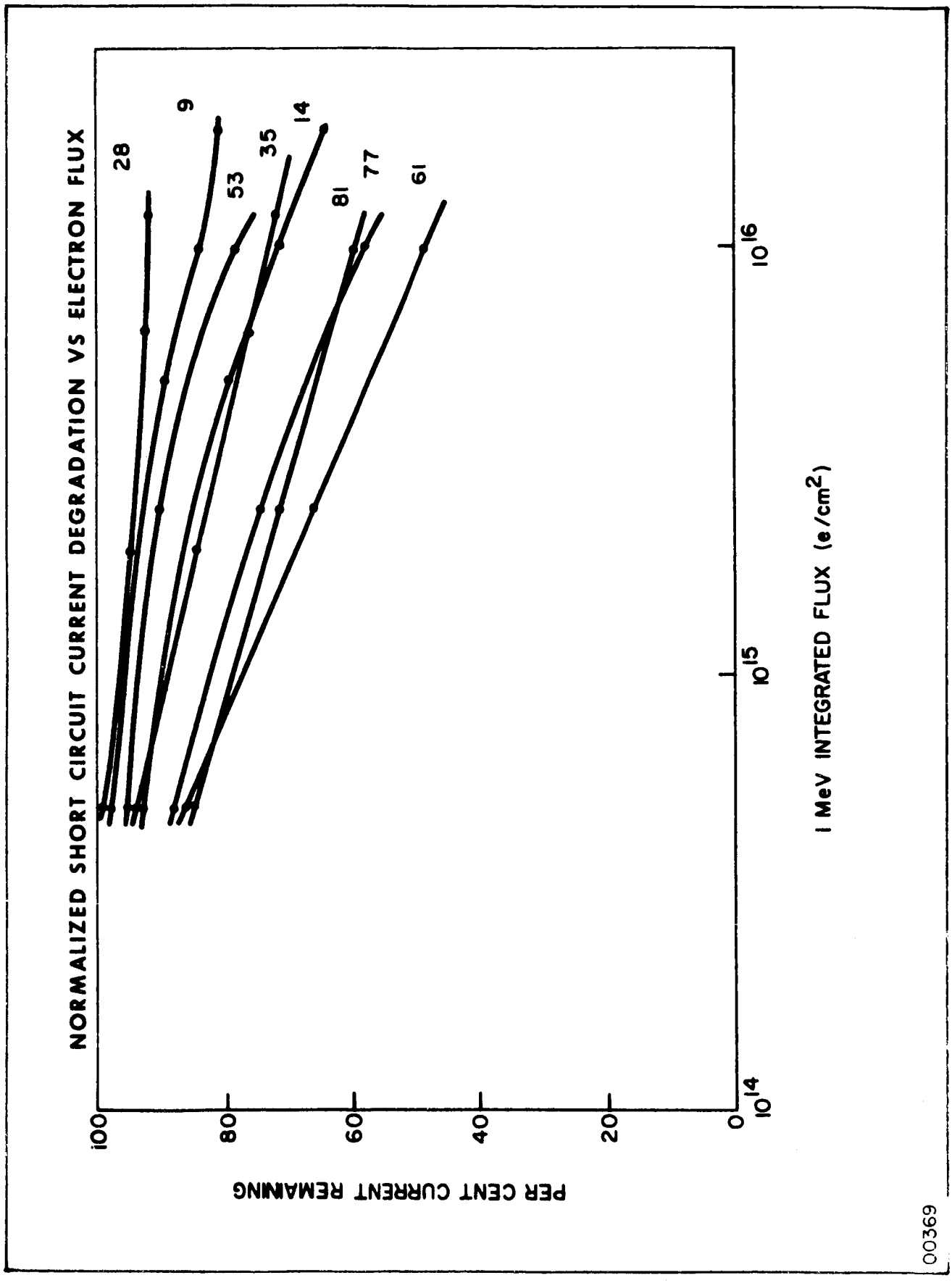

Fig. 11. Representative Short Circuit Current Degradation Data

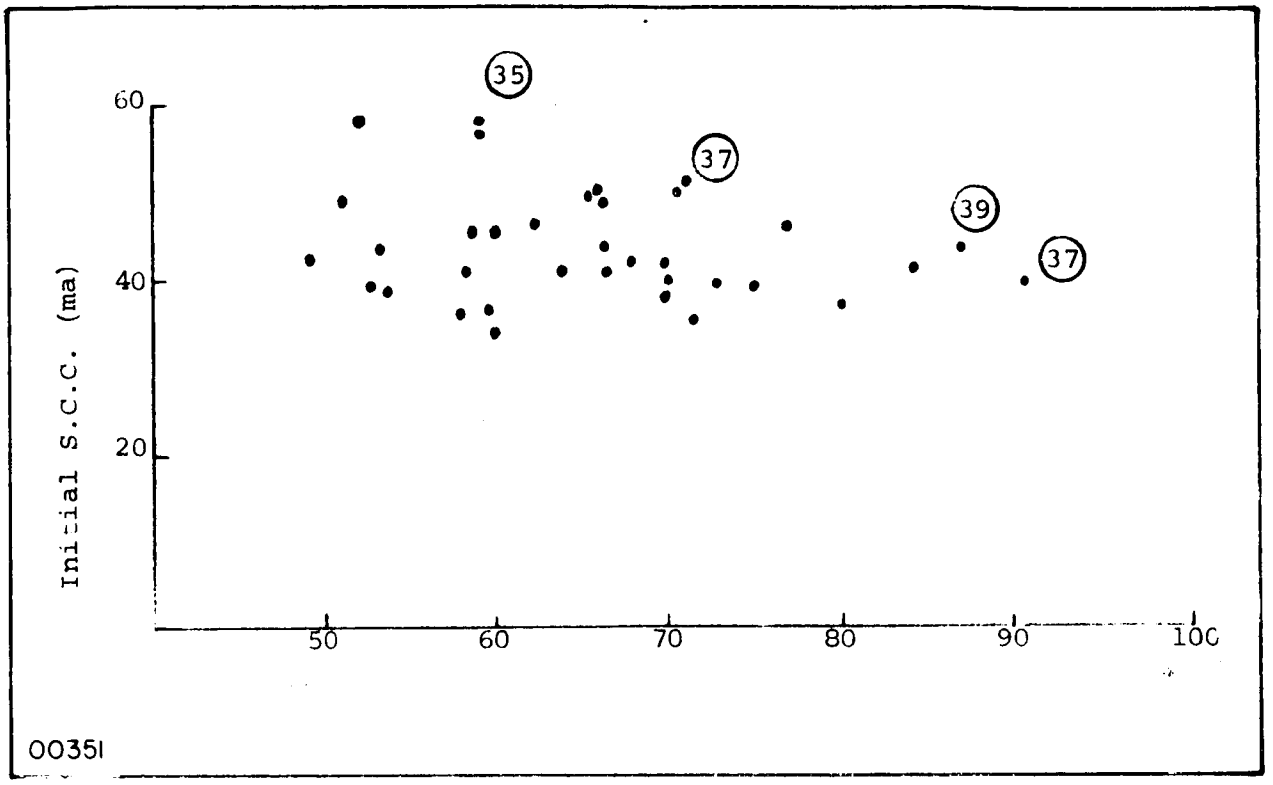

Fig. 12. Initial Short Circuit Current versus Fraction of Current Remaining after a Total Flux of 10^{16} electrons/cm^2. The Circled Numbers Are Final Currents.

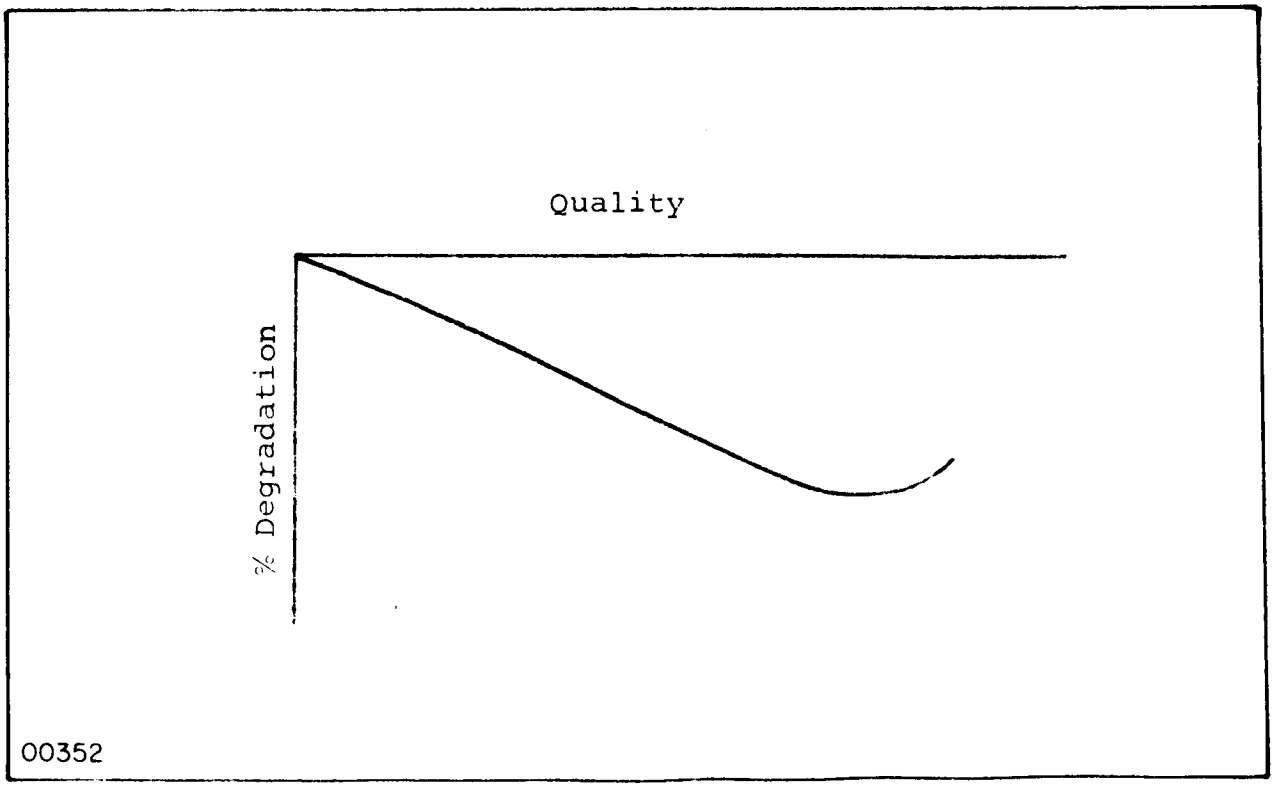

Fig. 13. Per Cent Degradation versus Initial Cell Quality

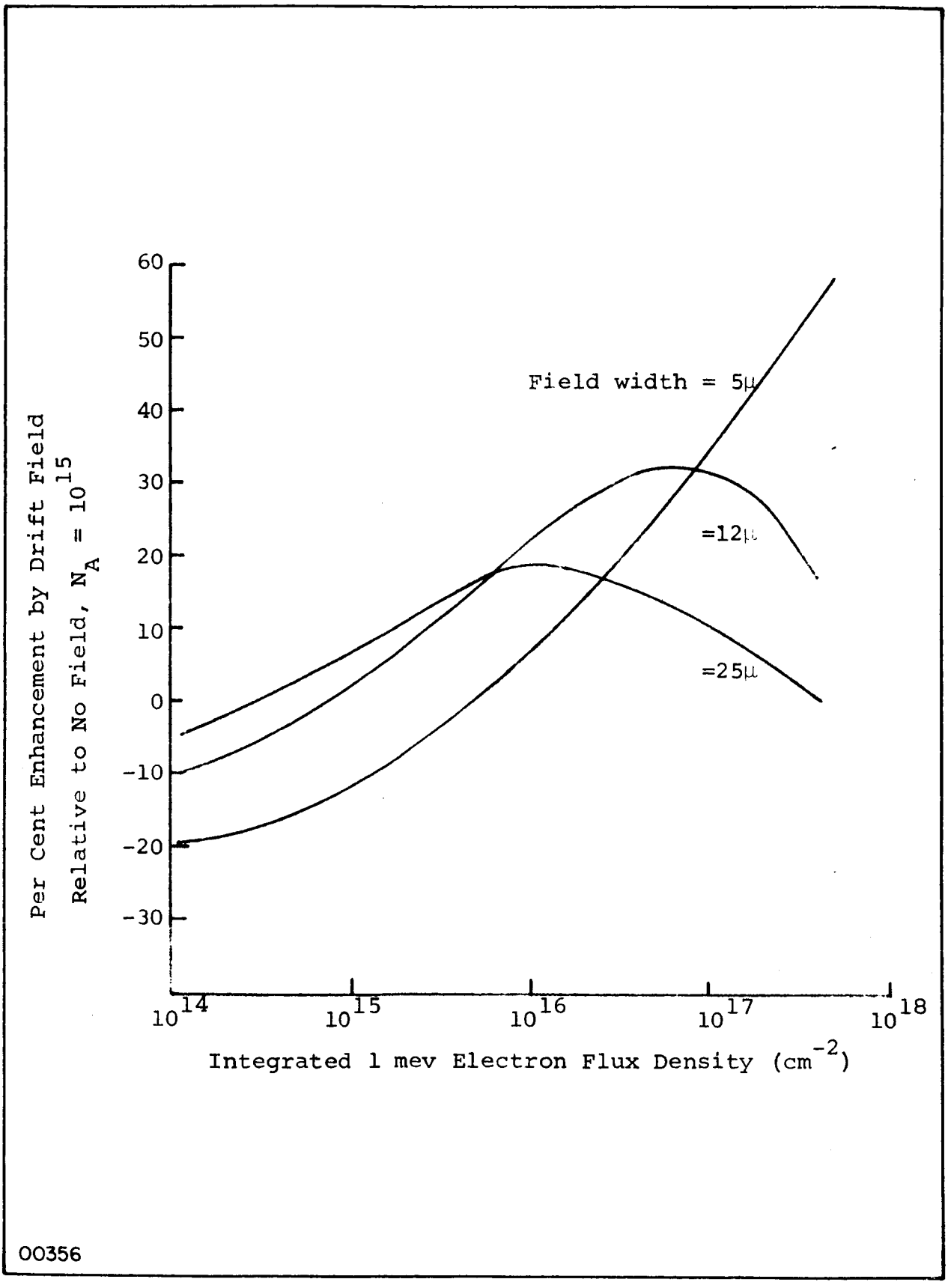

Fig. 14. Theoretical per cent enhancement in short circuit current, as a function of total flux, for three order of magnitude fields and field widths of 5, 12 and 25 microns

Discussion

Green - Underwater Sound Lab: What is the difference between a normal cell and one with a built in field?

Runyan: With regard to what?

Green: Do not all solar cells have a built in field?

Runyan: A normal cell has a built in field only between the front surface and the junction. Usually however, only about 15% of the carriers are absorbed in that region, so most of them recombine behind the junction. It is an additional field added in this region to which the paper referred.

Green: Why not make the initial field itself thicker?

Runyan: Usually solar cells with deeper junctions are somewhat less efficient than those with shallow junctions.

Pearson - Session Chairman: I think this conversation should be delayed and continued during the coffee hour.

Loferski - Brown University: Did you say that the only parameter you have looked at on these cells has been short circuit current?

Runyan: Yes.

Loferski: And there was not much improvement in that over ordinary cells?

Runyan: That is correct.

Loferski: What about the other characteristics of the cells? Are they even worse?

Runyan: This is rather an embarrassing question because we have neither made a theoretical analysis nor have we examined the data for either total power output or open circuit voltage.

Chidester - Lockheed: I realize that this was not the primary purpose of your study, but are you saying that if we are using cells in a radiation environment that we should not be too concerned with the initial performance of that cell - that we could use poorer cells and get the same performance at the end of life?

Runyan: Yes I said that, but if you consider the total power then you will have less total power delivered to the load with the poor cells. I think one wants to start with the best cell available. My point was that the kinds of data one sees on radiation effects depend on the kind of cell it was to start with, and that one should take this into account when analyzing the data.

Ralph - Heliotek: In regard to Loferski's questions; I think I would like to make a comment. Maybe you would indicate what you have observed. We have seen a peculiar effect with drift field cells wherein the voltage degradation was lower when the current degradation was higher, and vice versa. Have you seen anything like that?

Runyan: No I don't think we have seen that exact thing.

Kaye - EOS: May I make a quick comment on that? I will be showing some data on voltage degradation and giving some discussion in my paper. Perhaps I might suggest that we leave this discussion until after that and then it can all be discussed at one time.

Ralph: That is agreeable with me.

Pearson: Could you have used avalanche breakdown to determine the concentration rather than the four-point probe?

Runyan: I think a single point spreading resistance probe would probably work, but I do not know how to analyze the data from the avalanche breakdown probe for the case in which the concentration is varying below the surface.

PIC-SOL 209/6
Section A-3

DRIFT FIELD DENDRITIC SILICON SOLAR CELLS*

Presented by

K. S. Tarneja

Westinghouse Semiconductor Division

Youngwood, Pennsylvania

18 October 1965

*Most of the work described here was supported by the U. S. Air Force Aeronautical Systems Division, Wright-Patterson Air Force Base, Ohio, under contract AF 33(615)1049.

PIC-SOL 209/6

17309

Abstract

Silicon solar cells are semiconductor devices which convert the sun's radiant energy into electrical power. Solar cells are being widely used on space vehicles, which requires them to be radiation resistant. Considerable effort is currently being expended to develop a radiation-resistant solar cell structure.

A drift-field structure for the fabrication of radiation-resistant solar cells will be presented and discussed. Epitaxial growth techniques were used to obtain graded layers for achieving the drift-field structure. Graded epitaxial layers of 10-50 microns thick were successfully grown on low resistivity, P-type silicon web and Czochralski crystal substrates. The N-P junction was formed using phosphorous diffusion. Evaporated Ti-Ag contacts were used for fabricating the device. The physical and electrical characteristics on these devices will be presented.

Radiation-damage studies using 1 MeV electrons were performed to optimize the structure for increased radiation resistances. Plots of efficiency and short-circuit current density vs. electron flux density will be presented and discussed. The results obtained will show the epitaxial graded base cells were more radiation resistant than the field-free (conventional) cells. The optimum drift-field structure for radiation resistant dendritic silicon solar cells will be presented and discussed. Integral quartz cover studies on these cells will be presented.

A slotted angle design for the fabrication of solar cell panel modules will be presented and discussed. Estimated weights and power density (watts/lbs) on the different cell design will be presented, and a study of fabrication in quantity for dendritic cells will be discussed.

Author

DRIFT-FIELD DENDRITIC SILICON SOLAR CELLS

K. S. Tarneja
R. K. Riel
V. A. Rossi
E. R. Stonebraker
Westinghouse Semiconductor Division
Youngwood, Pennsylvania

and

J. M. Hicks
Westinghouse Research Laboratories
Pittsburgh, Pennsylvania

Introduction

Virtually all of the solar cells produced in this country are being used on space vehicles as sources of primary power. A chief limitation of solar cell arrays is the degradation of power output from the space radiation environment. In the interest of mission economy, solar cell arrays should also have high power densities (watts/lb). This paper will outline the use of webbed dendritic silicon in a radiation- resistant and lightweight solar cell array. Superior radiation resistance is achieved through the use of the drift-field cell structure, and the unique mechanical properties of the webbed dendritic silicon strongly contribute to array power density.

Drift-Field Cells

Recent studies by several workers have indicated that an N/P type solar cell, of about 10 ohm-cm base resistivity, is optimum with respect to radiation resistance. Therefore, most of the present commercial cells are of this type.

Solar cell performance strongly depends upon the ability of minority charge carriers to drift into the N-P junction region from the base region. Space radiation inhibits this drift by generating minority carrier recombination centers in the base region. Therefore, it has been suggested that an electric field, in the base region of solar cells, will enhance charge collection for any given density of radiation-induced recombination centers, over that of field-free cells. Such drift-field cells, therefore, should display performance with damaging radiation superior to that of comparable field-free cells.

In the present drift-field approach, an epitaxially-grown layer, with a graded P-type impurity concentration, is employed. A cross-section of this cell, and an impurity concentration profile are shown in Fig. 1. Cells made by this method have shown efficiencies as high as 11% under filtered 3400°K illumination. This value of initial

efficiency, plus the radiation resistance of these units, results in superior performance for the duration of any mission. Table I shows some of the characteristics obtained on these cells. Large area drift-field cells were made and the results are shown in Table II. Figures 2 and 3 show the results of an irradiation in which both conventional and drift-field cells were irradiated for comparison purposes. If radiation resistance is regarded as the ratio of integrated flux density values necessary to reduce the efficiency to a given value, it can be seen that there is a factor of 3 superiority for the drift-field cell (Fig. 2). If one considers that the cells will be exposed to an equivalent integrated omnidirectional 1 MeV electron flux density of 7×10^{15} e/cm^2 per year (for a worst-case equatorial orbit), then it is readily seen that the daily integrated flux density is 1.9×10^{13} e/cm^2. Considering the crossover point of Fig. 2, it is evident that after less than seven days in the above space environment, the drift-field cells will be superior to the conventional cells, despite the fact that their initial efficiency was lower than that of the conventional cells. Fig. 4 also shows the performance of these cells as compared to commercial N/P cells.

The above analysis of solar cell space performance assumes that the electrical operating point of the cells will always be at maximum efficiency. However, on practical spacecraft, the solar cells generally work into a constant voltage load. This requirement actually enhances the performance of the drift-field cells, as can be seen from an examination of Figure 5. Therein is plotted the efficiency vs. integrated 1 MeV electron flux density, for both cell types, at different load voltage values. The advantage of the drift-field cells is greatest at the higher voltage, and decreases as the load voltage decreases.

It is expected that the superior radiation resistance of the drift-field cells can be utilized to increase the watts per pound ratio of future solar cell arrays by allowing thinner cover slips to be used over the cells. In this case, the lifetime of the array of drift-field cells would be the superior over an array of conventional cells. It may be possible to use recently-developed integral quartz covers of 1-3 mils thickness, instead of adhesive-bonded 6-mil covers. This approach has the additional advantage of eliminating effects of radiation damage to the cover slip adhesive.

A novel technique for the low-temperature deposition of SiO_2 was developed. Known methods for oxide deposition include the pyrolytic decomposition of tetraethylorthosilicate, the reaction of a silicon halide with CO_2 or H_2O, etc. Typically, these methods yield oxides that are porous, of low density and have a slow growth rate. The system chosen for study was Si X 4 (X = Cl, Br, or I) - H_2 - O_2. It was assumed that hydrogen and oxygen striking the hot silicon surface would react to form water and the water would react with the silicon halide according to the reaction,

$$SiCl_4(g) + 2H_2O(g) = SiO_2(s) + 4HCl_{(3)}.$$

This reaction is very favorable thermo-dynamically; in fact, the reaction proceeds to the right at room temperature. The $SiO_2(s)$ deposited is nonporous, approaches the theoretical density, and can be deposited at a high growth rate. These considerations make this technique very attractive for the fabrication of integral quartz covers for solar cells. Initial cells made using this technique had open circuit voltage of 0.54 volts and current density 22.5 ma/cm, and efficiency of 8% without antireflective coatings.

Solar Cell Module and Array Design

The purpose of this design study was to present a high power to weight ratio, self-erectable solar array, capable of displaying 20 square feet of high efficiency silicon webbed dendrite solar cells. The approach taken here was the modular one. The basic module selected was one of 3 inch by 12 inch nominal size containing eight dendritic solar cells. A slotted angle substrate was chosen for this module. The substrate was very suitable to long dendritic solar cells as it utilized the mechanical properties and physical dimensions of these cells. The substrate of the "slotted angle" design consisted of a 10-mil thick aluminum sheet. The aluminum sheet was rigidized using die forming techniques. Solar cells were attached to the substrate using a thin layer of RTV silastic adhesive. It should be noted that several wire leads were put on each cell and six mil quartz covers applied before they are mounted on the panel. Design details of a slotted angle panel are shown in Figure 6.

The modules fabricated using this design were tested environmentally for the following tests:

1. Acceleration - - - - 12 g's
2. Shock - - - - - - - 40 g's
3. Temperature - - - - 40°F to 200°C
4. Vibration - - - - - 15 g's

The details of this are shown in Figure 7. The modules passed the environmental tests satisfactorily.

Table III gives the details for power to weight ratios for a 20 ft^2 array. Figures 8, 9, 10 and 11 show the array concept and deployment technique. Twenty of the modules are tied together to form a five square-foot array segment. These array segments are then attached to either the supporting beam or a hard back containing supporting hinges. The array is held in the stored configuration by means of clevis joint. The pin in the joint is attached to pyrotechnic cartridge and can be retracted by firing the cartridge. Springs are provided to erect the panels.

Conclusions

A drift-field solar cell structure using silicon webbed dendrite has been developed. Efficiencies on these cells were as high as 11.2%. Drift-field cells 1 cm by 2 cm, 1 cm by 6 inch and 1 cm by 12 inch were fabricated.

A low temperature SiO_2 deposition technique for achieving integral covers on solar cells was tried and found feasible.

Solar cells in large quantities can be fabricated on silicon webbed dendrites. A pilot-line for this has been set up and presently is in operation.

The slotted angle panel design resulted in 15 watts/lb or more power output under tungsten testing conditions. With improvements in the present design, it is possible to achieve 25.0 watts/lb.

Acknowledgements

Most of the work described here was supported by U. S. Air Force Aeronautical Systems Division, Wright-Patterson Air Force Base, Ohio under Contract AF 33(615)-1049. The work described on the 20 ft^2 array was performed by the Aerospace Division of Westinghouse and we wish to thank Mr. C. Denton, Mr. F. England and Mr. J. Rew for this.

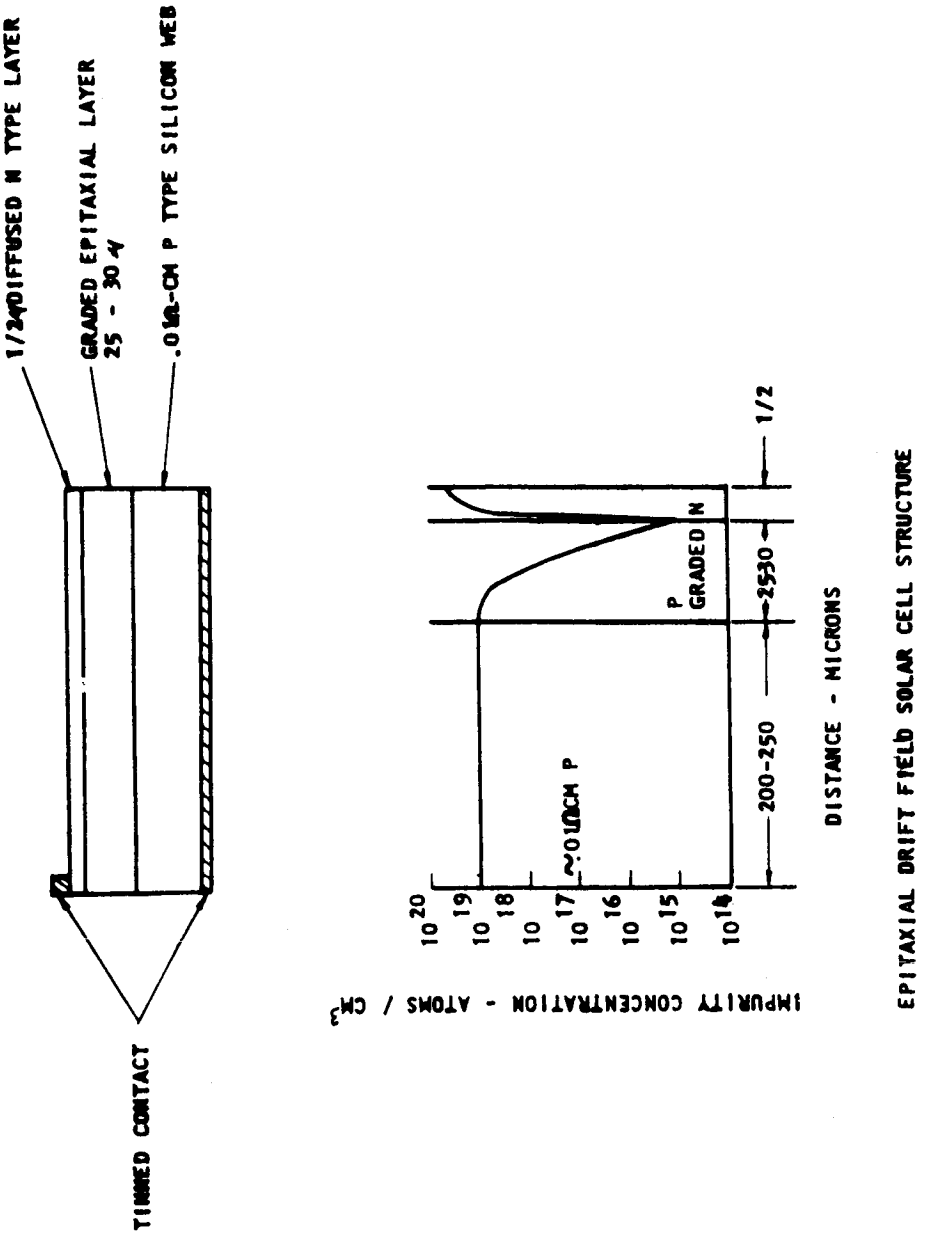

EPITAXIAL DRIFT FIELD SOLAR CELL STRUCTURE

Figure 1

TABLE I

TABULATION OF SOLAR CELL DATA ON

OPTIMUM DRIFT FIELD STRUCTURE USING SILICON WEBBED DENDRITES

PHYSICAL CHARACTERISTICS				ELECTRICAL CHARACTERISTICS UNDER ILLUMINATION					
Cell No.	*Area cm^2	Length cm	Width cm	V_{OC} Volts	I_{SC} ma	V_M Volts	I_M ma	P_M mw	n %
EP67-2	1.71	2.0	0.95	0.57	45	0.44	42.0	18.48	10.8
EP68-4	1.71	2.0	0.95	0.56	45	0.44	42	18.48	10.8
EP68-5	1.80	2.1	0.95	0.56	49	0.44	45	19.8	10.95
EP71-2	1.89	2.0	1.05	0.56	51.5	0.44	47	20.7	10.9
EP83-2A	1.71	1.9	1.0	0.55	47.5	0.44	43.5	19.14	11.2
EP90-3A	2.16	2.0	1.2	0.55	58.0	0.44	53.0	23.3	10.75
EP90-3C	2.16	2.0	1.2	0.55	56.5	0.44	51.5	22.62	10.45
EP110-2C	2.16	2.0	1.2	0.57	55.8	0.47	49.7	23.4	10.8

* Effective Area Only .9 (LxW)

Intensity mw/cm^2: 100

Type of Source: Tungsten

Color Temperature: 3400°C

TABLE II

Cell No.	Area Cm^2	Length Cm	Width Cm	V_{OC}	I_{SC}	V_M	I_M	P_M	N%
EP1-182A	13.68	15.2	1	.55	315	.44	286	126	9.23
EP1-183A	13.68	15.2	1	.56	330	.42	310	130	9.5
EP1-174A	13.68	15.2	1	.54	340	.42	295	124	9.06
EP1-184A	13.68	15.2	1	.54	325	.42	295	124	9.05
EP1-172C	13.68	15.2	1	.55	335	.42	310	130.2	9.55
EP1-181B	13.68	15.2	1	.55	335	.42	310	130.1	9.53
91-1	12.39	15.2	0.9	0.55	320	.44	290	127.6	10.3
76	24.62	22.8	1.2	0.55	640	0.40	585	234	9.5
90-3	24.62	22.8	1.2	0.55	640	0.40	585	234	9.5

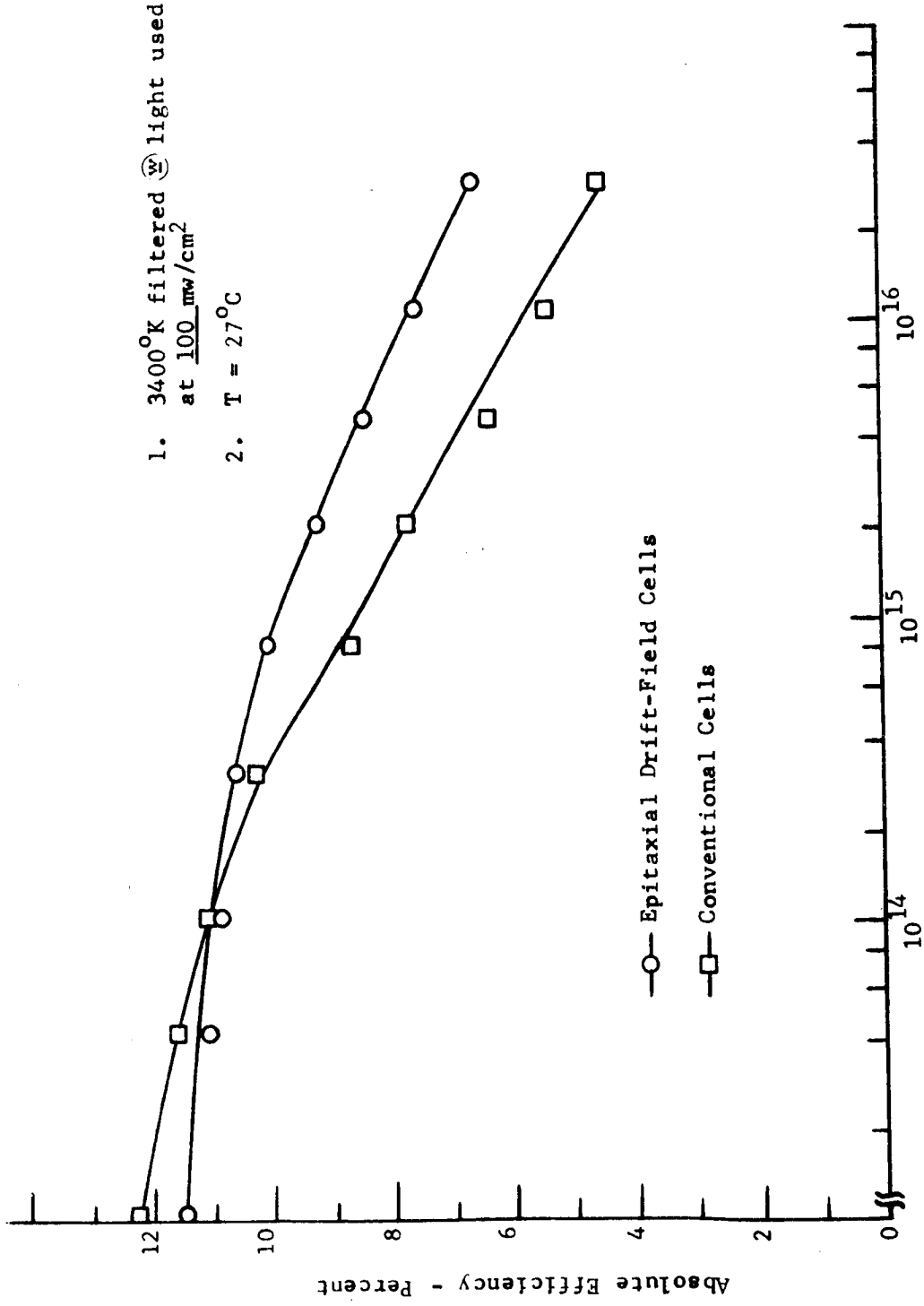

Absolute Efficiency of Westinghouse Silicon Solar Cells vs. 1 MeV Electron Flux Density

Figure 2

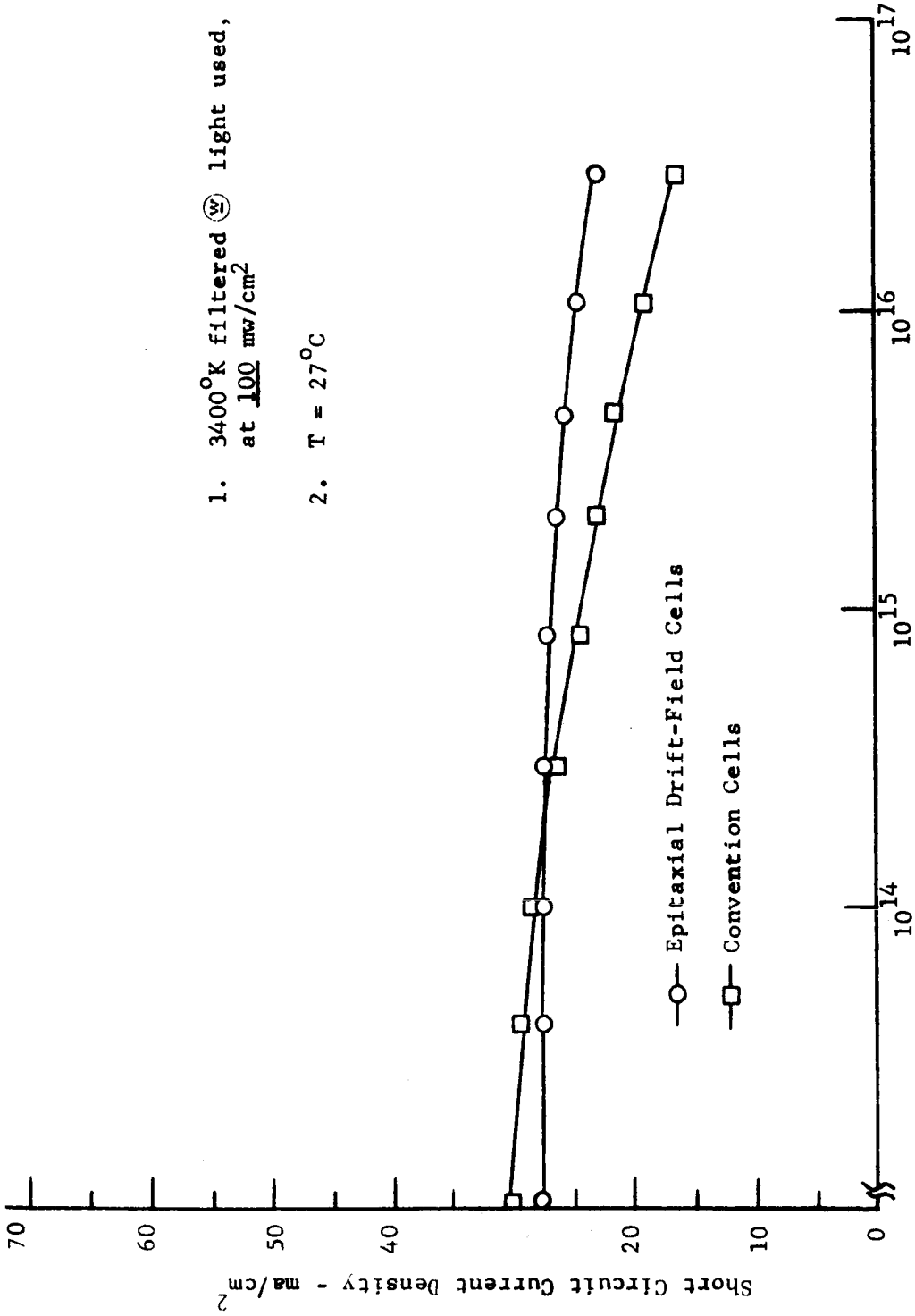

Absolute Short-Circuit Current Density of Westinghouse Silicon Solar Cells vs. 1 MeV Electron Flux Density

Figure 3

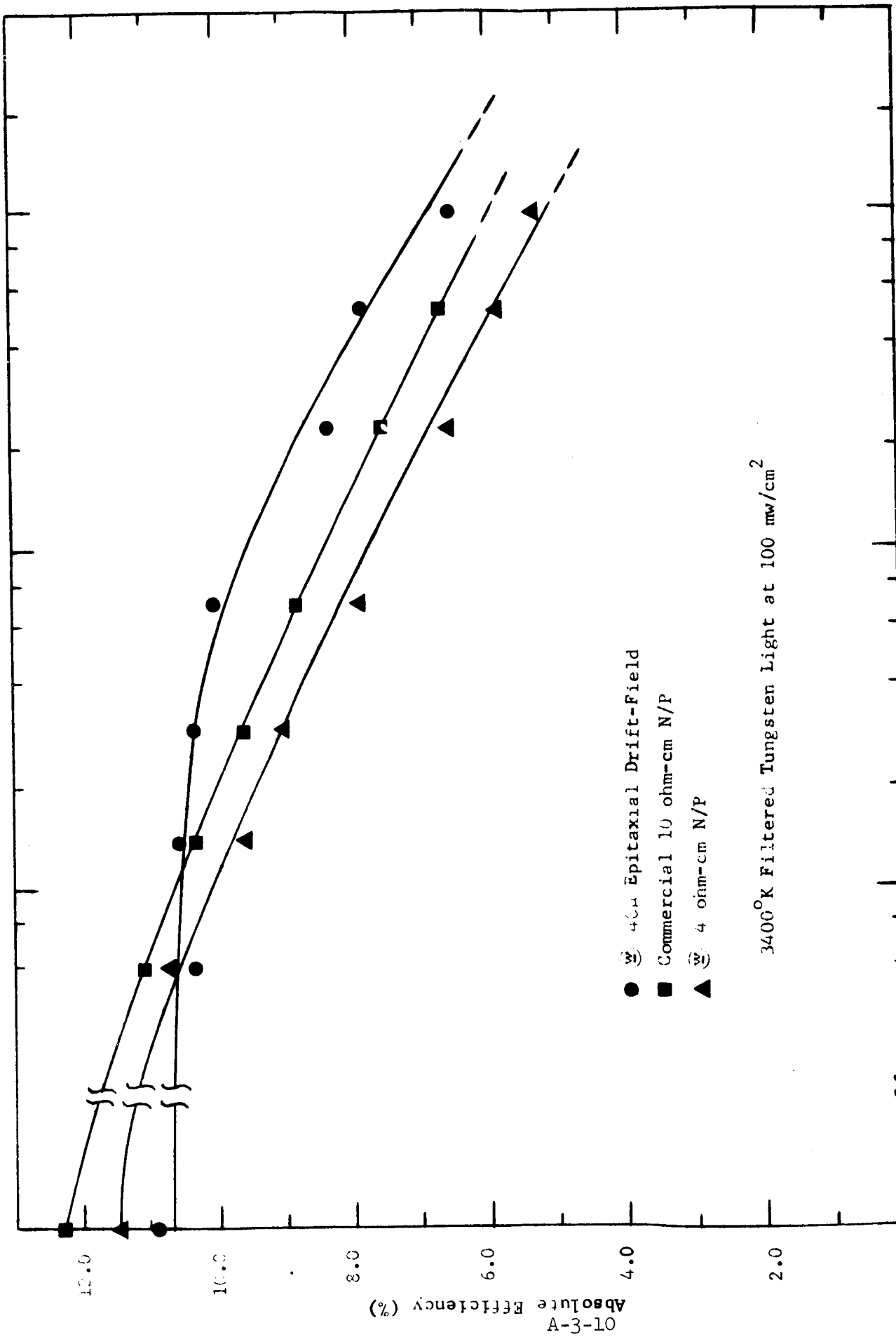

ABSOLUTE EFFICIENCY VS. 1.0 MeV ELECTRON FLUX DENSITY FOR SILICON SOLAR CELLS

Figure 4

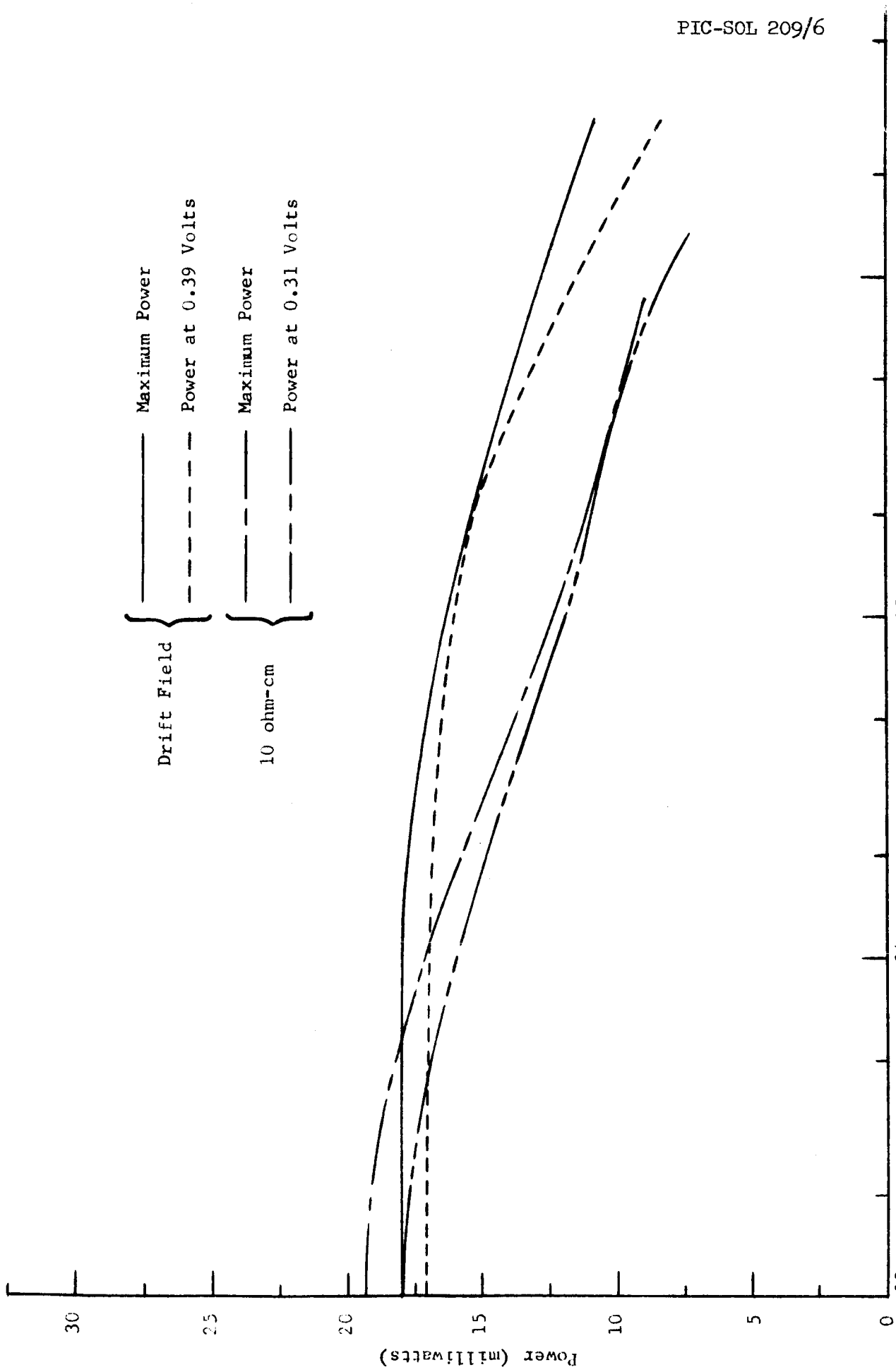

POWER OUTPUT VS. 1.0 MeV ELECTRON FLUX DENSITY FOR SILICON SOLAR CELLS

Figure 5

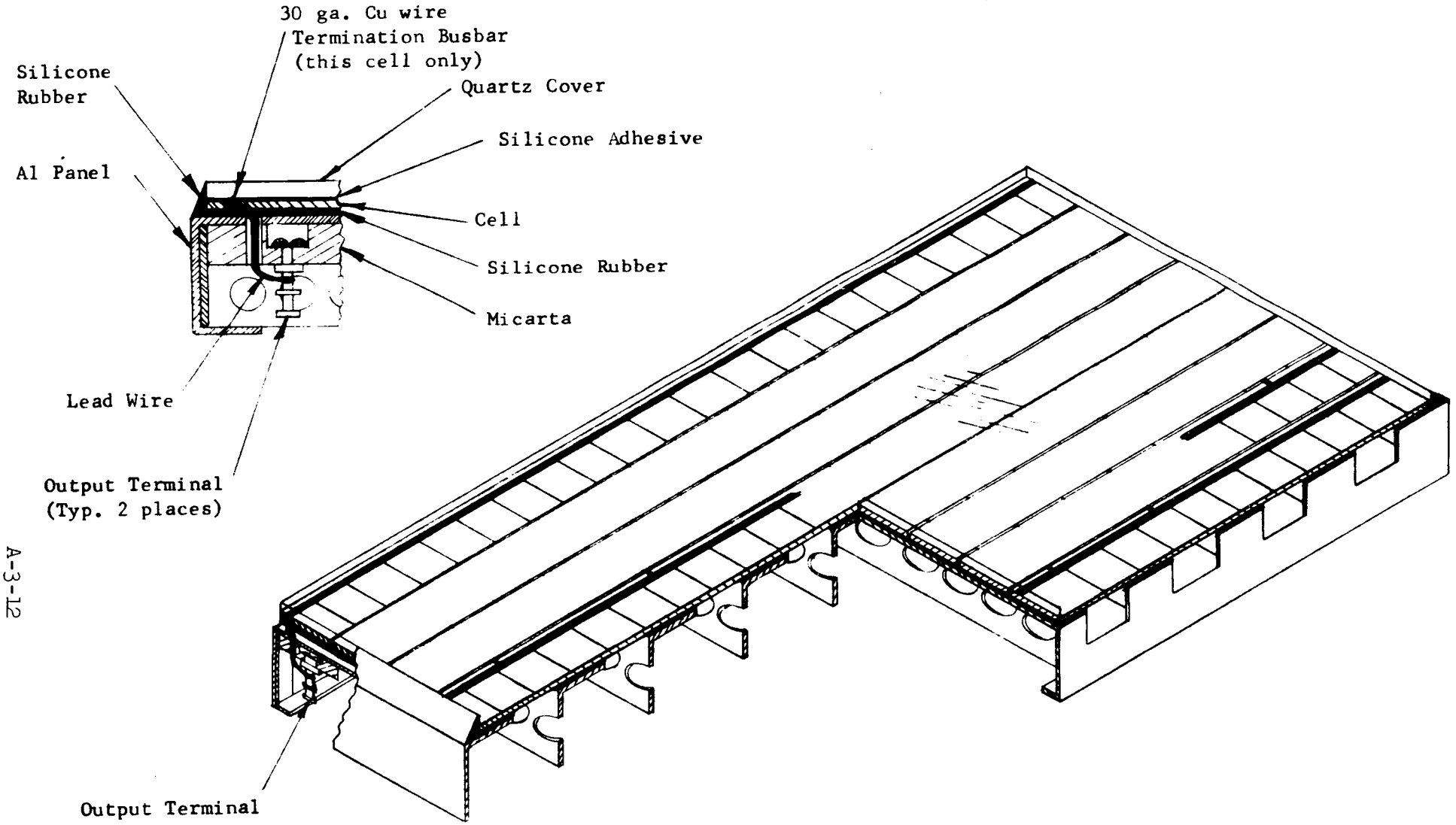

SLOTTED ANGLE SOLAR CELL POWER MODULE

Figure 6

Test Requirements

1. Acceleration

The solar cell panels will be subjected to 12 g's acceleration force for a duration of ten minutes in each direction of each of the three (3) mutually perpendicular axes.

2. Shock

The solar cell panels will be subjected to a shock pulse with a magnitude of 40 g's and a pulse duration of six (6) milliseconds. The solar cell panels will be subjected to three (3) shocks in each direction of the three (3) mutually perpendicular axes.

3. Temperature

The solar cell panels will be subjected to three (3) complete temperature cycles. Each temperature cycle will consist of starting at room temperature, increasing the temperature to +200°F, then reducing the temperature to -40°F and finally returning to room temperature.

4. Vibration

The solar cell panels will be vibrated in each of three (3) mutually perpendicular axes under the following conditions:

Type of Vibration	Frequency	Input
Sine Wave	5 to 14 cps	0.5 inch D.A.
	14 to 40 cps	5.0 g's
	40 to 400 cps	7.5 g's
	400 to 3000 cps	15.0 g's
Random	20 to 2000 cps	0.05 g^2/cps spectral density

The sine wave vibration will be applied separately from the random vibration. The sine wave cycling will consist of 5 to 3000 cps in 2.50 minutes and 3000 to 5 cps in 2.50 minutes. The random vibration will be applied for 5.0 minutes.

Figure 7

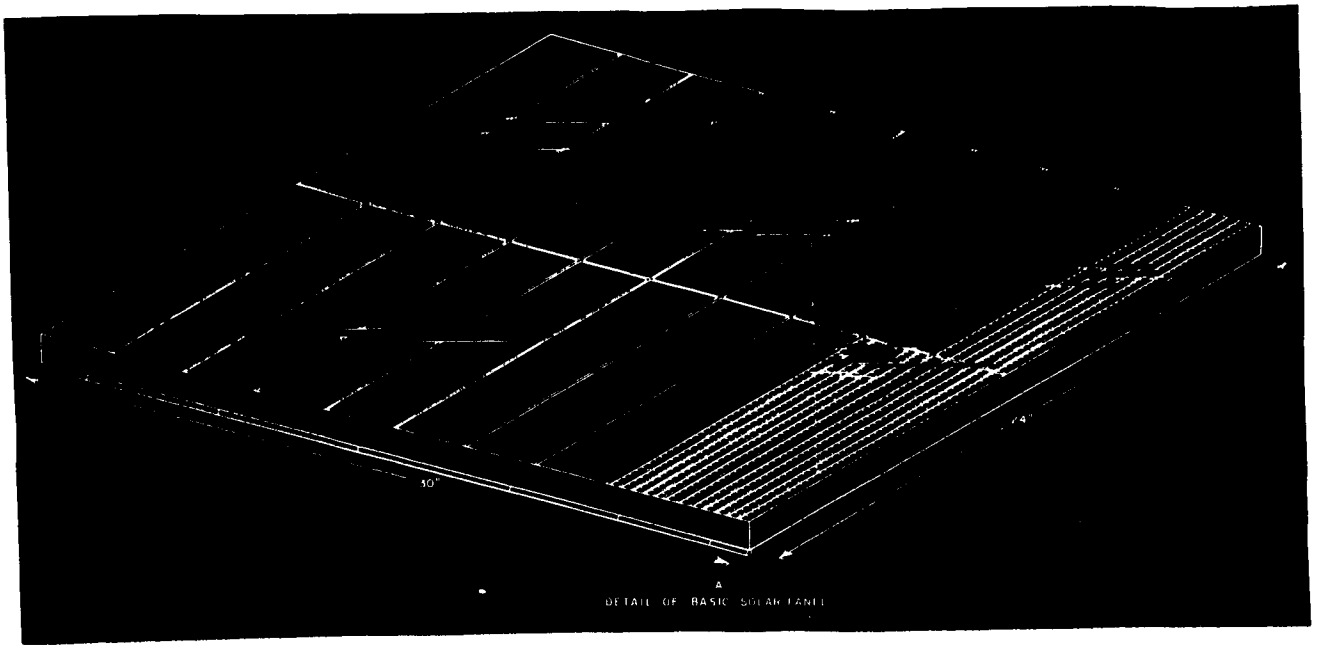

Figure 8

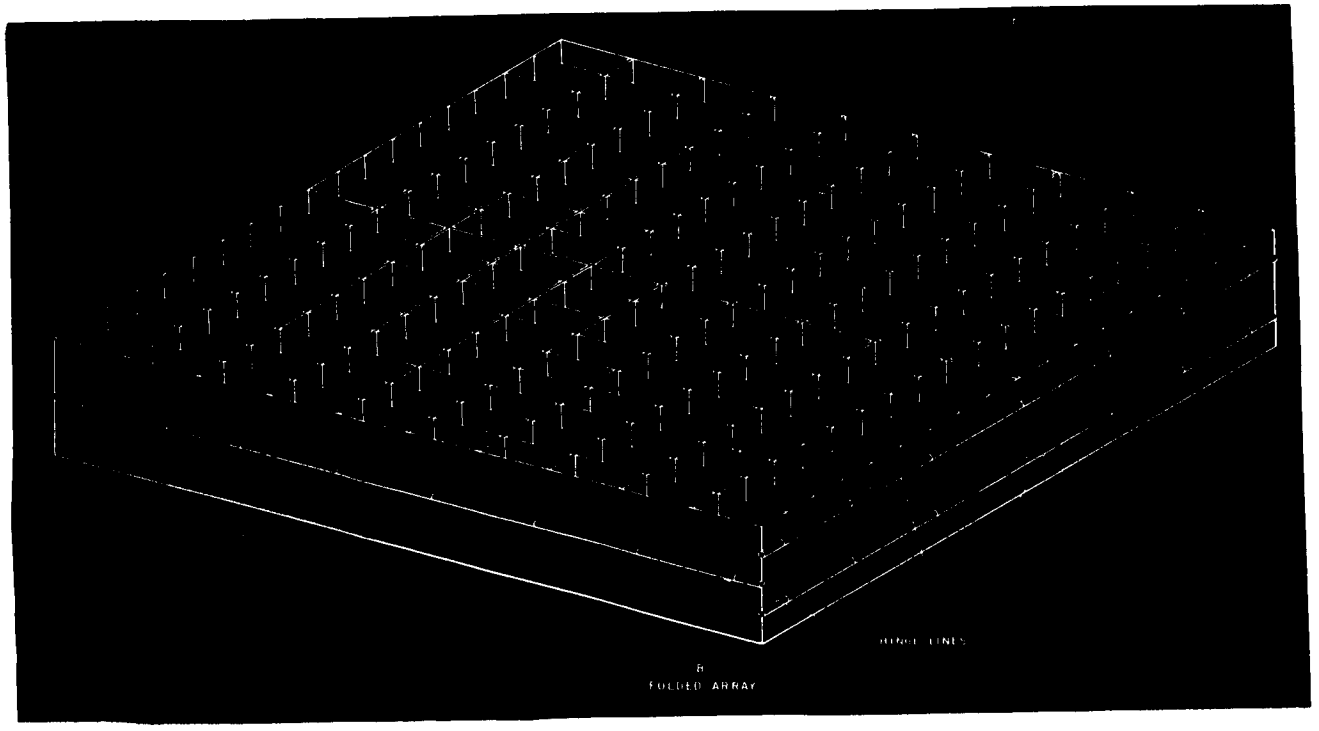

Figure 9

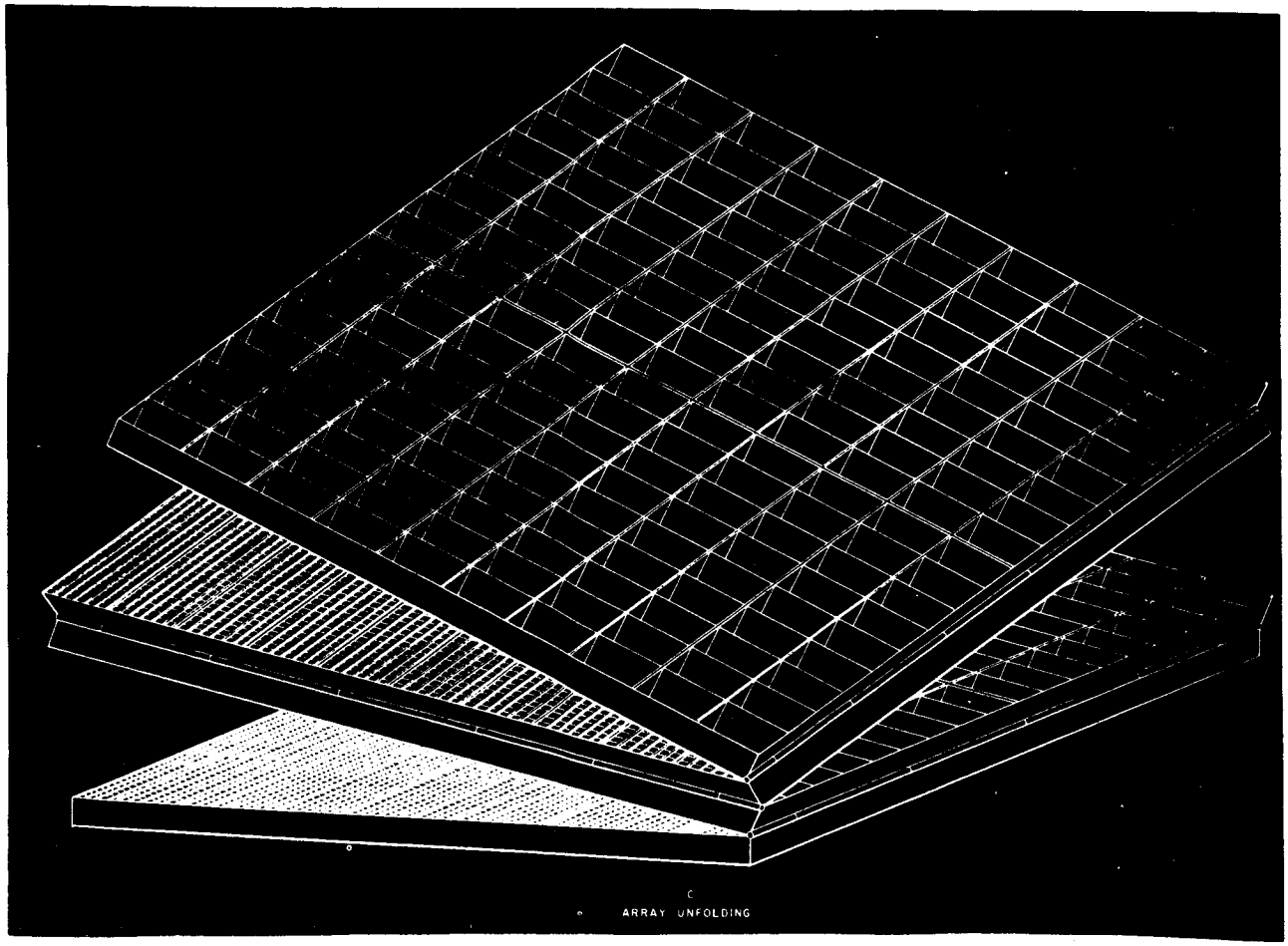

Figure 10

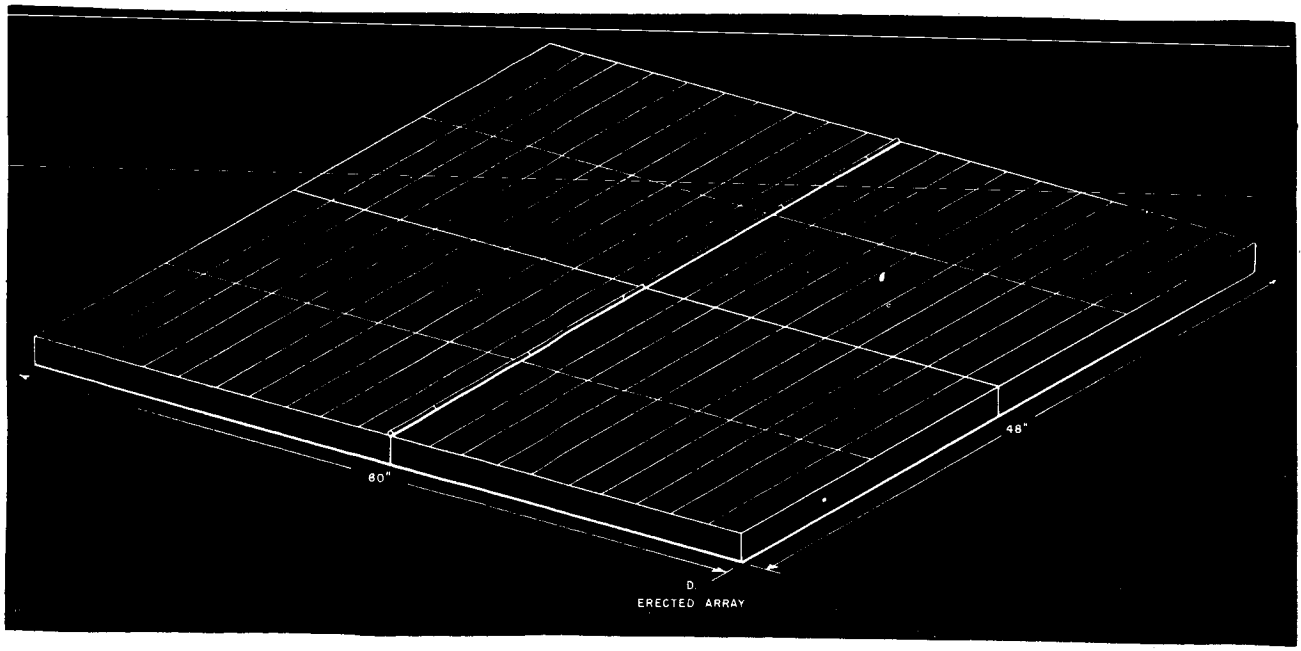

Figure 11

TABLE III

Power to Weight Ratios for a 20 Sq. Ft. Array

Present Available		Present Possible	
A. Module Weight Size: 3 in by 12 in (nominal)		A. Module Weight Size: 3 in by 12 in (nominal)	
6 mil covers	8.0 gms	3 mil covers	4.0 gms
Si solar cells (soldered, 15 mils thk.)	32.0 gms	Si solar cells (solderless, 7 mils thk.)	11.2 gms
Al substrate	21.0 gms	Al substrate	17.0 gms
Silicone Rubber Adhesive	7.5 gms	Silicone Rubber Adhesive	7.5 gms
Transparent Adhesive	5.5 gms	Rest	1.6 gms
Rest	3.7 gms		
TOTAL	77.7 gms	TOTAL	41.3 gms
B. 20 Sq. Ft. Area		B. 20 Sq. Ft. Area	
80 modules at 77.7 gms each	13.6 lbs	80 modules at 41.3 gms each	7.37 lbs
C. Array Hardware		C. Array Hardware	
Weight	2.60 lbs	Weight	2.60 lbs
D. Total Weight		D. Total Weight	
B + C	16.20 lbs	B + C	9.97 lbs
E. Total Power Output		E. Total Power Output	
Using 10% cells	248.8 watts	Using 10% cells	248.8 watts
F. Watts/lb		F. Watts/lb	
$\frac{E}{D}$	15.5	$\frac{E}{D}$	25.2

Discussion

Campbell - NRL: I want to ask about that low temperature and what do you predict for the radiation stability as far as discoloration? Seeing as how it's grown from ....

Tarneja: Well, as I said earlier in the paper, the work is in the initial stages. We can right now deposit as thick as 1 mil and probably thicker, but we have no radiation data available at this time. But we predict that we can probably deposit up to 3 mils, with some refinements in the present techniques.

Campbell: What do you predict on the radiation stability for discoloration?

Tarneja: Well, I would not like to make a prediction right now.

Runyan - TI: Two questions: one, with regard to the layer of oxide you're depositing, how do you keep the thermal mismatch from causing such severe bowing that the whole thing breaks?

Tarneja: Well, as I said, the approach which we have taken in this is to grow this at fairly low temperatures, and we did see some mismatch; but now, if we use a silicon web piece right after diffusion, before the contacts are put on, we do not have this problem.

Runyan: At what temperature is this done?

Tarneja: This is around 600 degrees.

Runyan: OK, I see.

Tarneja: We are trying to go lower.

Runyan: One other quick question. That was, your data on the effect of the built-in field, centered around measurements made with a filtered light bulb 3400 degrees K light. Now what would be the effect on your data if you had used the solar simulator rather than the tungsten lamp?

Tarneja: We have some data. I think that later on a paper is going to be given on the balloon flight measurements where the dendritic solar cells were put on the balloon flight, but the air mass zero efficiencies of the balloon flight measurements, if I can recall correctly, were in the vicinity of 9%.

Toole - RCA: Did you observe degradation for silicon-web cells and conventional cells under a tungsten source? Could you make any kind of statement as to how the spectral response of the silicon-web cells compares with the conventional cells?

Tarneja: If we compared the spectral response of the silicon-web conventional cell with a conventional silicon crystal cell, there is no difference whatsoever. Now, in the drift-field cells, we did not have the other drift-field cells available; but the spectral response on the drift field cells which we make is what we would expect. It is good in the blue region, but in the far infrared or in the red region it is a little lower because initially of the lower resistivity of the substrate and the lifetimes of the structure.

Toole: And they're lower in the red - the silicon web cells.

Tarneja: The drift-field silicon-web cells - not the conventional silicon-web cells.

Voice - RCA: OK.

Kaye - EOS: Do these dendrites have a twin plane running through the center of them?

Tarneja: Yes, they do normally.

Kaye: Have you noticed what effects you get with the presence of the twin planes ....

Tarneja: We have conducted an experiment and we do not see any effect of the twin plane on a solar cell and other devices.

Kaye: How do you account for that?

Tarneja: Well, I think ... (laughter) But, probably, I have my own explanation. It will take some time, but I could get together with you later on. Because I think that in the solar cell structure where we are using the top and bottom as contacts, the twin plane really doesn't play any role. Although we have grown silicon-web with no twin plane at all.

Kaye: I expect it to act as a recombination plane?

Tarneja: With respect to the recombination planes, we had an experiment where we would start with a piece where the twin plane is within a short distance from the surface and the other away from the top surface; and we did not see any degradation, or effects whatsoever.

PIC-SOL 209/6
Section A-4

STATUS OF ADVANCED SOLAR CELLS AT ELECTRO-OPTICAL SYSTEMS, INC.*

Presented by:

S. Kaye

Electro-Optical Systems, Inc.

Pasadena, California

18 October 1965

* A portion of this work was supported under Contract NAS 5-3560

ABSTRACT

17310

This paper describes the results of recent work carried out at Electro-Optical Systems on silicon drift field and thin single crystal solar cells. The 0.004 inch thick cell was designed for use on light weight weather balloon panels. Data taken under tungsten and sunlight illumination is presented that shows sample cells to have approximately 9 to 10 percent conversion efficiency.

Also discussed is a radiation resistant cell employing a built-in electrostatic drift potential. The results of a computer calculation, which takes into account the variation of lifetime and mobility due to changes in doping, are presented and compared with experimental data. The results indicate an optimum field width of 50 to 75 microns.

The important question of open-circuit voltage degradation and the results of a calculation that accounts for the anomalous degradation often observed is presented.

Author

STATUS OF ADVANCED SOLAR CELLS AT ELECTRO-OPTICAL SYSTEMS, INC.

S. Kaye and G. P. Rolik
Electro-Optical Systems, Inc.
A Subsidiary of Xerox Corporation

Introduction

This discussion will consider two advanced types of solar cells: radiation resistant drift field cells, and thin (0.004 inch) cells. In the drift field case, it can be shown that the calculations of the current collection efficiency from distributed field in the base of the cell predict an optimum field strength-width ratio. These calculations take into account a varying mobility and lifetime due to changes in the doping level producing the field. Also, it can be shown that the open-circuit voltage degradation, with increased radiation fluxes, is dependent not only on the short-circuit current degradation but, more heavily, on the increase of the junction saturation current. Cells 0.004 inch thick have been developed primarily as power sources for instrumented balloon flights. These cells, fabricated by an extension of present solar cell processing techniques, are capable of a 9 to 10 percent conversion efficiency both in tungsten illumination and air mass one sunlight.

Drift Field Cells

In considering the calculations for the current collection efficiency, two types of field profiles were considered (Fig. 1). Case I assumes a linear change of field strength through the active base region, with the highest field at the p-n junction. Case II again assumes a linearly changing field but with the high field at the back of the active region. It should be noted here that if the field is formed by a long diffusion of an acceptor type dopant into p-type base material from the back, the impurity distribution being an erfc, a field profile approaching Case I is attained. Also, the average field strength (assuming a 10^5 ratio in the number of impurities) is approximately $0.3/w$ volts cm^{-1}, where w is the field width. This would give a field varying linearly from zero to $0.6/w$ volts cm^{-1}. Also, for the purpose of approximation both μ and τ were assumed to decrease linearly with position as one proceeds toward the heavily doped portions of the base region. The results of the calculation are shown in Figs. 2 and 3. No vast difference is seen between the two cases, although a smaller optimum field width and lower base collection efficiency is predicted for Case II.

The sample cells were fabricated by diffusing the field forming impurity (boron) into the back of the cell to the optimum depth

indicated by the calculation for Case I. A profile measurement made on sample cell substrates by alternate sheet resistivity and etching steps showed the impurity distribution to have an erfc shape. Since a cell with a total thickness equal to the optimum thickness indicated by the theory (75-80μ) would be too fragile for conventional use, a 0.004 inch thick low resistivity epitaxial layer was deposited on the back of the cell. The front of the cells was then lapped and etched to the desired point along the impurity distribution. The junction was placed 0.3-0.4μ below the front surface with a conventional phosphorus diffusion. Sintered silver-titanium contacts and silicon-monoxide antireflection coatings were applied to complete the process.

Cells were submitted to Dr. P. Fang of Goddard Space Flight Center for irradiation testing with 1 MeV electrons. The data obtained on EOS cells (designated #1) and those of other manufacturers is shown in Figs. 4 to 6. Figure 4 shows the percentage degradation of short-circuit current as a function of integrated flux. The graph shows the degradation slopes to be reasonably well behaved, the slope of EOS cells being shallower than the slopes of the cells of other manufacturers. However, in considering the slopes of the values of absolute efficiency versus electron flux (Fig. 5), considerable variation is noted, which cannot be explained on the basis of I_{sc} degradation alone, but must stem from anomalous behavior of the open-circuit voltage, V_{oc} (Fig. 6).

In analyzing data of the degradation due to irradiation of several types of cells, it was noted that the degradation of V_{oc} is faster than $\ell n I_{sc}$. This prompted a closer inspection of V_{oc} dependence on other parameters.

If one plots the logarithm of the absolute value of the current I minus I_{sc} versus voltage of typical cells before and after irradiation, an extrapolation to V = 0 yields a value of saturation current I_o (Fig. 7). The validity of this procedure can be shown by considering Eq. 1 of Fig. 8, as $V \to 0$, $\ell n \left| I - I_{sc} \right| \to \ell n I_o$. However, since the 'A' factor changes with voltage, the plot of $\ell n \left| I - I_{sc} \right|$ versus voltage will not be a straight line, and the extrapolation to $V_{sc} = 0$ must be made from that portion of the function where $1 < A < 2$. The value of I_o thus obtained is characteristic of operation near the maximum power point of the I-V characteristic. From this value of I_o, the minority carrier lifetime can be calculated from Eq. 2 of Fig. 8, this being the expression for the dependence of saturation current generation on minority carrier lifetime in the space charge region as expressed by Jonscher (Ref. 1).

Results of calculations of τ for two representative drift field cells, one with a small degradation of V_{oc} (Cell E34-2A) and the other with larger degradation of V_{oc} (Cell E35-2C), are shown in Fig. 9. Values of w_s were taken from graphs given by Ref. 2 under zero bias condition and assuming the junction potential to be 0.7 volts. The values of τ shown are reasonable and in fair agreement with published data (Refs. 3 and 4).

This indicates that the excess degradation of V_{oc} is probably only a further manifestation of a decrease in lifetime and is consistent with the lifetime change deduced by the degradation of short-circuit current. This investigation is still proceeding.

Thin Solar Cells

Silicon solar cells, 0.004 inch thick, 1 by 2 cm, were recently fabricated as power supplies for instrumented balloon flights. The cells were n-on-p type with sintered silver-titanium contacts and were fabricated by an extension of presently accepted cell manufacturing procedures from 1 ohm-cm base material. Approximately 300 cells were made and incorporated into panels of 100 cells (Fig. 10). The panel substrate was of polyimide ("H" film) 0.010 inch thick, onto which a copper printed circuit interconnection pattern had been deposited.

Spectral response measurements were taken on several cells. A typical response curve compared to that of a standard 0.012 inch thick cell is shown in Fig. 11. It is apparent that the longer wavelength response is reduced, which predicts a decrease in I_{sc} and power output compared to thicker cells. Figure 12 shows the theory of Wolf and Ralph (Ref. 5) for the variation of short-circuit current with thickness. Also shown in this curve are their experimental data and a point for a short-circuit current of the ten best cells made during the present investigation. This point lies on an extrapolation of the experimental points obtained by Wolf and Ralph and falls below their theoretical prediction.

Figure 13 shows a table comparing the short-circuit current and total efficiency in tungsten and sunlight illumination of the 10 best cells obtained. It should be noted that the device parameters were optimized for air mass one operation due to the requirements of the balloon flight mission.

Acknowledgements

A portion of the work described was supported by NASA, under contract NAS 5-3560. The technical monitors on this contract were Mr. M. Schach and Dr. P. Fang. The authors are particularly grateful to Dr. Fang for providing the data on radiation damage and to Mr. E. Monastersky, of the Mathematics and Computing Branch of Goddard Space Flight Center for carrying out the computer program.

References

1. A. K. Jonscher, "Principles of Semiconductor Device Operation," John Wiley & Sons, Inc., 1960.

2. H. Lawrence and R. M. Warner, Jr., "Diffused Junction Depletion Layer Calculations," Bell Telephone Laboratories Monograph, No. 3517.

3. J. M. Denney and R. G. Downing, "Summary of Radiation Damage Studies at STL," paper presented at the Solar Working Group Conference, Feb. 1962.

4. "Radiation Damage to Silicon," Final Report; work performed by RCA, David Sarnoff Research Center, for NASA, Contract NAS 5-457.

5. M. Wolf and E. L. Ralph, "Effect of Thickness on Short-Circuit Current;" paper presented at the fourth Photovoltaic Specialists Conference, June 1964.

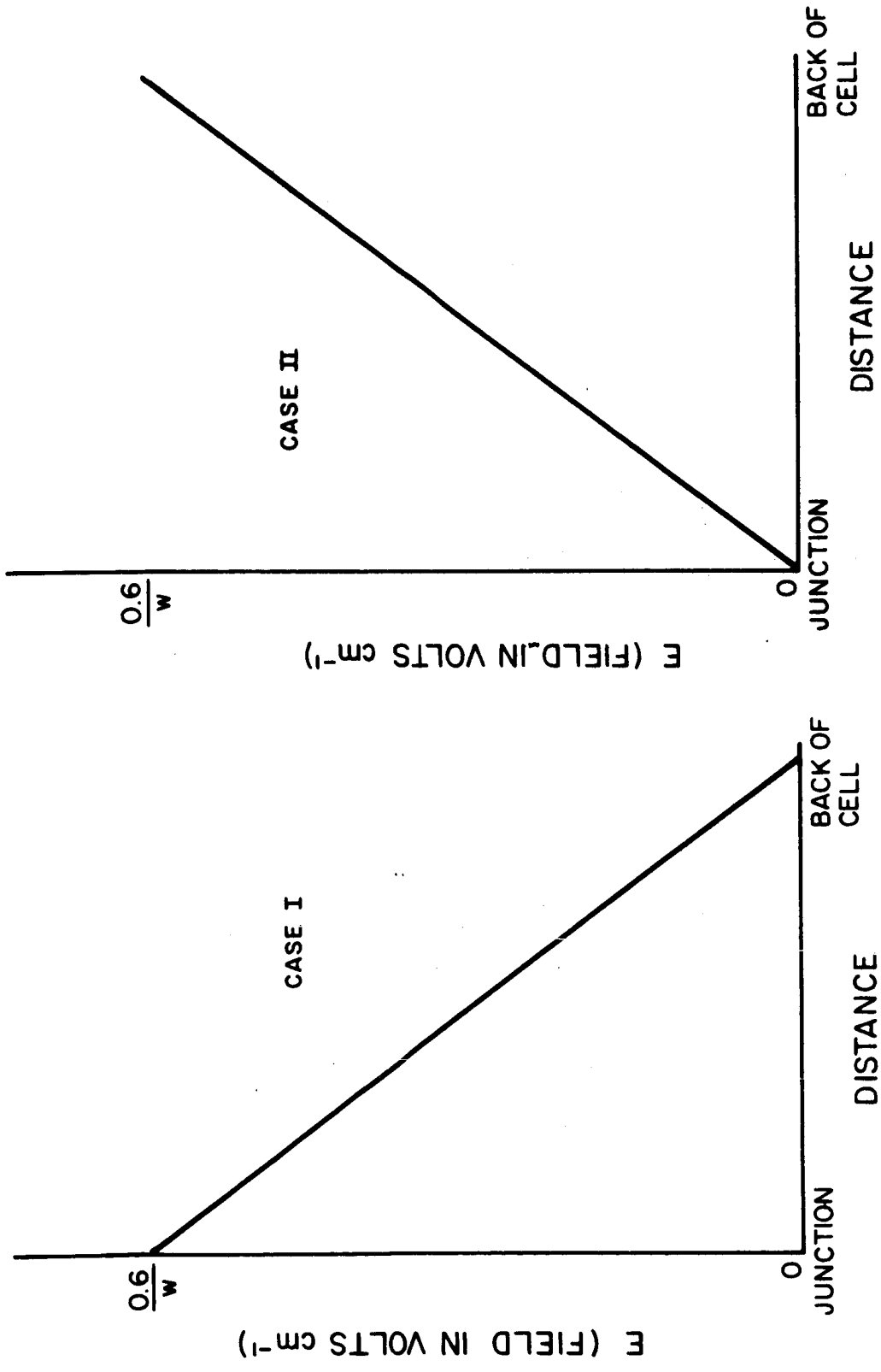

FIGURE 1. FIELD DISTRIBUTION VERSUS DEPTH IN DRIFT CELL

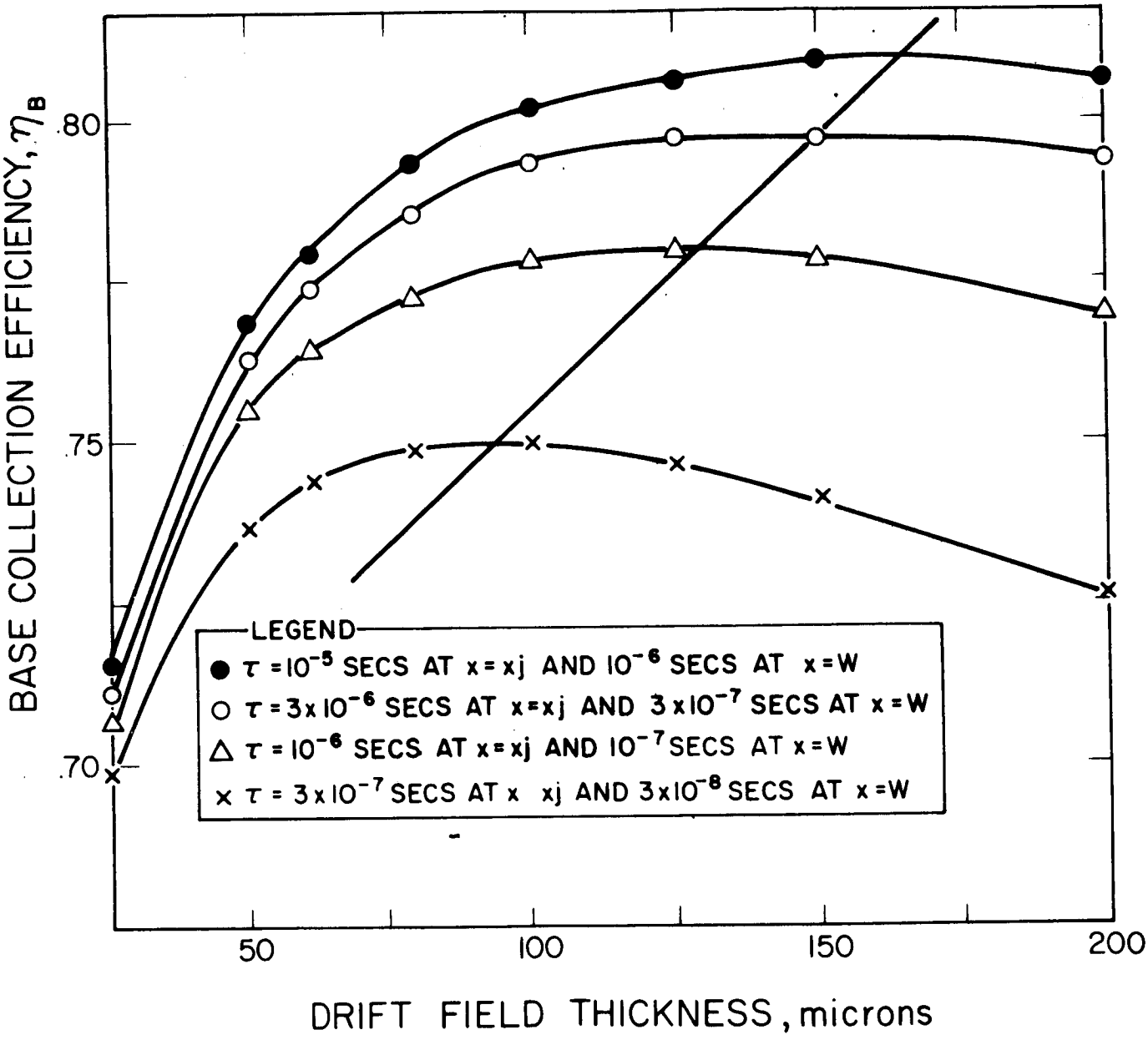

FIGURE 2. RESULTS OF COMPUTER SOLUTION FOR DRIFT FIELD CELL WITH HIGH FIELD NEAR THE JUNCTION (CASE I)

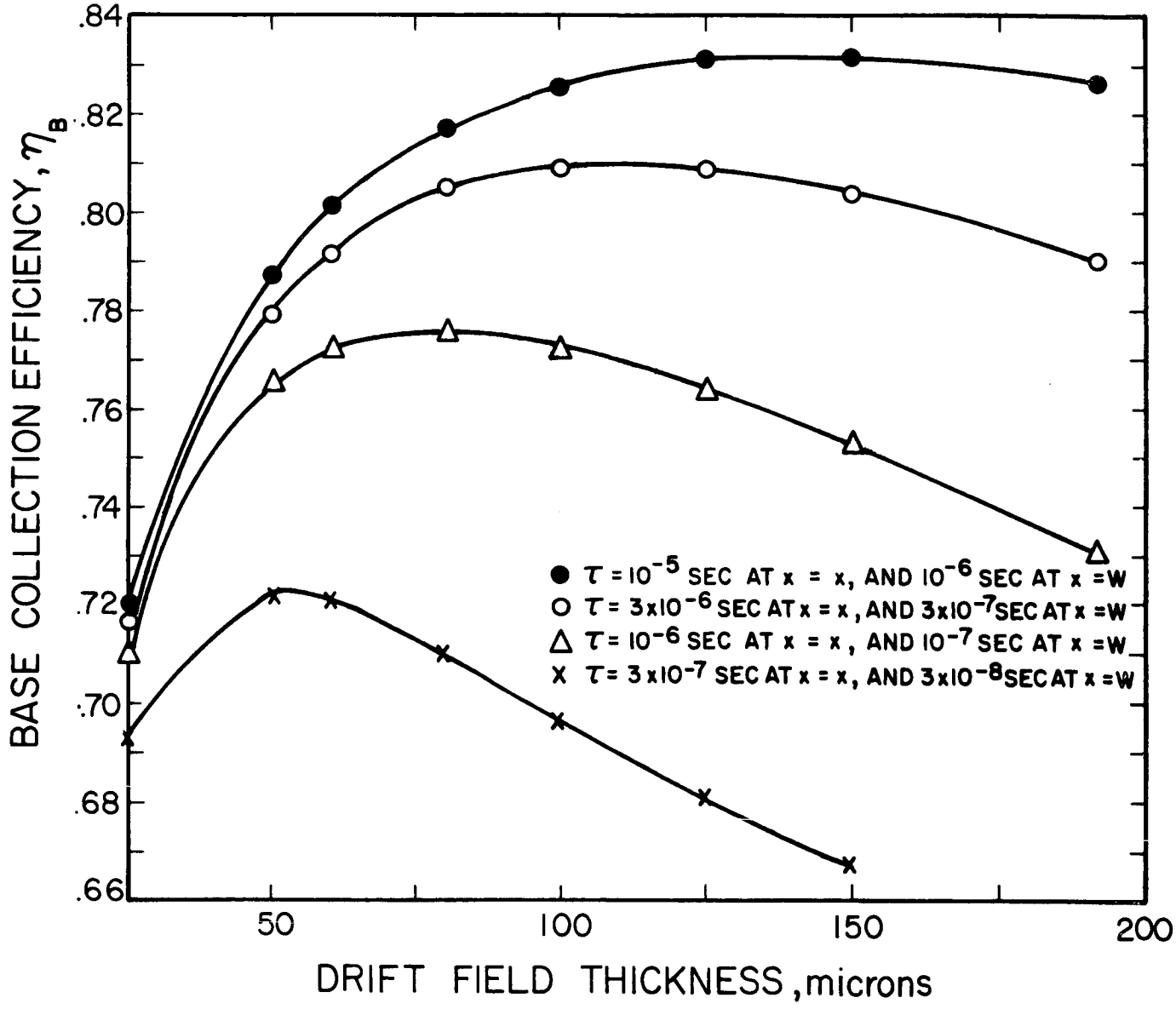

FIGURE 3. RESULTS OF COMPUTER SOLUTION FOR DRIFT FIELD CELL WITH HIGH FIELD AT THE BACK (CASE II)

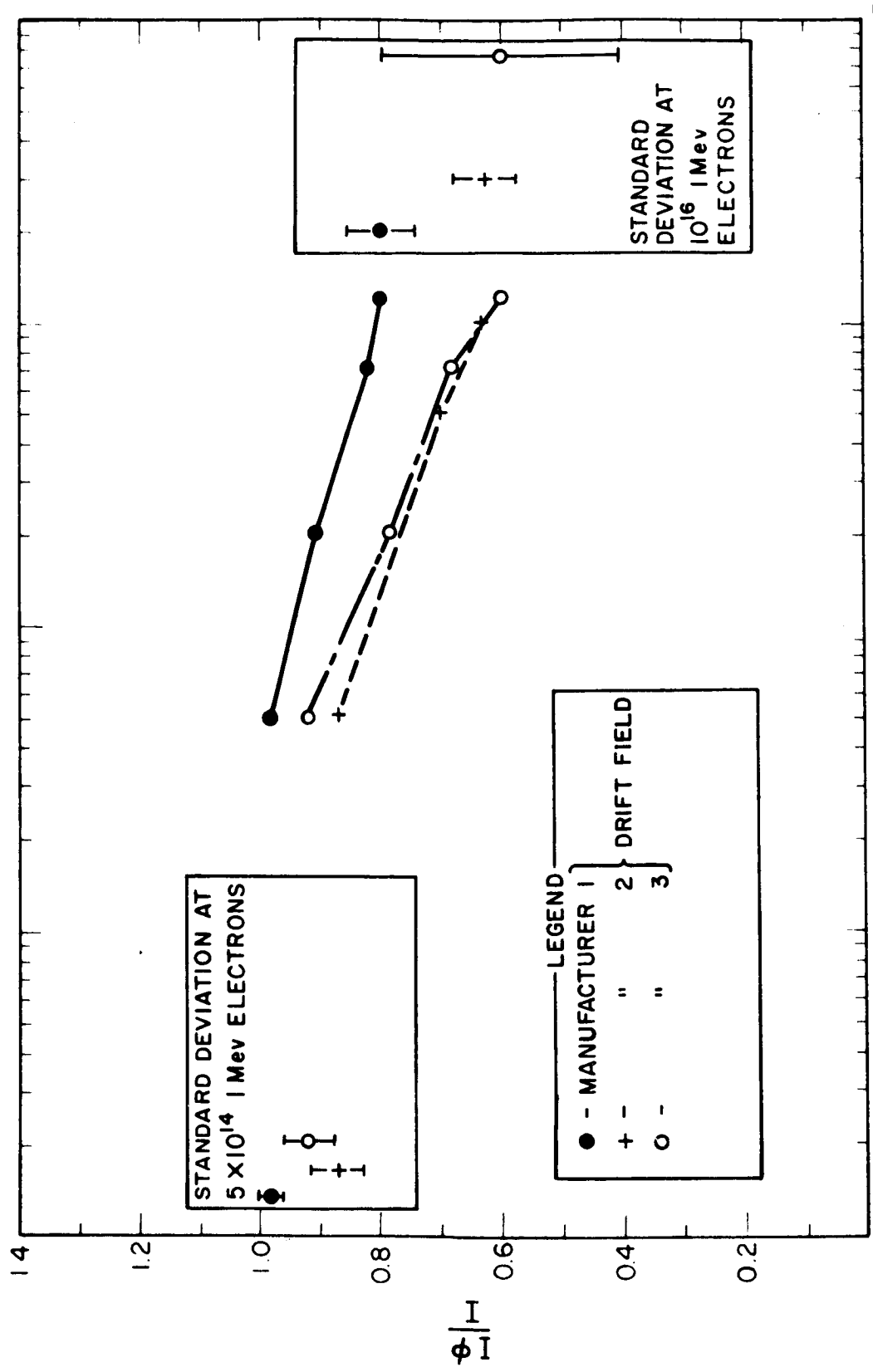

FIGURE 4. MEAN CELL OF EACH MANUFACTURER, PERCENT SHORT-CIRCUIT CURRENT RETAINED.

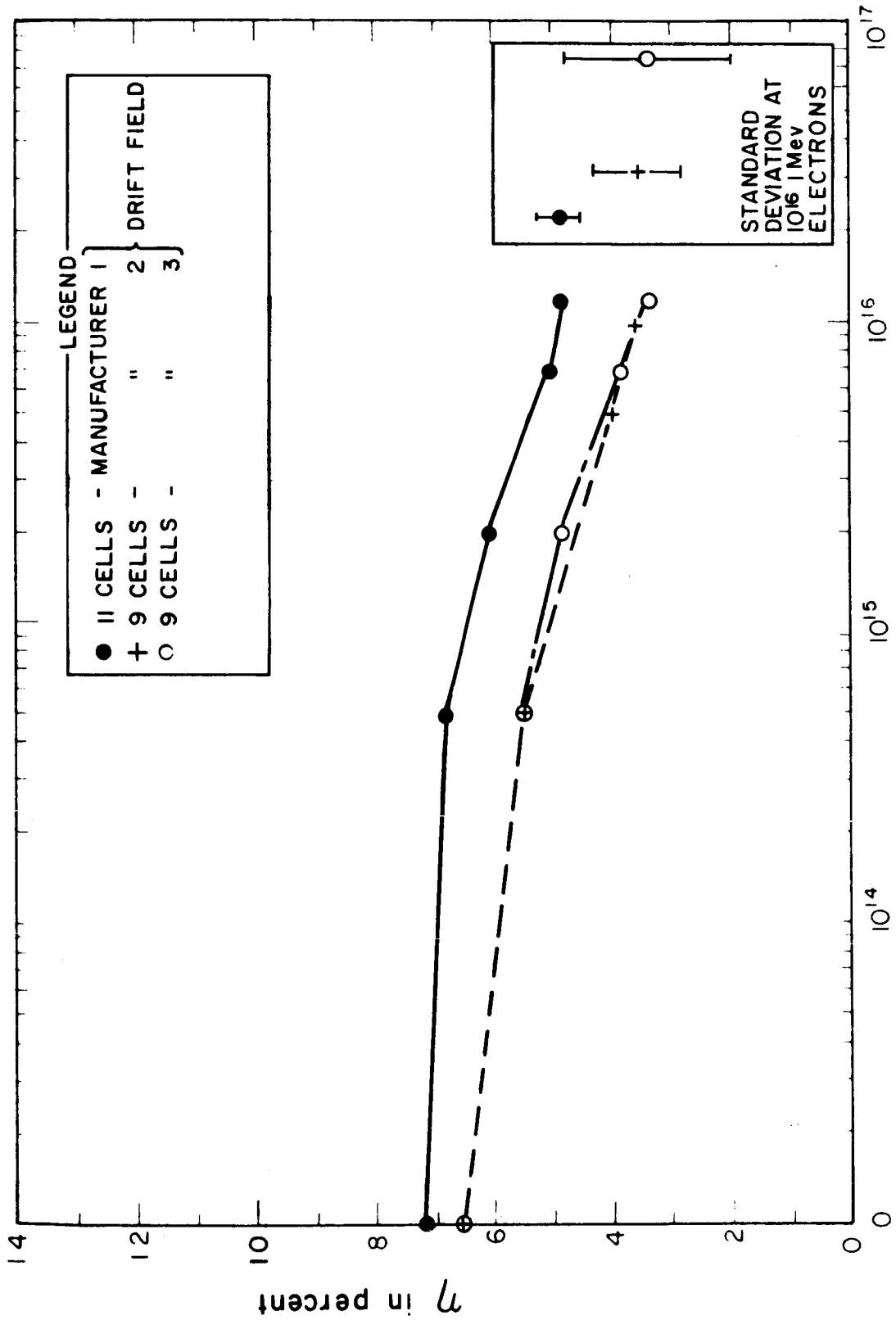

FIGURE 5. MEAN CELL OF EACH MANUFACTURER, ABSOLUTE EFFICIENCY

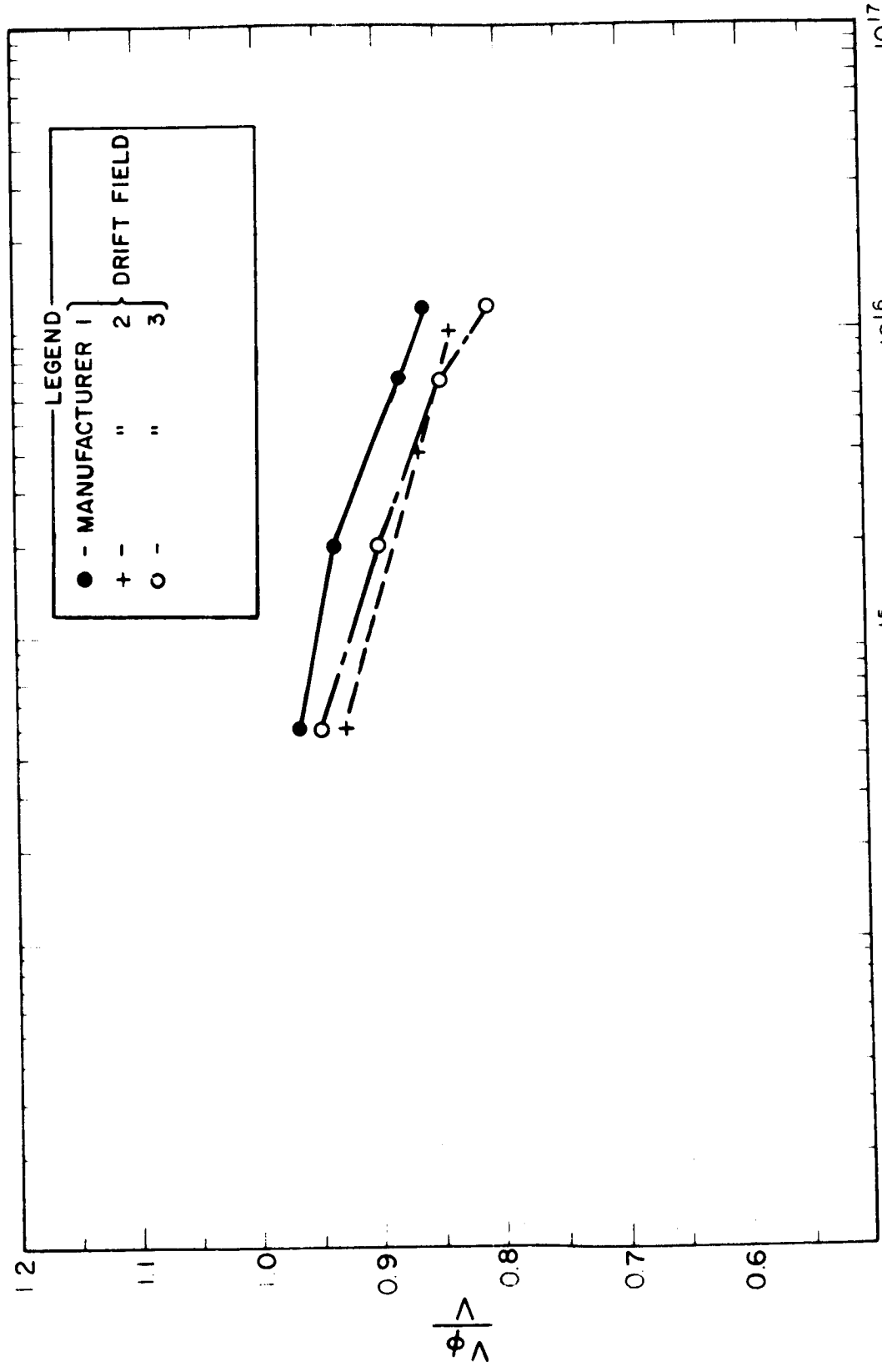

FIGURE 6. MEAN CELL OF EACH MANUFACTURER, PERCENT OPEN-CIRCUIT VOLTAGE RETAINED

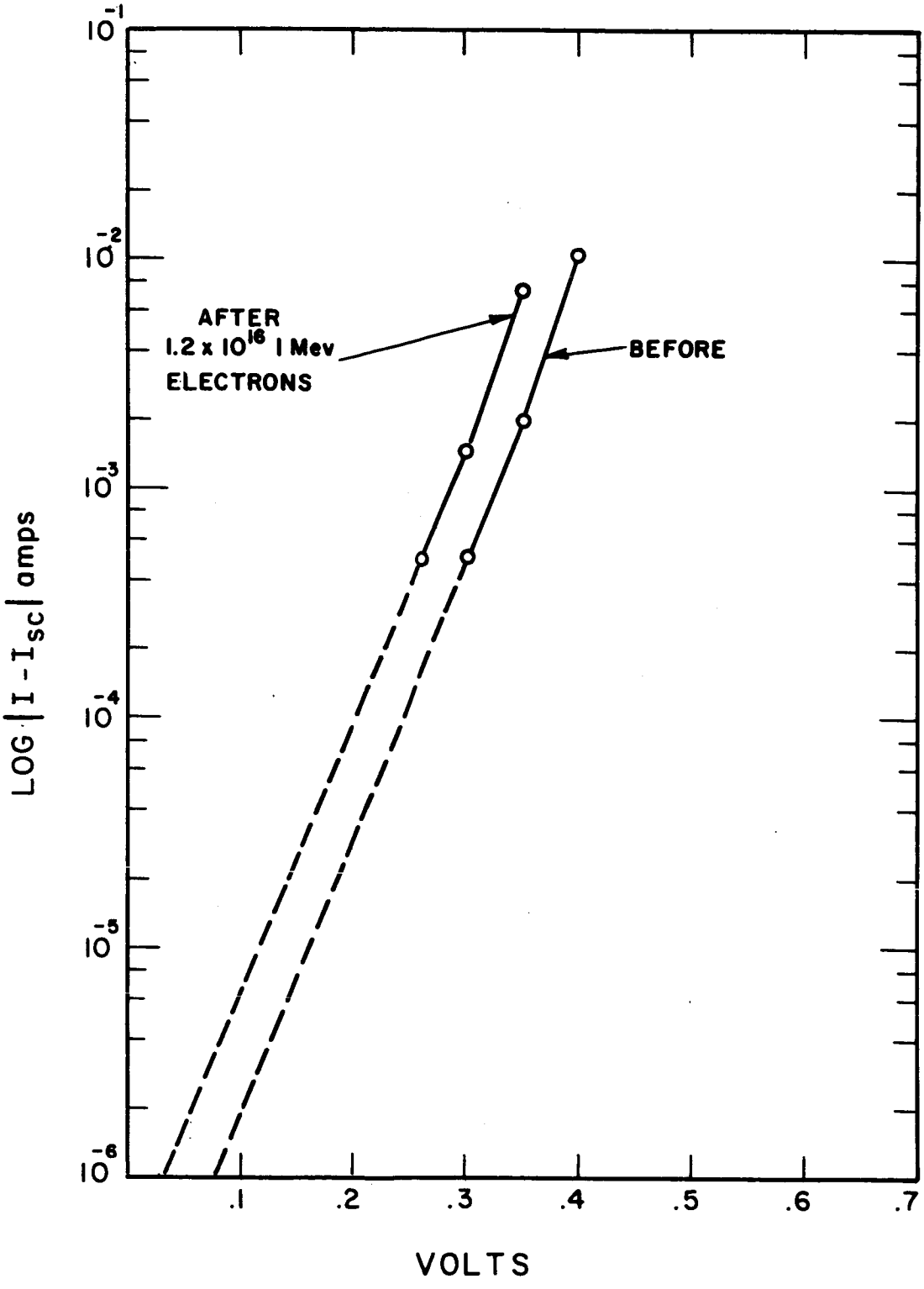

FIGURE 7. LOG I VERSUS VOLTAGE PLOT OF EOS CELL NO. E34-2A BEFORE AND AFTER IRRADIATION

$$\ln \left| I - I_{sc} \right| = \frac{qV}{AKT} + \ln I_o \,, \quad \frac{qV}{AKT} \gg 1 \qquad (1)$$

$$J_g = q\, n_i\, w_s / 2\tau \qquad (2)$$

WHERE q = ELECTRONIC CHARGE

n_i = INTRINSIC CARRIER DENSITY OF SILICON AT 300°K

w_s = SPACE CHARGE WIDTH

τ = MINORITY CARRIER LIFE TIME

I_o = JUNCTION SATURATION CURRENT

J_g = SATURATION CURRENT DENSITY

A = JUNCTION CHARACTERISTIC "FUDGE" FACTOR

FIGURE 8. EQUATIONS USED IN CONSIDERING OPEN-CIRCUIT VOLTAGE DEGRADATION

CELL NUMBER		I_o	W_s	τ	L_n
E34-2A	BEFORE	1×10^{-7} AMPS	1.5×10^{-4} cm	3×10^{-6} SECS	110μ
	AFTER 1.2×10^{16} ELECTRONS	4×10^{-7} AMPS		8×10^{-7} SECS	55μ
E35-2C	BEFORE	5×10^{-7} AMPS	5×10^{-5} cm	2×10^{-7} SECS	27μ
	AFTER 1.2×10^{16} ELECTRONS	1.5×10^{-5} AMPS		3×10^{-9} SECS	3.5μ

FIGURE 9. CALCULATIONS OF MINORITY CARRIER LIFETIME τ, BEFORE AND AFTER IRRADIATION

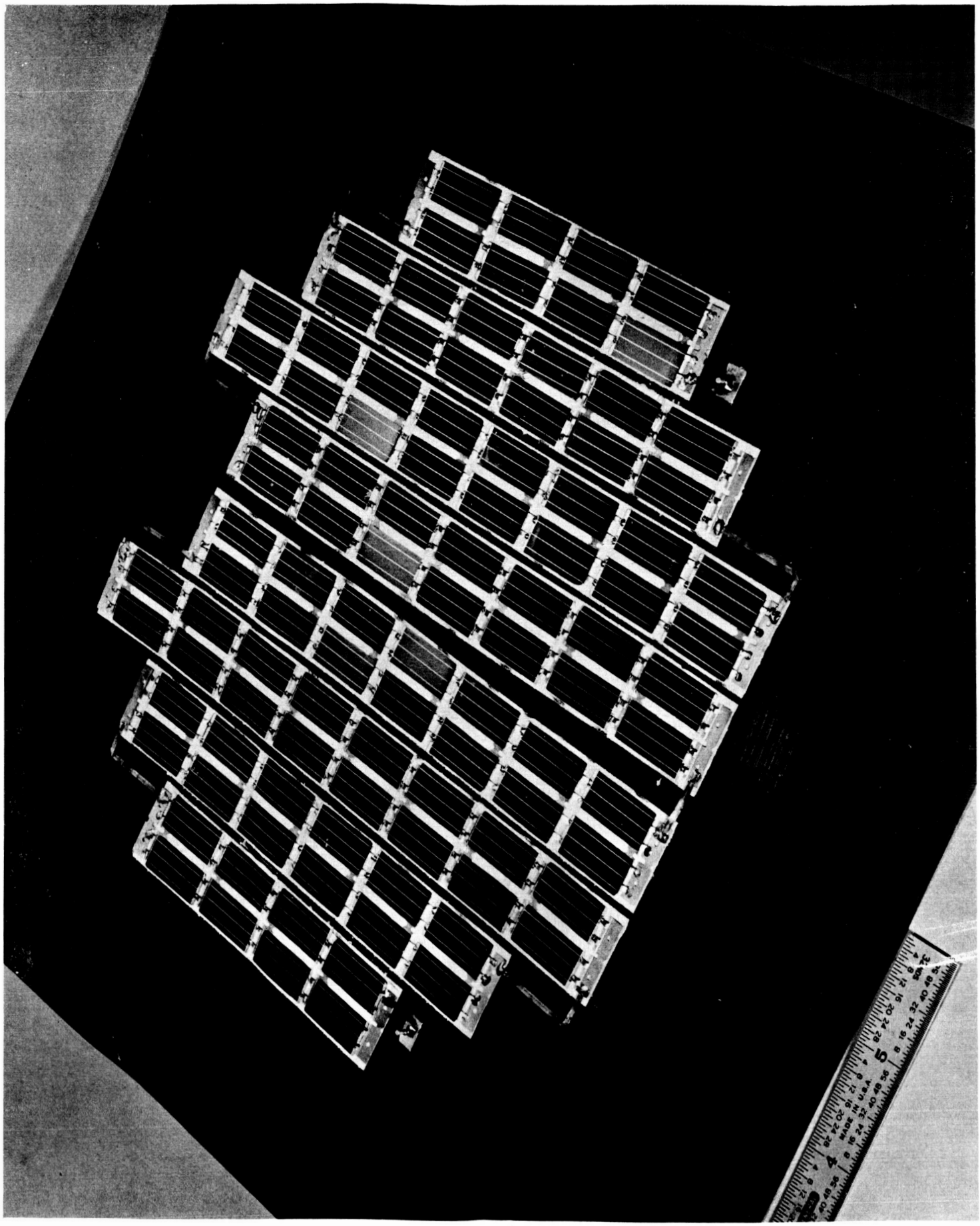

FIGURE 10. 0.004" SOLAR CELLS ASSEMBLED ON 0.010" 'H' FILM

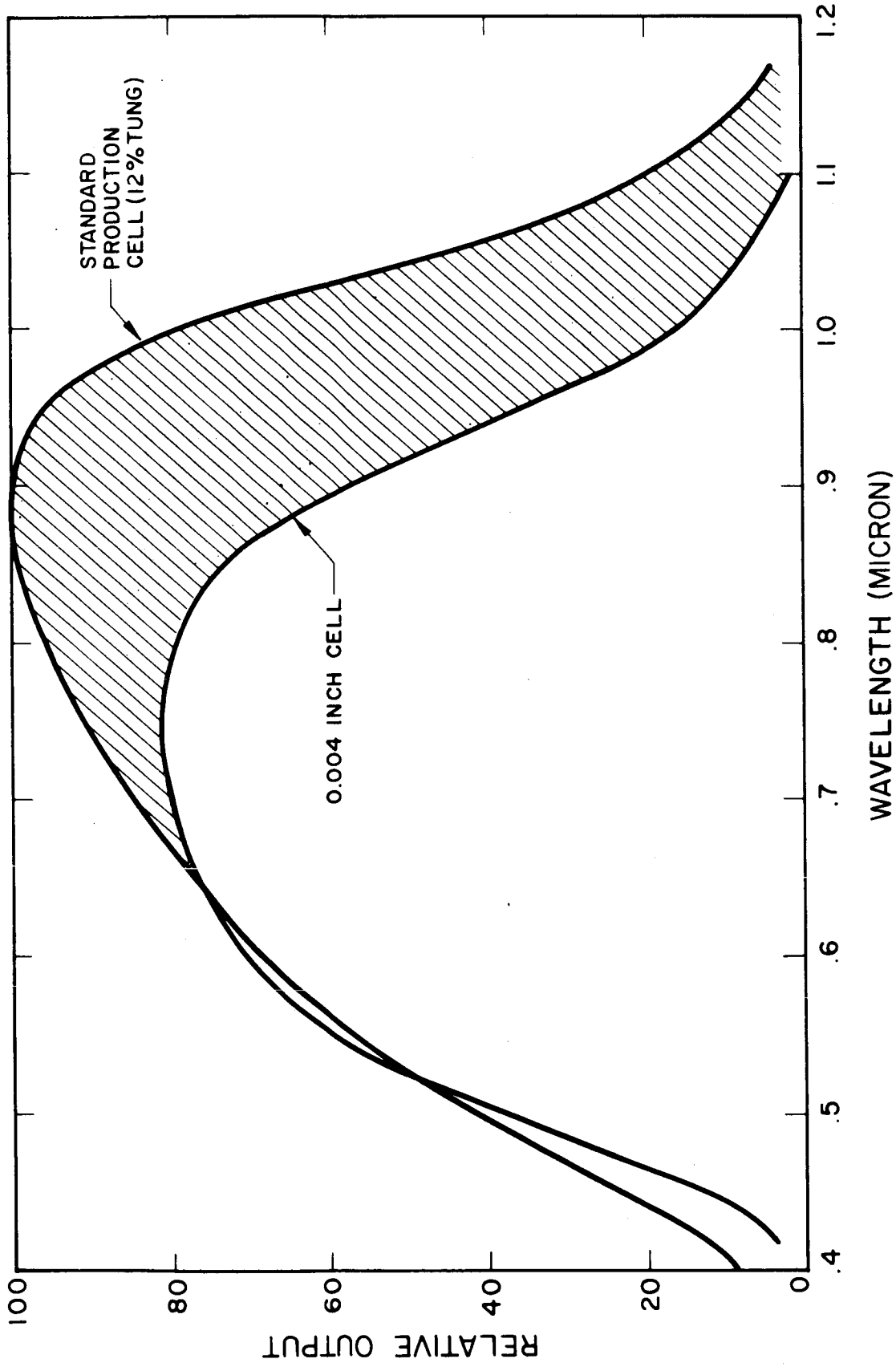

FIGURE 11. RELATIVE SPECTRAL RESPONSE OF N/P SOLAR CELLS

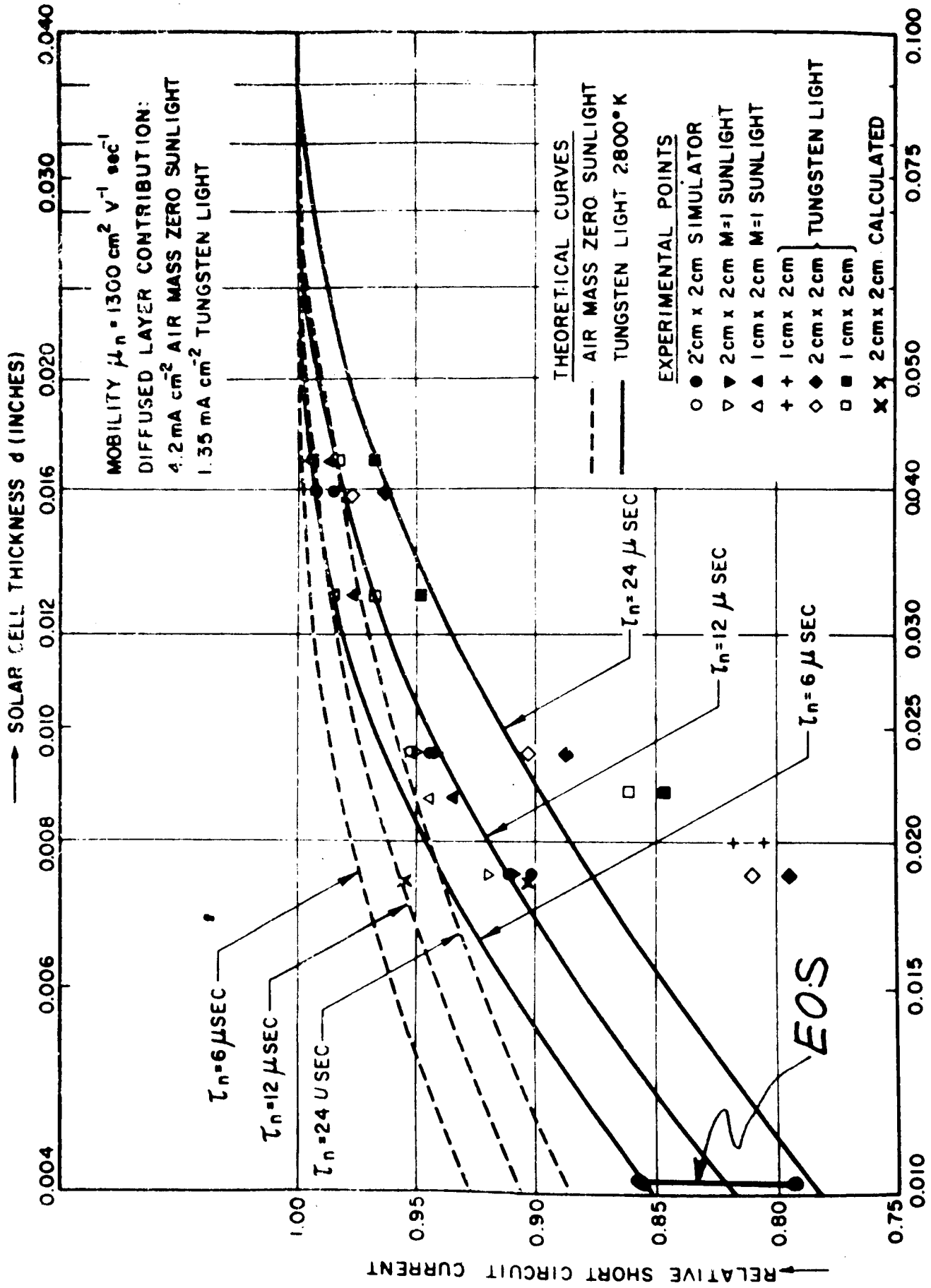

FIGURE 12. COMPARISON OF EOS RESULTS OF I_{sc} ON 0.004" CELLS COMPARED TO DATA OBTAINED BY WOLF AND RALPH

CELL NO.	TUNGSTEN		SUNLIGHT, A M = 1	
	I_{sc} in ma	η in %	I_{sc} in ma	η in %
1	45.5	10.6	41.5	9.6
2	46.0	10.3	41.0	9.2
3	43.5	10.4	38.0	9.1
4	45.0	10.7	39.5	9.3
5	45.0	10.1	40.5	9.1
6	44.0	10.2	39.5	9.2
7	43.5	10.1	39.0	9.0
8	45.0	10.7	40.0	9.4
9	43.0	10.4	39.0	9.4
10	43.0	10.3	38.5	9.2

FIGURE 13. TUNGSTEN AND SUNLIGHT EFFICIENCIES OF TEN BEST 0.004" CELLS

Discussion

Pearson: Before I open up for discussion, do you have a watt per pound figure for this 4-mil solar cell?

Kaye: It is rather difficult to give a general answer to this question, since the watt per pound for a complete system depends very much upon the method of mounting interconnections, etc. that are used. For the cell itself, the weight of a 1 by 2 cm, 0.004 in. thick cell will be about 0.08 grams compared to 0.16 grams for a 0.013 in. thick cell with silver-titanium contacts; and 0.25 to 0.3 grams for a 1 by 3 cell, 0.018 in. thick, with soldered contacts.

Baicker - Princeton Research & Development Co.: I would like to make a comment on this open-circuit-voltage problem. We've been analyzing some Texas Instrument drift field cells and some Heliotek drift field cells and comparing them with some standard RCA cells. We have made some I-V curves similar to the plots that you showed. A principal difference we found was that there seemed to be two clearly separated regions in the I-V curve. One is the standard thermal current region that one would expect and which would fit with the kind of expression that you wrote on the board with an A factor, which is in the neighborhood of 1 1/2 or 2. The other region looks very much like the excess current that one sees in tunnel diodes. I don't want to suggest that this is a tunnel current or anything like that, but it looks very much like that, and it affects the squareness of the I-V curve a little bit - not appreciably, but it's clearly there and it dominates the forward current in the region up to about 0.4 volt. This region has a much lower exponential slope; consequently, one would expect that the voltage would drop more rapidly under bombardment in the drift field cell that exhibits this kind of excess current, if you want to call it that.

Kaye: How does this excess current change with radiation damage?

Baicker: We do not have enough data to answer that question, but it is several orders of magnitude higher than in conventional cells, at least conventional RCA cells made on 1 and 10 ohm-cm base material.

Kaye: I would certainly appreciate looking over your data if it is available.

Loferski - Brown University: Perhaps I misunderstood, but early in the course of the presentation you showed some slides with the high field of the junction and a drift field with the high field at the back of the cell. You then said that there wasn't much difference one way or the other. That means that without any drift field, there is also no difference - right?

Kaye: No. I must apologize for not clearly expressing myself in

discussing that point. Another way of expressing my point is that the mean transit time of the carrier across the base region of the cell does not vary appreciably with a change in field configuration; that is, whether there is a high field at the back or at the front of the cell or even a uniform field across the base region of the cell. However, the transit time does differ from the case of a field free cell and is, of course, less than in that case. This calculation was carried out because there had been some speculation that one might get a considerable difference between these two cases. I think the calculation shows that there is some difference, but it's not very important.

Loferski: Was the field in the same direction in both cases?

Kaye: In both cases the field was such as to accelerate the minority carriers toward the junction. It's merely a question of the distribution of field in the base region of the cell.

Ralph - Heliotek: On Figure 12 was the data for the EOS cells that you presented tungsten or air mass 1.

Kaye: The data points shown on that figure are for AM1 short-circuit current for the 10 best cells shown in Figure 13 and were plotted assuming that a 1-ohm-cm thick cell would have a short-circuit current of 50mA when illuminated with AM1 light. These points fall on your extrapolated data points for AM1 cells. If, however, one looks at the tungsten short-circuit currents (also shown in Figure 13) and assumes that a thick cell illuminated by tungsten light would have a short-circuit current of 55mA, then these tungsten data points would fall on your theoretical curve for tungsten illumination.

Tarneja - Westinghouse: In one of your slides you showed the diffusion length of your drift field cell as 100μ. Would you care to comment on what the structure of the drift field cell was?

Kaye: That wasn't a real diffusion length. As you recall, I calculated the i_o of the cell from the forward I-V characteristics, and from that I calculated a lifetime. Since many of us are accustomed to thinking more in terms of diffusion lengths, rather than lifetime, I put in a diffusion length equivalent to the lifetime I had calculated. I am not suggesting that this was the actual diffusion length in the cell.

Tarneja: What is the structure of your drift field cells?

Kaye: The cells were not all the same, but generally, they had field widths in the base region varying between 75μ and 100μ. The acceptor concentration in the vicinity of the junction was $2 \times 10^{14}/cm^2$ increasing to approximately $10^{20}/cm^3$ at the rear of the field region followed by 4 - 6 mils of epitaxially heavily doped material having 10^{19} - 10^{20} atoms/cm^2.

Wiener - RCA: Have you compared the temperature of your 4-mil solar array

mounted on film against a conventional solar array?

Kaye: No, we haven't.

Wiener: How can we get more information on this array and its characteristics? Is there a formal paper on it?

Kaye: Unfortunately, there is not a formal paper available at this time.

PIC-SOL 209/6
Section A-5

[redacted]

PRESENT STATUS OF SILICON SOLAR CELLS

PANEL DISCUSSION

Moderator: W. R. Cherry NASA-GSFC

Panel: Eugene L. Ralph - Heliotek
Peter Iles - Hoffman
K. S. Ling - RCA
Robert L. Cole - Texas Instruments
Robert K. Riel - Westinghouse

18 October 1965

SOME CONSIDERATIONS REGARDING THE PRODUCTION OF IMPROVED SOLAR CELLS

by
E. L. Ralph
Heliotek, Div. of Textron Electronics, Inc.

Introduction

Four areas of consideration in regard to the present state-of-the-art of solar cell production are discussed. There is a brief discussion of some recent advances in solar cell production. Future possibilities for advancement are mentioned with some technical discussion being made regarding the problems associated with these changes.

The first area of discussion considers the changes in spectral response that have been made on typical production cells during the past few years and the reasons for these changes.

The second area considers the effect of increasing the cell size, thus increasing the active area of the cell and the benefits or disadvantages that can come out of this type of change.

The third area covered is the effect of decreasing cell thickness and how this affects cell performance.

The fourth area compares the Air Mass Zero efficiencies of bare cells for the past few years based on production history for specific space programs.

Spectral Response

The spectral response of production type silicon solar cells has undergone several minor changes since 1961. In 1961 a major change took place when the blue shifted P/N type solar cell was introduced by Heliotek. This type of cell had a shallower junction depth which resulted in improved short wavelength response. Quantitatively, this response improvement provided about 8% more power in sunlight, compared to the standard practice of making measurements in a tungsten light source, than the cells available prior to this change. Since that time no significant change in response has taken place in production type P/N cells.

In 1962 the first N/P type solar cells were made available in production quantities. At that time Heliotek produced N/P type solar cells with a lapped silicon surface and nickel plated contacts. These N/P cells had a SiO interference type antireflection coating on the lapped surface and the spectral response was shifted somewhat toward

the short wavelengths compared to the P/N type solar cell. This slight improvement in spectral response amounted to about 2% more power output, when operated in sunlight (compared to tungsten measurements), than that obtained with the P/N type cells.

In 1964 Heliotek made available production quantities of N/P solar cells with a polished silicon surface and a silver-titanium sintered contact. This solar cell also had a SiO interference type antireflection coating on the surface. As a result of optimization studies which were made on this coating, it was designed to give the maximum output for an Air Mass Zero sunlight spectrum.[1] As a result of this study another slight improvement in spectral response at the short wavelength was made. In this case the improvement amounted to about 3% more output in sunlight (compared to tungsten measurements) relative to the production type N/P cells previously available. Relative spectral response curves corresponding to these most recent type cells were shown in the above referenced work.

Cell Size

The size or area of production type solar cells has historically been predominantly of the 1 cm by 2 cm size. The primary reason for the acceptance of this particular size appears to be the ease of handling for both cell manufacturers and solar panel manufacturers. As early as 1959 larger sizes of 2 by 2, 2 by 5 and 2 by 7.5 cm were available in laboratory quantities, however, no general acceptance or production was started at that time. Gradually 2 by 2 cm sizes were accepted, but even today the 1 by 2 cm size is produced in the largest quantities.

The use of larger solar cells is not only a matter of acceptance by manufacturers and users, even though there is a great deal of resistance in changing from an existing configuration type. In addition, however, there are technical and economical considerations which must be weighed as the cell size is changed. In almost all cases the solar cell panel manufacturer has found that increasing the cell size to 2 by 2 cm has decreased panel costs, due to a reduction of the soldering and handling operations. Also, the cell manufacturers have found that a larger cell, such as the 2 by 2 cm size, can be produced more economically on a cost-per-milliwatt basis. Again, this is primarily due to less handling operations per unit of power output.

The above logic implies that much greater economical advantages can be obtained in the future by increasing cell size still further. This conclusion is not necessarily accurate since the economical advantages above were obtained even though several disadvantages of large cells were present. As the size increases these disadvantages must be studied and it is likely that they will become the controlling factors.

Of significant importance in increasing cell size is the effect on material utilization and breakage. In the case where the solar cell blank is cut from a single crystal ingot, there is a definite material utilization dependence which is associated with size. Figure 1 shows several curves that represent the relative utilization merit factor for various silicon ingot diameters and several cell sizes. The solid curves represent theoretical utilization factors assuming that all cell sizes considered could be cut as efficiently and with the same breakage factors as a 1 by 2 cm blank. Even under this idealistic condition a definite penalty is experienced if a 4 by 4 cm cell was to be made. The dashed curves are obtained after a typical cutting loss and breakage factor is applied to the solid curves. These curves show that these cutting losses and breakage factors become larger as the size increases and obviously would add a significant amount to the raw material costs. In the case of the 2 by 2 cm cell these increases were offset by production process cost reductions associated with less handling (per unit area), so that the result was a net decrease in costs. This is likely to be reversed as utilization factors are decreased.

Even though cell costs may not be able to be decreased or may even need to be increased for very large sizes, this may not necessarily mean that the over-all effect is bad. It may turn out that panel manufacturers can decrease costs further with larger cells so that the net effect again would be a decrease in costs of the solar power system.

In addition to the cost factors associated with cell size there is also a performance design aspect which must be considered. Figure 2 shows a solar cell grid design situation that develops when the cell width (or grid length) is increased from 1 to 3 cm. For the three centimeter cell width case where the grid thickness is 1.5μ, (typical for 1 by 2 cm cells) there is about 5% loss in power output after the grid width is optimized for maximum performance. This loss can be decreased to 0.5% by increasing the grid thickness, t, by a factor of 4 (to 6μ), but this adds cost and may have a deleterious effect on the contact strength properties. Figure 3 shows the power output ratios (relative to a 1 by 2 cm cell design) expected as the cell size is increased for several grid thicknesses. It is obvious that typical grid thicknesses of 1.5μ are not sufficient for large cells. As cell sizes are increased the losses due to grid design or interconnections become very important and are likely to make very large cells appear undesirable.

There are other factors of importance relating to the applicability of larger cells which need further consideration. For instance, small arrays can not use large cells and achieve the desired voltages without increasing the complexity of the interconnections and wasting panel area. Furthermore, for many arrays, reliability is actually decreased when larger area cells are employed, unless special contact designs

are used. Thus, it is not necessarily advantageous to move toward larger cells.

Cell Thickness

The effect of solar cell thickness on short circuit current was studied and reported a year ago.[2] Since that time additional work has been done which verified the short circuit current losses with thickness, that were reported. These losses were about twice as large as expected by theory. In addition to the current losses, the recent work has shown that a voltage loss is also associated with cell thickness. This voltage effect amounts to about a 20 mV drop in open circuit voltage as the cell thickness is decreased from 16 mil to 8 mil.

In addition to studying the cell output characteristics as a function of thickness, the radiation resistance characteristics were also studied. Figure 4 shows the effect of 1 MeV electron irradiation on cell short circuit current for various thicknesses. The solid curves are theoretical curves from the previous work.[2] The dashed curves are the experimental results observed. As mentioned above, the 8 mil thick cells show lower short circuit current than theory predicts. In both cases (i.e., 8 mil and 16 mil cells) the radiation degradation characteristics behave as expected. Degradation at the high flux levels for all thicknesses follow the same degradation curve even though the initial values are at different levels.

Figure 5 shows the open circuit voltage degradation characteristics as a function of 1 MeV electron flux for several cell thicknesses. The solid curve in this case was data from a previous radiation experiment on thick cells.[3] In this figure the effect of thickness on open circuit voltage is apparent at the low flux levels. As in the case above, however, the radiation characteristics are as expected and at high flux levels all cells follow the same degradation curve.

Air Mass Zero Efficiency

Air Mass Zero solar cell efficiencies have been gradually increasing during the past few years. There have been no sharp increases as was observed with the introduction of such basic changes as the gridded solar cell and the blue shifted cell, but instead, the improvements have been due to better production control and optimization of the various cell design parameters.

With the introduction of the N/P solar cell in 1962 there was a significant differential in the production yield between N/P and P/N cells. The average M = 0 efficiency of the N/P cell was more than 10% below that of the P/N cell. Since that time the efficiency of N/P

cells has been increased by as much as 10%, but the average efficiency of P/N cells has also been increased. Today the average efficiency of N/P cells is typically about 6% below that of P/N cells.

Another way of evaluating the present state-of-the-art of production capabilities is to consider the space program efficiency requirements which have been met. In this type of analysis only deliveries meeting space program requirements are considered, without specific reference to the number of cells produced which do not satisfy the program requirements. What it does show, however, are the efficiencies which were available and indicates the general trend in solar cell production history. Figure 6 shows Heliotek's solar cell production experience for the past four years. The cell average M = 0 efficiency and the quantity of cells delivered for each specific program was evaluated. Only programs with greater than 10,000 cells were included in this study. Figure 6 is a population distribution diagram showing the average efficiency distribution over each yearly period. For both the P/N and the N/P cells there was a general trend to supply higher efficiencies versus time. Also, the relative quantities of N/P cells produced has increased so that this type of cell now comprises the major portion of the market. Of interest is the slight increase in the N/P efficiencies delivered. As was mentioned above, average N/P production yeilds have increased by almost 10%, or double that shown in Figure 6. The reason deliveries show a smaller increase is that in 1962 space program requirements for N/P cells were specified near the P/N levels even though the production yields were not equivalent.

The sharp efficiency increase in P/N deliveries in 1964 and 1965 was partially due to increased yields, but was also due to the decreased demand for this type of cell, except where very high efficiencies were needed and where radiation environments were not a significant factor.

It is clear from Figure 6 that the average cell efficiency delivered to the space program over the past four years has increased by about 5%, combining the data for both P/N and N/P type cells. With the improvement of production methods and controls this same pattern is expected to continue in future years.

References

1. E. L. Ralph and M. Wolf, "Effects of Antireflection Coatings and Coverglasses on Silicon Solar Cell Performance", Photovoltaic Specialists Conference, Cleveland, Ohio, June 1964.

2. M. Wolf and E. L. Ralph, "Effect of Thickness on Short Circuit Current", Fourth Annual Photovoltaic Specialists Conference, Cleveland, June 1964.

3. Martin, Teener, Ralph, "Some Effects of Electron Irradiation and Temperature on Solar Cell Performance", 17th Annual Power Sources Conference, Atlantic City, New Jersey, May 1963.

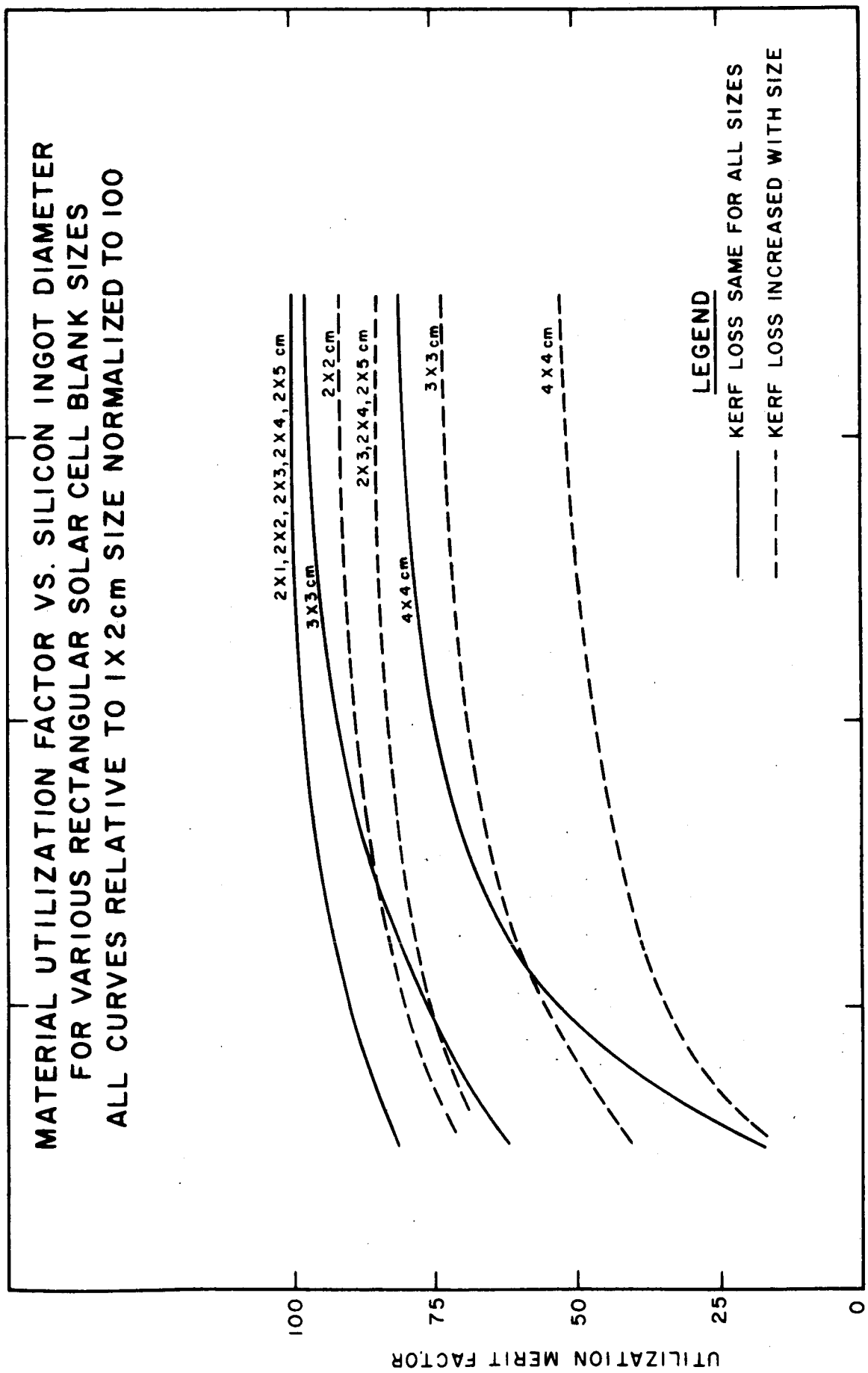
MATERIAL UTILIZATION FACTOR VS. SILICON INGOT DIAMETER
FOR VARIOUS RECTANGULAR SOLAR CELL BLANK SIZES
ALL CURVES RELATIVE TO 1X2cm SIZE NORMALIZED TO 100
2X1, 2X2, 2X3, 2X4, 2X5 cm
3X3cm
2X2cm
2X3, 2X4, 2X5 cm
4X4 cm
3X3 cm
4X4 cm
LEGEND
KERF LOSS SAME FOR ALL SIZES
KERF LOSS INCREASED WITH SIZE
UTILIZATION MERIT FACTOR
100
75
50
25
0
1.5
1.75
2.00
2.25
SILICON INGOT DIAMETER (INCHES)

Fig. 1

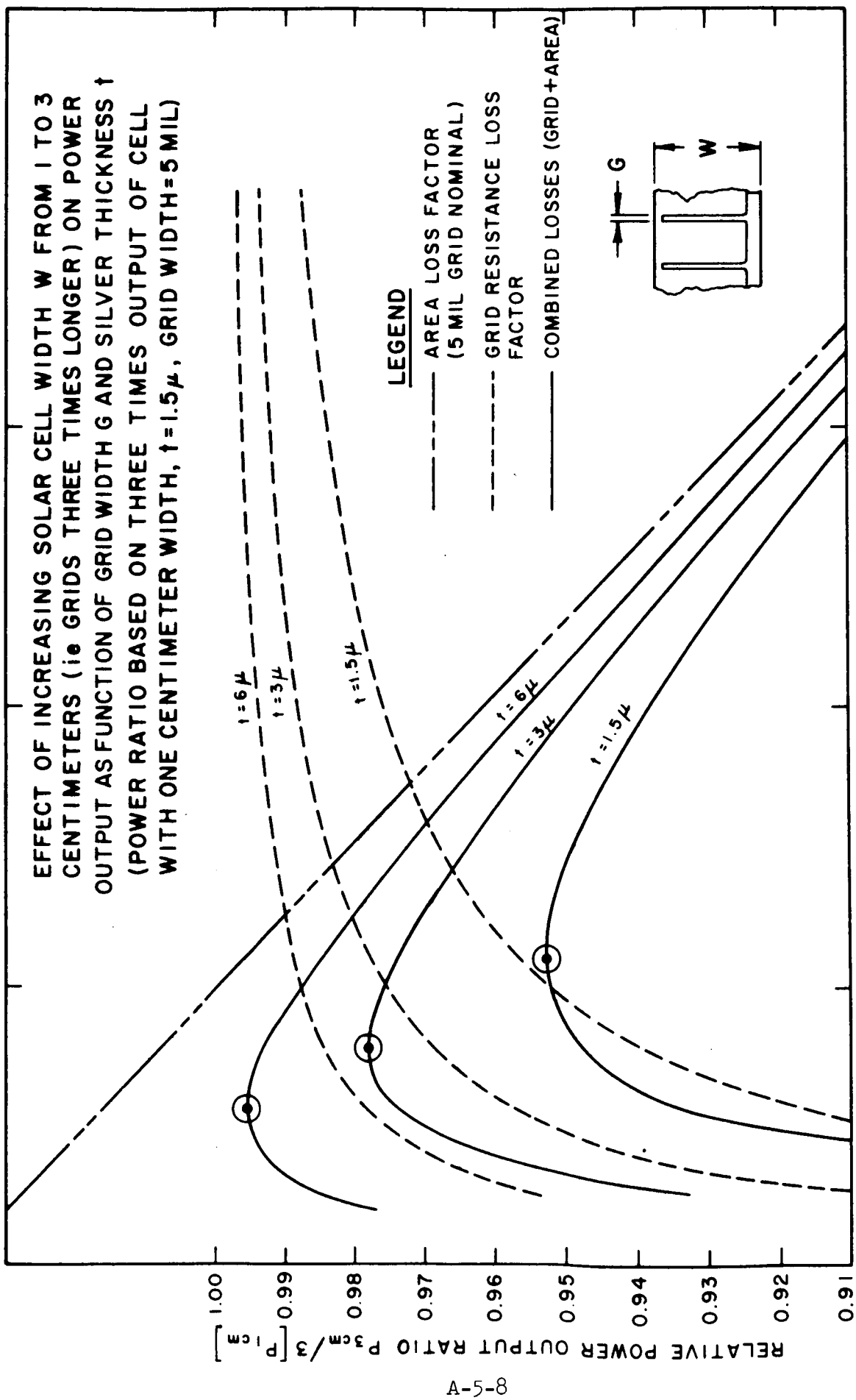
EFFECT OF INCREASING SOLAR CELL WIDTH W FROM 1 TO 3 CENTIMETERS (ie GRIDS THREE TIMES LONGER) ON POWER OUTPUT AS FUNCTION OF GRID WIDTH G AND SILVER THICKNESS t
(POWER RATIO BASED ON THREE TIMES OUTPUT OF CELL WITH ONE CENTIMETER WIDTH, t=1.5μ, GRID WIDTH=5 MIL)
LEGEND
AREA LOSS FACTOR (5 MIL GRID NOMINAL)
GRID RESISTANCE LOSS FACTOR
COMBINED LOSSES (GRID+AREA)
t=6μ
t=3μ
t=1.5μ
G
W
RELATIVE POWER OUTPUT RATIO P3cm/3[P1cm]
1.00
0.99
0.98
0.97
0.96
0.95
0.94
0.93
0.92
0.91
0
5
10
15
20
GRID WIDTH G (mil)

Fig. 2

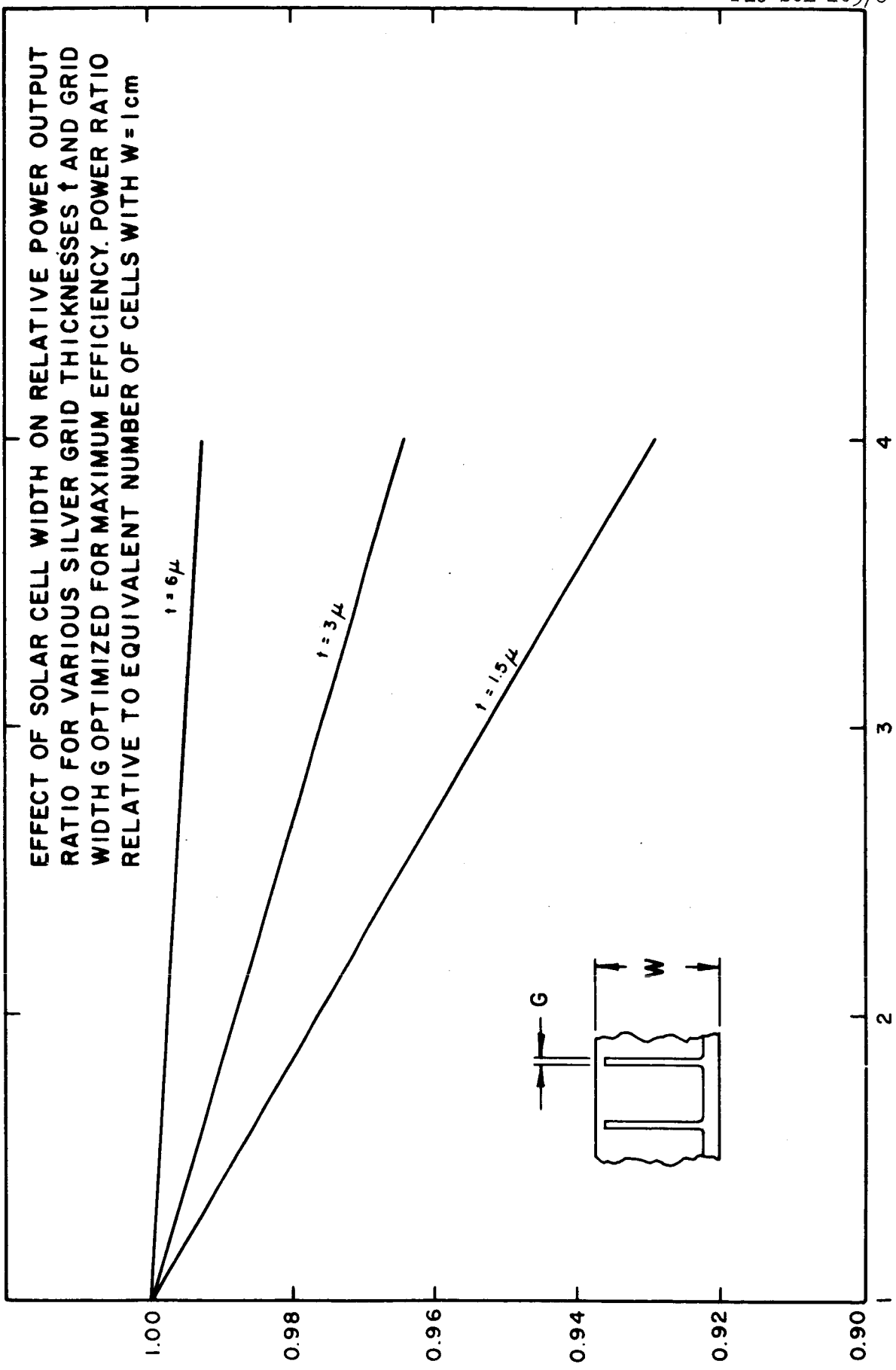
EFFECT OF SOLAR CELL WIDTH ON RELATIVE POWER OUTPUT RATIO FOR VARIOUS SILVER GRID THICKNESSES t AND GRID WIDTH G OPTIMIZED FOR MAXIMUM EFFICIENCY. POWER RATIO RELATIVE TO EQUIVALENT NUMBER OF CELLS WITH W = 1cm
t = 6μ
t = 3μ
t = 1.5μ
G
W
RELATIVE POWER OUTPUT RATIO
1.00
0.98
0.96
0.94
0.92
0.90
1
2
3
4
SOLAR CELL WIDTH W (cm)

Fig. 3

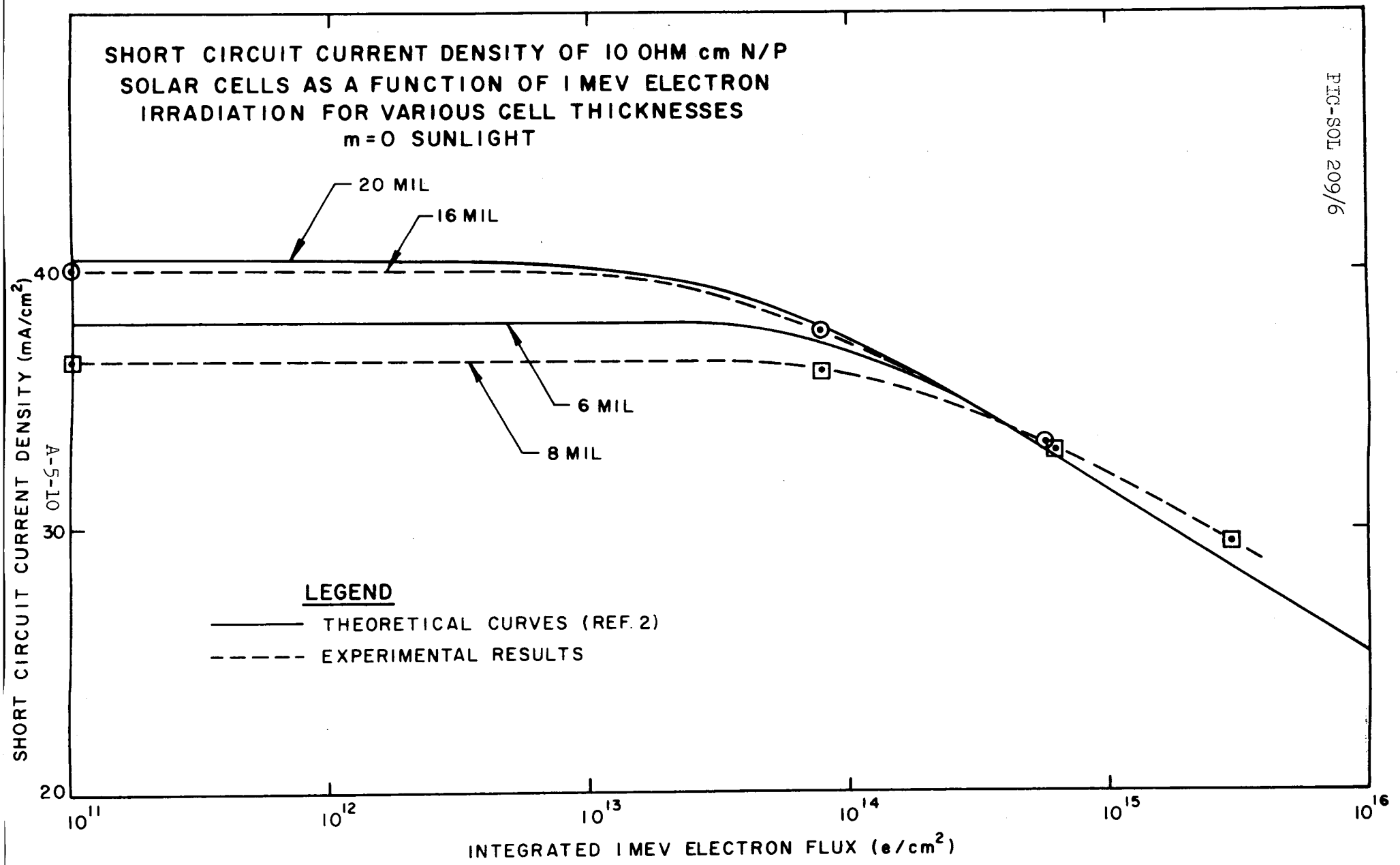
SHORT CIRCUIT CURRENT DENSITY OF 10 OHM cm N/P SOLAR CELLS AS A FUNCTION OF 1 MEV ELECTRON IRRADIATION FOR VARIOUS CELL THICKNESSES
m = 0 SUNLIGHT
PTC-SOL 209/6
20 MIL
16 MIL
6 MIL
8 MIL
A-5-10
LEGEND
THEORETICAL CURVES (REF. 2)
EXPERIMENTAL RESULTS
SHORT CIRCUIT CURRENT DENSITY (mA/cm²)
40
30
20
10¹¹
10¹²
10¹³
10¹⁴
10¹⁵
10¹⁶
INTEGRATED 1 MEV ELECTRON FLUX (e/cm²)

Fig. 4

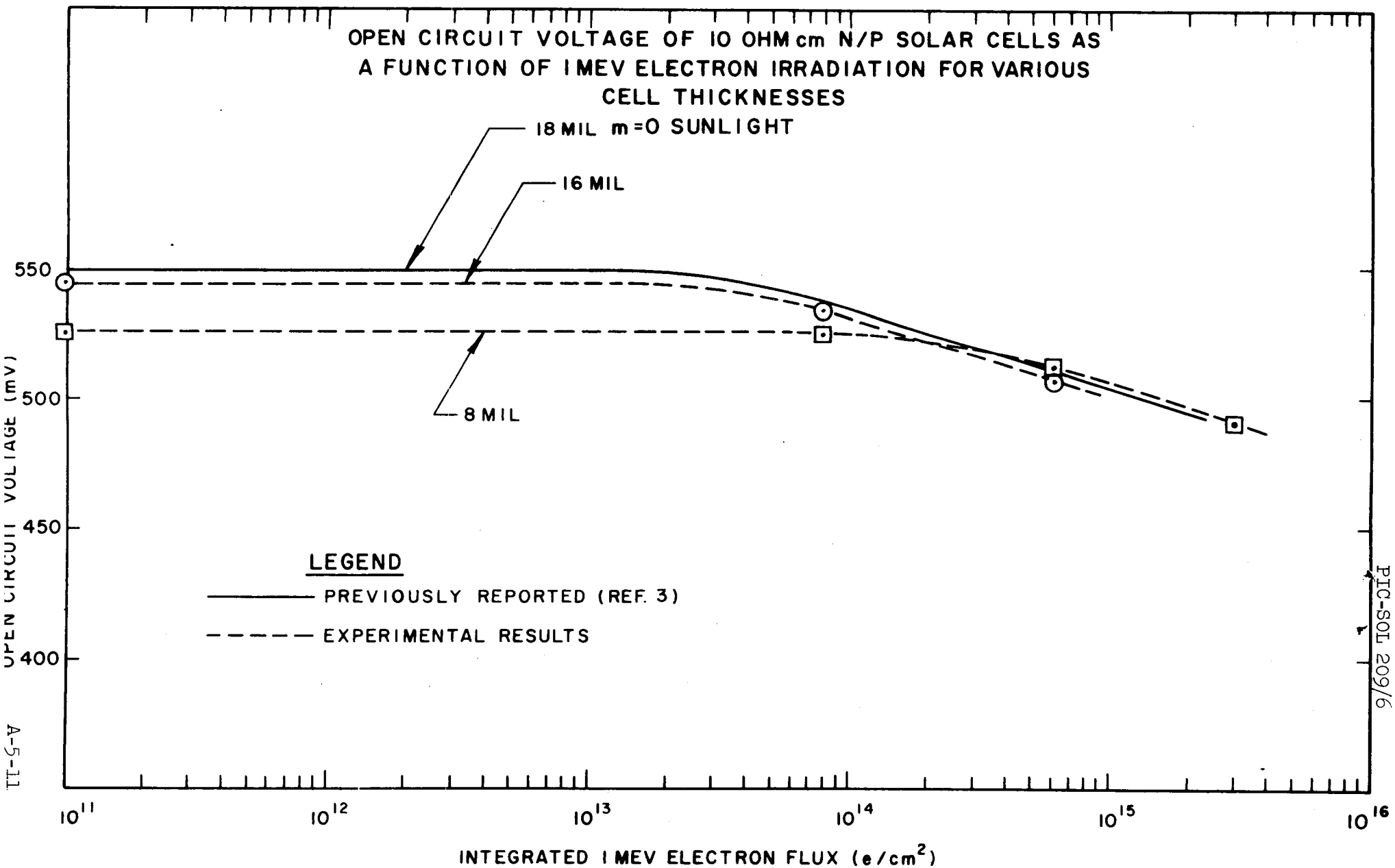
OPEN CIRCUIT VOLTAGE OF 10 OHM cm N/P SOLAR CELLS AS A FUNCTION OF 1 MEV ELECTRON IRRADIATION FOR VARIOUS CELL THICKNESSES
18 MIL m=0 SUNLIGHT
16 MIL
8 MIL
LEGEND
PREVIOUSLY REPORTED (REF. 3)
EXPERIMENTAL RESULTS
OPEN CIRCUIT VOLTAGE (mV)
550
500
450
400
10^{11}
10^{12}
10^{13}
10^{14}
10^{15}
10^{16}
INTEGRATED 1 MEV ELECTRON FLUX (e/cm^2)
PIC-SOL 209/6
A-5-11

Fig. 5

AVERAGE SOLAR CELL EFFICIENCY MARKET REQUIREMENTS AS REFLECTED BY HELIOTEK SPACE PROGRAM DELIVERIES FOR FOUR YEARS ALL CURVES BASED ON m=0 SUNLIGHT AND 28° CELL TEMPERATURE (ONLY PROGRAMS WITH GREATER THAN 10,000 CELLS INCLUDED)

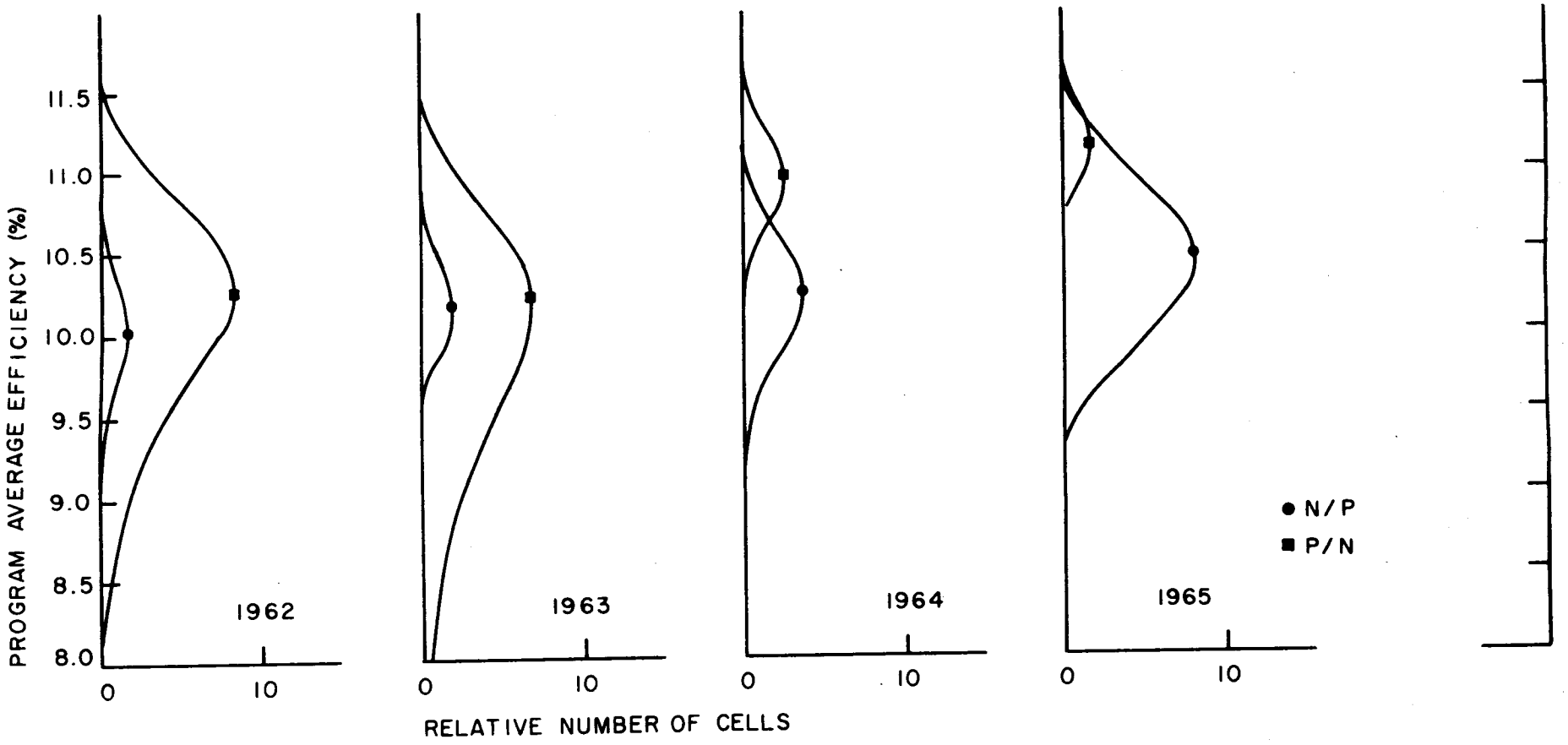

Fig. 6

PIC-SOL 209/6
Section A-5.1

PRESENT STATE OF SOLAR CELL PRODUCTION

Presented by

P. A. Iles

Hoffman Electronics Corporation

El Monte, California

18 October 1965

PRESENT STATE OF SOLAR CELL PRODUCTION

P. A. Iles
Hoffman Electronics Corporation
El Monte, California

Preamble

We have been asked to survey the changes over the last three years in production silicon solar cells, particularly in AMO output and spectral response, with comments on cell area and thickness.

During these three years, the main change for space missions has been the replacement of P/N cells by N/P cells to gain greater radiation tolerance. There has been greater emphasis on meeting the individual requirements (electrical, mechanical or visual) of customers, and it is common to find several designs of cells, differing in dimensions, bulk resistivity, diffusion schedule and test parameters, being manufactured at the same time. This variety of mission requirements has prevented either the use of high volume production methods, or the practice of stockpiling. Nevertheless, the cost per watt has decreased appreciably in this three year period, even though the specifications have been increasingly severe.

We have derived benefit from 100% testing with reliable solar simulators, and good agreement exists between cell and submodule measurements and the array output in space.

Hoffman has produced two different forms of N/P cells, as follows:

Plated Contact N/P Cells

These are characterized by a rough surface finish, a shallow PN junction, a diffusion-produced antireflecting coating, and plated gold-nickel contacts.

Sintered Contact N/P Cells

These are based on the Western Electric cell design and have a polished surface finish, a shallow PN junction, sintered titanium-silver contacts and an antireflection coating of evaporated silicon monoxide.

For equal active areas, the two cell forms give similar current output. However, the sintered contact cells can have slightly lower series resistance, and therefore more power output. Also, the evaporation process allows greater active area (economically) and closer control of the yield.

Plated cells offered more chance of cost reduction because there was less slice preparation required, inexpensive grid masking methods were used, and the additional a/r coating step was eliminated. However, the main impetus to the trend to sintered contact cells was the higher bond strengths available (>800 grams for edge contact pull-test) although it is of interest that present plated cell contacts generally allow a pull-test minimum of 600 grams. Present sintered contact cells when pull-tested, generally fail in the silicon rather than in the contact. The present contact strength is adequate for currently used module methods, and may be sufficient for the automated interconnection methods being developed.

We consider the main advantage of sintered contact cells is the fact that unsoldered cells have as much output as soldered cells, thus reducing cell weight per milliwatt. Also, the grid lines can be left free of solder, with the chance of a better bond with the cover slides.

To make best use of these advantages, we begin our sintered cell fabrication with mechanically polished slices. This surface finish gives the best optical tuning of the a/r coating, and avoids the pillow-effect of etch-polished slices, thus ensuring a thin cover adhesive layer for the whole cell, rather than a layer several mils thick near the edges. If some solder is needed on part of the cell, the fabrication steps can be arranged to solder only selected areas, such areas being the minimum required for interconnections. Solar panel people at Hoffman and elsewhere have devised very good methods for connecting solderless cells with minimum solder, resulting in lighter, more flexible modules with electrical output and mechanical strength equal to or greater than that for the best soldered cell modules. As is often the case, the end product appears simpler than those formed by earlier methods.

It is difficult to show a clear production picture because of the varied configurations and resistivities used. In general, however, the electrical characteristics change predictably (lower I_{sc} and greater V_{oc} as the resistivity is decreased), although recently the bulk perfection of cells made from silicon around 2 ohm-cm has approached that of cells using 10 ohm-cm silicon. Here we have compared 1 cm x 2 cm cells made from 10 ohm-cm silicon, with three grid lines extending from a contact along the 1 cm edge.

AMO Output

Figure 1 shows the cumulative percentage (the percentage greater than the corresponding abscissae) versus simulator output (as abscissae) for such cells. The shifted abscissa zero exaggerates the differences, but shows the trend. Instead of using AMO efficiencies, we prefer to use milliwatts available from the cell, because this latter quantity is really what the buyers need. The values given are for reasonably large production runs. Curves A, B and C are as described. Curve D is Curve B replotted assuming an active area equal to that of the cells used for Curve C, and shows the sintered contact cells to be slightly superior in output. The

power per pound available from more than 50% of the cells increased from 54 watts for Case A to 68 watts for unsoldered cells in Case C.

Spectral Response

This has remained fairly stable, Figure 2 showing a typical curve, with 2 limits. The slight variations observed can generally be traced to differences in bulk perfection (predictable changes as the bulk resistivity is changed), to differences in the diffused layer properties or in the coatings.

Effect of Varying Area

We will consider only cell slices cut from large single crystal ingots (other people will deal with web-dendrites). At present, there is good ingot yield for either 1 cm by 2 cm, or 2 cm by 2 cm cells. For larger slices, either the ingot yield decreases, or a greater spread of crystal properties (resistivity, perfection, oxygen content) must be tolerated. The larger slices require fewer handling steps per milliwatt, and thus lower costs, but mechanical losses are relatively more serious. Larger area cells should allow greater active area, but may mean a change in the grid structure. Long, narrow cells require fewer configuration changes than large square cells, but the latter give better uniformity in the production steps of a/r coating and possibly in diffusion.

Larger cells require fewer interconnections in arrays, and probably larger covers, but need more area per volt in the array. There may be difficulties when covering irregularly shaped surfaces, and some filling-in with smaller cells will probably be needed for these cases.

Therefore, at present, the 2 cm by 2 cm size appears best, and before large size increases are made, a careful evaluation of the effects on the whole array system must be made.

Effect of Decreasing Thickness

Thinner cells will help to reduce array weight. Our results show that as the cell thickness was decreased from 16 to 8 mils, 5 to 6% of the cell output under the simulator was lost. The loss became greater below 8 mils as expected. Thus decreased cell weight means less power per array area. Also, the increased watts per pound for thin cells will not give significant increases for the whole system, until the main contributors to array weights, primarily the substrate, are also made lighter. NASA and other agencies realize this, and several promising approaches to lighter array design are evolving, some of them to be described in this meeting.

If the array and cover design are suitable, use may be made of the greater flexibility of thin cells. For thin cells, when one balances the relative weight contributions against the slight power loss and the greater production complexity (greater mechanical losses and handling problems),

we feel that caution is necessary to prevent unreasonable demands being made on cell manufacturers to produce thinner cells, rather than making a balanced approach to reducing the weight of the whole array system including the cells.

At present, 10 mils is a realistic lower limit for production numbers.

FIGURE 1 AMO OUTPUT TREND

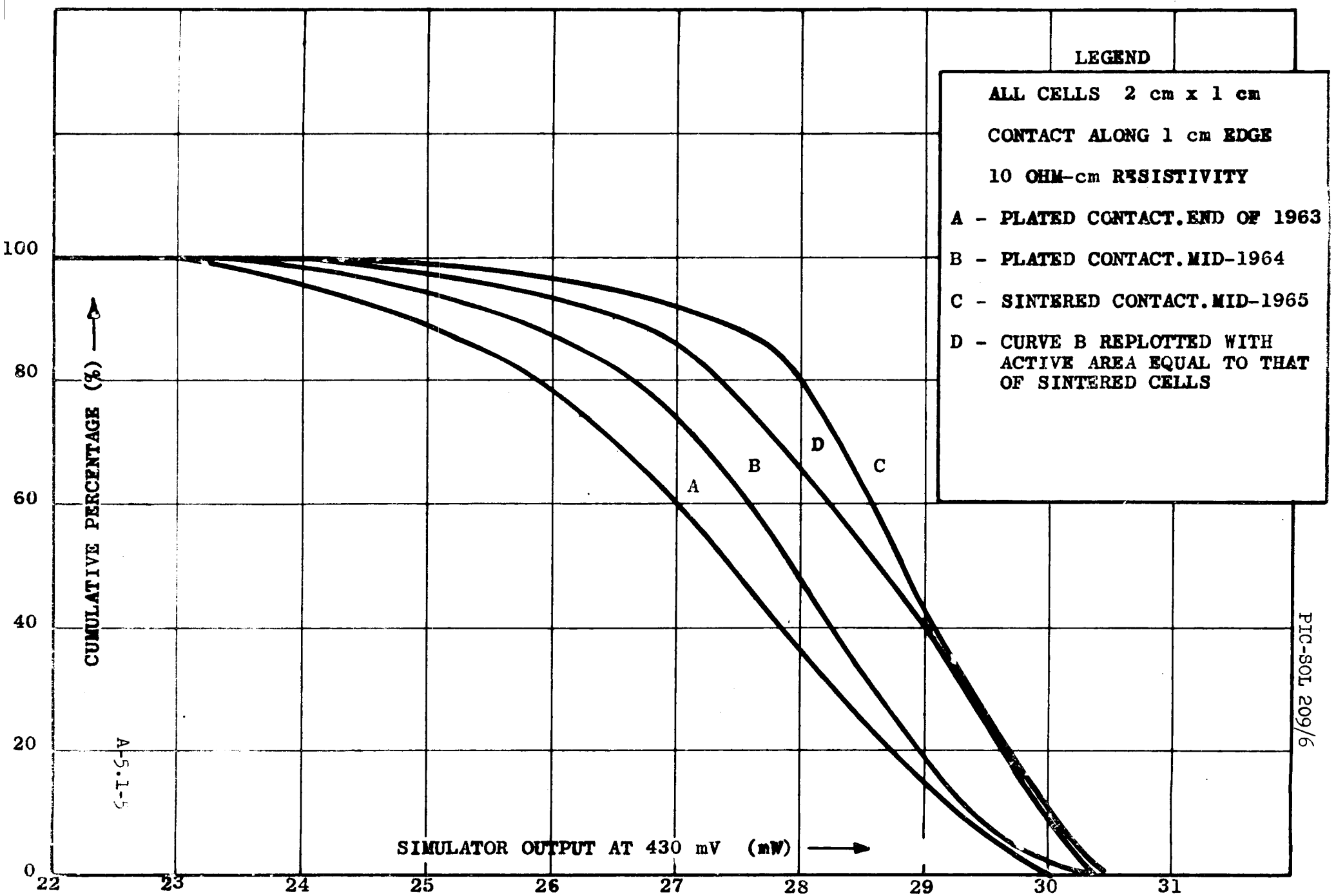

PIC-SOL 209/6

A-5.1-5

FIGURE 2 TYPICAL SPECTRAL RESPONSE

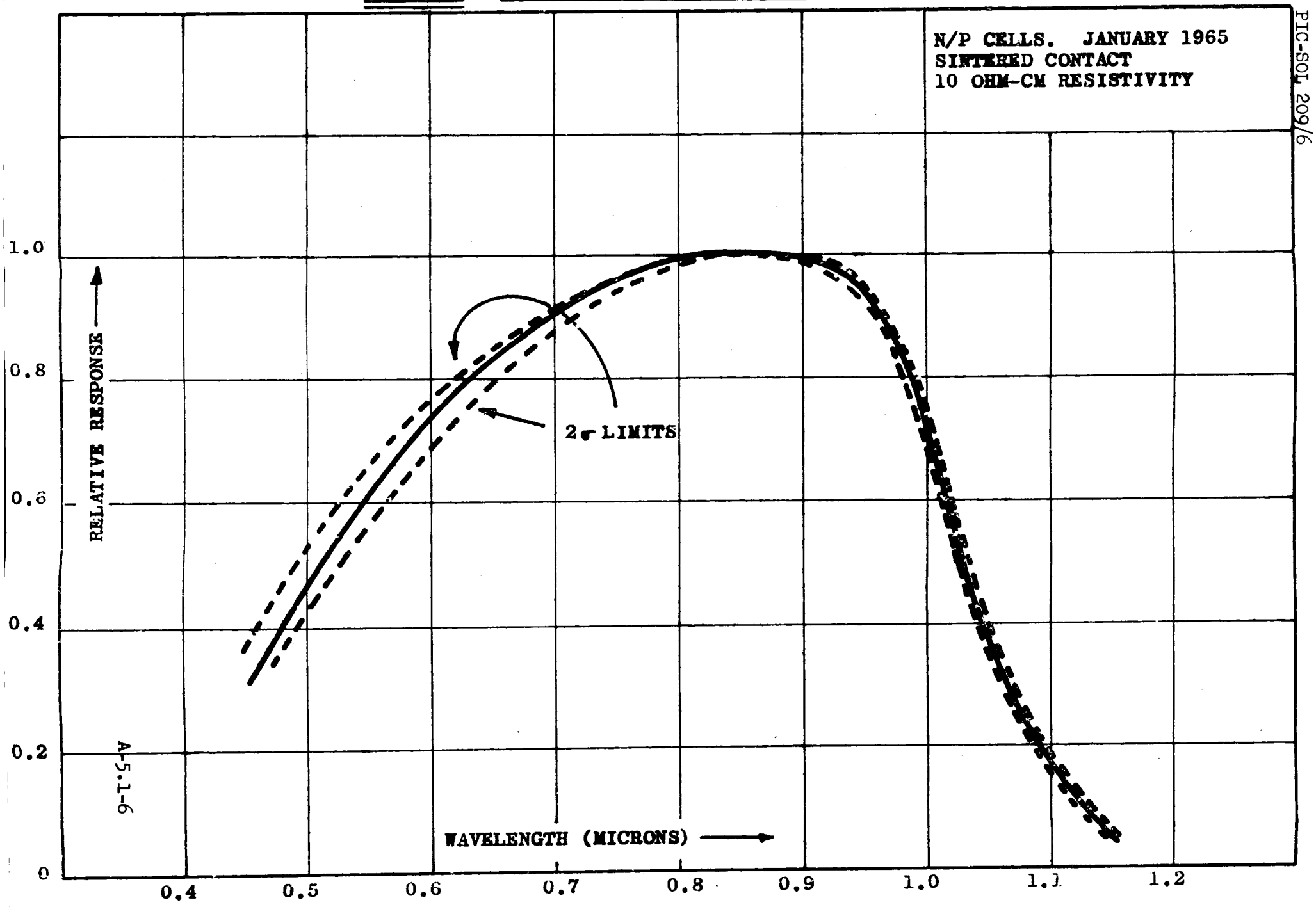

PIC-SOL 209/6

A-5.1-6

PIC-SOL 209/6
Section A-5.2

SUMMARY OF RCA DISCUSSION

Presented by

K. S. Ling

Radio Corporation of America

Electronic Components and Devices

Mountaintop, Pennsylvania

18 October 1965

SUMMARY OF RCA DISCUSSION

by
K. S. Ling
Radio Corporation of America
Electronic Components and Devices
Mountaintop, Pennsylvania

Efficiency

Examination of distribution of air mass zero efficiency on cells produced during the latter part of 63, 64, and 65 indicated that the efficiencies of cells have not changed. They range from 10% to 12%. Generally the users do not want cells under 10% efficiency. In 63 and 64 we had thought we had better cells than what we have today because the relative spectral method was used to determine the air mass zero efficiency. The conversion factor was calculated to be 1.22. Now that we have airplane-flown standard cells to calibrate the light source, the same conversion factor was found to be 1.16. If the airplane flown standard cell is used to measure the cells produced in 63 and 64, the air mass zero efficiency was found to be comparable to that of present cells.

Another factor that has influenced the efficiency of the cell is a demand for cells made with higher bulk resistivity material.

In 1963, the cells were made with 1-2 ohm cm material and now most of the cells are made with 7-14 ohm cm material. The efficiency of the low resistivity cell is lsightly higher than that of the high resistivity cell as the former has the maximum power point at 0.47 or 0.48 volts while the latter has the maximum power point at 0.44 or 0.45 volts.

In conclusion, a major breakthrough is required to increase the efficiency beyond what can be obtained today. However, no evidence of such a breakthrough is in sight.

Spectral Response

The spectral response of the RCA cells has not been changed for the past three years. The same diffusion parameters have been used for the last three years for materials of all resistivity range. We believe that the thickness of silicon monoxide coating probably has a more pronounced effect on the spectral response than minor changes in the diffusion parameters. The thicker the SiO coating, the more red-shifted is the cell response.

Area

RCA has only made a very small quantity of 3 by 3 cm cells. No sufficient data are available to determine accurately the effect of area on efficiency. Based on thousands of cells produced, there is an indication that the efficiency of 2 by 2 cm cells is slightly higher than that of 1 by 2 cm cells.

Thickness

We agree with what Mr. Iles and Mr. Ralph said. The efficiency of the cell is lower as the thickness of the cell is reduced. No appreciable difference was observed between cells of 0.013 inch and 0.017 inch in thickness. Cells of 0.008 inch or less show a loss in efficiency mainly due to the loss in the red response.

PIC-SOL 209/6
Section A-5.3

SUMMARY OF TEXAS INSTRUMENTS DISCUSSION

Presented by

Robert L. Cole

Texas Instruments Incorporated

Dallas, Texas

18 October 1965

SUMMARY OF TEXAS INSTRUMENTS DISCUSSION

Robert L. Cole
Texas Instruments Incorporated
Dallas, Texas

QUESTION: AMO efficiency of bare cells at peak of production distribution now, a year ago, and two years ago.

ANSWER: Silicon solar cell efficiency has increased significantly over the past several years. In 1963, the Telstar satellite typically used cells in the 9% AM1 range. Using this as a base point, Figure 1 shows how efficiency has increased over the years 1963 to 1965 for nominal 10Ω-cm base resistivity cells. Nominal 1Ω-cm cells usually exhibit 1/2 to 3/4% higher AM1 efficiencies than 10Ω-cm cells. From 1963 to the third quarter of 1965, the cell efficiency has increased rather rapidly. Cell efficiency in 1966 and 1967 will begin to level out as anticipated by the dotted line.

QUESTION: Spectral response of the typical production solar cell now, a year ago, and two years ago. This should be relative response at constant energy vs. wavelength in microns.

ANSWER: Silicon solar cells spectral response over the past several years has shifted both into the shorter wavelength as a result of improved cell characteristics and shallow junctions and into the longer wavelength due to preservation of lifetime in the base material.

Figure 2 shows how spectral response has changed over the past two years. This shift in spectral response is responsible to some extent in the increase in cell efficiency.

The spectral response as shown in Figure 2 is plotted on a normalized basis. Data were taken using a Perkin-Elmer Spectrophotometer Model 12C using a tungsten light source, a quartz prism for wavelength separation and a thermocouple for detector.

QUESTION: Performance of silicon cells as a function of area, i.e., 1 by 2 cm, vs 2 by 2 cm, vs. 1 by 30 cm, etc.

ANSWER: Figure 3 shows typically how the AM1 power varies with size of solar cells.

Power is plotted on a normalized basis.

The white cross-hatched area for each resistivity shows what typical spread in power can be expected fron standard production. Note the 1Ω-cm cells consistently give higher power output than the 10Ω-cm cells. All

bar charts in Figure 3 are for nominal 13 mil thick cells in the solderless condition with titanium-silver contacts and SiO antireflective coating. Soldered cells generally fall slightly below the power of solderless cells.

QUESTION: Performance of silicon cells as a function of thickness.

ANSWER: Cell power output drops as the cell thickness is reduced. Figure 4 shows approximately what happens to a cell as the thickness is reduced fron 20 mils to 8 mils where the cumulative photon absorption drops fron 98% to about 95%, respectively. Relating this to power output by actual measurements, the power for an 8 mil cell runs about 90-92% of the power of a 20 mil cell, other cell characteristics remaining essentially the same.

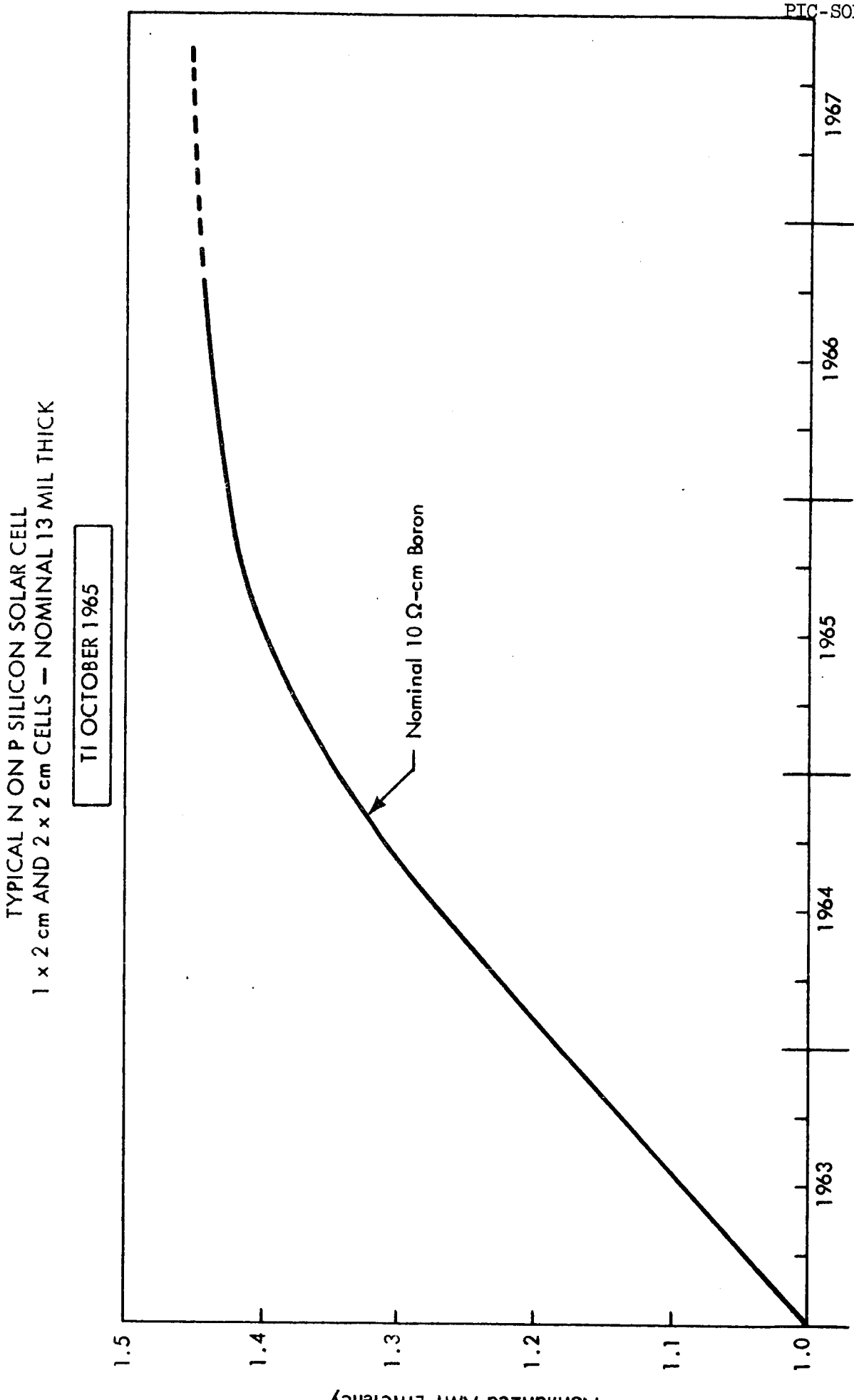
TYPICAL N ON P SILICON SOLAR CELL
1 x 2 cm AND 2 x 2 cm CELLS — NOMINAL 13 MIL THICK
TI OCTOBER 1965
Nominal 10 Ω-cm Boron
Normalized AM1 Efficiency
1.5
1.4
1.3
1.2
1.1
1.0
1963
1964
1965
1966
1967

FIGURE 1

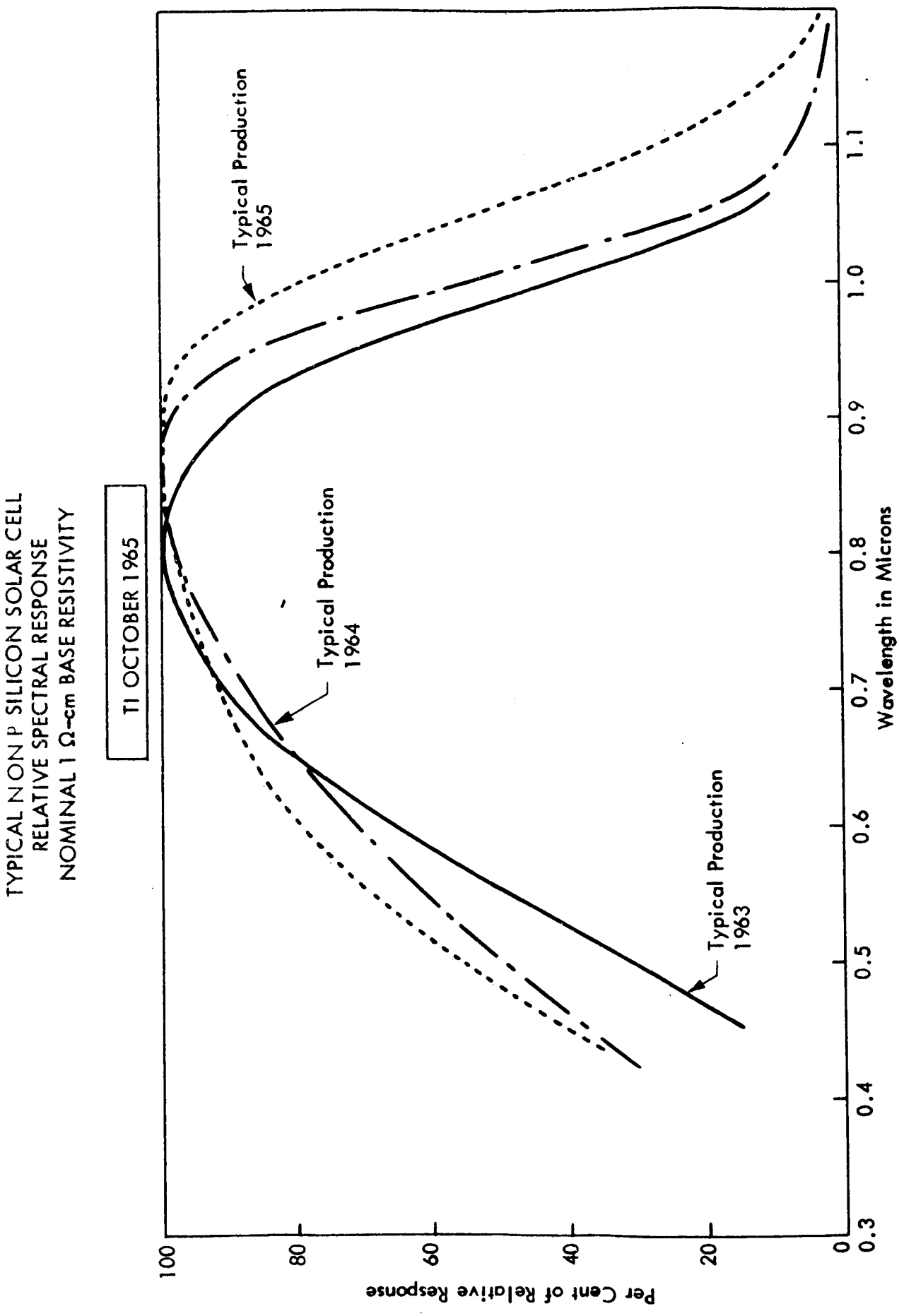
TYPICAL NON P SILICON SOLAR CELL
RELATIVE SPECTRAL RESPONSE
NOMINAL 1 Ω-cm BASE RESISTIVITY
TI OCTOBER 1965
Typical Production
1965
Typical Production
1964
Typical Production
1963
Per Cent of Relative Response
100
80
60
40
20
0
0.3
0.4
0.5
0.6
0.7
0.8
0.9
1.0
1.1
Wavelength in Microns

FIGURE 2

TYPICAL N ON P SILICON SOLAR CELL

NORMALIZED AM1 POWER OUTPUT VS CELL GEOMETRY

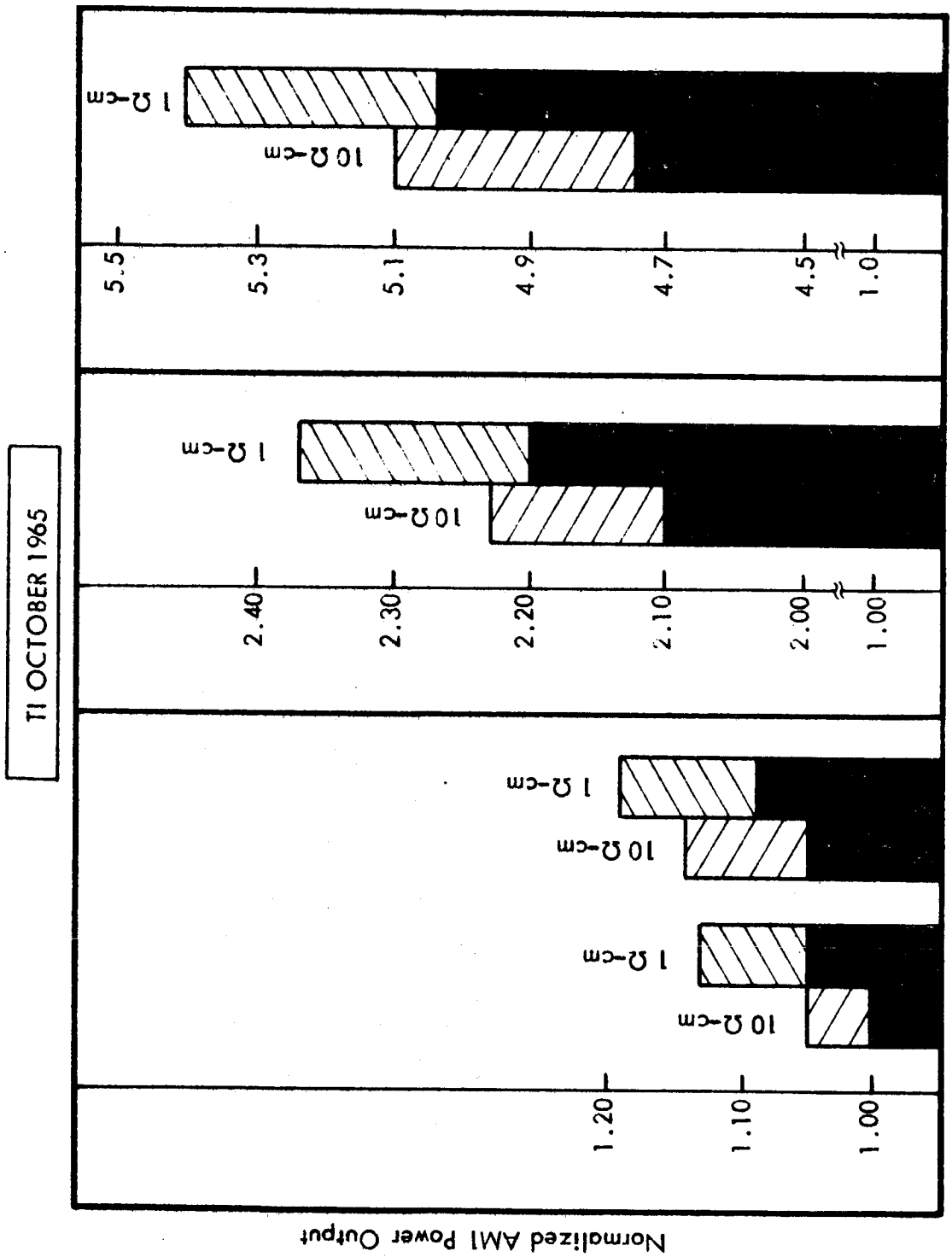

FIGURE 3

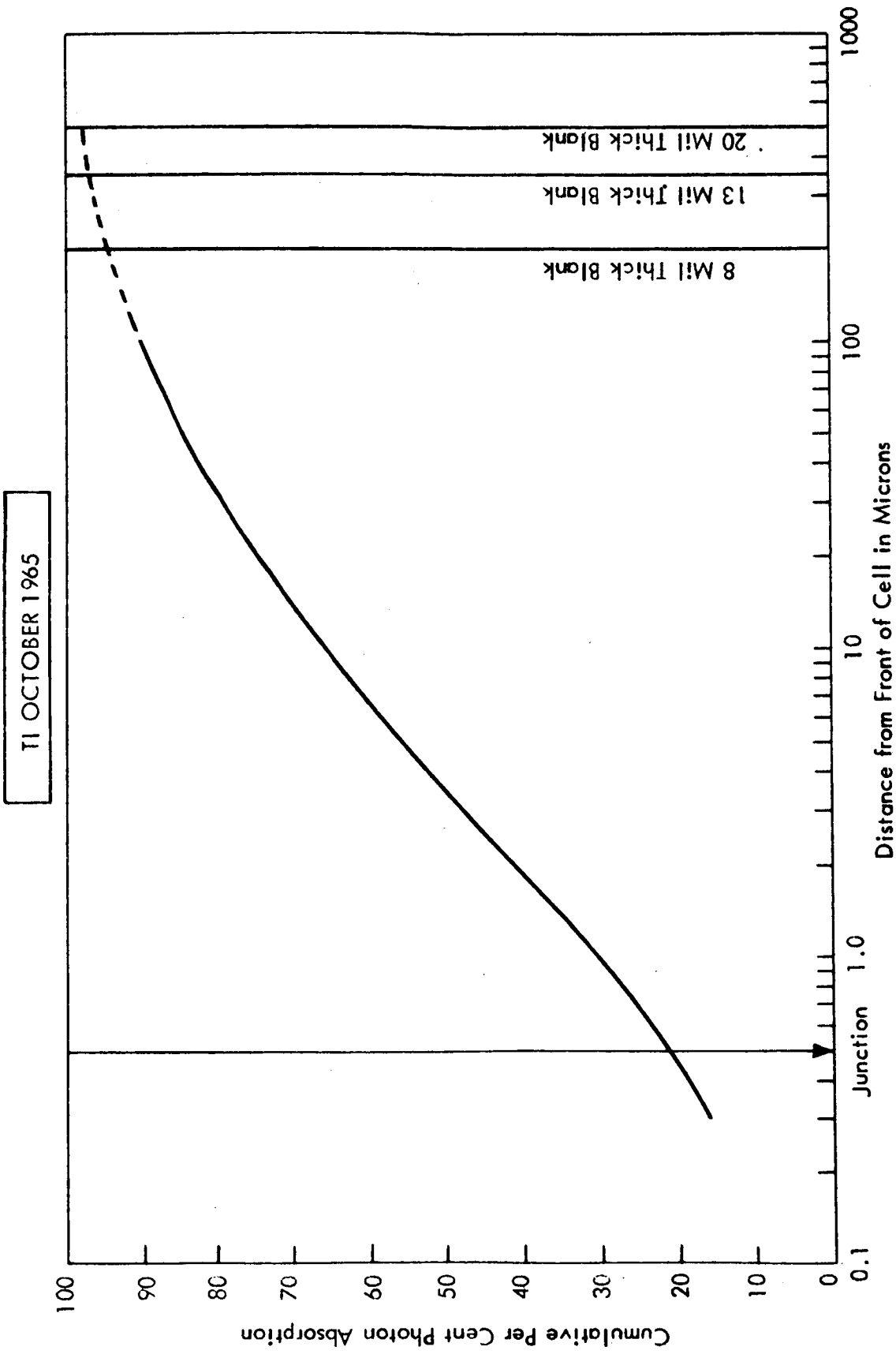
PHOTON ABSORPTION FOR JOHNSON'S SPECTRUM IN 1-10 Ω-cm BORON SILICON
TI OCTOBER 1965
8 Mil Thick Blank
13 Mil Thick Blank
20 Mil Thick Blank
Cumulative Per Cent Photon Absorption
100
90
80
70
60
50
40
30
20
10
0
0.1
1.0
Junction
10
100
1000
Distance from Front of Cell in Microns

FIGURE 4

PIC-SOL 209/6
Section A-5.4

STATUS OF SILICON WEB SOLAR CELLS

Presented by

R. K. Riel

Westinghouse Electric Corporation

Youngwood, Pa.

18 October 1965

STATUS OF SILICON WEB SOLAR CELLS

R.K. Riel
Westinghouse Electric Corporation
Youngwood, Pa.

Introduction

Westinghouse has been engaged in the development of solar cells since 1959. Most of the work done in the area of solar cells on silicon webbed dendrites has been under the sponsorship of the United States Air Force. At present, Westinghouse is involved in the fabrication of N/P conventional and epitaxial drift-field cells.

Results

Presently, the peak distribution for N/P conventional cells is around 10.5% AMO, and it was 9.5-10% a year ago and 9% two years ago. The drift-field cell distribution is around 9% and a year ago was at 8%. Slide 1 shows the details of some of the Balloon Flight Data obtained through the courtesy of J.P.L. The Plates 6A and 6B are representative of present conventional cells and Plates 2A, 2B, 4A, 4B of conventional cells a year ago. In the case of drift-field cells, Plates 7A-11B show the present distribution. It is anticipated that AMO efficiencies of 11% on conventional cells and 10% on drift-field cells can be achieved in the near future.

Slide 2 shows the status of the spectral response on the conventional cells. The effort in this area has been to improve the blue response of the cells. This has been mainly achieved by shallower diffusion depths coupled with improved grid structure design.

Cell thickness was varied from 7-15 mils. No significant decrease in efficiency of these cells was observed. The opinion is that thinner cells can be fabricated and breakage problems of thinner cells can be solved.

An experiment was made to determine the effect of efficiency as a function of area. Silicon web material was cut in different lengths of 2 cm, 3 cm, 4 cm, 5 cm, 6.0 cm, 15.0 cm and solar cells fabricated on these using the conventional process. There was no significant variation in the efficiencies achieved on these samples. These were within $\pm$ 5%.

Last, but not least, we would like to mention that we have a process to fabricate solderless cells. Slide 3 shows the characteristics over some of the N/P conventional solar cells. Solderless solar cells result in weight reduction and high temperature contacts suitable for integral quartz covers.

Advantages

One of the major differences in our development is the use of silicon webbed dendrite materials instead of the conventional silicon crystals. There are several advantages of using silicon webbed dendrites, among these the major one being the fabrication of large area solar cells, 1 cm wide by 30 cm long. Silicon webbed dendrite material is grown to the desired width and thickness and the material is ready for fabrication after the dendrites are trimmed and the web cut to suitable lengths. When one compares this with the Czochralski pulled crystals, the material savings in the fabrication become apparent. The present standard silicon web solar cell can compete with other cells in cost. The cost would only be increased by 10% when using drift-field solar cells.

SLIDE 1

BALLOON FLIGHT CALIBRATION OF WESTINGHOUSE WEB DENDRITE SOLAR CELLS

PLATE NO.	CELL TYPE	EFFICIENCY (PERCENT)			
		Ⓦ TUNGSTEN[3]	Ⓦ SUNLIGHT[4]	J.P.L. TABLE MOUNTAIN[6]	J.P.L. BALLOON MEASUREMENT[5]
2A	Conventional	11.62	11.21	9.47	9.39
2B	↓	12.72	12.20	10.18	10.12
4A	↓	12.05	11.79	10.13	10.10
4B	↓	12.22	11.94	9.20	9.09
6A	↓	11.97	12.50	10.61	10.47
6B	↓	11.48	12.32	10.31	10.36
7A	Drift Field	10.82	10.82	8.90	9.01
7B	↓	10.78	11.00	9.22	9.17
10A	↓	10.72	NA	8.90	8.79
10B	↓	10.20	10.61	9.01	8.71
11A	↓	10.80	NA	9.42	9.37
11B	↓	9.80	NA	8.86	8.73

SLIDE 2

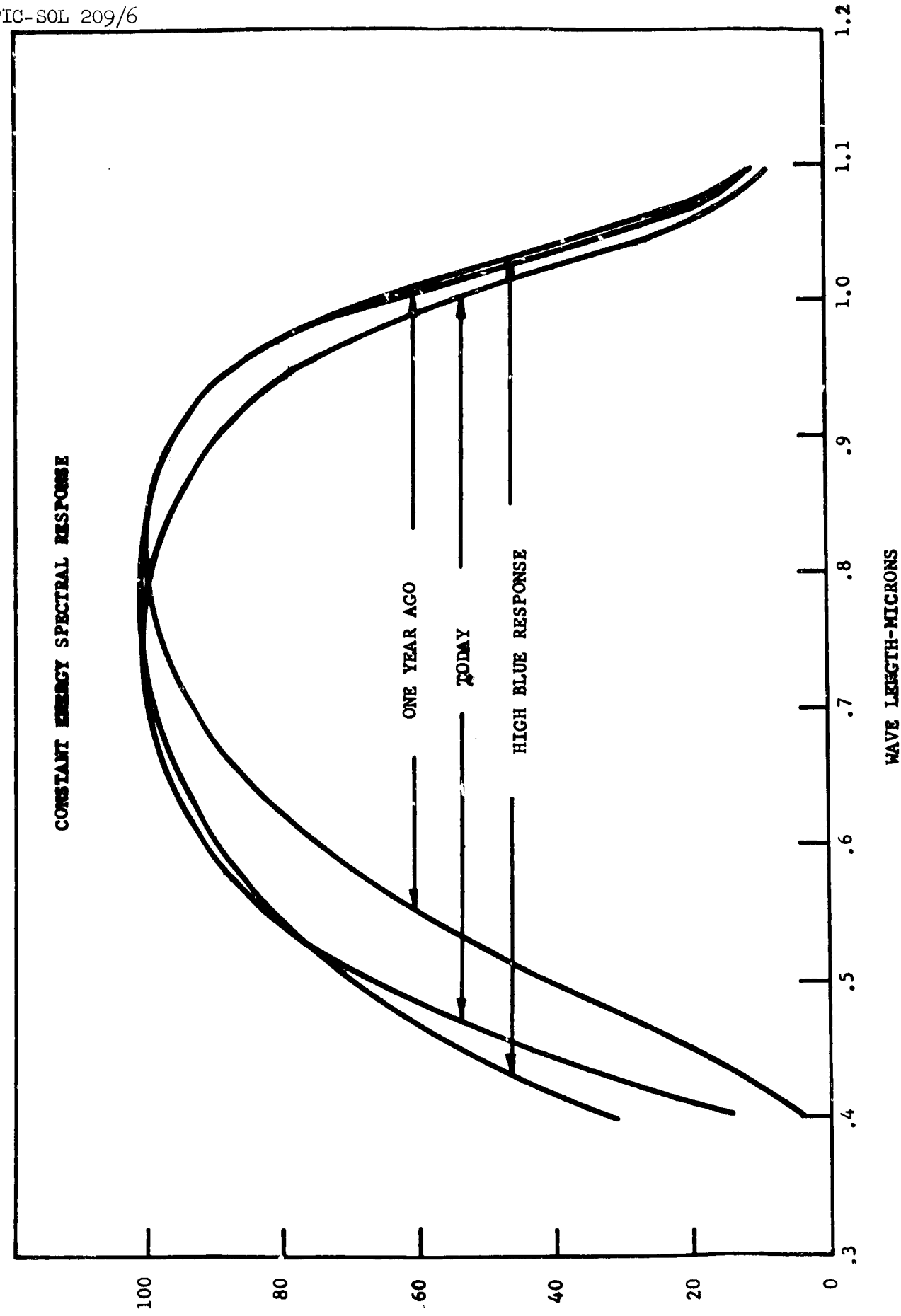
CONSTANT ENERGY SPECTRAL RESPONSE
ONE YEAR AGO
TODAY
HIGH BLUE RESPONSE
% RELATIVE RESPONSE
0
20
40
60
80
100
.3
.4
.5
.6
.7
.8
.9
1.0
1.1
1.2
WAVE LENGTH-MICRONS

SLIDE 3

TABULATION OF SOLDERLESS SOLAR CELL DATA

PHYSICAL CHARACTERISTICS				ELECTRICAL CHARACTERISTICS			
Cell No.	*Area Cm^2	Length Cm	Width Cm	V_{OC} Volts	I_{SC} ma	V_m Volts	n %
IQ-2A	13.86	15.4	1.0	0.54	410	0.42	11.36
IQ-2B	13.86	15.4	1.0	0.54	420	0.38	10.55
IQ-7A	13.68	15.2	1.0	0.53	410	0.40	10.8
IQ-7D	13.68	15.2	1.0	0.52	385	0.42	10.6
IQ-11	13.77	15.3	1.0	0.54	435	0.44	12.2

*Effective Area Only .9 (LxW)

PIC-SOL 209/6
Section B-1

ION IMPLANTATION AS A PRODUCTION TECHNIQUE

Presented by

J. T. Burrill

Ion Physics Corporation

Burlington, Massachusetts

18 October 1965

Abstract

17314

Progress in the ion implantation process for producing N on P solar cells has advanced to the stage where production methods are being developed. Ion implanted cells are presently competitive with diffusion produced cells in conventional materials. Air mass zero efficiencies of 11% have been achieved even though the process is not yet optimized. A high current production machine capable of producing 10,000 cells/week has been constructed and is being applied to further cell development.

The implantation technique is currently being adapted to the fabrication of dendritic material cells where air mass zero efficiencies >9.3% have been obtained. Recent developments in this area, with respect to material (commercial), and fabrication techniques will be discussed.

Investigations have been carried out on fused silica integral cover-slips and compatible antireflection coatings. The latter have involved single layer coatings with indices of refraction more nearly optimized for cover-slipped cells than SiO. It can be theoretically shown that this technique may produce cover-slipped cells with higher efficiencies than non-cover-slipped cells.

The overall objective of this Air Force supported program is the assimilation of the above techniques into a method of fabricating integral cover-slip 1 by 30 cm dendritic cells. Possibilities for achieving this goal will be briefly discussed.

Author

ION IMPLANTATION AS A PRODUCTION TECHNIQUE

J. T. Burrill, W. J. King, S. Harrison
Ion Physics Corporation
Burlington, Massachusetts

Introduction

The basic concepts on which the ion implantation process is founded have been described in detail in prior publications.[1,2] The ultimate objective of this Air Force Aero Propulsion Laboratory (Contract AF33(615)-2292) supported program has been development of a process for producing very high efficiency silicon cells under high yield conditions. Because of the inherent reproducibility and uniformity of the junctions made by this technique and the automation potential, it is particularly attractive as a means of fabricating cells from dendritic material.

Results in this paper concern investigations conducted over the past twelve months on N on P-type cells made by implanting P^{31} in P-type Si. In particular, the present status in terms of efficiency, spectral response and radiation damage is given. Most of the data to be presented were taken from cells made recently for a flight test to be conducted by the Air Force in November 1965. Some modest investigations have been conducted on integral cover slip cells with very encouraging results.

Finally, the implantation process as applied to silicon solar cells has reached the stage where production techniques are being developed. It is notable that the successful application of ion implantation in the solar cell field has generated considerable interest in the process in the semiconductor industry for application to other devices and materials. Work in these areas is being conducted at IPC and at other industrial and university laboratories. The production apparatus to be described, however, represents the first full scale application as a production process.

Production Techniques

Junction Profiles

In order to upgrade ion implantation to a production process, it was necessary to change the basic method of varying the concentration profile of the implanted ions and therefore of the junction. Control of the profile relies on the basic phenomenon that heavy ions have a relatively discrete range in matter. Previously the profile was controlled by fixing the ion energy and rotating the sample in the beam.[1] This led to a flux problem which could only be avoided by going to a system in which the ion energy and current, and implantation time, are varied to obtain the proper number of substitutional ions at each point in the surface region. All

implantations in this method are carried out with the beam entering the crystal at 7° to the (111) plane and the sample position fixed.

Since all prior results were obtained using the sample rotating system, it was necessary to test the validity of the new system. This was done by implanting samples at four energy levels (80, 120, 160 and 200 keV) with implantation times varied so that the envelope of the implanted distribution would approximate the 100:1 - linear fall-off (surface to junction) used in the better cells made by the rotation method. The straggle in the range of the ions is sufficient to smooth the distribution between the energy peaks.

The impurity distributions of these samples were determined by the anodization-etching technique coupled with sheet resistivity measurements. As shown in Figure 1, the distributions are sufficiently similar, within experimental error, that the junction and cell characteristics were almost identical.

Fabrication Procedures

Although many minor variations have been introduced into the fabrication procedure during the optimization process, the same basic steps are used for all cells. In this general procedure, the samples are first lapped and the front surface is etch polished and then anodized to a depth of approximately 1,000 Å. After implantation the samples are annealed at 750°C for 16 hours and contacted on the front with Ti-Ag and on the back with alloyed Al followed by Ti-Ag. In our laboratory by using this technique, the contact resistance has been reduced to an almost negligible value on 10Ω-cm material. Finally an SiO antireflective coating is applied and the cells are tested.

The annealing process can be shortened if necessary. This was demonstrated by annealing an implanted sample at temperatures from 200°C to 750°C for periods of one hour each, and monitoring the sheet resistance after each step using a conventional four-point probe. The resulting annealing curve is shown in Figure 2. Subsequent heating of the sample for 16 hours at 750°C gave no further decrease in sheet resistance. Angle-sections also showed no junction movement between the 1 hour and 16 hour anneals. Temperatures as low as 700°C may be used with little effect on sheet resistance.

Cell Characteristics

Conventional Material

The group of cells produced for the flight test although small (87) by production standards, represented the first case in which a fairly large number of implanted cells were made with the same parameters. One of the finished panels is shown in Figure 3. The cells were made from material with the following characteristics:

Material:	Lopex
Resistivity:	10 Ω-cm
Thickness:	15 mils
Dopant:	Aluminum
Lifetime:	>100 μsec

The variable energy technique was used and the implantation (80 and 100 keV) were done on the 400 keV Van de Graaff accelerator described previously.(1,2) Due to time problems associated with operating this accelerator at relatively low energies, these cells were made with junction depths slightly deeper (0.5μ) than optimum for maximum blue response. A fourteen-finger front grid configuration and SiO antireflection coatings were used.

In setting up this small pilot line, a problem was encountered initially in the soldering step. After this problem was solved, a high yield of high efficiency cells was obtained as shown in Figure 4, which gives the tungsten efficiency distribution. The AMO efficiency of 70% of these cells was 10% or better with some cells better than 11%. The center of the distribution was about 10.5%. AMO efficiencies were obtained using a method similar to the Bell Laboratories' technique but with the filter wheel replaced by a Bausch and Lomb grating monochromator. Curve factors on these cells averaged 0.74 to 0.75 with some cells as high as 0.77.

Spectral response curves of these cells are shown in Figure 5. For comparison, the spectral response obtained on cells with implanted junctions of 0.25μ depth is shown. The slight red shift was due to a difference in the characteristics of the bulk material used to make the two cells. The improvement in blue response that can be achieved is clearly evident.

Dendritic Material

The general process described previously has been used in investigations on dendritic material with the major exception being the use of the as-grown surface. Cells made with Westinghouse material using a 0.5μ junction depth have shown AMO efficiencies of >9.3%. Cells made with commerical material have had somewhat lower efficiencies with primary limitation appearing to be the material. Over the period of a few months in which we have been studying commercial dendritic material, the material being delivered has shown some slight improvement in characteristics. Handling this material presents problems at present because of breakage due to crystal faults.

Figure 6 shows the relative spectral response of some dendritic cells compared with a similarly implanted conventional material cell. There is a wide variation in response above 6,000 Å depending on the particular dendritic crystal, with an apparent tendency for better response with lower dislocation density and less slippage. This curve also shows an apparent increase in blue response for the dendritic material which occurs because these are relative response curves normalized to the peak value.

However, there is no apparent technical reason why, with future material improvement, competitive cells cannot be produced from dendritic material.

Coatings

Investigations have been carried out on antireflection coatings and fused silica integral cover slips. Antireflective coatings for silicon cells should be peaked around 6,000 Å to maximize the peak of the product of the solar photon spectrum and the photon response spectrum of a typical cell. The antireflective characteristic occurs when the reflections from the upper and lower surfaces are of equal intensity and opposite phase. The equality of reflected intensity is set when the relative refractive indices at the top and bottom interfaces of the coating are equal. This occurs when the well-known condition

$$n_{layer} = \sqrt{n_o n_{si}}$$

is satisfied, where n_o is the index of air for a bare cell or of the cover slip or adhesive on a cover-slipped cell.

SiO meets this condition fairly well for a non-cover-slipped cell since

$$n_{SiO} = 1.95 \approx \sqrt{1 \times 4}$$

We have been attempting to optimize the situation for a cover-slipped cell in which case the antireflective layer should have

$$n \approx \sqrt{1.45 \times 4} = 2.41$$

Using evaporation and high vacuum sputtering techniques, several materials have been investigated as the n = 2.41 intermediate layer, including TiO_2 and SiC. TiO_2 has proven effective down to approximately 5,000 Å but has shown a tendency to cut off below this wavelength which is about 800 Å higher than expected. SiC has been difficult to locate in the purity and form necessary for sputtering and for the material available has in general shown a tendency to relatively high absorption.

When cover slips, both integral and normal, are applied to SiO coated cells, the color almost disappears. When applied to TiO_2 coated cells there is a gain in color and efficiency over the range of effectiveness. These titania coated cells were of approximately equal efficiency to SiO coated cells when cover slips were applied. The lack of efficiency increase was due to the high (5,000 Å) blue cut-off. Coatings of indix 2.4 which do not have this cut-off should provide the best single-layer antireflective coating for use with cover slips.

Integral cover slips of approximately 1 mil thick fused silica have been applied to 8 cells using an IPC high vacuum (2×10^{-6} torr) sputtering

apparatus. Excellent adherence of the coating is obtained. These coatings have been thermally cycled from +100°C to -100°C without cracking or peeling. There is no change in the curve factors with application of these coatings. Starting with cells with tungsten efficiencies (2800°K) of 11.2 to 12.3%, final cell efficiencies of 10.6 to 11.6% tungsten were obtained. The loss in efficiency was primarily due to absorption in the coatings. This absorption was due to impurities and can be eliminated with more refined techniques.

Radiation Damage Investigations

A comparative investigation of solar cells irradiated with 1 MeV electrons at fluxes up to 1.8×10^{16} electrons/cm^2 has been made. Details of the investigations are given in a recent contract report.(3)

One comparison was between cells produced by IPC and other manufacturers. The IPC cells and those of two of the manufacturers had 10Ω-cm base material while the other manufacturer had 1Ω-cm base material. Results of these tests, given in Figures 7 through 10, show the superior radiation resistance of the 10Ω-cm material as observed previously by other investigators. No appreciable difference was observed within experimental error between cells produced by implantation and those produced by diffusion.

A comparison among IPC cells only also gave an increase in radiation resistance with increasing base resistivity, as shown in Figures 11 and 12. This comparison was made as part of a study currently being conducted on the effects of bulk dopant, resistivity, lifetime and crystal growing techniques on radiation resistance. It was felt that the implantation process would help in the elucidation of the effects of these parameters since the process has little or no effect on bulk material characteristics. No detectable difference in radiation resistance was observed for cells implanted at ambient or LN_2 temperatures.

Of special interest is the preliminary result that there was a larger decrease in I_{SC} for the aluminum doped cells than for the boron doped cells but almost equal decreases in efficiencies. Both of these sets of cells were 10Ω-cm and had lifetimes greater than 100μ sec.

Production Apparatus

As described previously, most of the earlier work on this program has been conducted on Van de Graaff accelerators because of their inherent stability and energy control. The Van de Graaffs being used are, however, inherently unsuitable for production of large area devices such as solar cells, because of their limited current capability (<1 μamp/cm^2) for boron and phosphorus beams. As the energy range of interest for this work got narrower, it became possible to design a production apparatus with higher ion current capability.

An implantation apparatus, shown schematically in Figure 13, has been designed and built which operates on the variable energy technique rather than the older rotating sample technique. This machine consists of an IPC high-current, low-density plasma ion source, a pre-acceleration analyzing magnet and a sample implantation chamber.

The source is run on a phosphorus-containing gas. A large diameter P^{31} beam is drawn from the source at approximately 5 keV and passed through the analyzing magnet to remove undesired impurities. After analysis the ions are accelerated on to the samples at energies up to 150 keV by voltages applied to the sample holder. The high voltage is supplied by a single stacked rectifier power supply coupled to the sample holder through the chamber wall by an IPC bushing.

Profile programming is accomplished by varying the input voltage to the high voltage supply and the implantation time. The sample holder, which can be maintained at temperatures from LN_2 to ambient, is a six-sided drum with each side (5 cm by 15 cm) being capable of holding 70 cm^2 of cells for implantation. The cells are mounted at 7° to the incoming beam direction to avoid channeling. One side of the drum is scanned in front of an aperture which limits the large diameter beam to a uniform 2 by 6 cm area. This therefore gives uniform implantation of all cells on one side. The scanning rate of the samples (6 inches/sec) is fast compared to the time in which the high voltage is varied so that all cells on the side see the same energy variation. After one side is implanted the drum is indexed to the next side and the implantation procedure repeated.

This system has a stainless steel ten-inch diffusion pump system with a continuously refrigerated optical baffle. Pumping speed is sufficient to allow a cycle time of one hour for sample insertion, pumpdown and sample removal. The implantation time varies depending on the desired junction characteristics. For a uniform distribution of 10^{21} ions/cm^3 throughout a 0.5 μ layer it will take approximately 12 minutes/side or 72 minutes for all six sides. Allowing for overscan of the sample holder increases the total implantation time to about 1-1/2 hours and the total cycle time to 2-1/2 hours.

This time is based on an already available 1 mA P^{31} beam (83 μ amps/cm^2 over the 2 by 6 cm area) and a 15 cm long sample plate. Each sample plate holds thirty-five 1 by 2 cm cells and therefore 6,300 cells can be implanted per week assuming a two-shift operation. If the longer (30 cm) plate is used, or the beam current increased, the system will implant well over 10,000 samples per week. Both of these changes can be made on this machine whenever necessary.

The sample holder has been designed to accommodate 1 by 15 cm dendritic cells and may be converted to handle 1 by 30 cm cells. An economical dendritic cell production process could be set up if sufficient high quality dendritic material were available.

Figure 14 gives a view of the actual apparatus showing the electronics, sample implantation chamber with bushing and clean bench for loading the samples. The entire apparatus is mounted on a bench in the IPC chem lab in order that a line may be set up around it. At present, the machine is in the final debugging stage and some experimental cells have been produced. Pilot line runs will be made in the near future for further optimization of implanted cells through improved profiles, lower sheet resistivities, and shallower junctions.

Conclusion

The present status of the ion implantation process as applied to solar cells has been described. Cells are currently being made by implantation with efficiencies equivalent to those of the best production line diffusion cells. An inherent high yield capability has been demonstrated although this has not been tried on a production line basis. Further improvements in implanted cells are possible, and significant progress could be made in dendritic material if enough good material were available. Finally, the implantation process has reached the stage where a production line can be set up.

References

1. King, W. J. and Burrill, J., "Solar Cells Produced by Ion Implantation Doping;" Fourth Photovoltaic Specialists Conference, June 1964.

2. Reports on Contracts AF33(657)-10505 and AF33(615)-1097.

3. Quarterly Technical Progress Report No. 3 on Contract AF33(615)-2292, August 1965.

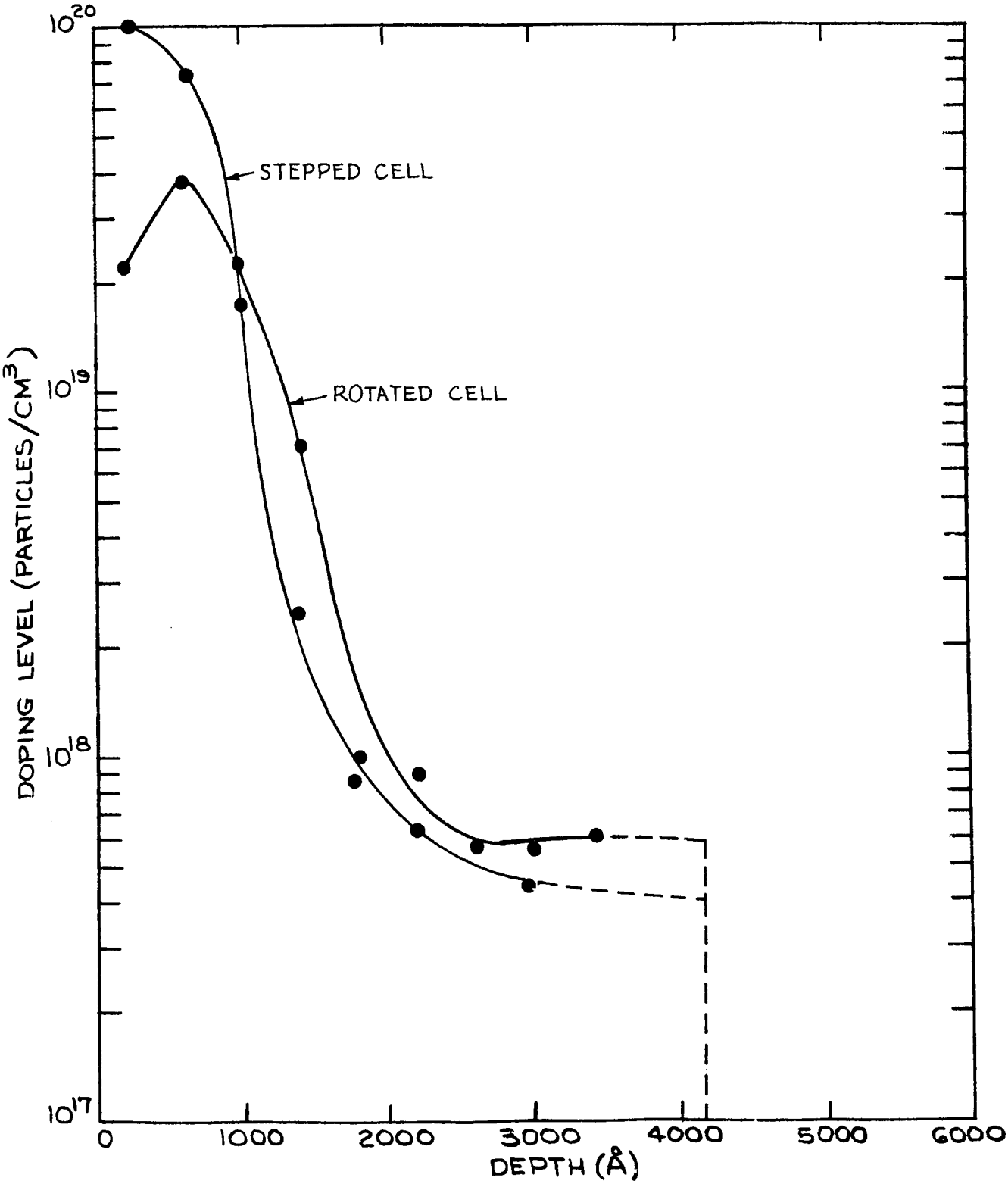

FIG. 1 DOPING LEVEL VERSUS DEPTH

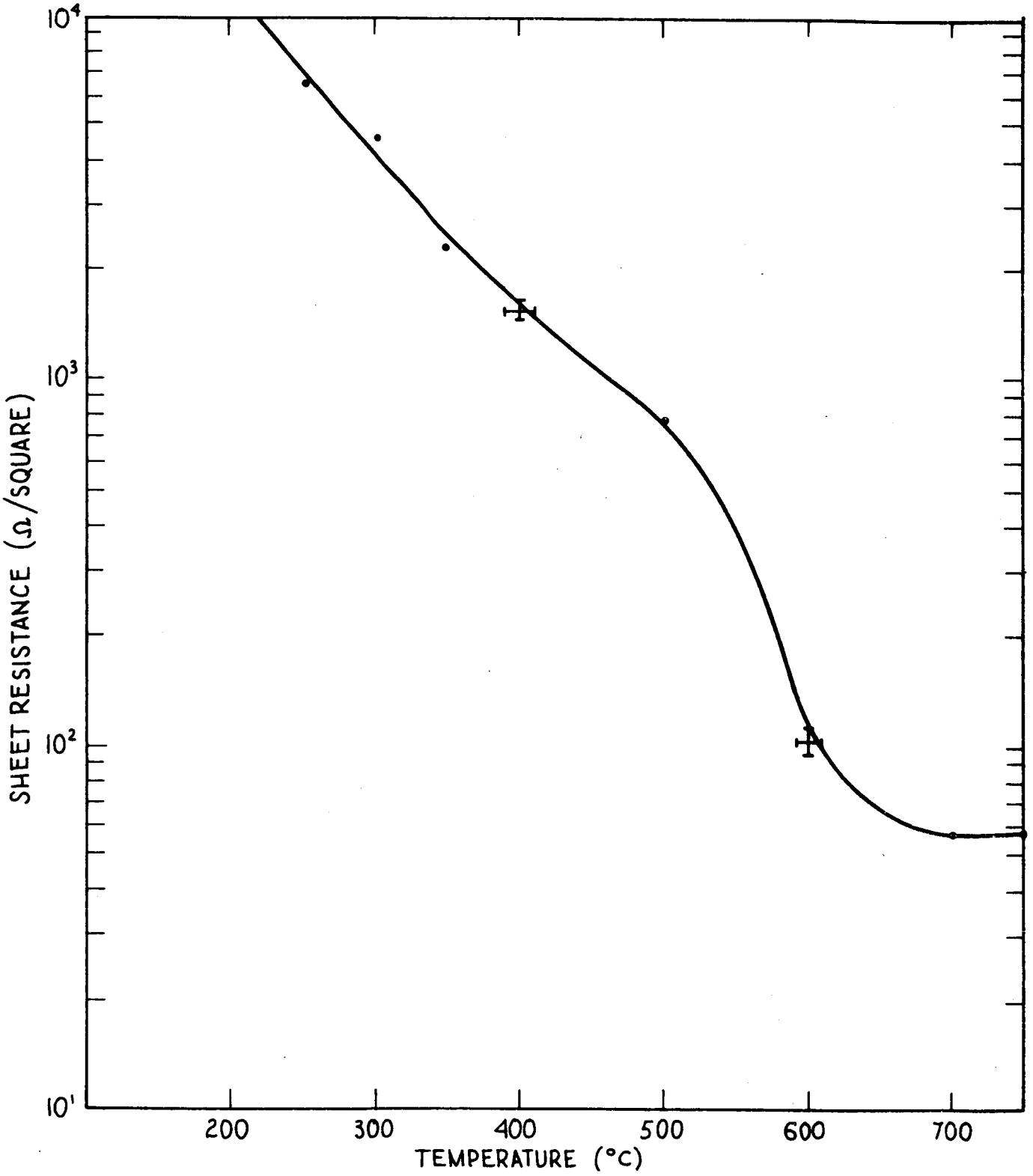

FIG. 2 SHEET RESISTANCE VS. ANNEALING TEMPERATURE

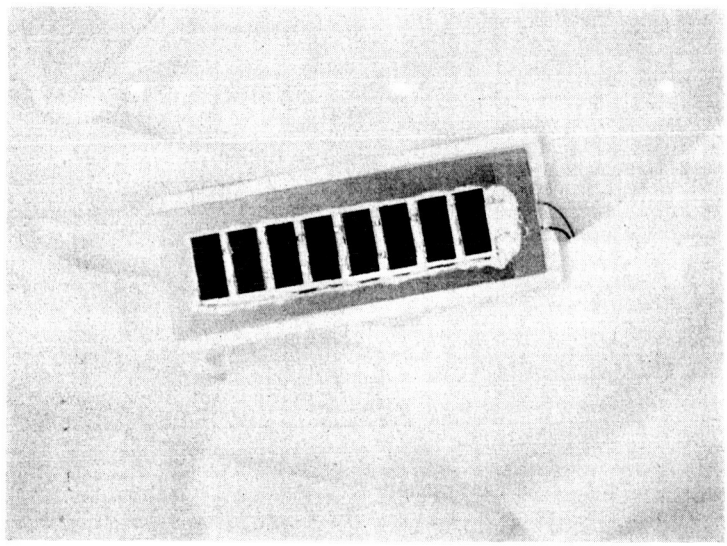

Fig. 3 Experimental Solar Cell Panel

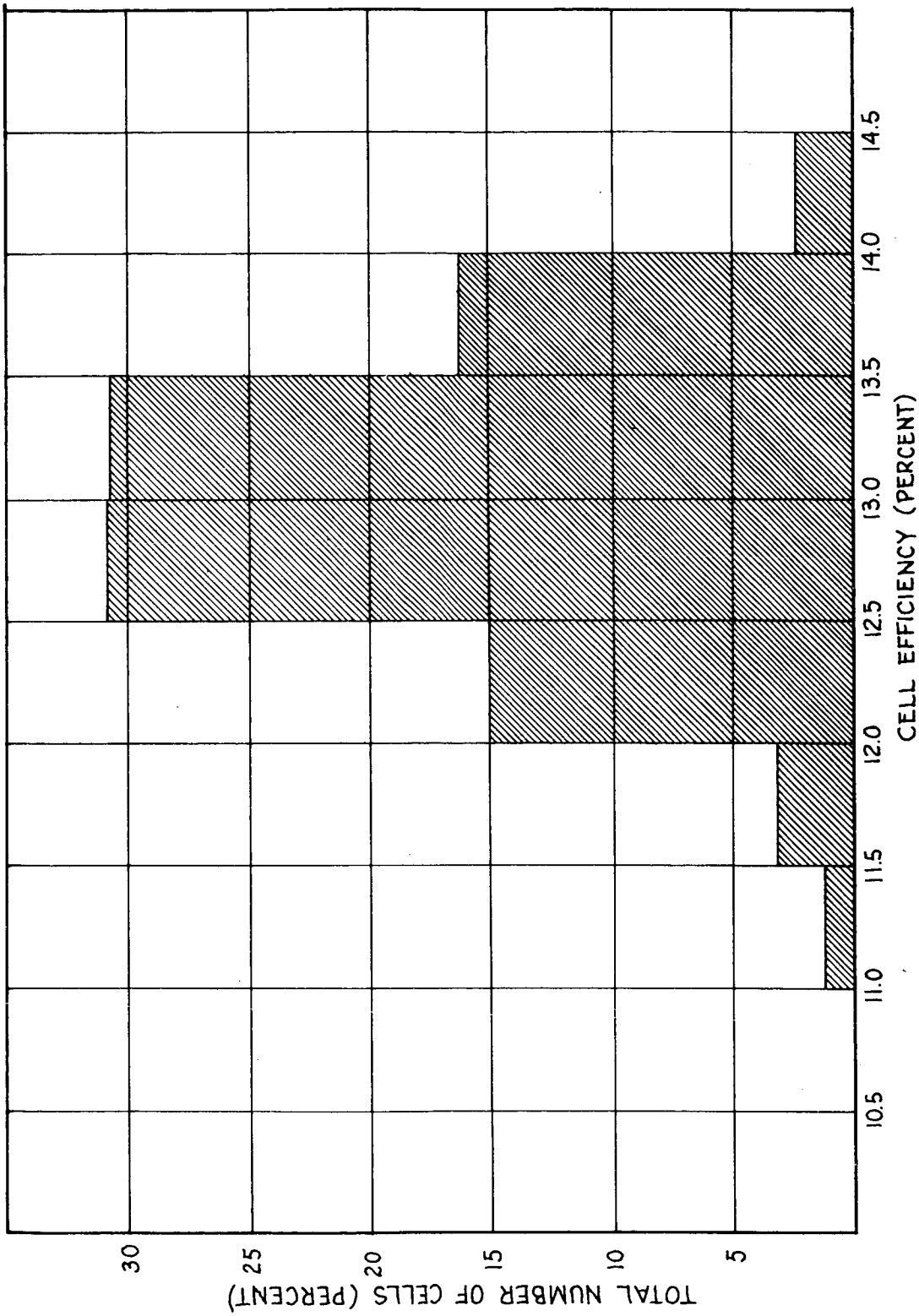

PERCENTAGE OF TOTAL CELLS WITHIN EFFICIENCY GROUP INDICATED ON ABSCISSA (10 OHM-CM-A1 DOPED BASE MATERIAL)

FIG. 4

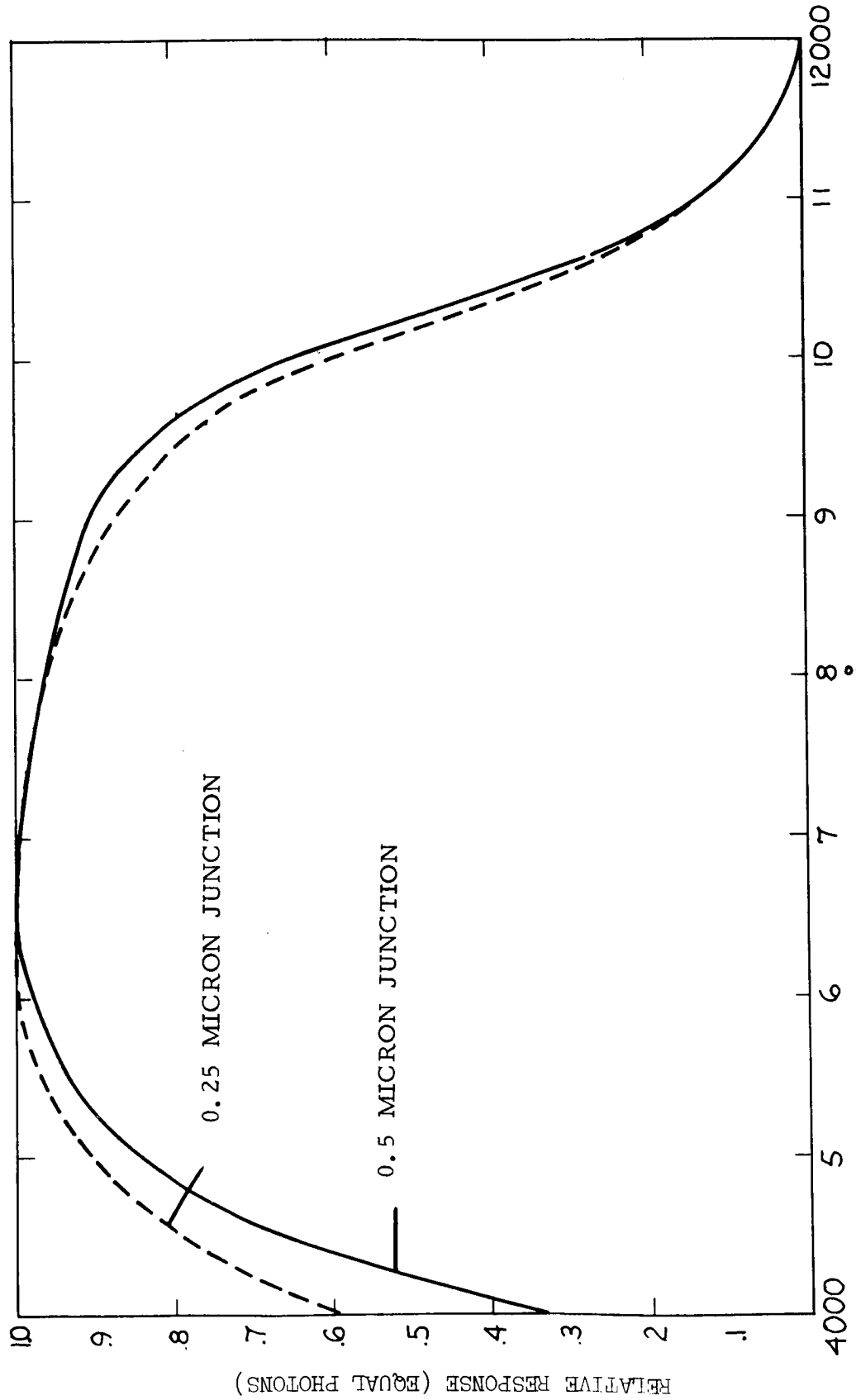

FIG. 5 SPECTRAL RESPONSE

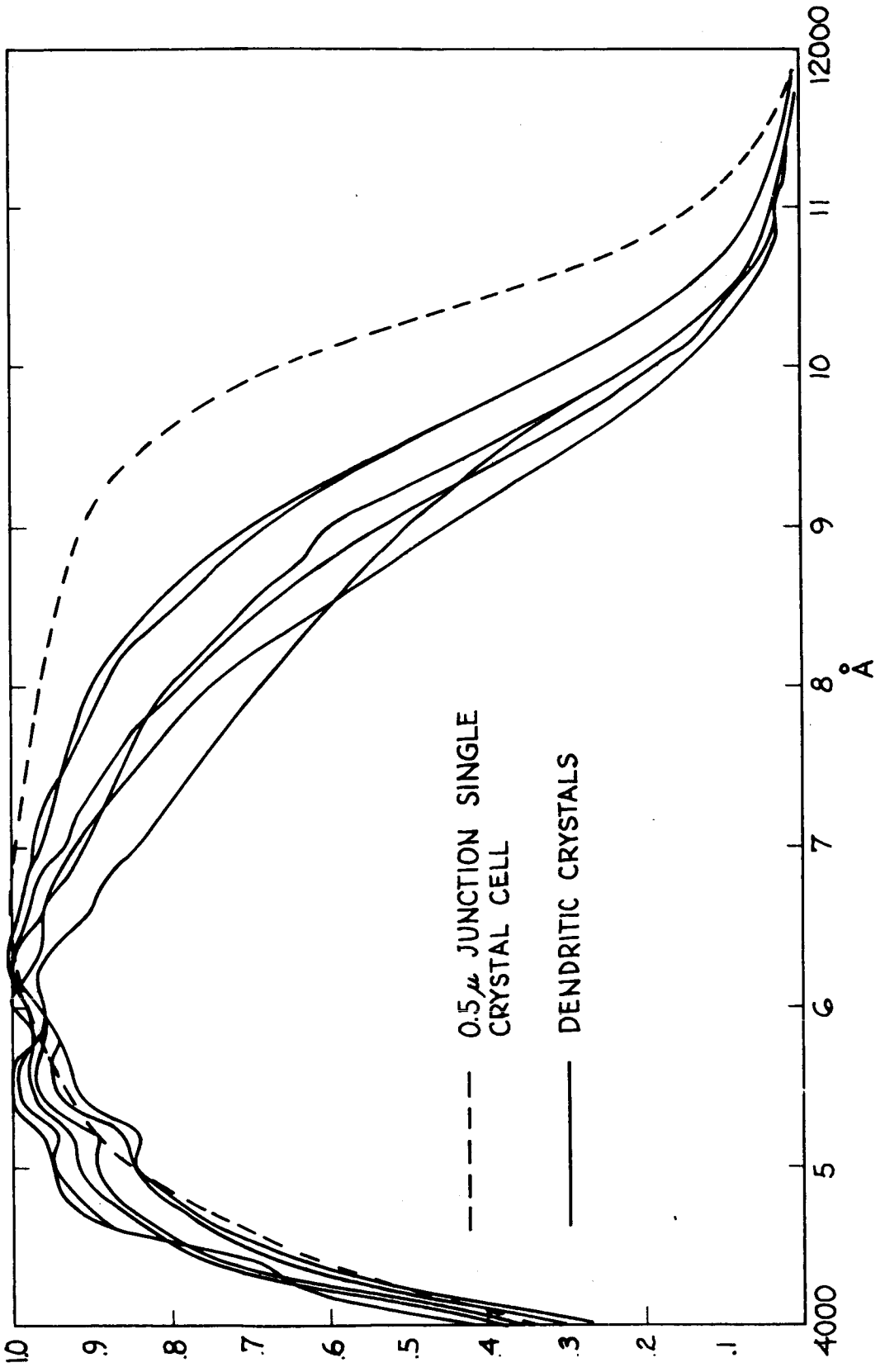

FIG. 6 **SPECTRAL RESPONSE**

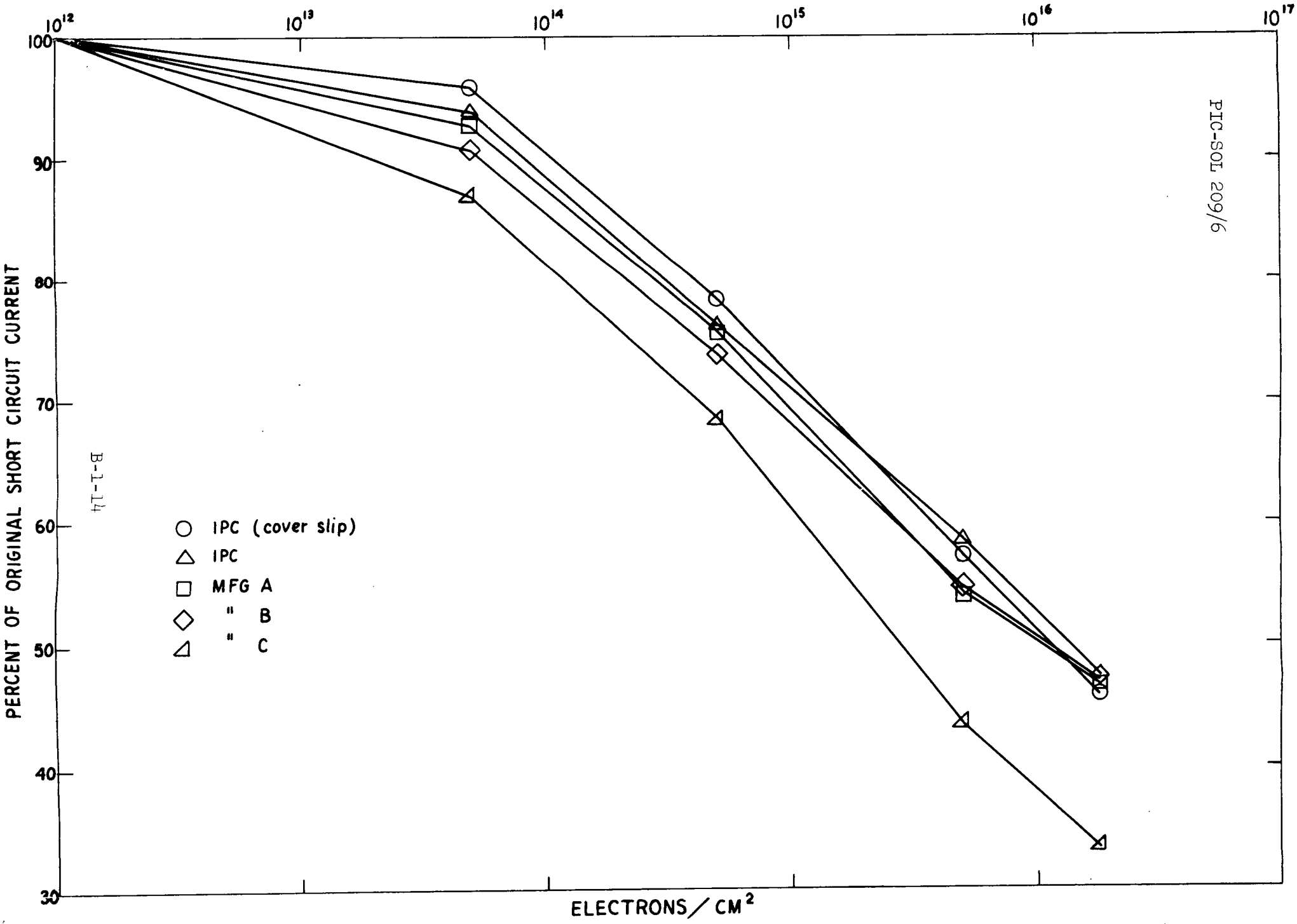

FIG. 7 PERCENT OF ORIGINAL SHORT CIRCUIT CURRENT VS DOSE (2800° K TUNGSTEN)

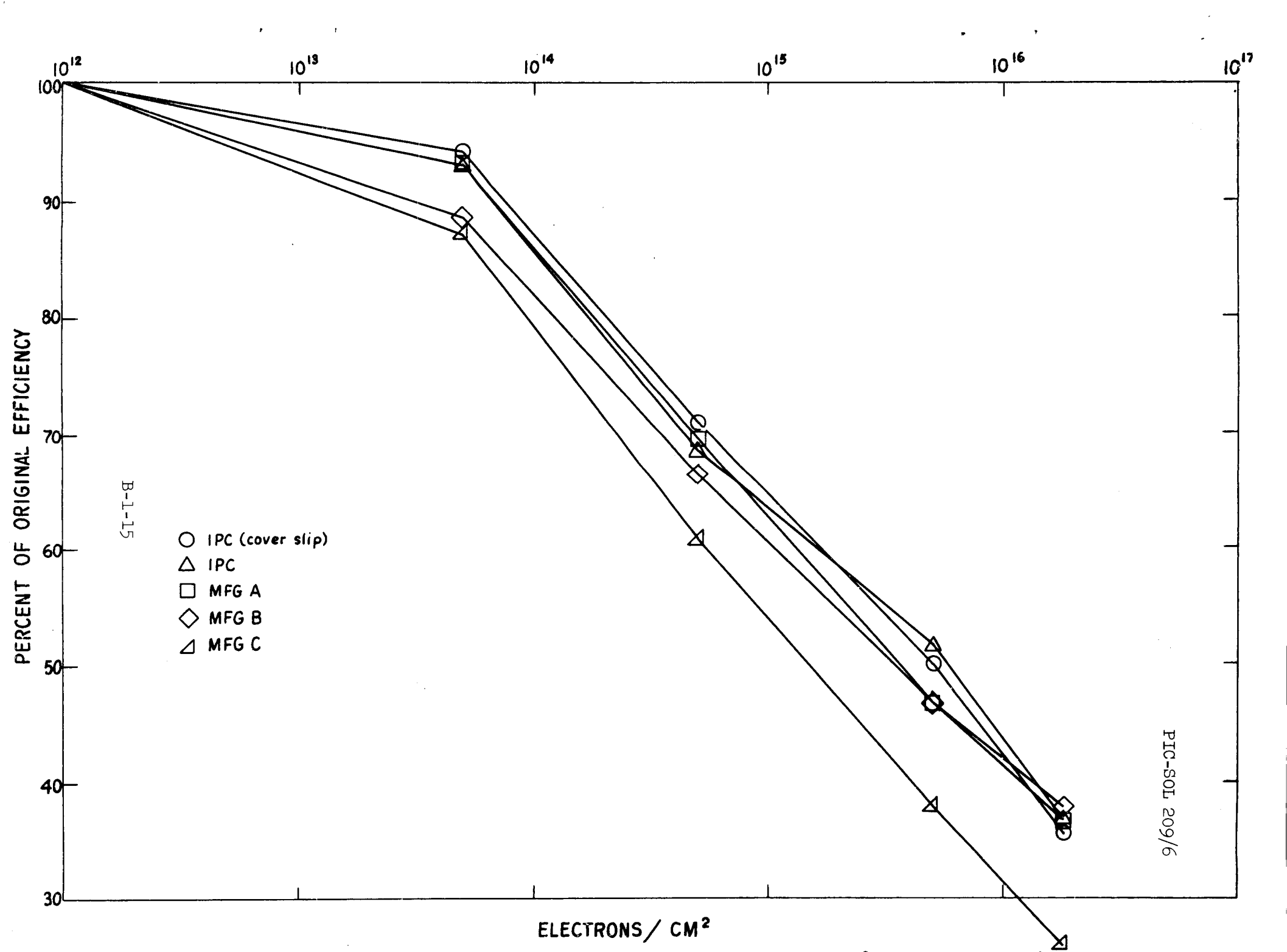

FIG. 8 PERCENT OF ORIGINAL EFFICIENCY VS DOSE (2800° K TUNGSTEN)

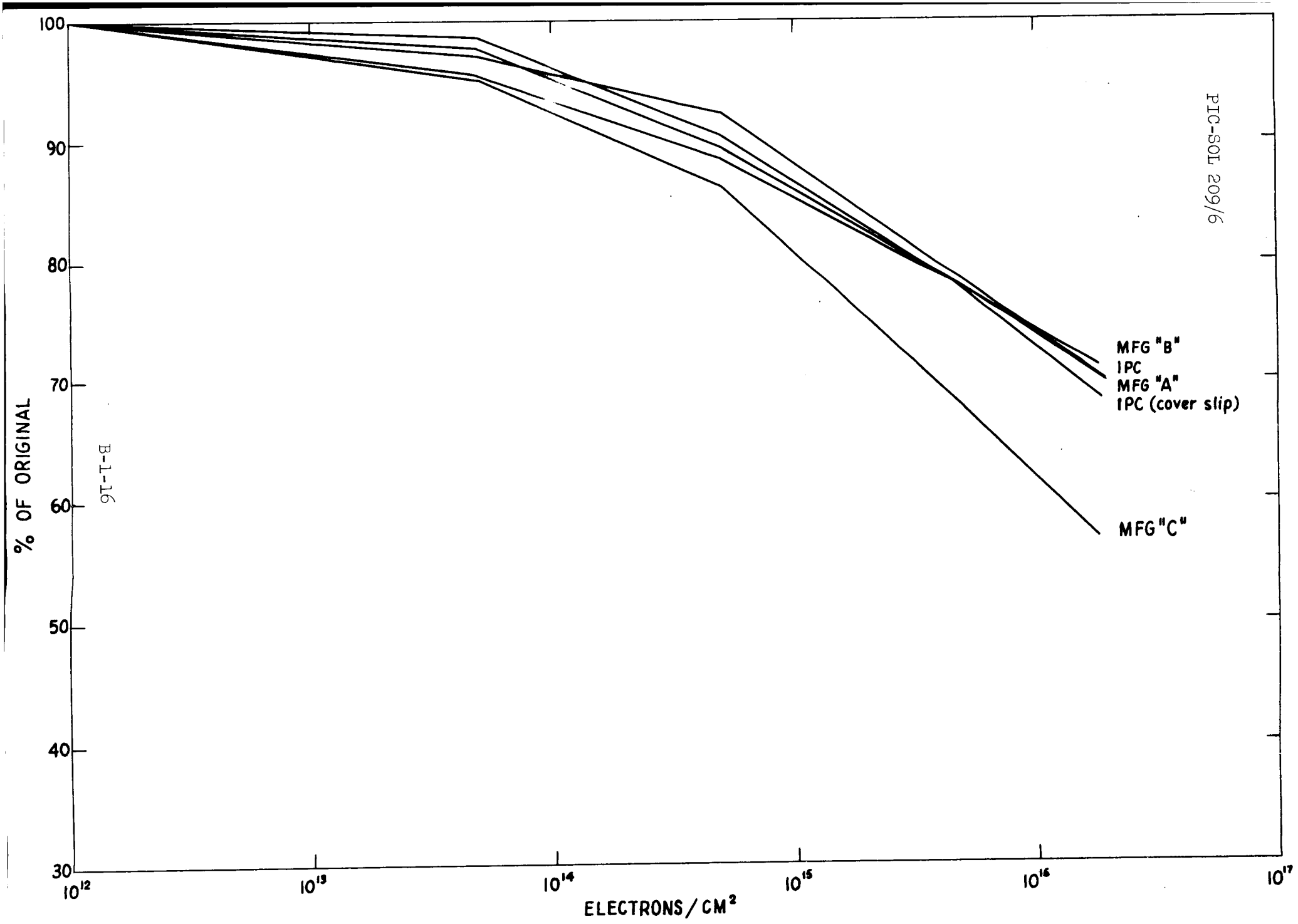

FIG. 9 PERCENT OF ORIGINAL SHORT CIRCUIT CURRENT VS DOSE (AMO)

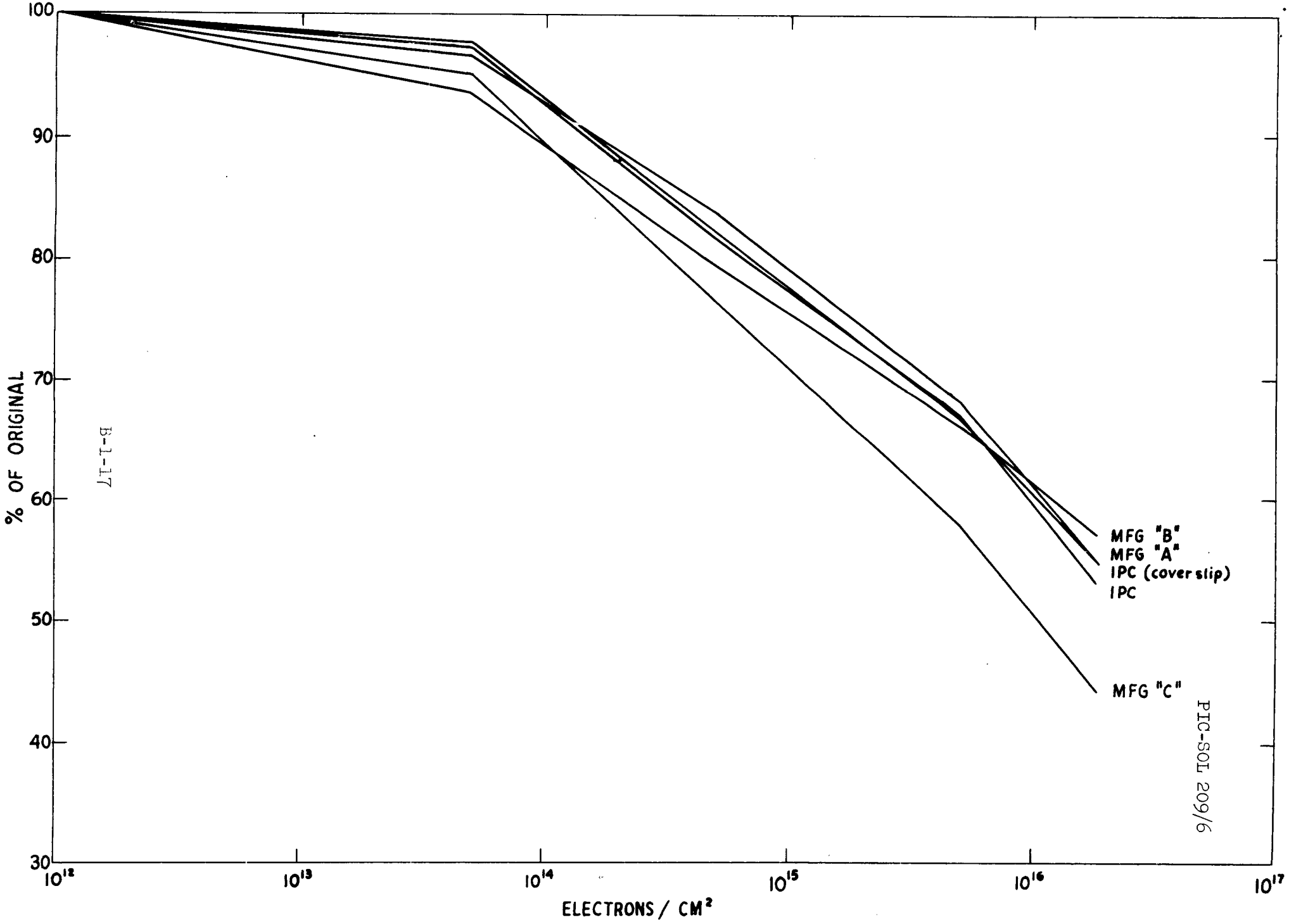

FIG. 10 PERCENT OF ORIGINAL EFFICIENCY VS DOSE (AMO)

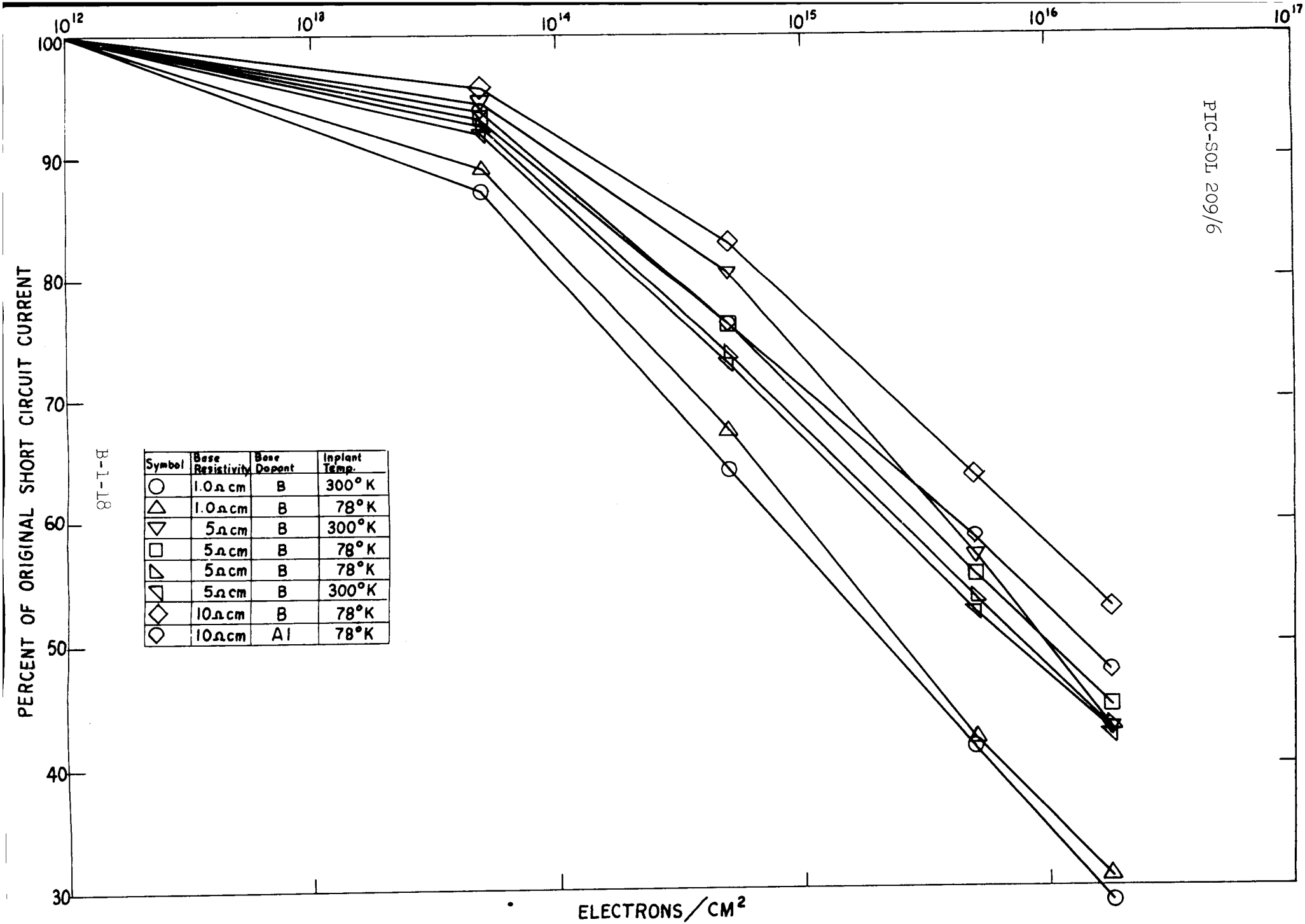

FIG. 11 PERCENT OF ORIGINAL SHORT CIRCUIT CURRENT VS DOSE (2800° K TUNGSTEN)

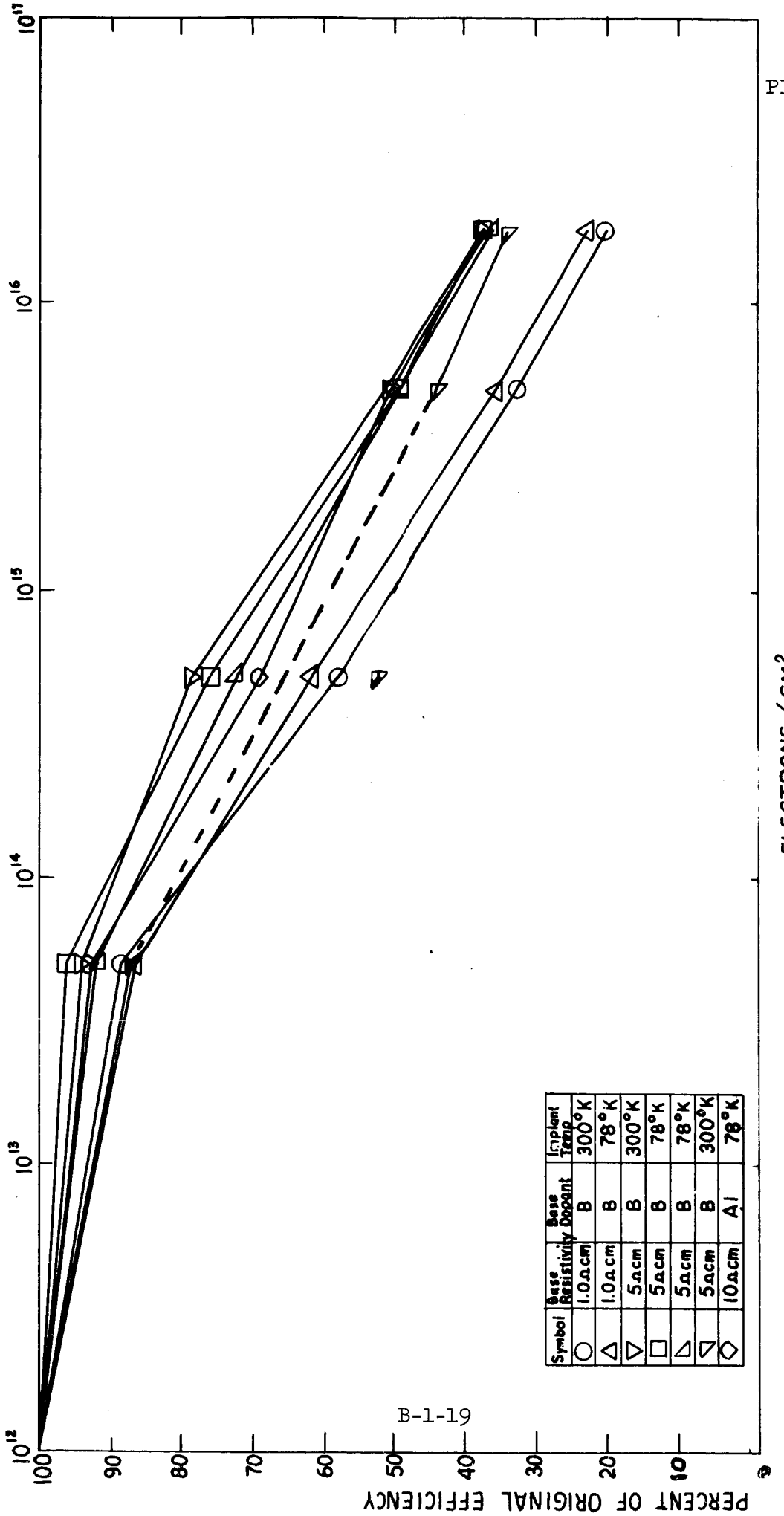

FIG. 12 PERCENT OF ORIGINAL EFFICIENCY VS DOSE (2800°K TUNGSTEN)

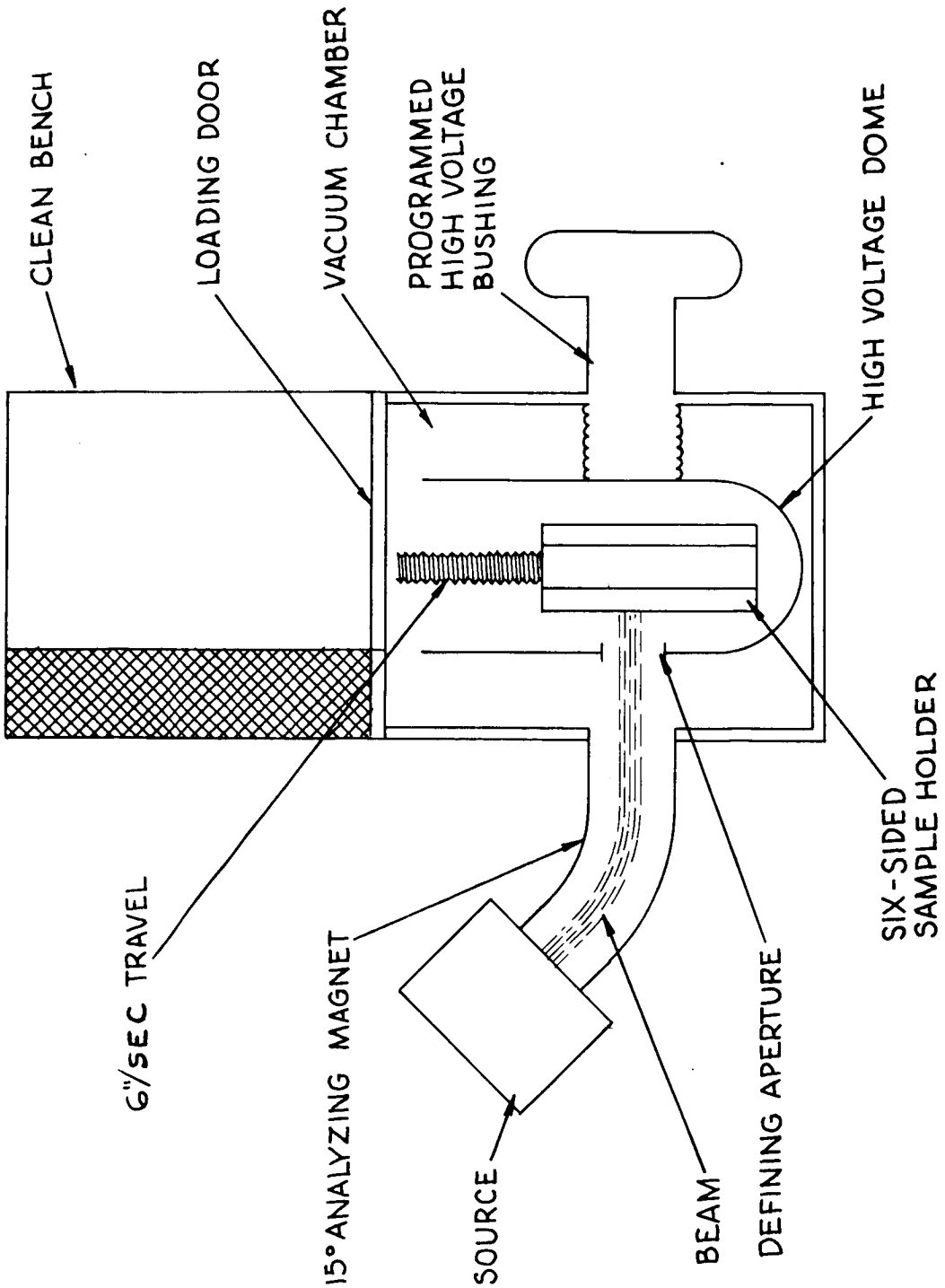

FIG. 13 **PRODUCTION MACHINE SCHEMATIC**

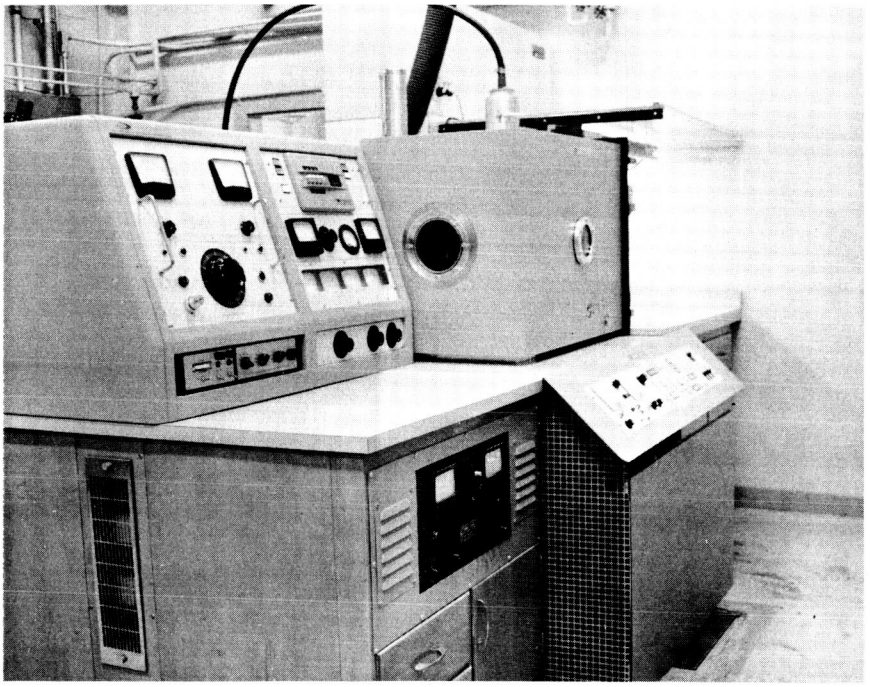

Fig. 14 Production Machine

Discussion

Oman: Thank you Mr. Burrill. Now, are there questions?

Weiner - RCA: I have several questions. One, what is the dimension of the cells you make?

Burrill: These are all 1 by 2 cm cells.

Weiner: Thank you. Secondly, you mentioned that you normally anneal these cells at 700 degrees for 16 hours.

Burrill: 750 at present...

Weiner: You also...

Burrill: Right.

Weiner: In other words, 600 degrees and annealing times as short as an hour.

Burrill: Right.

Weiner: What are the effects of these lower temperatures at shorter times?

Burrill: In that slide I think I showed that the annealing temperatures below about 700 degrees do not anneal completely. In other words, all the phosphorus ions implanted do not take up substitutional positions. At about 700 and above, they do, so that for optimum solar cell use, 700 probably would be about the minimum for annealing.

Weiner: And you mentioned that the time can be reduced...?

Burrill: The time can be reduced. That was about an hour, and going from one hour to 16 hours gives no change in shape or decrease in sheet resistance.

Weiner: I see.

Kaye - EOS: You mentioned life times before implantation of about 100 microseconds. Do you have any feel for the life time after implantation, and secondly, would you care to make some comments on the economic aspects. I understand you can make about 630 cells in an 8-hour shift on this machine. How would this compare in price with a - let's say a conventional diffusion furnace which could probably make a somewhat larger number of cells per shift?

Burrill: In answer to your first question, we have measured the life time after implantation and annealing, and there's no change.

Kaye: You're saying you still have 100 microseconds?

Burrill: On the particular 100 microsecond samples I can't say - those samples were the most recent and I haven't gotten the measurements back on them.

Kaye: Could you give us some further comparison before and after, then?

Burrill: Right. I can on data that we have on other cells, in which the life times start in the range of 20 microseconds. Those particular cells were measured before and after, and there was no change.

Kaye: How about the economic aspect?

Burrill: On the economics - we haven't, as I said, set up our production line at this stage, but there's no reason why it shouldn't be just as economical, if not more so, mainly because...

Kaye:...how about the capital cost of this machine, say compared with a 3 to 4 thousand dollar diffusion furnace which would have probably a higher output?

Burrill: Well, I don't know whether we want to get into the complete economics of it...

Kaye: Well, I think this is important. I mean, at this point you're saying you can make cells that are equivalent and you haven't made any projections that you can make better cells, so that the only advantage would appear to be one of cost, at this point, anyway.

Burrill: I think it's both. I think we did say that we can make better cells and that we have better control over the junction profile and that we can have better yield because of better control over this junction. And, also, it can be economical because one machine can produce 10,000 per week, and...

Kaye: But that's compared with the five thousand dollar diffusion furnace...

Burrill: But the difference isn't that much.

Kaye: Well, the only question I'm asking...do you have any idea...

Burrill: The mechanical parts of this machine will run somewhere around $25,000.

Kaye: Thank you.

King - IPC: The cost of the machine and parts is something over $20,000, with something like six months of a technician's time involved in building that apparatus. On the capital write-off; that machine can be used for a great variety of projects. It can be used to implant almost anything. It can be used to implant solar cells, radiation detectors, and many of the

other devices that we are making. Now, the capital cost, which can vary - I couldn't finalize it now - but it would be somewhere between 25 and 50,000 dollars to reproduce that machine on a production line basis - is not a deterring factor. This is a machine which will run ad infinitum. If you look at almost any production line, introducing a 25 to 50,000 dollar capital investment isn't that much. We appreciate the fact that the machine itself costs more than a diffusion furnace. But I think when one wants to make a comparison on how much a production unit is going to cost, one has to look at all aspects. You have to look at yield figures, you have to look at write-off on all your capital equipment, everything else that goes with it. You can't look at the machine itself - it's part of a process.

Voice: You use a diffusion furnace anyway to bake them.

King: The furnaces we use to bake these are nothing complex - nothing in comparison to good diffusion furnaces.

Oman: Maybe we should go into the technical aspect. There's a question in the back row.

Weiner: I'd like to pursue the financial one for a moment. (laughter) In the context of the question this morning, what would a 2 by 2 cost based on a 100,000 lot?

Burrill: I don't think any of them were particularly explicit on this either. (laughter)

Prince - EOS: I'd like to get back to the technical aspect, if you don't mind. You mentioned that you anneal at 750 degrees for 16 hours.

Burrill: Right.

Prince: Have you made any analysis of the distribution of impurities in the vicinity of the junction?

Burrill: I think my first slide showed the distribution.

Prince: I see. Okay. I'll try to get with you later.

Medved - EOS: I would like to pursue that question just one further step. Is it clear whether or not you're getting radiation enhanced diffusion?

Burrill: Yes. It's fairly clear that we're not. In other words...

Medved: On what basis do you make that statement?

Burrill: Because the implanted profiles, which we calculate when we want to implant and those that we measure after implantations are, within experimental error, the same.

Medved: You measure the profile before implant - before annealing?

Burrill: We theoretically calculate what we're going to implant and then we measure after the annealing step what was implanted. These are identical within our experimental error.

Medved: Well, we'll have to pursue that in private, but one further question in the same area; it also ties back to the original questions on economics. It wasn't clear to me what kind of stability requirements one will have in a machine of this type where you're moving a sample in a beam of reasonably small area compared to some of the large-area, large-diameter beams which are now available. I'm talking about beams which are hundreds of square centimeters of high uniformity and extremely high stability which have been employed in other programs, as you all well know. In this case, you have a beam which is no more than a few inches across, and you're making a sample traverse across it over a period of some time. What is the stability in this beam? And its uniformity?

Burrill: The stability is very good, and uniformity...

Medved: "Good" is not a scientific answer. I'd like to know what your stability is. (laughter)

Burrill: The stability, I don't know in what form you want to put it, the beam variation versus time?

Medved: Beam variation per hour.

Burrill: Beam variation is within a few percent over a time. And, as I said, the scan rate is 6 inches per second, which is quite rapid, considering the time of implantation.

King: It's absolutely irrelevant anyway, because it has nothing to do with it; a few percent of even 10% or 20% variation of that beam current has no effect on the cell. It's quite obvious if you look at the profile and consider what effect it's going to have on the cell performance, a 10% variation at some point in that curve is going to have no effect at all on the cell performance. The machine is designed primarily as a production apparatus. Now, if you want to design a research tool, go ahead. Now, we have research tools around which work pretty well. We have Van de Graaffs which we use for research in order to define the device parameters which are controlled, as you know, to 1 kilovolt in 400 kilovolts, or 1 kilovolt in 2 Mev, with very good current control. But the point is, this machine is designed as a productive apparatus; it's made to produce cells cheaply and in that context it is quite adequate in every respect. If you want us to go into exact details, I think some of them are what we consider proprietary, and the ones that we don't consider proprietary, we give.

Oman: I propose that you and he fight afterwards. (laughter) We'll have one more question.

Rappaport - RCA: I'm always concerned about the $64 question which comes

up with respect to ion implantation, that is, how much of it are you getting from the diffusion and how much are you getting from the acceleration of the ion into the semiconductor. Have you done the following experiment? Apparantly you can operate from something like 80 kv up to a few 100. Have you tried looking at like 80, 150 and 200 kv with the same current coming into the ion current going into the sample and then diffusing all of them under the exact same conditions and then see if your profile is indeed different?

Burrill: Yes, we have.

Rappaport: And the other question is: Have you tried just holding your annealing temperature to about 400 degrees even though it may take a long time, where probably you get less diffusion, much less than you would at 700? Because I think you can get solar cells with phosphorus baked at 7 to 750 for, you know, 20 to 30 minutes.

Burrill: I think one thing I did say was that one hour is sufficient and that we see no change in that extra time.

King: We have actually done very elaborate experiments in order to determine whether or not the concentration gradient changes a function of annealing time and implanted concentration. I'm giving that the latter part of this week at the IEEE meeting over at the Sheraton Park.

Rappaport: Could you discuss this a little.

King: Sure, if you want me to. The point is this; if one looks at a standard distribution curve for implanted ions of a given energy, one gets a Gaussian distribution with a mean range and a certain straggle, or peak width at the half-height. The junction depth is determined by the point where the active implanted concentration, after annealing, equals the number of impurity ions corresponding to the background resistivity. For this purpose, it is important to note that almost all of the ions we implant become substitutional after annealing. By controlling the number of ions implanted per cm^2, one can control the absolute height of the distribution, and the cross-over point, or junction depth. Therefore, by controlling the number of ions one puts in, and the implantation energy, one can predict the junction depth as a function of energy. Now, we have done experiments by first implanting a given number of ions/cm^2 - in some uses with a predetermined controlled distribution - in which we successively anneal at 400°, 500° and up to 900° C, measuring the junction depth after each anneal. Within the accuracy of our experiment (approximately 0.1 micron), we see no detectable difference in junction depths from a 600° to a 900°C anneal. We see a slight decrease in sheet resistivity from 600° to 700°C as shown by the slide shown previously. We standardly anneal our solar cells at 750°C for 16 hours simply because it happens to be convenient. We put them in overnight and take them out next morning. Returning to the junction

---

Author's note: This section has diagrams on a blackboard; it has been rewritten to avoid including diagrams.

depth; one gets as a function of background resistivity, a family of curves (for a given implanted ion concentration) of junction depth versus implantation energy. Our experimental data agrees quite well with the calculated curves. So the standard range - energy curves which people have derived over a long period of time are quite effective in predicting junction depth and in predicting distributions that one achieves.

PIC-SOL 209/6
Section B-2

SOLAR CELLS FROM EXPITAXIAL GALLIUM ARSENIDE ON GERMANIUM

Presented by

K. H. Maxwell

Philco Applied Research Laboratory

Blue Bell, Pa.

18 October 1965

SOLAR CELLS FROM EPITAXIAL GALLIUM ARSENIDE ON GERMANIUM

K. H. Maxwell, L. C. Bobb, H. Holloway, and E. Zimmerman
Philco Applied Research Laboratory
Blue Bell, Pa.

Introduction

While gallium arsenide solar cells have some specific advantages, particularly for high temperature conditions, enthusiasm for the devices has been tempered by their high cost. The cost is due, largely, to the fact that good quality, single crystal gallium arsenide is expensive. Consequently, there has been much interest in the possibility of using epitaxial techniques to put down thin layers of GaAs on suitable substrates, Single crystal germanium is an obvious choice as a substrate for gallium arsenide deposition, principally because of the very small lattice mismatch between the two materials and the closeness of their coefficients of thermal expansion. Various methods have been tried in attempts to achieve epitaxy but the layers, while good by the normal standards applied to epitaxial films, are not perfect enough for the fabrication of semiconductor devices. This paper describes the techniques of preparation and characterization that have been evolved to produce high quality GaAs films on germanium substrates and the characteristics of some diodes that have been prepared in the epitaxial layers. Comparison is made with results obtained from epitaxial GaAs grown on single crystal gallium arsenide.

Preparative Method

The preparative method is a chemical deposition technique that has been used previously for the growth of GaAs films on GaAs substrates. The essentials are as follows: Pure hydrogen gas was bubbled through $AsCl_3$ at room temperature (vapor pressure $\sim$ 10 torr) and passed over metallic gallium which was held in the hot end of a two zone furnace. The resulting gaseous mixture then passed over germanium blanks (1 cm by 1 cm) at the cool end of the furnace, whereupon GaAs was deposited on the substrates.

Deposition Conditions

The effect of varying the preparative conditions was studied and the results are summarized below.

a. Temperature. The gallium boat was always held at 900°C while the temperature of the substrates was varied between 700° and 800°C in 10°C intervals. The best deposition was found to occur at around 760°C; below 730°C there was a definite decline in crystal perfection while above 780°C there was a drastic deterioration of the layers.

b. Flow Rate. The best range for flow rates in the one inch (O.D.) quartz tube was 200-400cc/minute. Lower flow rates than 200 cc/minute produced poorer epitaxial layers while increasing flows over 400cc/minute yielded diminishing amounts of deposition and, eventually, net etching of the substrates. Typically, the deposition rate was 50-70 microns GaAs per hour.

c. Saturation of Gallium with Arsenic. It was found necessary to saturate the gallium with arsenic before using it in a reaction, otherwise arsenic did not transport down the tube but merely dissilved in the gallium. The solubility was about 2 molar percent.

d. Introduction of Reactants. It was found important that the $AsCl_3$ flow should be started over the substrates before inserting the gallium boat. The initial deposit was thus formed in the presence of a considerable excess of arsenic.

Crystal Perfection of the Epitaxial GaAs

Perfection of the epitaxial layers was evaluated by measurement of the width of the Bragg peak using a double crystall diffractometer. With a low dislocation density germanium (111) first crystal and $CuK\alpha_1$ radiation, the layers prepared under optimum conditions exhibited rocking curves similar to those from bulk GaAs and with widths differing by less than ten percent from that calculated from the Darwin-Prins equations.

We have found that the width of the X-ray rocking curve provides a useful, though semi-empirical, measure of perfection which correlates well with the device quality of the epitaxial layers. Thus, poor quality layers contain large numbers of low-angle boundaries which provide paths for anomalously rapid diffusion of dopants hence degrade the quality of the diode. The presence of these low-angle boundaries is indicated by an increase in the width of the X-ray rocking curve. The rapidity with which the X-ray measurement can be made has proved invaluable in optimization of the conditions for growth of gallium arsenide on germanium.

Orientation Dependence of Perfection

We have found that growth of good-quality arsenide on germanium requires careful selection of the substrate orientation. Attempts to grow the GaAs on a Ge(100) or (110) substrate give poor quality layers because the GaAs can nucleate in two orientations both of which are parallel to the Ge substrate but which differ in the arrangement of their polar <111> axes; this is true of growth of GaAs in any nonpolar direction. With growth of the GaAs in a polar direction, one may have a difference in energy between the nuclei of the two kinds of parallel oriented nuclei, (the nuclei may be distinguished as having their A or B faces next to the substrate). However, growth on Ge(111) does not lead to high-quality layers. We suspect that this may be a consequence of residual contamination in the epitaxial growth system. Thus, none of the three low-index faces of Ge have given high-quality epitaxial layers. In an attempt to compromise between the substrate orientation-dependent occurrence of doubly oriented nuclei and the residual contamination, which we would also expect to depend upon

substrate orientation, we have grown layers upon Ge substrates with orientations intermediate between the polar (111) and the nonpolar (100) faces. This has led to high-quality epitaxial GaAs on Ge. The optimum substrate orientation is not yet well-defined. Most of our work has been with Ge(311) but we have also obtained good results with Ge(511) substrates.

Electrical Properties

Studies were made of the electrical properties of the GaAs films epitaxially deposited on Ge and GaAs substrates. The approach used was to fabricate junction diodes in the film and deduce the electrical properties of the material from diode analysis. Diodes were prepared by diffusion using a sealed tube containing both As and Zn maintained at a temperature of 720°C for one hour. Angle lapping and staining showed a flat parallel junction approximately 2 microns deep. Standard techniques were used to fabricate mesa diodes. Junction cleanup was accomplished by chemical etching and measurements were made directly on the diodes without any further surface treatment. Detailed I-V plots were made of the diodes as were C-V measurements. The C varied as the inverse square root of V indicating that these are abrupt junctions and the barrier height was found to be 1.25 volts. The I-V measurements were made as a function of temperature from 77°K to 300°K and above 150°K the forward characteristic showed an $e^{qV/nkT}$ dependence with $n \approx 2$.

The characteristics of a diode fabricated in the GaAs film deposited on Ge(311) are shown in Figure 1. If the forward characteristic is extrapolated to zero volts, a space charge generated current of about 6×10^{-13} A is predicted. Using the Sah, Shockley, Noyce assumption and combining this space charge generated current with the diode area and the diode zero bias capacitance a value of lifetime $(\tau_p \tau_n)^{\frac{1}{2}}$ of 2.5×10^{-10} was calculated on this diode. In the upper right hand corner is the curve tracer photo of this diode showing a diode breakdown of 5 volts.

In Figure 2 is shown the characteristics of a diode made from GaAs deposited on a GaAs substrate of (110) orientation. The epitaxial film for this diode and for the one shown in Figure 1 were deposited simultaneously. The same type of analysis showed a space charge generated current of 3.5×10^{-12} A, and a lifetime of 6.5×10^{-10}. The reverse breakdown was 15 volts. The donor concentration was found to be 3.2×10^{15} in this case, while, for the diode (Figure 1) where the substrate was Ge rather than GaAs, $N_D \simeq 1.9 \times 10^{17}$. This difference can be attributed to Ge doping of the film deposited on Ge.

This analysis indicated that GaAs epitaxed on Ge substrates was of good quality both metallurgically and electrically and should be adequate for solar cell fabrication. The fabrication process used for the GaAs solar cells was as follows. The epitaxed wafer of GaAs on Ge (1cm by 1 cm) was cleaned and given a light chemical etch before the junction was formed by diffusing zinc. The junction depths after diffusion were 1-2 microns. The back (Ge side) and edges were lapped and chemically polished to remove

the back junction before the bottom contact was made. This contact consists of a Sn-Sb deposit. The top contact which is Au-Ag is then evaporated. At this point we alternately etched the junction and tested the cell using a 100 mw/cm^2 simulator to optimize the junction depth. While it has been possible to make a number of 1 cm^2 cells using this technique a problem arose in the majority of large area cells. Many of the large cells showed a shunt resistance which, while it could be eliminated by continued etching, usually resulted in the junction depth being reduced until it was too shallow. At this point while the V_{OC} measured was on the order of 0.8 - 0.9 V the I_{SC} was so low as to make the cell useless. A number of 1 cm^2 cells which showed this shunt resistance initially were cut into smaller area cells (10^{-1} cm^2) instead of being subjected to vigorous etching. In most cases it was possible to locate the area which was responsible for the shunt. Examination of the problem area has not yet revealed the cause of this shunt resistance.

Figure 3 shows the I-V characteristic of one of the GaAs-Ge cells that was cut from a 1 cm^2 cell which showed this type of resistance. Efficiencies of 7-9% were typical values for these small cells. No particular effort was made to optimize the cell structure, i.e., no grid structure contacts were used nor was any attempt made to use an antireflection coating. Thus, further improvement is possible even with the present films.

Conclusions

We have demonstrated that GaAs may be grown heteroepitaxially upon Ge to give diodes with properties equivalent to diodes in bulk GaAs. This could make possible the production of GaAs solar cells at a cost significantly lower than is possible using bulk GaAs.

There remains a major technical problem. Our diodes have been made with small areas and attempts to extend the work to areas around 1 cm^2 give diodes which are shunted. This behavior is similar to that caused by low-angle grain boundaries which provide a rapid path for diffusion of the Zn depant down to the Ge substrate. However, examination of these layers by X-ray topography fails to reveal grain boundaries. We speculate that the shunts are caused by failure to completely clamp the growth to a single orientation. The boundary between the two orientations is incoherent and would be expected to behave like a grain boundary. We know that contamination can produce, even on Ge(311), layers whose surfaces are mixtures of (311)A and (311)B, but detection of small amounts of the second parallel orientation is difficult.

Work is in progress to check our hypothesis that the shunts are due to double orientation and to attempt to eliminate them by growth under more rigorously controlled conditions.

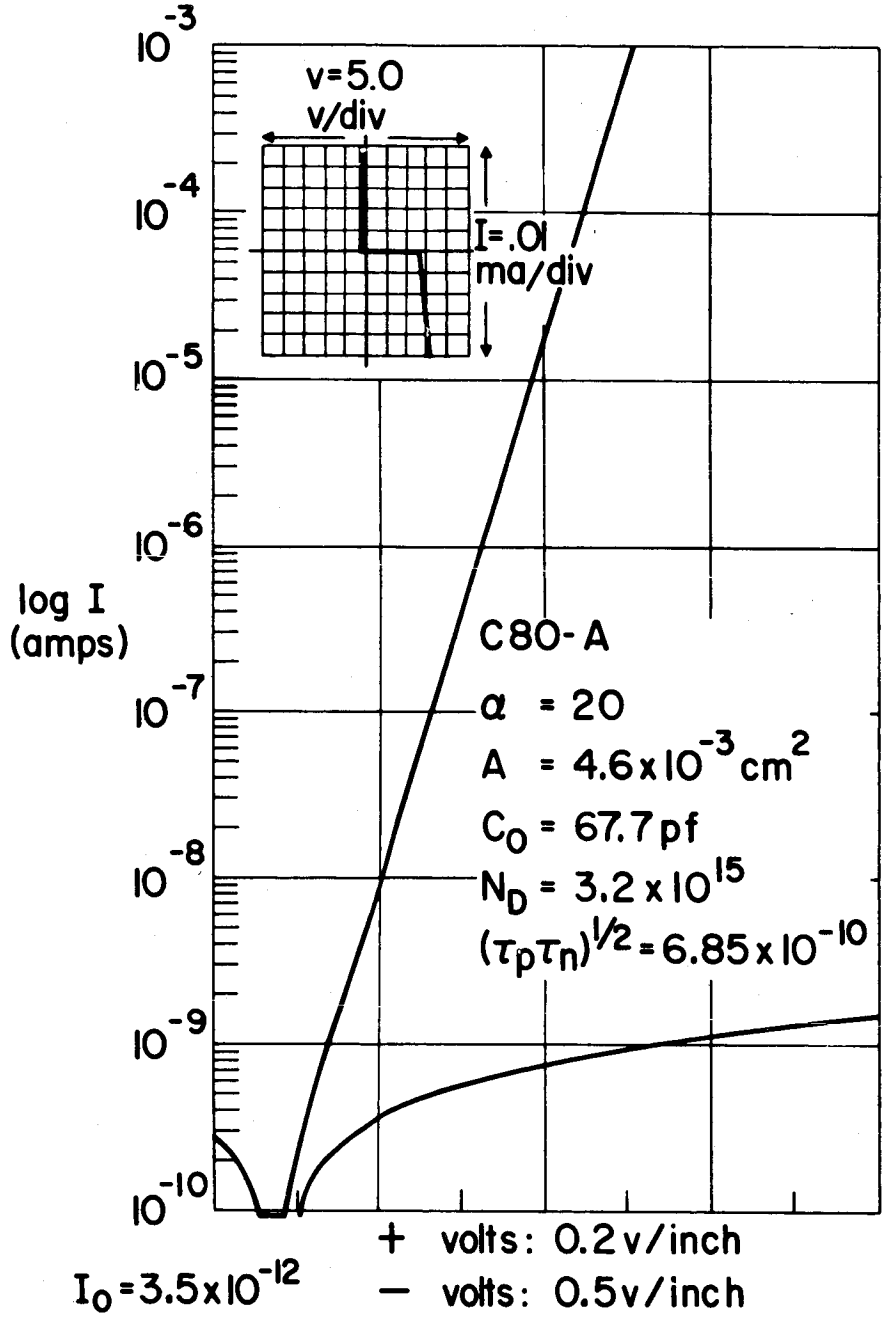

Figure 1. Characteristics of Diode in Epitaxial GaAs on Ge.

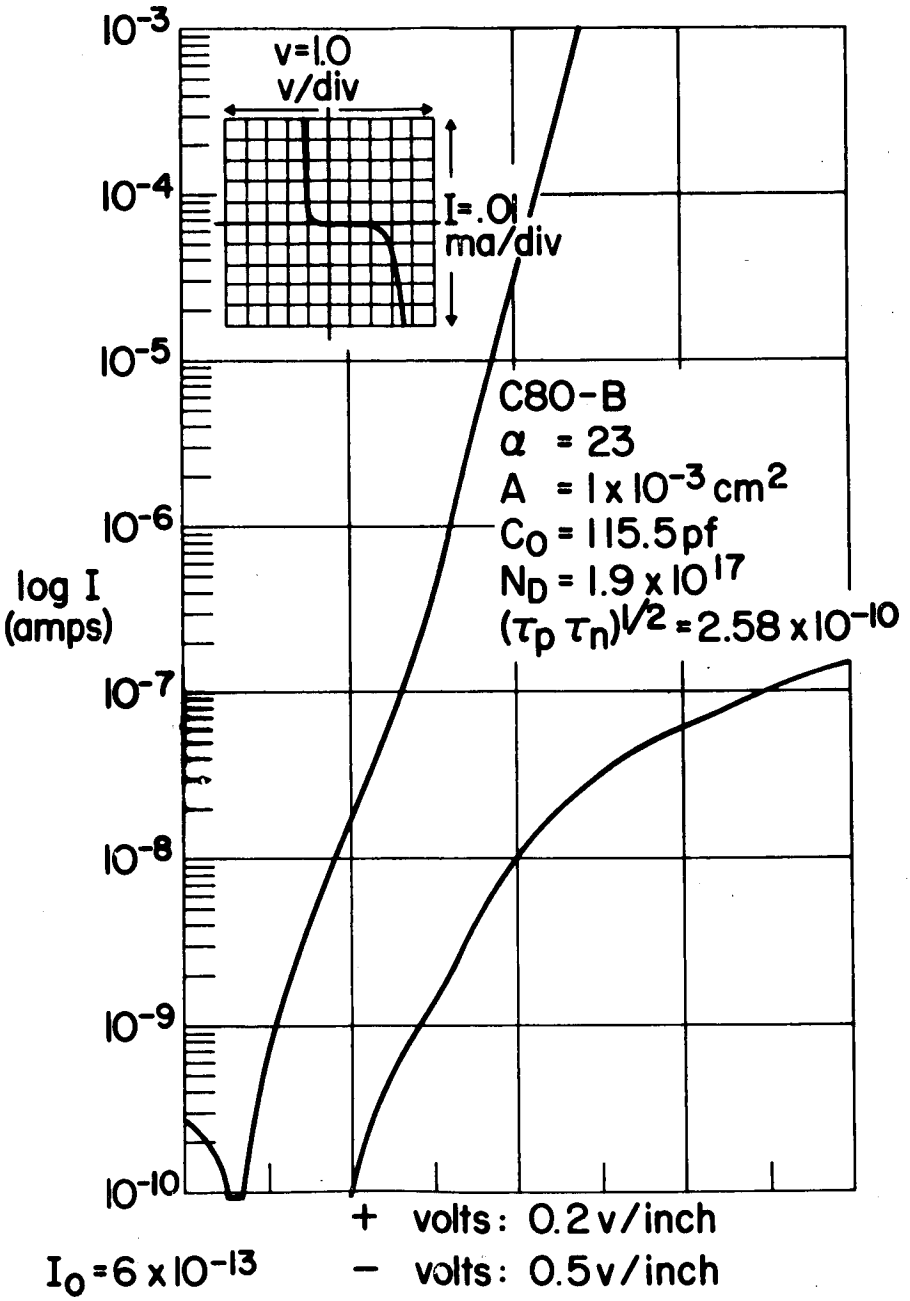

Figure 2. Characteristics on GaAs.

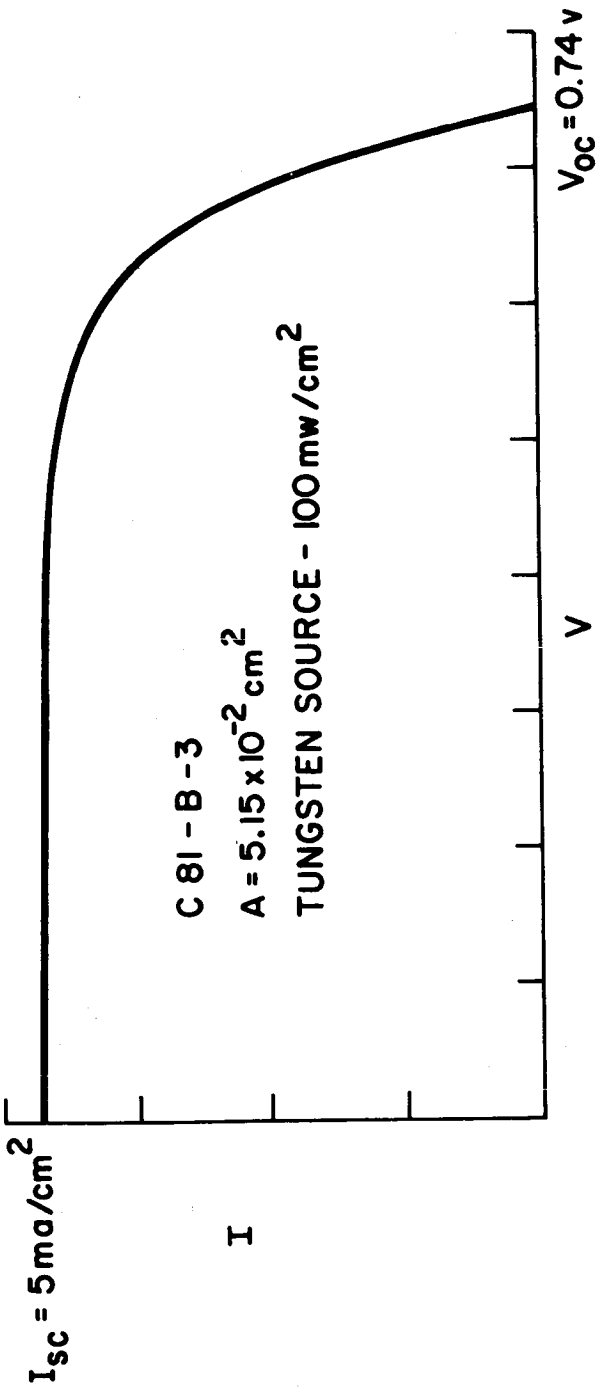

Figure 3. Photoresponse of Diode from GaAs on Ge.

PIC-SOL 209/6
Section B-3

IMPURITY PHOTOVOLTAIC EFFECT IN CADMIUM SULFIDE*

Presented by

John Blair

Department of Electrical Engineering

Massachusetts Institute of Technology

18 October 1965

* Work supported in part by the National Aeronautics and Space Administration Grant NsG 496

17316

Abstract

Photovoltaic cells were fabricated by evaporating a thin copper layer on low resistivity single crystal n-type cadmium sulfide. It was found that the spectral response of the cells in the infrared was enhanced by as much as two hundred fold when the cell was illuminated by radiation with energy corresponding to the energy gap (green light). The enhancement of the infrared photovoltaic response is attributed to creation of additional minority carriers by transitions of electrons from the valence band to impurity levels. These impurity levels were emptied by the green excitation making infrared transitions to the impurity states more favorable. The net effect is the broadening of the spectral response of the cell. Transient measurements of the emptying and filling of the impurity states were made by illuminating the sample from two monochromatic light sources. The recombination statistics of holes was analyzed. A single recombination level model was adequate to explain the results. Recombination center concentration and hole and electron capture cross sections were calculated with the results:
$N_r = 1.3 \times 10^{17}/cm^3$, $S_n = 1.2 \times 10^{-23} cm^2$ and $S_p = 2.08 \times 10^{-20} cm^2$.

Author

IMPURITY PHOTOVOLTAIC EFFECT IN CADMIUM SULFIDE*

Nguyen Duc Cuong** and John Blair
Department of Electrical Engineering
Massachusetts Institute of Technology

Introduction

High efficiency solar cells can be achieved with a proper material which makes a better use of the solar spectrum. It has been proposed(1) that the presence of impurity levels in the forbidden gap can facilitate the generation of carriers by photons with energy lower than the gap energy. Such possibilities are investigated in CdS single crystals.

Properties of CdS single crystal devices were studied. The crystals had a high conductivity, 0.4/ohm-cm, a good mobility, 280 cm^2/volt sec., an electron concentration of $10^{16}/cm^3$, all values at room temperature. Shallow traps and deep impurity levels were detected.

The photovoltaic effect (PVE) was studied in a Cu-CdS structure. A thin layer of copper was evaporated onto one side of the crystals, with no heat applied afterward. In general cells made this way were good diodes and operated similarly to silicon pn junction solar cells when illuminated. It is shown here that minority carriers were the origin of the effect.

Spectral response curves were recorded. Response in the infrared was fairly marked. It was observed that the response of the cell in the long wavelength region was enhanced considerably when green light was present. A model was derived to explain this effect. Impurity levels were the origin of the enhancement. The relaxation processes of these levels were studied from which basic parameters were calculated.

---

* Single crystals of cadmium sulfide were supplied by the Clevite Corporation, Cleveland, Ohio.

** This paper is based in part on an Electrical Engineer's thesis submitted to the department of Electrical Engineering, M. I. T., in June 1965.

The PVE in Cu-CdS structure has been observed by many workers but there is no uniformity of opinion concerning the origin of the photo-EMF.

With the copper layer deposited by electroplating and no heat subsequently applied, Williams and Bube[2] argued that electrons are being emitted from the metal side.

E. D. Fabricius[3] argued, however, that electrons are coming from the semiconductor side, in other words excited in the depletion layer mostly, and holes created conduct through the 3d copper level. However, in this case cells were submitted to a heat treatment and some copper had difussed into the semiconductor.

Woods and Champion[4], as well as Grimmeiss and Memming[5], supported this theory. One effectively has a pn junction at the contact. Copper is believed to be an acceptor in CdS and a very thin layer of p-type CdS is formed. The highest value of open circuit voltage reported is 0.63 volt.

D. C. Reynolds et al.[6] postulated the existence of an intermediate band in the forbidden gap, consistent with the model of conduction formulated by Brosser et al.[7]. Holes are believed to be bounded and cannot migrate to the metal, but electrons located in the intermediate band are assumed to be mobile and always in thermal equilibrium with the electrons.

It is also possible that one has here an heterojunction. Keating[8] reported good rectifying properties with diodes made with Cu_2S and CdS. It is conceivable that copper has reacted partially with sulfur atoms to form Cu_2S. However in this case minority carriers would still be the dominant effect.

It is believed in this work that minority carriers are the main cause in the creation of the photo-EMF. The mechanism is similar to that of a pn junction. Holes generated optically diffuse toward the boundary layer, then are accelerated through the depletion region by the existing static field. This model explains more satisfactorily the results obtained. It is still open to question, however, whether one

has a pn junction, in the sense that a thin layer of p-type CdS is formed, or a metal-semiconductor contact, or an heterojunction. Electron emission from the metal is discarded, or if it exists, it should be a second effect only.

Sample Preparation

Cut into the size of 5 by 5 by 1 mm, samples were polished, then rinsed with ammonium hydroxide for about two or three minutes then etched[2] with a strong solution of HCl and HNO_3 for roughly 30 sec. The copper contact was then evaporated onto one side, under a 1.5×10^{-5} mmHg pressure in a modified 18A Coater (Consolidated Electrodynamics). The thickness of the copper layer on all samples was about 400A, 500A. Indium contact was then made to the other face with an ultrasonic soldering iron. Copper wire was glued to the copper layer with "silver paint", whereas it was soldered directly to the indium contact.

The sample geometry is shown in Figure 1. It is believed that during the whole process no copper diffuses into the semiconductor. No heat was applied except for a brief moment during the soldering of the indium contact. A thin layer of copper is fairly transparent thus allowing both front and back illumination.

It was observed often during the etching process that the two large faces, which are perpendicular to the optical axis were not alike. One side was shiny, the other side was dull. Copper evaporated on different sides had also a different appearance. A metallic look was obtained when evaporation was done on the shiny side, a bluish look was obtained when it was done on the dull side of the crystals.

It is believed that this behavior in II-VI compounds is similar to that of III-V compounds. Gatos[9,10] had observed two different types of surfaces in InAs, designated surface A and B, with the orientation (111) and $(\bar{1}\bar{1}\bar{1})$. Due to the crystal structure, layers of In and As atoms alternate, such that is one face is In atoms the opposite face is As atoms. This kind of picture may be observed here. Copper might have reacted with sulfur to give some copper and sulfur compound that has a bluish look. It was observed that cells with this surface had poor rectifying

properties. However, when the copper layer had apparently not reacted with CdS, the cells had good rectifying properties.

Recorded on the curve tracer, the V-I characteristic in the dark showed good rectifying properties (Figure 2). In general, the experimental diode relation was found to be:

$$I = I_s(e^{qV/AkT}-1) \qquad (1)$$

where A varies between 1.5 and 2.0. It has been reported as high as 4.

Generally the reverse bias current saturated. A further increase in reverse bias produced a gradual breakdown at about 10-15 volts.

Under illumination, the cell behaved similarly to silicon solar cells (Figure 3). The maximum open circuit voltage recorded was 0.4 volt when the cell was illuminated by a focused microscope lamp. Cells deteriorated when exposed to air, after a period of two months, the open circuit voltage was reduced and the rectifying properties became poor.

Impurity Photovoltaic Effect

Spectral Response and the Effect of Combined Radiation

Under weak illumination, the photovoltaic current can be written:

$$I_L = I_{so}(e^{qV/AkT} -1) = I_{so}qV/AkT \qquad (2)$$

This approximation is fairly good for V less than 15 mv. or so since A is about 1.8. Open circuit voltage was recorded in all subsequent experiments.

The same set up for photoconductivity measurement was used to record the spectral response of the cells. The signal, chopped at 13 cps, was fed to an a-c amplifier then to the Speedomax G recorder. Responses were then normalized to incident unit energy. Of more than a dozen cells made and tested, a typical response is shown in Figure 4. For front illumination (copper layer side), the response peaked at the energy 2.45 ev., which corresponds to the band gap energy, then dropped off rapidly toward longer wavelength. It also dropped off rapidly toward shorter wavelength because the response is proportional to the number of incident photons and the curves here were normalized to incident unit energy. For back illumination (crystal side), the response cut off roughly at the band gap, because the

crystal is an effective filter for wavelengths shorter than 0.51 micron. However, response in the long wavelength region was larger when illuminated from the back, probably because the copper layer absorbed some of the radiation before it reached the junction whereas the crystals did not absorb as much. A difference by a factor of two or three was usually observed.

A secondary source of radiation simultaneously illuminated the cell and the spectral curve was recorded again. In most cases, no appreciable change in response was observed. However, one cell, subsequently designated Cell A, showed a very interesting behavior under secondary illumination. It should be noted here that the secondary illumination was a d-c light, whereas the spectral response was due to chopped light from the Perkin-Elmer monochromator referred to as primary illumination. The following observations were made:

As the wavelength of the secondary illumination was changed, the primary response peaked when the secondary illumination was green (0.51 micron), then dropped off on either side.

With green light as secondary illumination, the primary response was much enhanced in the long wavelength region. A factor as high as 200 was recorded. Figure 5 shows the striking difference.

As the intensity of the secondary illumination was increased, the primary response increased accordingly. Figure 6 shows the ratio of the response with secondary illumination (designated as activated response) to the response with no secondary illumination (designated as dark response). There are different peaks in the enhancement that shift noticeably toward longer wavelength as the intensity of green light is increased. The enhancement did not seem to saturate, it probably would at higher green light intensity.

A similar enhancement effect has been reported by Woods and Champion[4], due to secondary illumination of wavelength equal to 0.9 micron, and only at 0.7 micron of the primary response. A factor of four was reported in the enhancement of the short circuit current.

The effect of the impurity levels of the PVE is believed to be observed here. The presence of green light disturbs the equilibrium of the impurity levels in such a manner as to give rise to an enhancement. The rest of the paper is concerned with the investigation of this effect. An attempt to explain it and to represent it by an adequate model will be made.

Relaxation of Recombination Centers

The response in the long wavelength region is attributed to the presence of impurities in the forbidden gap. To study the relaxation processes of those levels, i.e. the change in population of those levels with time when the excitation is on or off, the following method was used, as illustrated in Figure 7.

This "continuous probing" method[11] is basically the modulation of two excitations at two different frequencies so that by observing the total signal on an oscilloscope screen, it is possible to discern the effect due to each illumination separately when they are both on simultaneously. It is obvious that this method can be extended to more than two excitations. The two different frequencies used were 13 cps and d-c light.

Different wavelengths were probed in this manner. It was observed that they all behaved in the same way, with a difference in relaxation time. Figures 8 and 9 show the result for $\lambda = 0.93$ micron. Secondary illumination was green light provided by a grating. Figure 10 shows the relaxation for $\lambda = 0.63$ micron. The relaxation time is about twice as large (the relaxation time is defined as the time to reach half the steady state value). Due to the long relaxation times observed, the secondary illumination was turned on and off manually.

The following conclusions are made:

1. The presence of green light (d-c) enhanced considerably the infrared response (13 cps) as was recorded before. This method, however, allowed the direct observation of the relaxation processes.
2. Relaxation time is relatively long, compared to visual phenomena observed in semiconductors. It varies between 0.5 sec. and 1.0 sec.

3. The difference between the lower and upper envelope is obviously the relaxation of the level corresponding to the wavelength being used.

4. Difference in relaxation time means probably that the levels are discrete, having different relaxation constant.

In order to see the effect of the infrared on the green, the infrared beam (13 cps) was turned on when the response to green light had already reached a steady state value. Figure 11 shows the result. A large transient was observed in the infrared response, whereas the green response was decreasing slowly (lower envelope). This transient behavior was not observed when no secondary illumination was present. It was also observed to vary in relaxation time for different wavelength.

Population of Recombination Centers and Minority Carrier Lifetime

The previous observations can be explained in qualitative terms as follows: The presence of green light depopulates the impurity levels (Appendix I); as a result two things occur:

1. More states are available for transitions from the valence band; the quantum yield is then increased and more holes are created for the same number of photons.

2. Since hole lifetime is inversely proportional to the number of electrons in the recombination centers, assuming that all recombination processes are indirect, it also increased correspondingly.

For a quantitative analysis, an energy band diagram is shown in Figure 12. The generation rate, g, is due to green light and f due to infrared light. They are both assumed to be constant. It is also assumed that most of the infrared excitation is from the valence band to the impurity level.

Under equilibrium condition $g = 0$, $f = 0$ (Appendix I):

$$R_{ct} = r_c n_o p_{ro},\ R_{tc} = r_c n_{ro} n_1 \text{ and } R_{ct} = R_{tc} \qquad (2)$$

$$R_{tv} = r_v n_{ro} p_o,\ R_{vt} = r_v p_{ro} p_1 \text{ and } R_{tv} = R_{vt} \tag{3}$$

For the condition $g \neq 0$, $f = 0$, we have:

$$g = R_{ct} - R_{tc} = R_{tv} - R_{vt} \tag{4}$$

where $R_{ct} = r_c(n_o+\Delta n)\ (p_{ro} - \Delta n_r)$ (5a)

$$R_{tc} = r_c(n_{ro}+\Delta n_r)\ (n_1) \tag{5b}$$

$$R_{tv} = r_v(n_{ro}+\Delta n_r)\ (p_o+\Delta p) \tag{5c}$$

$$R_{vt} = r_v(p_{ro} - \Delta n_r)\ (p_1) \tag{5d}$$

and the neutrality condition is:

$$\Delta n + \Delta n_r = \Delta p \tag{6}$$

Δn and Δn_r and Δp are the disturbances introduced by g.

For the condition $g \neq 0$, and $f \neq 0$, we have:

$$g = R_{ct} - R_{tc} \tag{7}$$

$$f + g = R_{tv} - R_{vt} \tag{8}$$

where $R_{ct} = R_c(n_o + \Delta n + \Delta n')\ (p_{ro} - \Delta n_r - \Delta n_r')$ (9a)

$$R_{tc} = r_c(n_{ro}+\Delta n_r+\Delta n_r')\ (n_1) \tag{9b}$$

$$R_{tv} = r_v(n_{ro}+\Delta n_r + \Delta n_r')\ (p_o+\Delta p + \Delta p') \tag{9c}$$

$$R_{vt} = r_v(p_{ro} - \Delta n_r - \Delta n_r')\ (p_1) \tag{9d}$$

and the neutrality condition is:

$$\Delta n' + \Delta n_r' = \Delta p' \tag{10}$$

$\Delta n'$ and $\Delta n_r'$ and $\Delta p'$ are the disturbances introduced by f.

Combining Equation (2) with Equation (10), we obtain:

$$\Delta n_r' = \Delta n' \frac{p_{ro} - \Delta n_r}{n_o+n_1+\Delta n+\Delta n'} \tag{11}$$

and $f = r_v(n_{ro}+\Delta n_r+\Delta n_r')\ (\Delta p') + r_v(p_o+p_1+\Delta p+\Delta p')\ (\Delta n_r')$ (12)

For small disturbances, we see that using Equation (11), the second term of Equation (12) can be neglected, and finally:

$$\Delta p' = f/r_v(n_{ro}+\Delta n_r+\Delta n_r') \tag{13}$$

$$= f/r_v N_r f_r \tag{14}$$

where f_r is the Fermi factor for the impurity level:

$$f_r = 1/(1 + e^{(E_r-E_{fr})/kT}) \tag{15}$$

E_r is the location of the level in the gap and E_{fr} the Fermi level for the impurity level.

The following conclusion can be made: For a given f, $\Delta p'$ could be made to increase by depopulating N_r, in other words decreasing the Fermi factor f_r. This process can be looked upon as increasing the hole lifetime, since normally hole lifetime is defined as:

$$\Delta p' = f(\tau_h) \tag{16}$$

However for this effect to be appreciable, the Fermi level E_{fr} has to move down at least as low as E_r from the equilibrium location which is near the conduction band. The impurity levels will be then almost empty.

This will not explain the smaller enhancement in the region of wavelength shorter than 0.51 micron. An increase in hole lifetime should give an enhancement that is the same for all wavelengths. As shown in Figure 6, such is not the case.

For a given number of incident photons, the number of excitations from the valence band to the impurity level is proportional to the number of electrons in the valence band and the empty states of the impurity levels into which the transition may occur. This can be written as:

$$f = KN_v p_r = KN_v N_r(1-f_r) \tag{17}$$

where K is a constant, N_v the effective density of states in the valence band and p_r the number of empty states in the impurity levels. Since:

$$1 - f_r = f_r\, e^{(E_r-E_{fr})/kT} \tag{18}$$

Equation (14) is reduced to:

$$\Delta p' = (KN_v/r_v)\ (e^{(E_r-E_{fr})/kT}) \tag{19}$$

Hence a small variation in E_{fr} can change $\Delta p'$ considerably.

The enhancement effect is thus shown to be due to two things:

1. An improvement in quantum yield for long wavelength by depopulating impurity levels.
2. A slight improvement in hole lifetime as a result of the depopulation, as observed in the region of wavelength shorter than 0.51 micron. There is no improvement in quantum yield in this region.

Relaxation Curves: Experimental and Theoretical

When green light is turned off, electrons fill up the impurity levels again, the infrared response decreases. The difference between the upper and the lower envelope is then the relaxation process as a function of time. The continous curve of Figure 13 was obtained in this manner from Figure 9. A theoretical curve for the process can be derived, from which a numerical value for the relaxation time can be obtained. Figure 14 depicts the model for this process.

When green light is turned off, the traffic between the impurity levels and the valence band establish "quasi-equilibrium" first, assuming for the moment that the levels have a larger capture cross section for holes than for electrons. Since the infrared response is directly proportional to the number of empty states at the impurity levels, we are concerned with the variation of Δn_r with time.

From Figure 14, we can write:

$$d(\Delta n)/dt = R_{tc} - R_{ct} \tag{20}$$

$$= r_c(n_{ro}+\Delta n_r)(n_1) - r_c(n_o+\Delta n)(p_{ro} - \Delta n_r)$$

Using the condition of Equation (2), and the neutrality condition:

$$\Delta p_r = \Delta n = \Delta n_r \tag{21}$$

Equation (20) can be written:

$$d(\Delta n)/dt = -r_c(n_o+n_1+p_{ro}+\Delta n)\ \Delta n \tag{22}$$

For small disturbances, and since:

$$n_o \gg n_1$$

$$n_o \gg p_{ro}$$

Equation (22) becomes:

$$d(\Delta n)/dt = -r_c n_o(\Delta n) \tag{23}$$

The solution is:

$$\Delta n(t) = \Delta n_o(e^{-r_c n_o t}) \tag{24}$$

Since the infrared response is assumed to be proportional to the number of empty states in the impurity levels, or:

$$\Delta p' = Ap_r \tag{25a}$$

$$\Delta p' = A(p_{ro}+\Delta p_r) \tag{25b}$$

$$\Delta p' = A(p_{ro}+\Delta n_o\, e^{-r_c n_o t}) \tag{25c}$$

Where A is a constant of proportionality.

Going back to Figure 9, the enhancement was measured to be about 10, which means that:

$$\Delta p'\ (t = 0) = \Delta p'\ (t = \infty) \times 10 \tag{26}$$

Using those boundary conditions, and dividing the vertical scale of Figure 13 into 10 arbitrary units, the final form of (25c) that fits best the experimental curve is:

$$\Delta p'\ (t) = 9e^{-1.5t} + 1 \tag{27}$$

Hence: $r_c n_o = 1.5\ (\text{sec.})^{-1}$ (28)

Minority Carriers vs. Electron Emission

The basic assumption made so far is that the origin of the photo-EMF is the existence of minority carriers. In this section, additional informations will be gathered to support the assumption.

Recovery time of the cells were recorded for different reverse bias voltages. A light pulse of 5μsec. duration was provided by a xenon lamp.

The short circuit current was observed across an 11 ohm resistor, as shown in Figure 15a.

When the cells were illuminated from the front side, two regions were observed in the recovery time: a fast region, with a time constant of about 15μ sec., and a slow region with a time constant of about 100μ sec. As the reverse bias was increased, the magnitude of the response increased. The time constant of the fast region decreased and approached the shape of the light pulse in the limit, whereas the time constant in the slow region stayed the same. Figures 15b and 15c show the recovery times for various bias conditions.

When the cells were illuminated from the back (crystal side), the same phenomena were observed, except that there was no change in time response of the fast region with increase in back bias.

The following conclusions can be made:

1. Such slow recovery time rules out electron emission as the mechanism in the creation of the photo-EMF, at least not as a first order effect.

2. The RC effect is discarded, because increasing the back bias actually increases the RC effect: R becomes large faster than C decreases. The two regions in the recovery time can be explained as follows: The bulk of excited carriers is located within a distance equal to $1/\alpha$ from the surface, where α is the absorption constant. For wavelength shorter than 0.51 micron, α is roughly 2.5×10^6 m^{-1} (12) or larger. For wavelength longer than 0.51 micron, α is smaller. The first region in the recovery time is then due to the diffusion time of the minority carriers within a diffusion length from the boundary layer. The concentration at the boundary is zero, and the transit time across the depletion region is negligible. The second region in the recovery time is due to decay of minority carriers through recombination, and it should stay unchanged.

3. As the reverse bias was increased, the depletion region width

increased, from about 6.3×10^{-8} m. at zero applied voltage to about 1.5×10^{-7} m. at -2 volts. Since the penetration of light is always $1/\alpha$ or less, which is 4×10^{-7} m. in this case, the increase in width of the repletion region means that there are less minority carriers to diffuse toward the boundary layer, hence a shorter time, as it was observed.

4. When illuminated from the crystal side, the bulk of the generated carriers would be on the crystal side, near the surface. No change in recovery time was observed as the same amount of charge is diffusing, independently of the reverse bias.

5. The increase in response with increase in reverse bias was probably due to some leakage current. Good photodiodes do not display this kind of behavior. During the time the light was on, the cell was effectively short-circuited, a current due to minority carriers as well as a current from the circuit were flowing through the 11 ohms resistor. The first current is constant but the second current is not.

A Model for CdS

In order to explain the results obtained so far, the following model is proposed.

An idealized band diagram is shown in Figure 16. Shallow traps are omitted since they do not play any role in minority carrier behavior.

All impurity levels are represented by a single level, having an effective density of state and located at an effective level. The value 1.4 ev. was chosen from Figures 5 and 6. It is the value at which the spectral response cuts off and at which the enhancement is large. However the location of the level is not critical in the calculation of various parameters.

In the presence of green light, which corresponds to the absorption edge, the impurity levels depopulate. It is shown in Appendix I that the change in electron population of the impurity levels can be written as:

$$\Delta n_r = \frac{(r_c p_{ro} - r_v n_{ro})\Delta p}{r_c n_o + r_v \Delta p} \tag{29}$$

where Δp is the change in minority carrier concentration. Since in equilibrium, most states of the impurity levels are occupied, the condition:

$$r_c p_{ro} \gg r_v n_{ro} \tag{30}$$

can be satisfied, and as a result Equation (29) can be written simply as:

$$\Delta n_r = \frac{-r_v n_{ro} \Delta p}{r_c n_o + r_v \Delta p} \tag{31}$$

The depopulation has as a consequence an increase in available states for transition from the valence band to the impurity levels. The quantum efficiency, or the number of transitions per incident photon, is thus increased. It was thought that the depopulation process could be done with red light, corresponding to transitions from the impurity levels to the conduction band, but the enhancement effect was not observed and it is concluded that electrons located at those levels have a very small photon capture cross section, and transitions from the impurity levels to the conduction band are negligible compared to the transitions from the valence band to the impurity levels.

A quenching effect was observed instead of the enhancement when red light was used as secondary illumination. Red light is then populating the impurity levels and as a consequence decreases the states available for transitions from the valence band to the impurity levels. The quantum yield is thus decreased and a quenching effect is observed.

Initial large transients as shown in Figure 11 are also a consequence of the filling up of the impurity levels with electrons by the same excitation.

Determination of Some Basic Parameters

With the results obtained so far, it is possible to determine three basic parameters associated with the impurity levels: capture cross section for electrons, capture cross section for holes, and density of states.

As mentioned previously, all impurity levels are represented by an effective density of states, although there is evidence that they are actually discrete levels having different capture cross section for holes and electrons. The capture cross section calculated is also an "effective" capture cross section.

The following calculations are based on Figures 9, 13, and 15, and the results revealed in the discussion of Relaxation Curves.

From the relaxation of the impurity levels shown in Figure 8, and Figure 9, one can conclude that due to such long relaxation times, a short light pulse of 20μ sec. does not disturb the population of the impurity levels during the time it is on when photoconductive decay is measured. At the onset of the photocurrent decay, we should have:

$$\Delta n = \Delta p \tag{32}$$

Both holes and electrons are conducting. Assuming that holes are being captured first, the first decay time is due to hole decay, and since the impurity levels are still fully occupied, the time constant is:

$$\tau_h = (r_v N_t)^{-1} = 100\mu \text{ sec.} \tag{33}$$

When all holes are captured, the impurity levels are mostly empty, since Δn and Δp are very large, and electrons start falling down from the conduction band to the impurity levels with a time constant:

$$\tau_n' = (r_c N_r)^{-1} = 50 \text{ msec.} \tag{34}$$

It was shown in the section on Relaxation Curves.

$$r_c n_o = 1.5 \text{ (sec.)}^{-1} \tag{35}$$

Since:

$$r_c = S_n v_n \tag{36}$$

$$r_v = S_p v_p \tag{37}$$

where S_n and S_p are the capture cross section for electrons and holes respectively, and v_n, v_p the thermal velocity of electrons and holes respectively.

At room temperature:

$$v_n = (2kT/\pi m_e)^{\frac{1}{2}} = 1.2\text{x}10^7 \text{ cm/sec.} \quad (38)$$

$$v_p = (2kT/\pi m_h)^{\frac{1}{2}} = 3.7\text{x}10^6 \text{ cm/sec.} \quad (39)$$

m_e and m_h are the effective masses of electrons and holes with $m_e = 0.2m_o$ and $m_h = 2.1\ m_o$.

Combining Equations (32) and (39), and using:

$$n_o = 10^{16}/\text{cm}^3 \quad (40)$$

the following values are obtained for the capture cross sections:

$$S_n = 1.2\text{x}10^{-23} \text{ cm}^2$$

$$S_p = 2.08\text{x}10^{-20} \text{ cm}^2$$

and

$$N_r = 1.3\text{x}10^{17}/\text{cm}^3$$

for the trap density.

It should be noted here that hole lifetime is $\tau_h = (r_v N_r)^{-1}$ and this value checks also with the recovery time in the slow region as shown in Figure 15c.

For small disturbances, electron lifetime is:

$$\tau_n = (r_c n_o)^{-1}$$

Hole mobility was not measured directly, an attempt to use the Haynes-Shockley method failed. There has been no report on a direct measurement of hole mobility in n-type CdS as far as the author knows. Woods and Champion reported the mobility of holes in p-type CdS obtained by doping CdS heavily with copper. It was measured to be 20 cm^2/volt sec. at room temperature. This is fairly consistent with the values of effective masses since mobility is inversely proportional to effective mass.

An estimate of trapped carriers can be made now. We have[13]

$$\tau_r = \tau_n(1 + \Delta n_r/\Delta n)$$

Since $\tau_r \cong 7$ sec. for $\Delta n = 10^{14}/\text{cm}^3$, then

$$\Delta n_r \cong 10^{15}/\text{cm}^3$$

Conclusion

The PVE is thus shown to improve when green light is present. The effect of green light is to depopulate the impurity levels, thus increasing the number of states available for transitions from the valence band to the impurity levels. The crystals effectively absorb more infrared light in the presence of green light.

Relaxation time is relatively large compared to what is usually observed in semiconductors, but CdS is known to have such long relaxation time.

The numerical values calculated for various parameters satisfy all assumptions made and check well with the values found by R. Bube.[13,14]

Appendix I

The Shockley-Read Model[15]

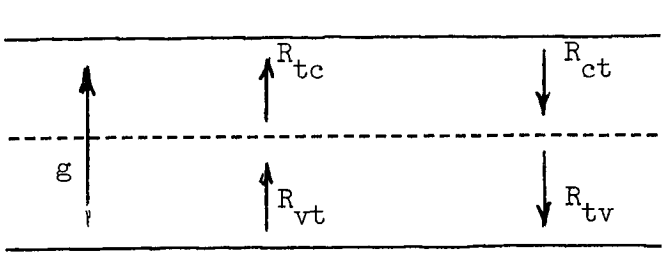

The various transitions are depicted above. Transitions are assumed to be proportional to the density of electrons available for transitions and the density of empty states into which transitions may occur. Hence:

$$R_{ct} = r_c n_o p_{ro} \tag{A-1}$$

$$R_{tc} = r_c' n_{ro} N_c \tag{A-2}$$

where r_c and r_c' are the constant of proportionality.

Under equilibrium condition, $g = 0$, we must have:

$$R_{ct} = R_{tc} \tag{A-3}$$

Since:

$$p_{ro} = N_r(1-f_{ro}) \tag{A-4}$$

$$n_{ro} = N_r f_{ro} \tag{A-5}$$

where f_{ro} is the Fermi factor for the level, we can deduce:

$$R_{tc} = r_c n_{ro} n_1 \tag{A-6}$$

where n_1 is defined as the electron concentration in the conduction band if the Fermi level were located at E_r:

$$n_1 = N_c\, e^{-(E_c-E_r)/kT} \tag{A-7}$$

The constant of proportionality r_c is also defined as:

$$r_c = S_n v_n \tag{A-8}$$

where S_n is the capture cross section for electrons and v_n the thermal velocity of electrons:

$$v_n = (2kT/\pi m_e)^{\frac{1}{2}} \tag{A-9}$$

Using the same argument for R_{tv} and R_{vt}, the following results are obtained:

$$R_{tv} = R_{vt} \tag{A-10}$$

$$R_{tv} = r_v n_{ro} p_o \tag{A-11}$$

$$R_{vt} = r_v p_{ro} p_1 \tag{A-12}$$

$$p_1 = N_v e^{-(E_r - E_v)/kT} \tag{A-13}$$

$$r_v = S_p v_p \tag{A-14}$$

$$v_p = (2kT/\pi m_h)^{\frac{1}{2}} \tag{A-15}$$

Under the non-equilibrium condition, $g \neq 0$, we have:

$$g = R_{ct} - R_{tc} = R_{tv} - R_{vt} \tag{A-16}$$

$$R_{ct} = r_c(n_o+\Delta n)\ (p_{ro}-\Delta n_r) \tag{A-17}$$

$$R_{tc} = r_c(n_{ro}+\Delta n_r)\ (n_1) \tag{A-18}$$

$$R_{tv} = r_v(n_{ro}+\Delta n_r)\ (p_o+\Delta p) \tag{A-19}$$

$$R_{vt} = r_v(p_{ro}-\Delta n_r)\ (p_1) \tag{A-20}$$

The neutrality condition is:

$$\Delta n + \Delta n_r = \Delta p \tag{A-21}$$

Combining Equations (A-3), (A-10) and (A-16) through (A-21), we obtain:

$$\Delta n_r = \frac{r_c p_{ro} \Delta n - r_v n_{ro} \Delta p}{r_c(n_o+n_1+\Delta n) + r_v(p_o+p_1+\Delta p)} \tag{A-22}$$

Since $n_o \gg n_1$, $n_o \gg \Delta n$, $\Delta p \gg p_o$, $\Delta p \gg p_1$ (A-23)

(A-22) can be simplified to:

$$\Delta n_r = \frac{r_c p_{ro} \Delta n - r_v n_{ro} \Delta p}{r_c n_o + r_v \Delta p} \tag{A-24}$$

Again using Equations (A-21) and (A-23):

$$\Delta n_r = \frac{(r_c p_{ro} - r_v n_{ro})\Delta p}{r_c n_o + r_v \Delta p} \qquad \text{(A-25)}$$

If furthermore:

$$r_c p_{ro} \gg r_v n_{ro} \qquad \text{(A-26)}$$

then:

$$\Delta n_r = \frac{-r_v n_{ro}\Delta p}{r_c n_o + r_v \Delta p}$$

Bibliography

1. M. Wolf, Proc. I.R.E., 48, p. 1246, (July, 1960).

2. R. Williams and R. H. Bube, "Photoemission in the Photovoltaic Effect in CdS Crystals", J. Appl. Phys., 31, 968, (June 1960).

3. E. D. Fabricuis, "Photoeffect in Au-CdS and Cu-CdS Photovoltaic Cells", J. Appl. Phys., 33, 1597, (April 1962).

4. J. Woods and J. A. Champion, "Hole Conduction and Photovoltaic Effects in CdS", J. Elec. and Contr., p. 243, (1959).

5. H. G. Grimmeiss and R. Memming, "P-N Photovoltaic Effect in CdS", J. Appl. Phys., 33, 2217, (July 1962).

6. D. C. Reynolds and S. J. Czyzak, "Mechanism for Photovoltaic and Photoconductivity Effects in Activated CdS Crystals", Phys. Rev., 96, 1705, (1954).

7. Brosser, Kallmann, and Warminsky, Z. Naturforsch 4A, 631, (1949).

8. P. N. Keating, "Hole Injection into CdS from Cu_2S", J. Phys. Chem. Solids, (Sept. 1963), p. 1101, 24.

9. H. C. Gatos, J. Appl. Phys., 32, 1232, (1961)

10. H. C. Gatos, The Surface Chemistry of Metals and Semiconductions, John Wiley and Sons, (1954), p. 384.

11. S. M. Ryvkin, Photoelectric Effects in Semiconductors, Consultants Bureau, (1964), Chapter X.

12. T. S. Moss, Optical Properties of Semiconductors, London, Butterworths, (1961), p. 214 and p. 2.

13. R. Bube, Photoconductivity of Solids, John Wiley, (1960), p. 348.

14. W. Shockley and W. T. Read, Jr., "Statistics of the Recombination of Holes and Electrons", Phys. Rev. 87, p. 835, (1952).

List of Symbols

E_c = energy of conduction band

E_f = Fermi energy

E_{fr} = Fermi energy of the recombination center

E_r = energy of recombination center

E_v = energy of valence band

f = generation rate by infrared light

f_r = Fermi function of recombination centers

g = generation rate by green light

N_c = effective density of states in conduction band

N_r = density of recombination centers

N_v = effective density of states in valence band

n_1 = $N_c \exp - (E_c - E_r)/kT$

n_o = equilibrium electron concentration in conduction band

n_{ro} = equilibrium

Δn = incremental electron concentration in conduction band due to green light

$\Delta n'$ = incremental electron concentration in conduction band due to infrared light

Δn_r = incremental electron concentration in recombination centers due to green light

$\Delta n_r'$ = incremental electron concentration in recombination center due to infrared light

p_1 = $N_v \exp - (E_r - E_v)/kT$

p_o = equilibrium hole concentration in valence band

p_{ro} = equilibrium hole concentration in recombination centers

Δp = incremental hole concentration in valence band due to green light

$\Delta p'$ = incremental hole concentration in valence band due to infrared light

r_c = recombination rate of electrons in conduction band

r_v = recombination rate of holes in valence band

R_{ct} = transition rate of electrons from the conduction band to the recombination centers

R_{tv} = transition rate of electrons from the recombination centers to the valence band

S_n = capture cross section for electrons

S_p = capture cross section for holes

t = time

τ_n, τ_h = electron and hole lifetimes

v_n, v_p = thermal velocity of electrons and holes

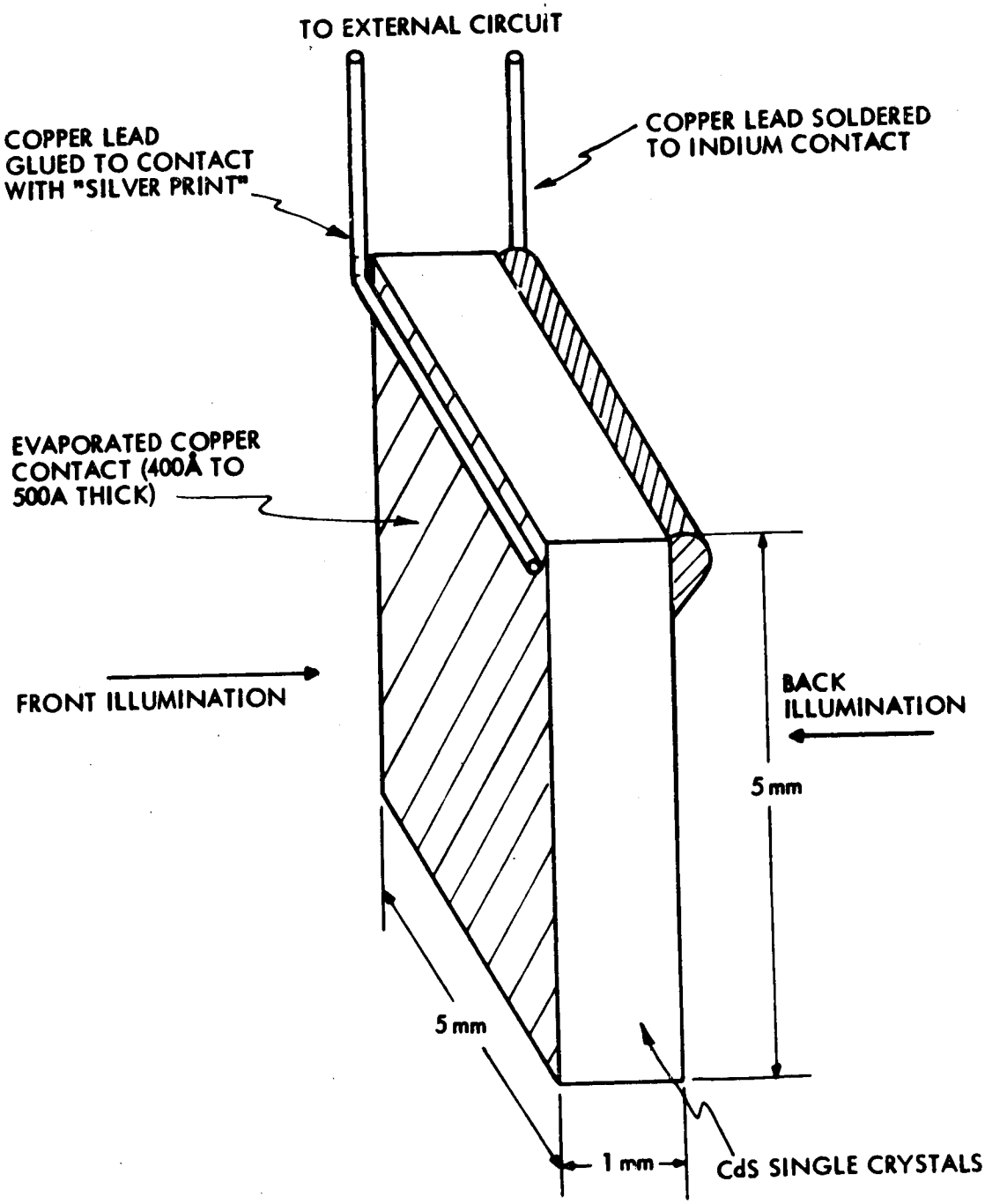

Figure 1. Cell Geometry

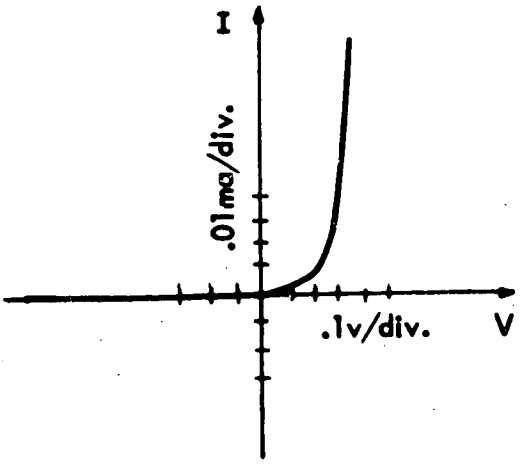

Figure 2. Dark I-V characteristics of a cell

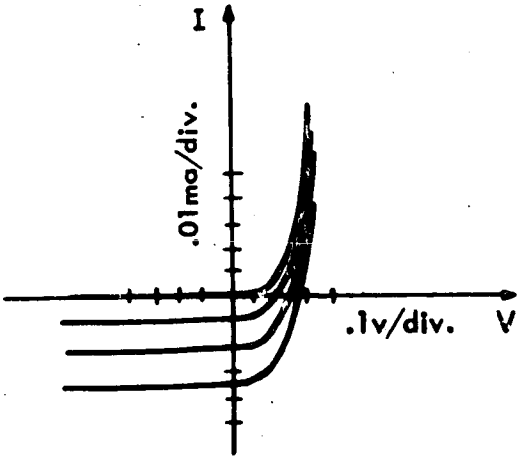

Figure 3. I-V characteristics of a cell under different illumination intensities

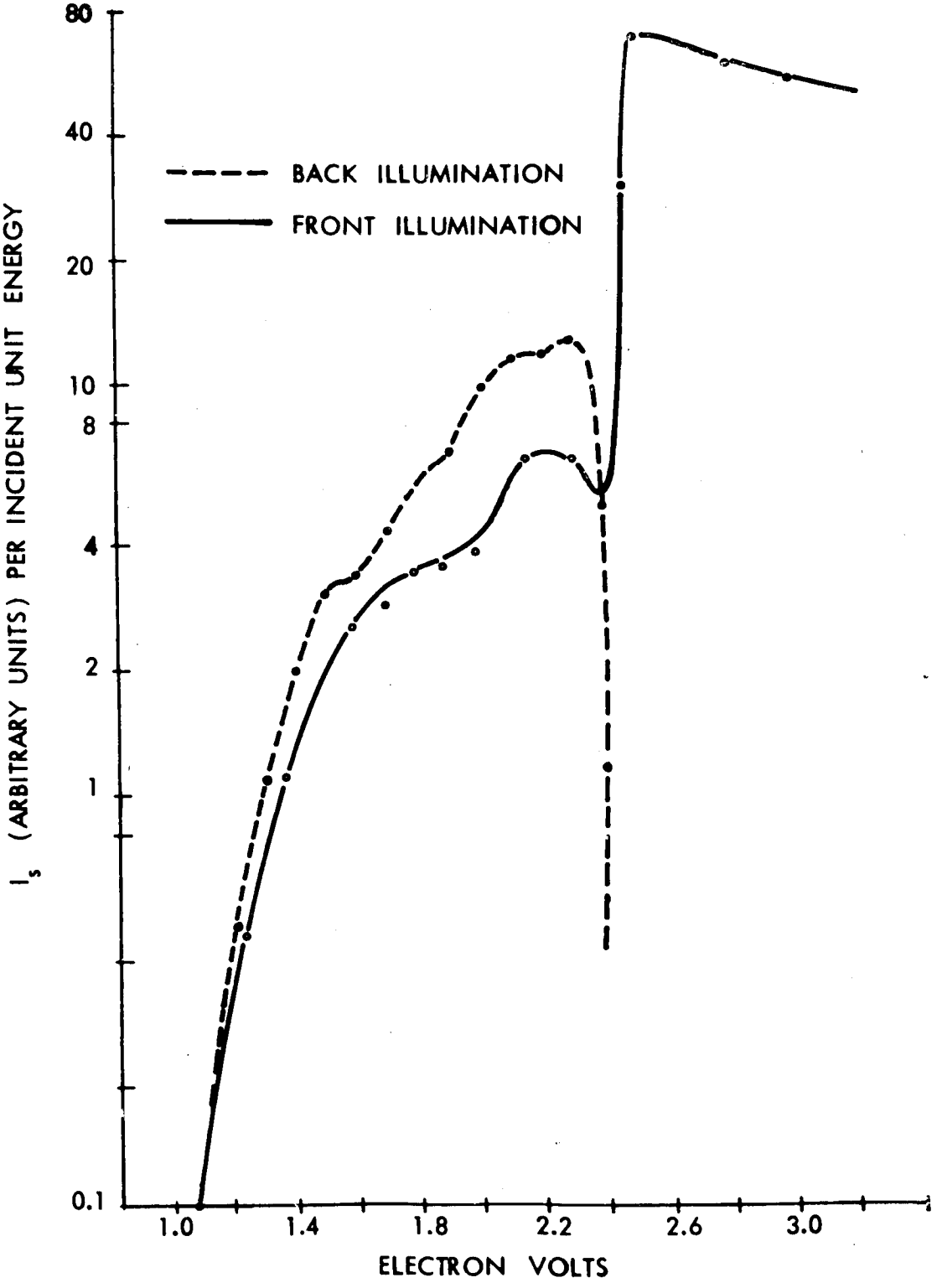

Figure 4. Spectral response of a typical cell

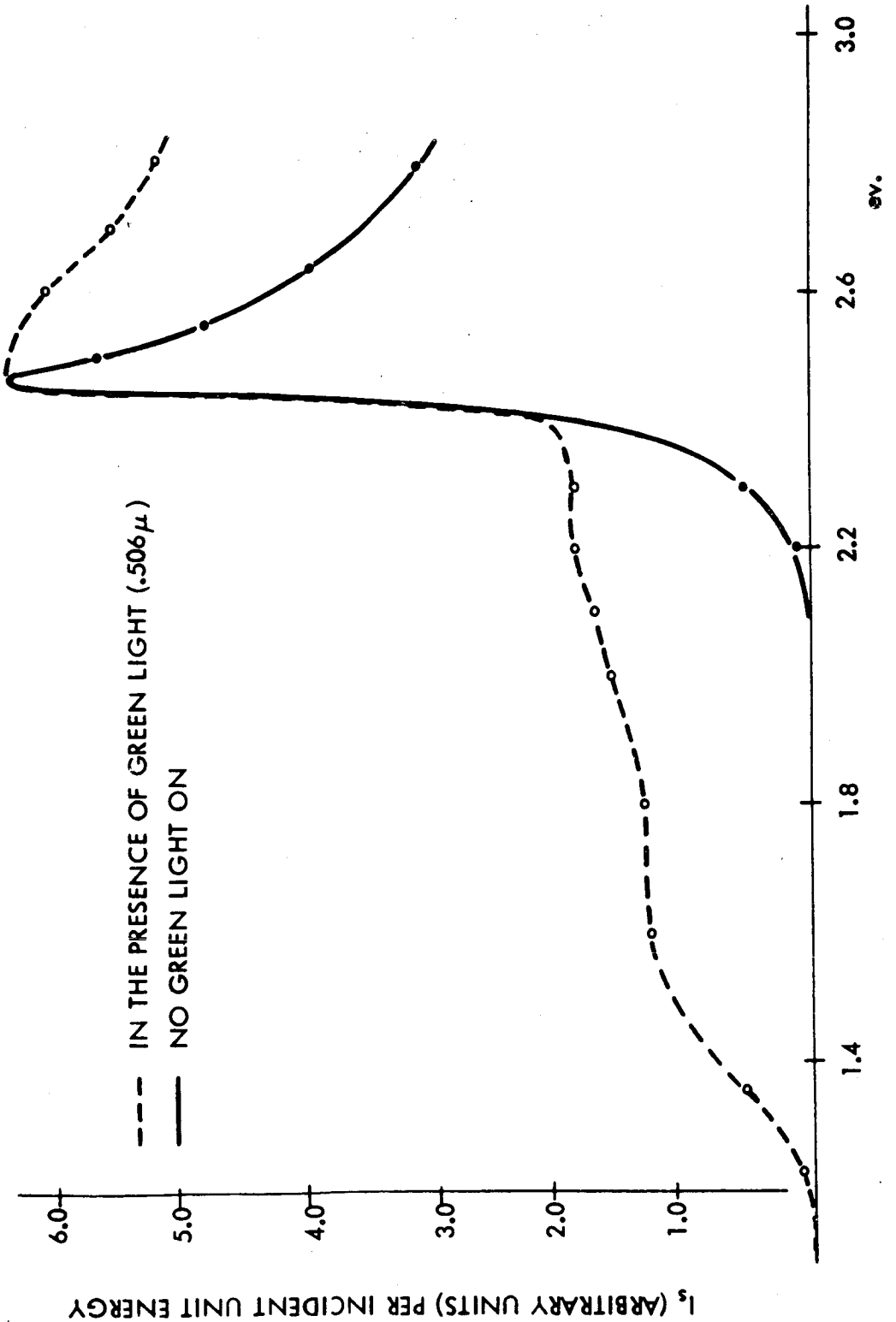

Figure 5. Spectral response of cell A

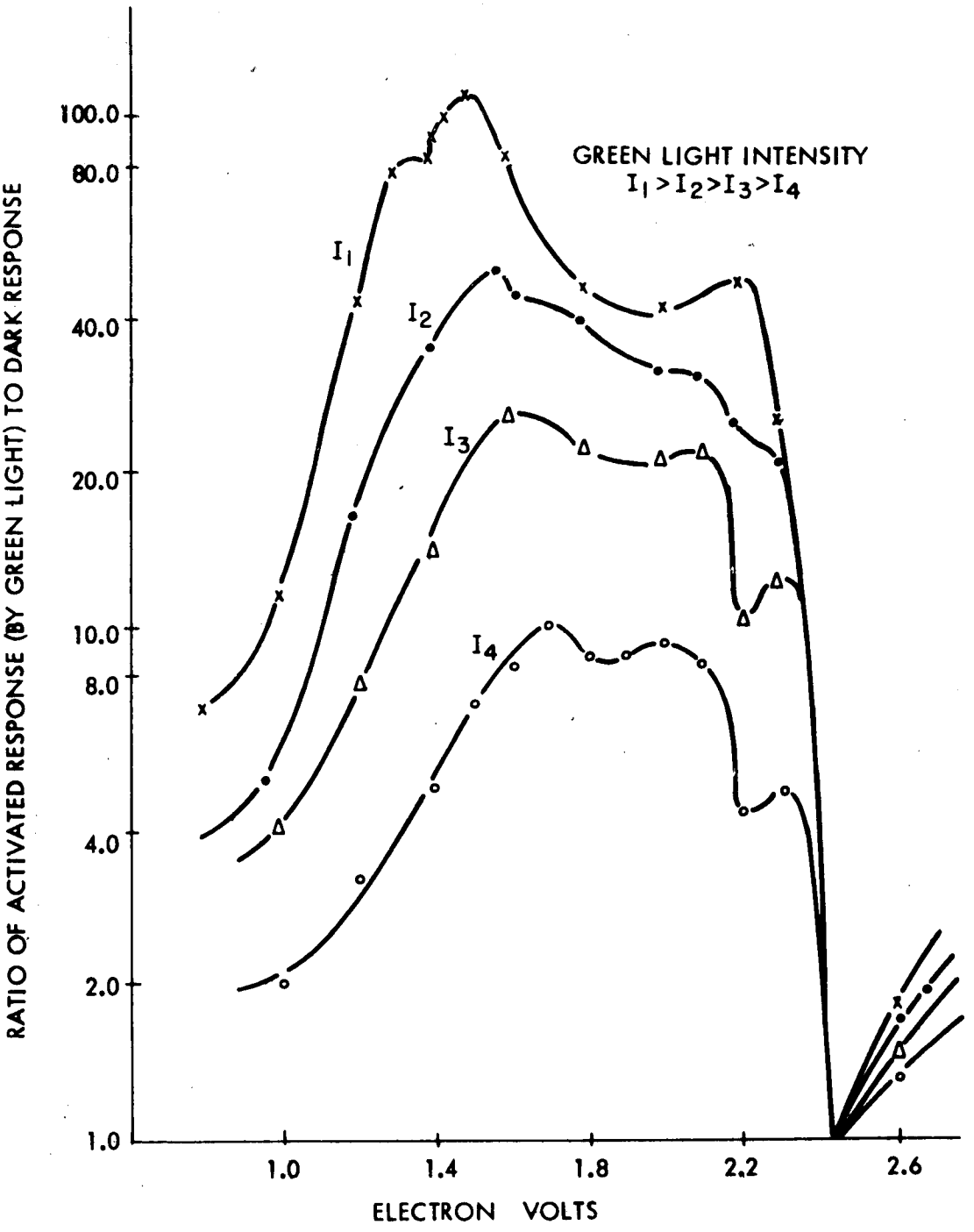

Figure 6. Enhancement of spectral response at each wavelength for different green light intensities

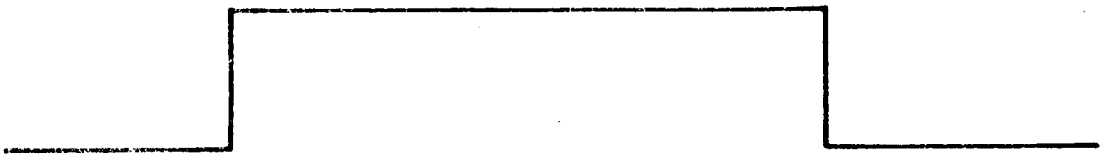

(a) GREEN LIGHT PULSE

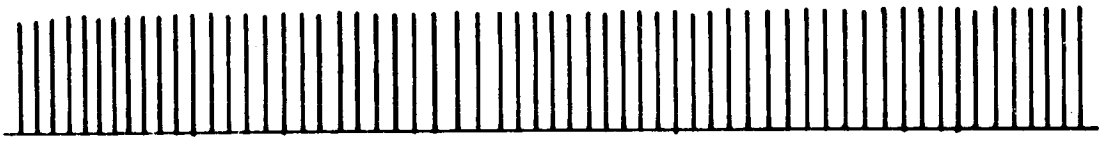

(b) LONG WAVELENGTH PROBING PULSES, CORRESPONDING TO IMPURITY LEVEL

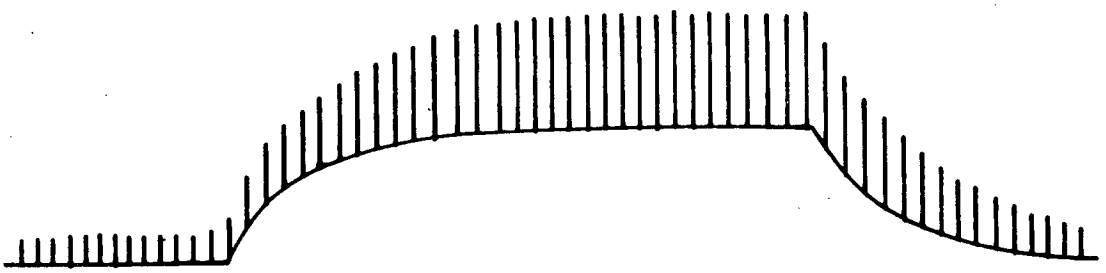

(c) THE WHOLE OSCILLOGRAM

(d) ENVELOPE OF PEAKS IS RELAXATION OF IMPURITY LEVEL

Figure 7. Continuous probing of the relaxation process of impurity centers

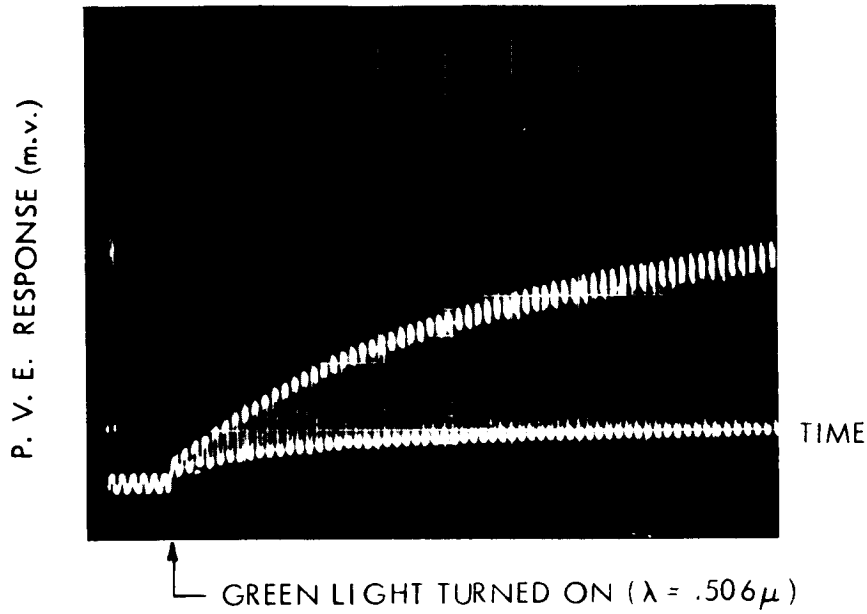

Figure 8. Impurity centers are being emptied when green light is turned on. Infrared beam (λ = .93μ) is chopped at 13 cps. The infrared response is enhanced considerably. Scale: 1 mv./div., .5 sec./ div.

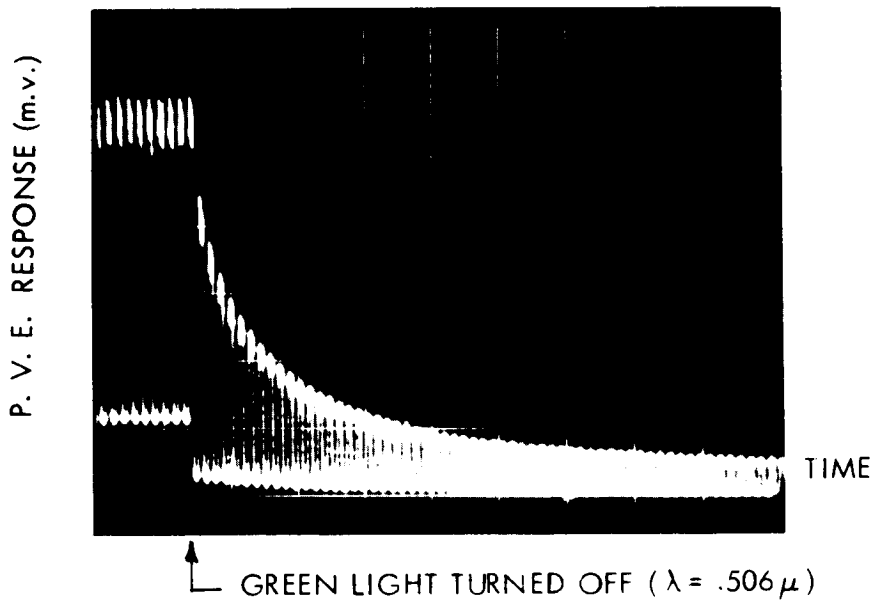

Figure 9. Impurity centers are filling up with electrons as green light is turned off. Same conditions as above. The difference between the upper and lower envelopes is the response to infrared (λ = .93μ) as a function of time. Scale: 1 mv./div., .5 sec./ div.

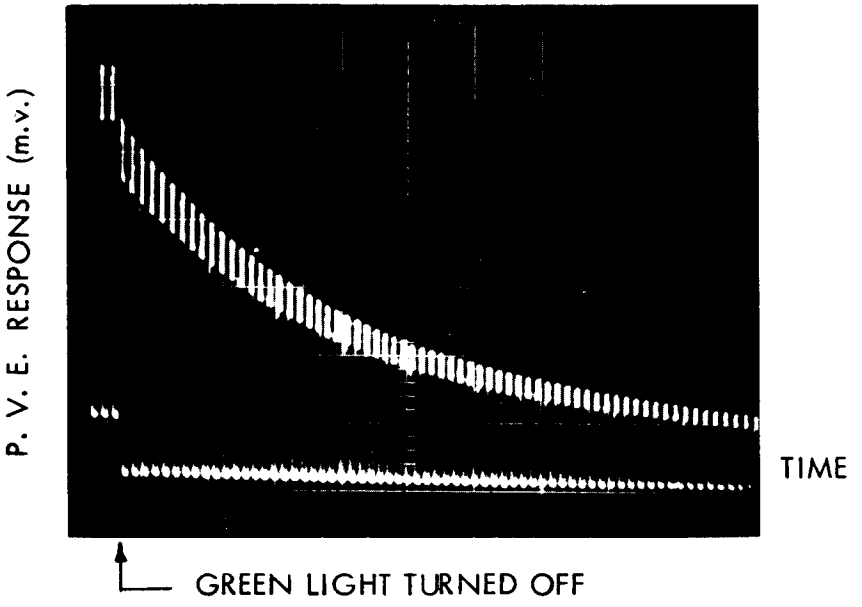

Figure 10. Impurity centers are filling up with electrons when green light (unchopped) is turned off. The chopped radiation corresponds to λ = .63μ. Scale: 2 mv./div., .5 sec./div.

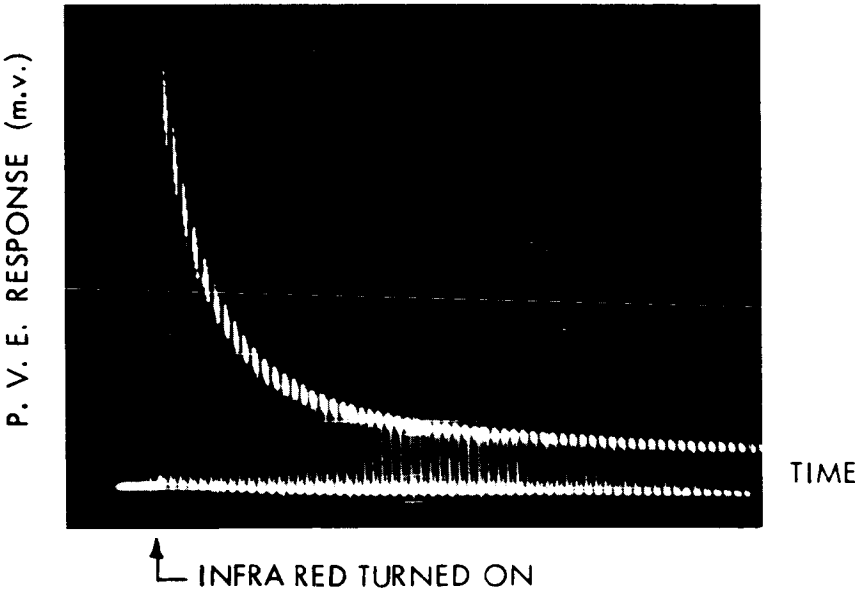

Figure 11. Transient due to infrared when it is turned on, with green radiation already on. There is a slight decrease in the green response (lower envelope), whereas infrared response decreases slowly as impurity centers are filling up with electrons. No such transient is observed when green light is not already on, λ = .93μ. Scale: 10 mv./div., .5 sec./div.

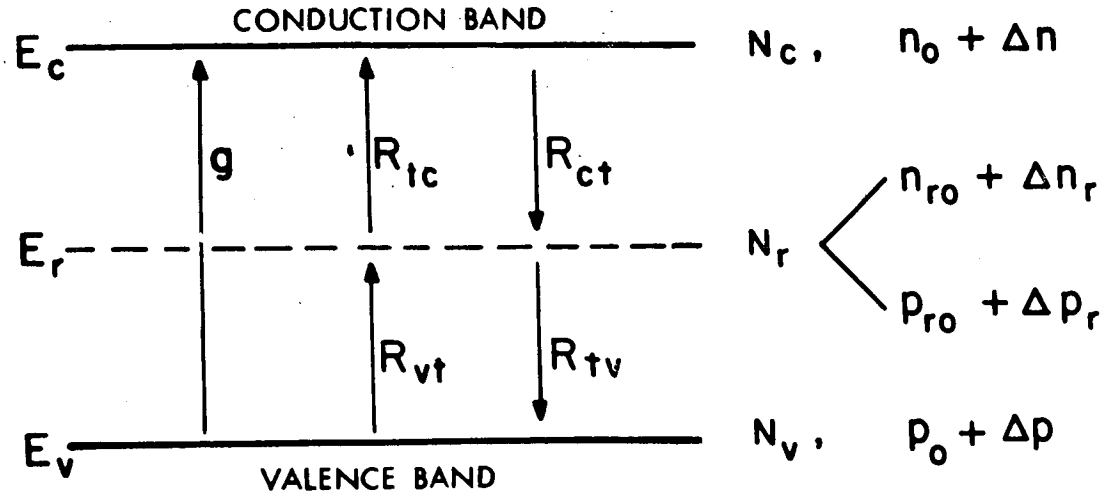

Figure 12. Transition rates and model for recombination statistics.

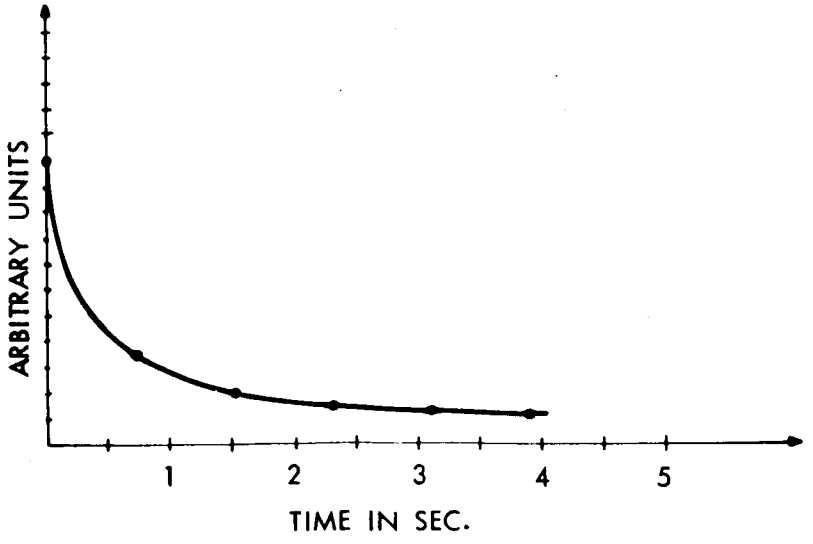

Figure 13. Relaxation of impurity centers is obtained by taking the difference between the upper and lower envelope of Figure 9. (Continuous curve) The dots are theoretical calculations of the same process ($\lambda = .93\mu$).

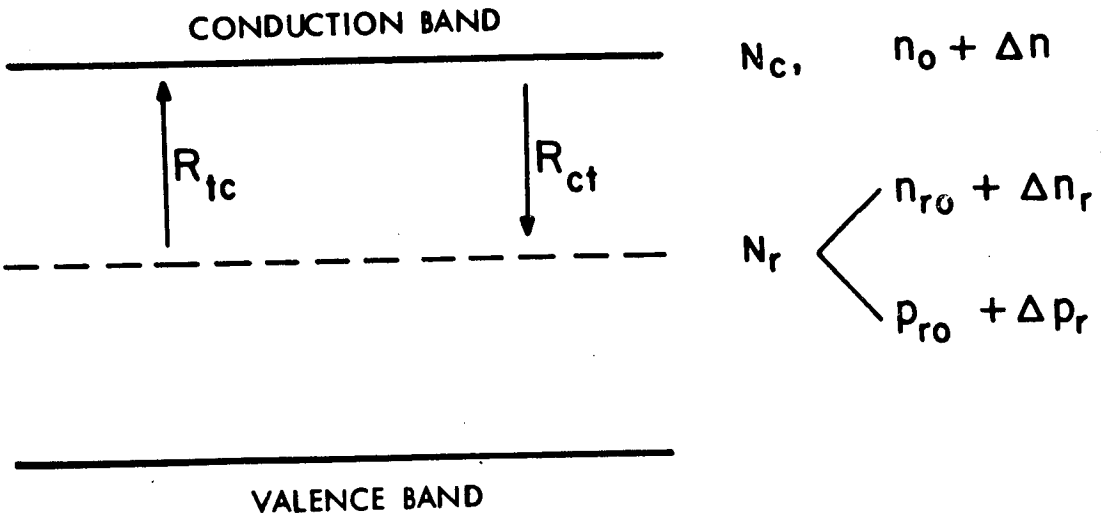

Figure 14. Transition rates and model for filling of the impurity centers

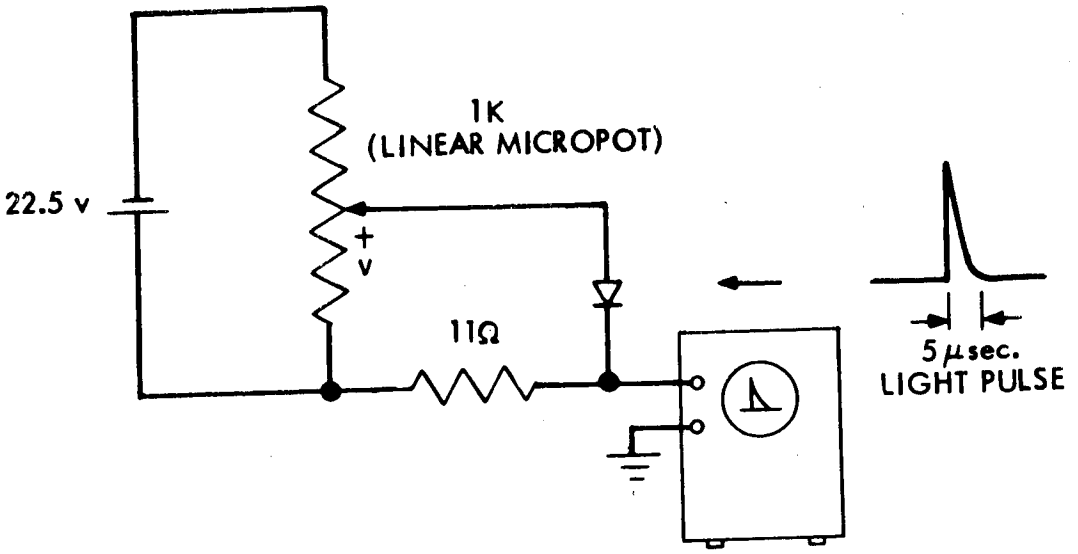

(a) the circuit

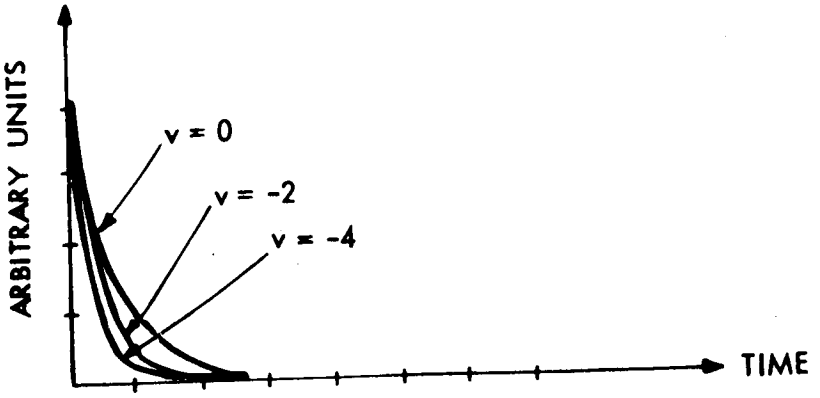

(b) fast decay region. Vertical scale is adjusted in order to compare time response with increase in back bias. Scale: 10μ sec./div.

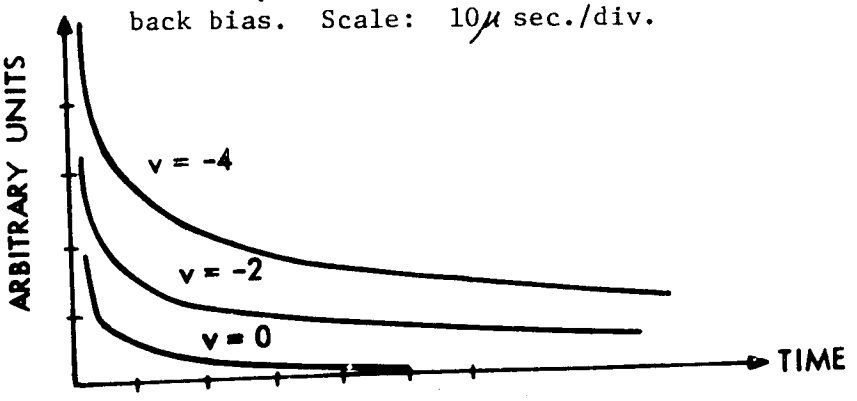

(c) slow decay region. No adjustment in scale. The response increases with back bias. No apparent change in time constant. Scale: 100μ sec./div.

Figure 15. Diode recovery experiment

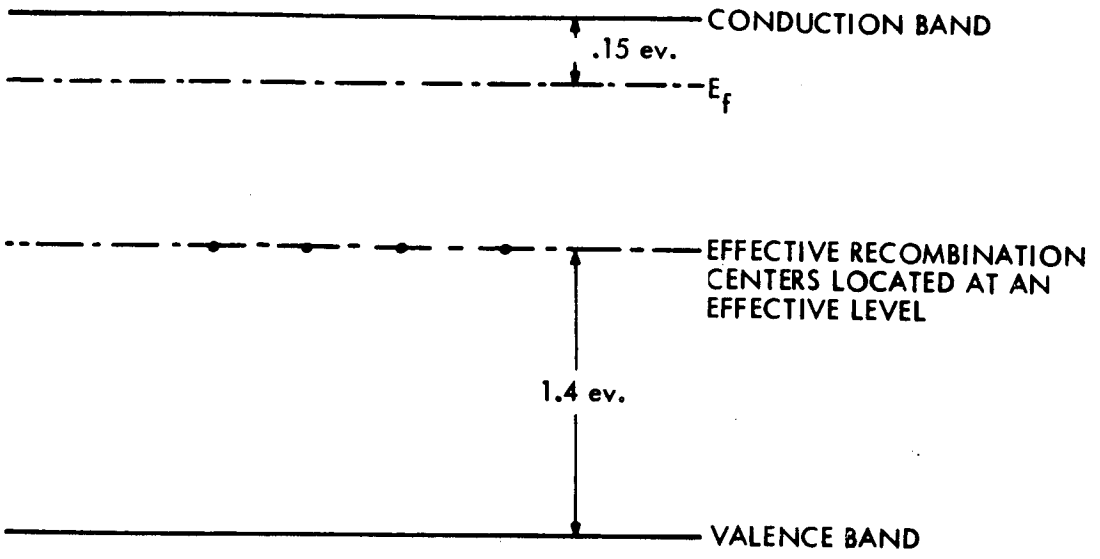

Figure 16. Proposed idealized model for the enhancement process. Shallow traps are neglected because they do not play an effective role in the behavior of minority carriers. Recombination centers are actually distributed over a larger region of the forbidden gap, but are replaced by an effective concentration located at an effective level in order to simplify the analysis.

Discussion

Kaye - EOS: Why do you ascribe the level to copper rather than a vacancy?

Blair: The 1.4 electron volt position of the level from photoconductive data indicates a copper acceptor level at this energy. But it could be a trap due to a vacancy as well.

Halstead - GE: I would like to ask one question. Have you measured the spectral width of the effective region of the spectrum? I would think in general in order to get sufficient concentration of energy in the green region for this to be a useful effect in connection with photovoltaic performance where you are concerned with response over a broad region of the spectrum, that there would be a rather narrow spectral region where there would be sufficient penetration by the green to help you much with the red?

Blair: I think that the comment is quite correct. We did span a spectral region around the green light to see what the effect on the enhancement is, and the most effective enhancement seems to be right at the absorption edge where there is a considerable penetration of the green light. If you fall to energies shorter than the energy gap, you do not get any enhancement, and if you go to energies larger than the energy gap, the absorption takes place too near the surface to sensitize the region within a diffusion length of the barrier.

Halstead: I would make a general comment, that is I think it is well established that the level would be copper and there is a fair amount of literature on the two-stage excitation in cadmium sulfide via copper level. There are several papers relevant to this. This has been proposed, although it hasn't been investigated, quantitatively, as a basis for this effect which you're describing.

Blair: Yes, that is correct.

Dr. Potter - NASA-Lewis: With regard to the more practical cell, it seems to me there are two things that still require more discussion and explanation. One is that, as you mentioned, in the more efficient cell there is a red response, which does not require a green light excitation. And it is a pretty healthy one. In many cases, the enhancement in a commercial cell is quite small. The other point that needs more explanation, probably, and discussion, concerns the fact that we do observe enhancement for wavelengths longer than the band edge; in other words, we can observe enhancement in some cases at wavelengths down to 1 micron, which is a very low energy indeed. So this is difficult to explain by your model. So I think it may be more complex still than we see from this.

Blair: I pointed out that the single level model is an idealization of the situation; in actuality there's a smeared-out series of levels in the forbidden region to which transitions take place. This may extend several

10ths of electron volts above and below the 1.4 electron volt level. Along the line of the comment that you made and perhaps in answer to the previous question, I would like to say that I am not trying to imply that the enhancement by the green light here has a very strong practical implication in improving the performance of cadmium sulfide cells. In this particular case, this was a very useful tool to populate and depopulate levels without any recourse to changes of the doping levels. In high-performance cadmium sulfide cells there is a proper compensation between the shallow donors and the deep-lying acceptors, which will leave these levels empty at all times for the transitions from the valence band to the impurity level to take place. I think that this is really the important practical consideration. This was a useful tool to study the mechanisms that are involved.

Goldstein - RCA: In some examples of similar materials, there should be a whole series of experiments and effects paralleling those that you have mentioned. Specifically involving those of wave length dependence and intensity dependence, which should involve such things as infrared quenching and infrared stimulation. Have you performed any of these experiments and are they consistent with the general picture that you have drawn?

Blair: The literature is rich in experiments which study the photoconductivity of cadmium sulfide and observe similar effects. I'd like to point out that there is a major difference between what we have seen and what exists in the literature. In photoconductive experiments. One always observes the behavior of the majority carrier, the electron. In this case, we have observed the behavior of the majority carrier, and this presents a novel approach to the study of cadmium sulfide.

Goldstein: Yes, that's correct, and I appreciate that. But the presence of the minority carriers are felt very often in certain experimental circumstances involving quenching and stimulation mechanism, even in the measurement of photoconductivity which is itself a majority carrier effect. Have you made any experiments along these lines?

Blair: We have made some photoconductive experiments but I think I'd rather not say much about them because at this time the results are not conclusive enough.

INTEGRAL GLASS COATINGS FOR SOLAR CELLS

Presented by

P. A. Iles

Hoffman Electronics Corporation

El Monte, California

18 October 1965

INTEGRAL GLASS COATINGS FOR SOLAR CELLS*

P. A. Iles
Hoffman Electronics Corporation
El Monte, California

Introduction

Bare solar cells have three limitations to their efficient operation in space. The front surface has low emittance, which increases the cell temperature and lowers the output, the antireflective coating, or the shallow PN junction are easily damaged by micrometeorite erosion, or the cell may be degraded by charged particle bombardment. Transparent covers have generally solved these problems, and in addition the radiation damage can be reduced by careful design of the solar cell. Nowadays, these covers are bonded to the cells by an elastomeric adhesive. This combination has the advantages of being well proven in many missions, in retaining most of the original cell power because of good transparency, and, because the adhesive cures at low temperatures, the covers can be applied to already connected modules. The elastomer can accommodate a large thermal mismatch between the cover and the cell, and this allows a wide range of radiation shield thickness. There are some disadvantages however. The finished cover, with its deposited coatings, especially the UV rejection filter which prevents darkening of the adhesive, can add costs of between 1/2 and 3 1/2 dollars for 2 cm^2 cells. The fragility of the covers adds to the complexity and costs of array assembly, and it is difficult to provide covers thinner than 5 mils. Finally, the adhesive sets the limits for the array in mechanical strength, and performance at high temperature.

These disadvantages provide the main reasons for investigating integral covers. The program outlined here was aimed at practicable evaluation of integral covers, particularly for missions where all the advantages of the discrete covers were not necessary. Convenient criteria for evaluation were maximum power available, simplified and less expensive array assembly, weight reduction and extension of the environmental performance of the finished array.

There are several available methods to apply transparent integral coatings and one of them will be described by the next speaker. We chose to develop an old technique which has been improved in recent years by research at IBM.

---

* This work was partly supported by Contract No. NAS 5-3857.

Glass Technology

Glass is ground to a fine powder, deposited on a solar cell slice and fused. The glass must be carefully chosen to have an expansion coefficient well matched to that of silicon for temperatures extending to the fusion range, it must have good fusing properties, and good transparency after fusing and preferably it should contain as few components as possible to minimize radiation darkening. Most glasses have adequate thermal emittance. Several borosilicate glasses were used successfully, with the minor penalty that their fusing temperatures were 100 to 200°C higher than those needed for many other glasses. In brief, the coating sequence was as follows:

1. Form a fine glass powder by ball-milling.
2. Make a slurry by dispersing the powder in liquids which prevent coagulation.
3. Adjust the optical density of the slurry by slow centrifuging or settling.
4. Deposit the glass powder on the silicon by fast centrifuging.
5. Fuse the glass.

The thickness of the deposited layer was controlled by the optical density adjustment, 3. Figure 1 shows an empirically determined curve relating the relative optical transmittance, and the fused layer thickness. This control worked well, and control of layer thickness to ± 3μ in layers 30μ thick was achieved. After some practice it was possible to obtain glass layers of good transparency, free from major flaws and drying patterns. For thickness above a few microns the layer was continuous, while for thickness greater than 1/2 mil, the top surface of the fused layer was fairly flat even when the glass was fused to a slice of rough surface finish. Figure 2 shows cleaved sections of a coated silicon slice, (a) before and (b) after dipping in hydrofluoric acid. The shiny surface layer in (a), when removed leaves a matte surface (b), which has the same transparency and slightly higher thermal emittance.

Solar Cell Fabrication

To accommodate the high fusing temperature (850°C - 950°C) the usual cell fabrication steps were altered slightly. Early cells were made by fusing glass to a diffused slice, making slots in the glass, and applying front contacts through these slots. Better methods were developed using two altered contact structures. The first method used deep diffused layers (2 to 5μ) under the front contact areas, the second

method relied on a thin dielectric buffer layer between the diffused layer and evaporated titanium-silver contacts. In the second method, during glass fusion, the contact metals moved into the dielectric layer and made low resistance, adherent contacts to the diffused silicon. Both of these methods allowed less exposed metal (wraparound contact cells were made successfully) and the high temperature stability of the contacts allowed build-up of the glass layer either by fusing a series of layers, or by using the first fused layer as a bond for thicker plates of a similar glass. After glass fusion the bulk silicon was exposed on the back surface, a back contact was applied, and the PN junction was cleansed of shorting paths.

The dielectric buffer layer, besides preventing metal penetration of the shallow diffused layer, must serve other purposes. It should be compatible with the fused glass and if possible provide an antireflecting coating on the silicon. Both the Hoffman diffusion-produced phospho-silicate glass antireflecting coating and evaporated SiO were used, on both rough and polished cell surfaces. In practice the best combination has been the phospho-silicate glass on a rough surface finish silicon.

Coated Cell Properties

Preliminary trials showed that the fusion process did not alter the junction depth or bulk resistivity of the silicon. The fusion cycle alone did not change the minority carrier lifetime in the bulk silicon, but when the glass layer was fused, a slight decrease in lifetime (and an accompanying drop in Isc) was observed. Typical decreases were 14 to 21 microseconds, with an associated Isc drop of 2mA. The Isc of the coated cell was mostly determined by the transparency of the fused layer.

The high-temperature contact structures allowed the use of completed cells to measure the transparency of the fused glass, and thus to optimize the fusing conditions. The next two figures, 3 and 4, show the degree of transparency possible. For Figure 3 (a) glass was fused to silicon or kovar, and the thin glass layer was stripped from the support and photographed in transmission. C is an airgap between two such slides. A is a layer fused at high temperature, with high transmission but some large flaws, B a typical layer. Figure 3 (b) shows the glass layer partly covering a grid line, and comparison of the line appearance above and below the arrows shows the degree of transparency. Figure 4 shows a cell where only half the surface was covered with glass.

To date, the combined effects of lifetime reduction and layer transparency limitations have been reduced to where Isc values for coated cells are consistently 90 to 93% of the Isc values for uncoated cells.

The rest of the cell structure can be designed to give output power up to 92% of the power from an uncoated cell. The next two figures, 5 and 6, compare the best cells made with 1 mil integral glass, with good production cells of equivalent bulk resistivity, diffusion parameters, and active area.

The relative spectral response was not changed much by the glass layer; the slight decrease in absolute response is fairly flat over the useful wavelength range of the cell.

So far, thinner layers have had greater transparency. Figure 7 shows how Isc decreases for the thicker glass layers. The advantage of a single fusion for the thicker layers can be seen. The I_{430} values for the single fusion case are also shown. As mentioned above, the most rapid way to build thicker layers is to use a thin layer of powder to fuse a prefabricated thick slide of a similar glass. In this way 20 mil slides were bonded to cells with good adhesion, but the decrease in output was larger than expected, in the best case being around 5% below the output of a cell with the fusing layer alone. Discussion below shows that the formation of thick layers is not the best use for integral covers.

The variation of cell output versus slice thickness for 1 mil integral glass layers was measured for the resistivity range 2 to 10 ohm-cm. As the slice thickness decreased from 16 to 8 mils, the power decrease was close to that measured for conventional cells, namely around 6%.

Other Measurements

Besides the cell output which is the most important quantity required, other measurements were made.

Thermal Emittance The coated cells, bonded to a heat source, were held inside a cooled, evacuated chamber, and the thermal balance for various input powers could be evaluated to give the total hemispherical emittance of the coated cells. Figure 8 shows several views of the equipment. Figure 9 plots the emittance values at 30°C versus glass thickness for two cell surface finishes. The thin layers are seen to have bulk emittance values for thicknesses above 1 mil. Thus, for thermal control, layers thicker than 1 mil have no advantages.

Particle Irradiation A dosage of 2×10^{15} 1 Mev electrons per cm^2 did not produce any additional damage in cells coated with integral glass. Preliminary trials have shown no degradation after dosage of 10^{16} 0.4 mev protons per cm^2.

Temperature Stability These integral glass cells have shown improved stability under prolonged exposure to high temperatures. Cells were

heated at 600°C for 4 hours before beginning to degrade. Several cycles of the cell between boiling water and liquid nitrogen did not affect the bonding or the cell output, thus showing the good match of the expansion coefficients for silicon and the glass layer. During post-irradiation trials it was found that complete annealing of the radiation damage followed 5 minute heating at 600°C.

Antireflective Coatings MgF_2 coatings increased the cell output by 1.5%, close to theoretical predictions.

System Considerations

The results to date have shown both the limitations and the possibilities of these integral coatings. Approximately 2,000 cells have been made, allowing preliminary cost estimates and showing the feasibility of reaching reasonable production rates. The cells have been combined with present methods for interconnecting solderless cells, and simplification and lowered costs of arrays appears possible. The main limitation is the 7 to 8% loss of output power.

Figure 10 shows the percentage of present cells with power greater than the corresponding abscissae. Figure 11 compares the output power and the mass for both conventional and integrally coated cells, as the silicon slice thickness decreases. Figure 12 converts these figures to Watts per pound versus slice thickness. This figure shows that integrally coated cells have a marked advantage over conventional cells with 6 mil covers, but that these advantages are minimized or lost when combined with present substrates.

Mission Design

During this work, some preliminary opinions have been formed about the best probable application for cells with integral covers. If severe particle densities are present and long life is required, there appears to be no alternative to thick covers (tens of mils) of pure quartz or sapphire. Even pure glass covers give inadequate shielding under these conditions and this fact, combined with the large thickness required, rules out integral glass covers for such applications. Dr. Fang, of NASA-GSFC has recently suggested that when electron radiation dosage is severe, cell output may be restored by annealing by heating the arrays above 400°C for 10 minutes, after periods where the dosage is less than 10^{14} electrons per cm^2. As mentioned above, cells with integral glass covers are well able to withstand such annealing, and if the practical problems of cell interconnection and heating can be solved, this is an intriguing possible use for cells with integral glass coatings.

There are also many missions where exposure to high energy particles will be low, and integral glass coatings appear better suited

to these missions. Reduced weight can be obtained by combining the minimum integral glass layer (1 mil for thermal control) with thinner cells. Also, because the bulk silicon does not need high radiation tolerance, lower resistivity silicon which gives more available power after integral coatings are applied, can be used for the cells. Figure 12 showed that if lighter substrates can be obtained, over 20 Watts per pound is available.

Summary

Solar cells with integral glass coatings have been made in sufficient numbers to show the feasibility of production, and to allow preliminary estimates of the output, costs, and weight. These cells can simplify array assembly and have good environmental stability. The results obtained have provided a firm quantitative basis for comparing other possible coating methods and study of alternative coating techniques is in progress.

PIC-SOL 209/6

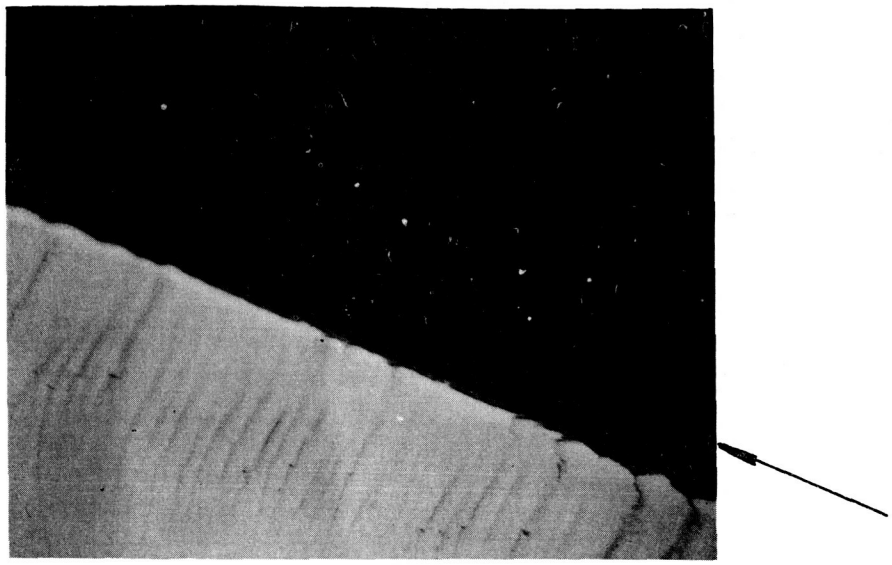

(a) SHINY SURFACE

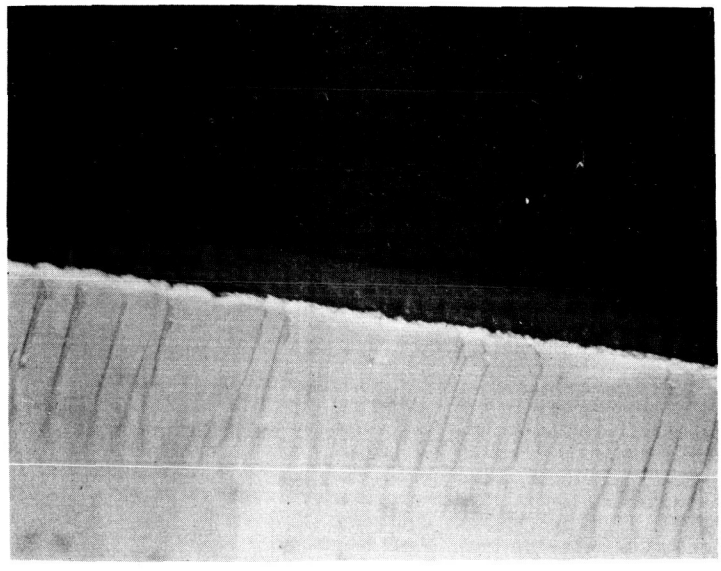

(b) MATTE SURFACE

FIGURE 2 - PHOTOGRAPHS (300X) OF CLEAVED SECTION OF SILICON SLICE WITH GLASS LAYER

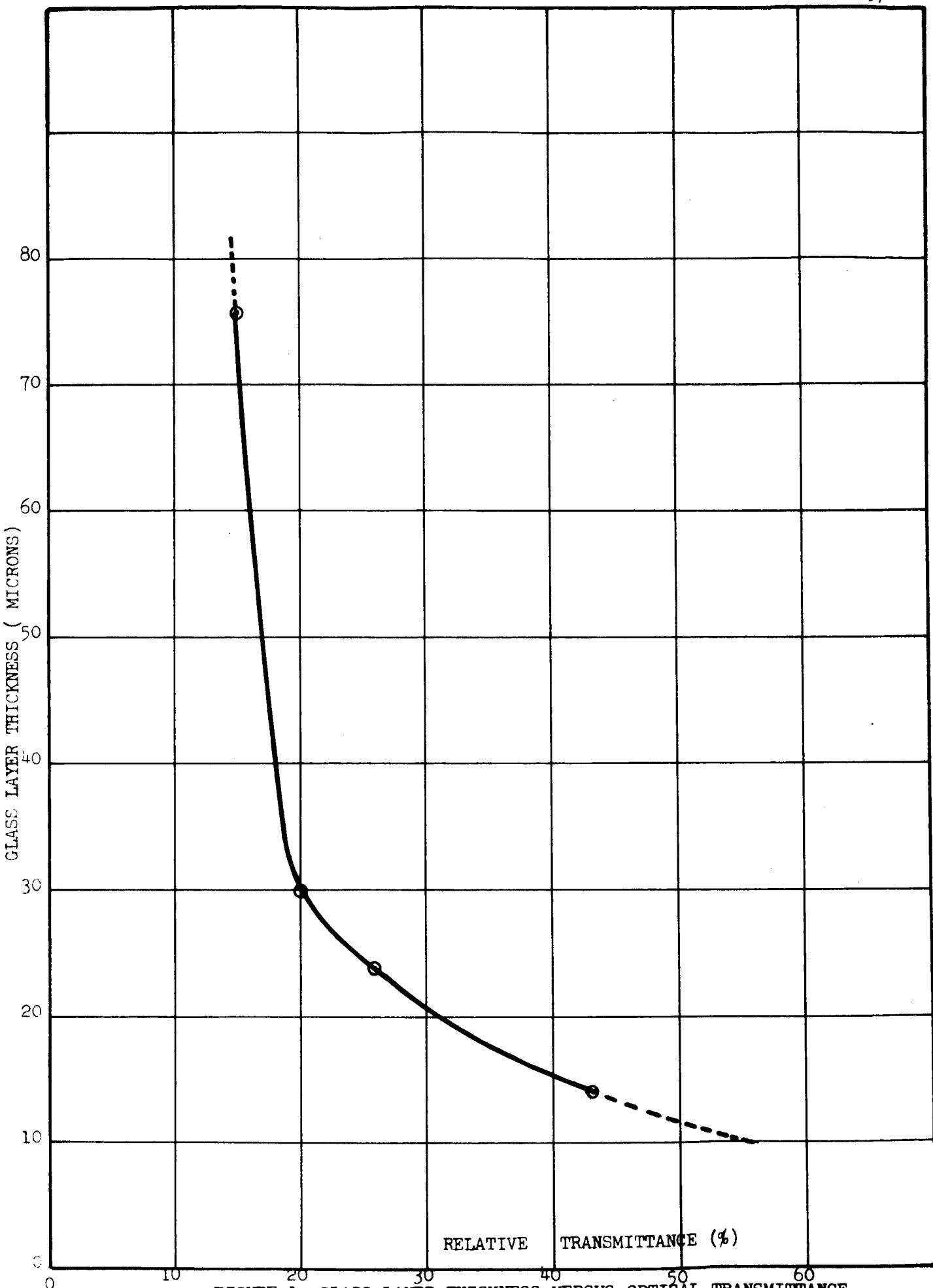

FIGURE 1. GLASS LAYER THICKNESS VERSUS OPTICAL TRANSMITTANCE OF SLURRY.

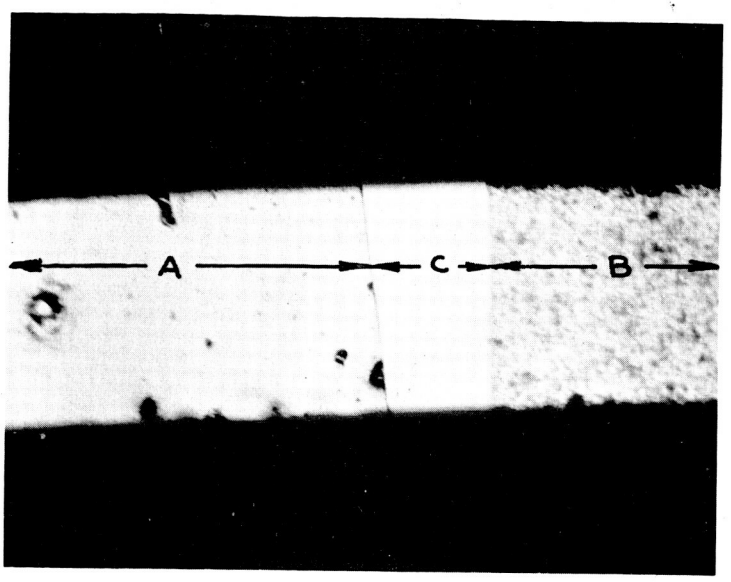

(a) TRANSMISSION PHOTOGRAPH

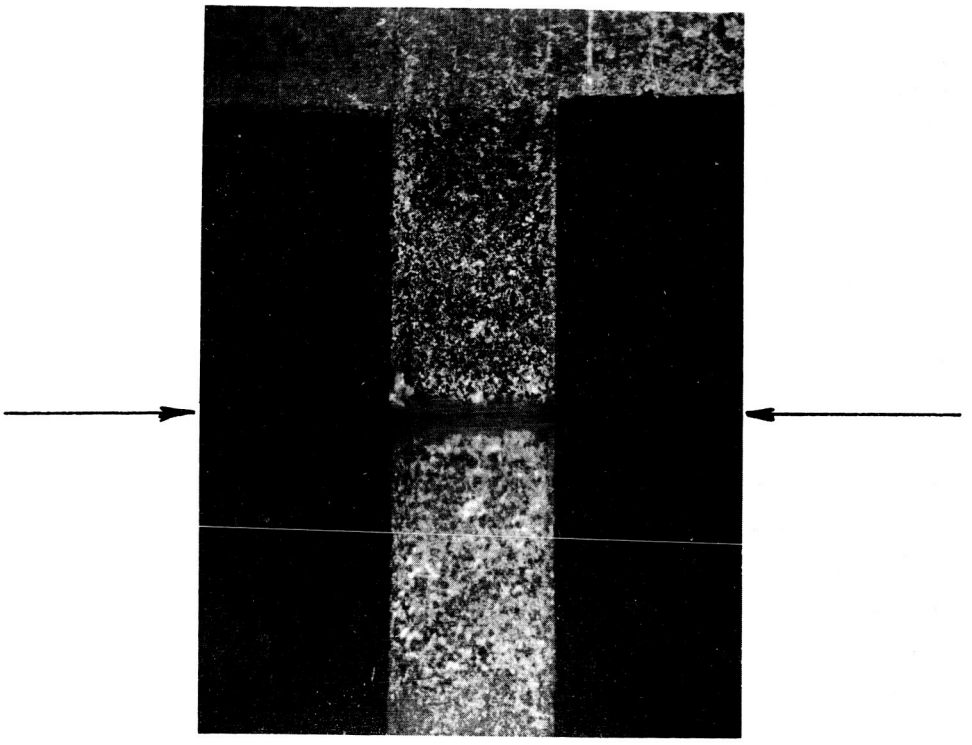

(b) FUSED GLASS ON CELL

FIGURE 3 - PHOTOGRAPHS SHOWING TRANSPARENCY OF FUSED GLASS

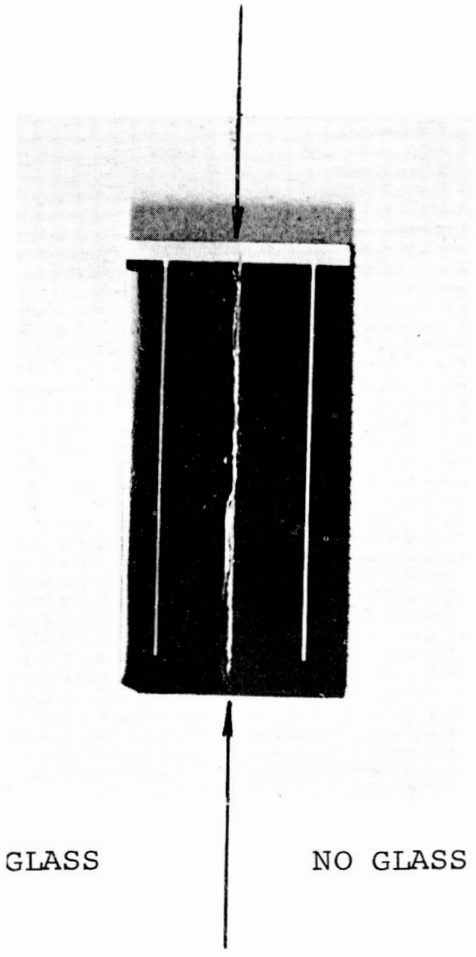

FIGURE 4 - SOLAR CELL PARTLY COVERED WITH INTEGRAL GLASS.

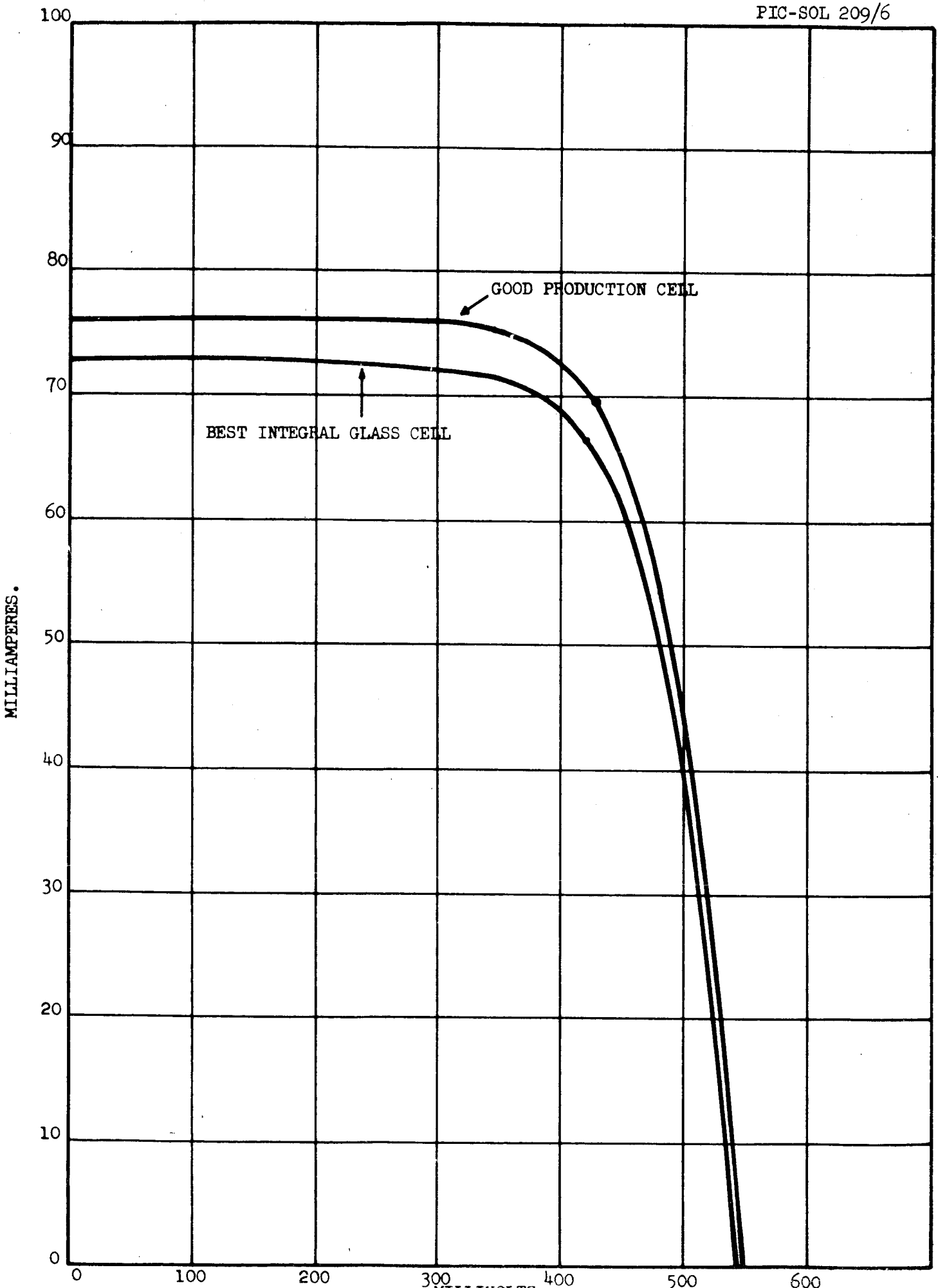

FIGURE 5. SOLAR SIMULATOR I-V CURVES. N/P. 2 cm^2. 10 OHM-cm.

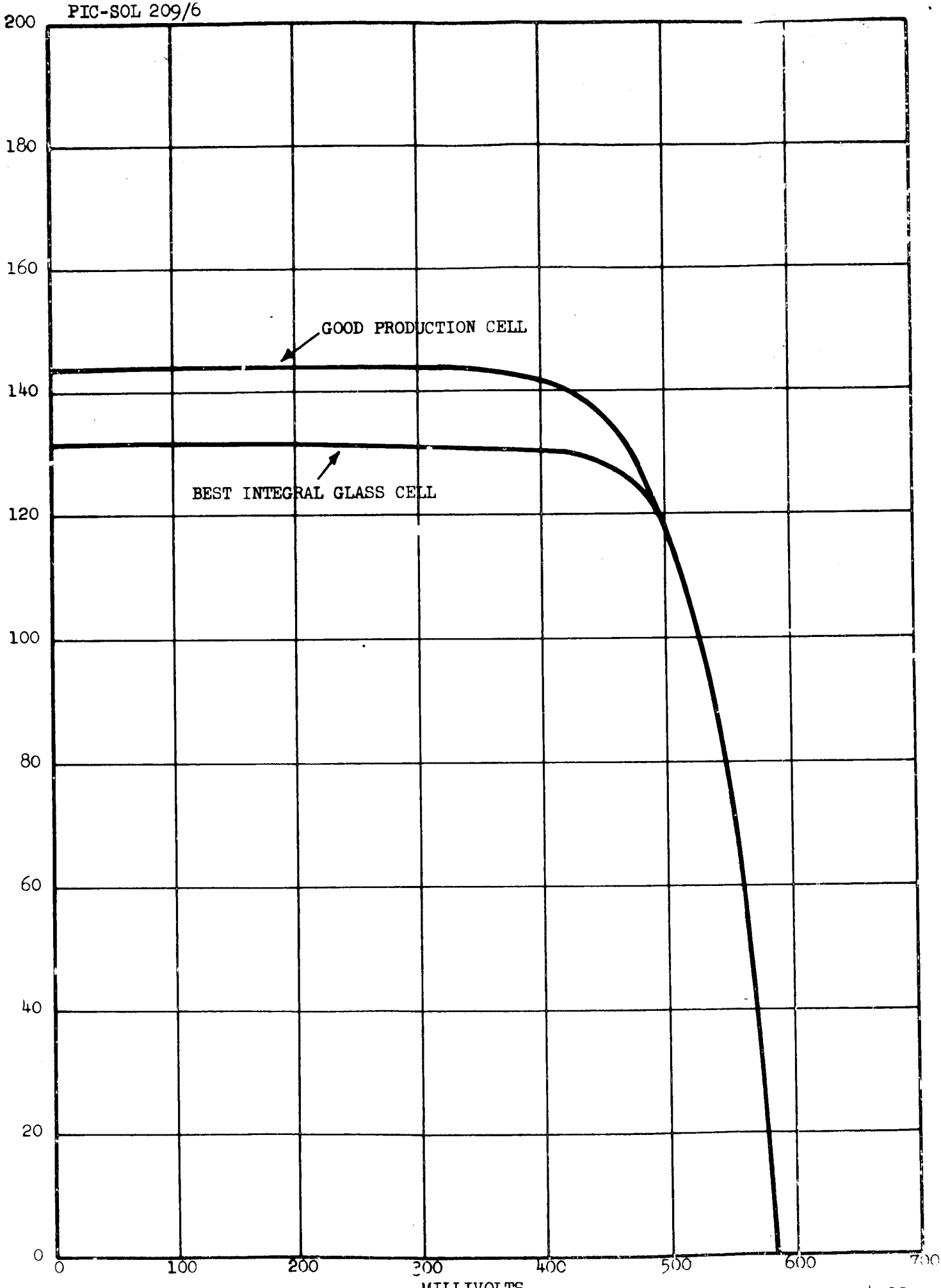

FIGURE 6. SOLAR SIMULATOR I-V CURVES, N/P, 4 cm^2, 2.5 OHM-cm.

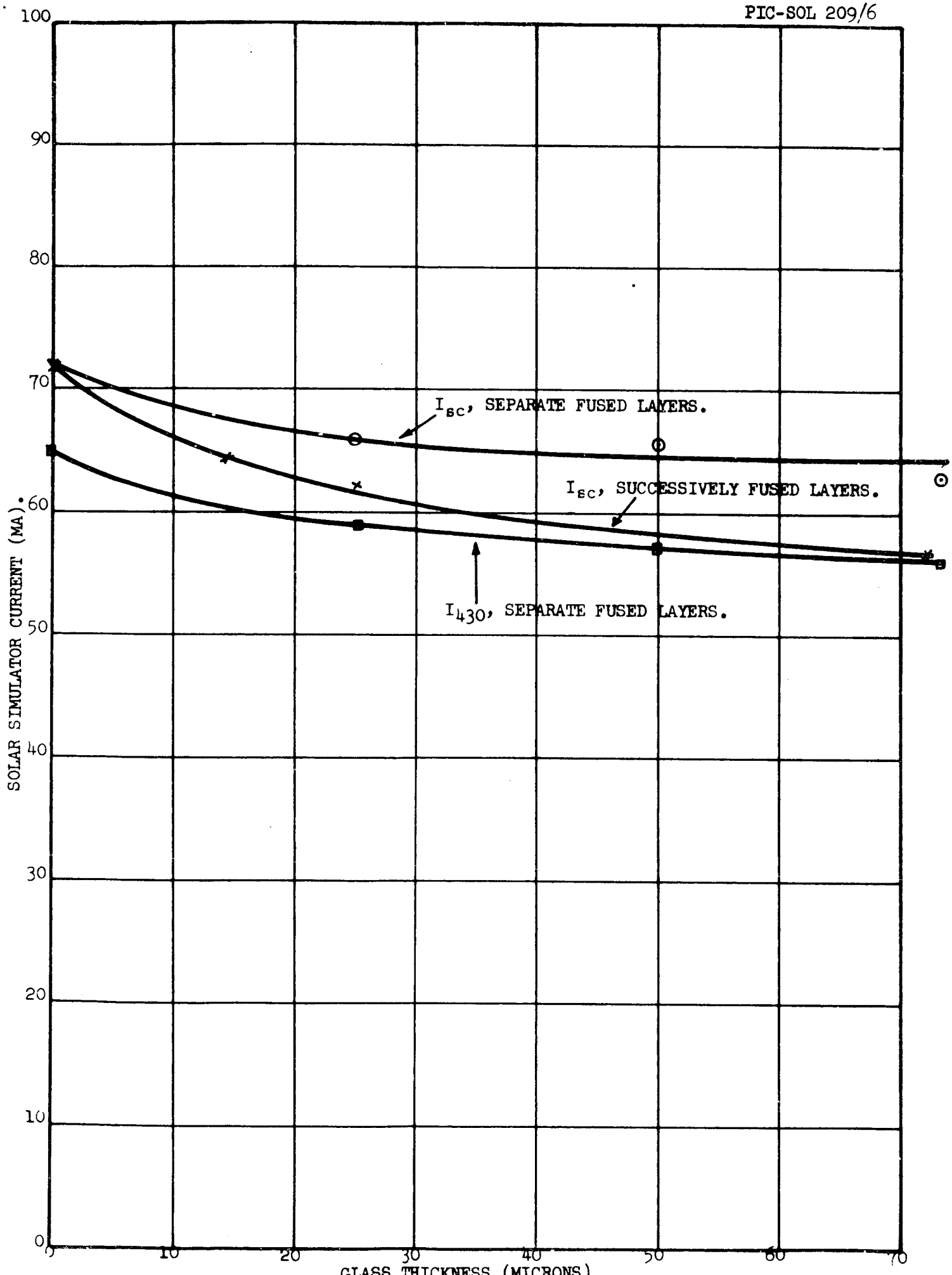

FIGURE 7. CELL CURRENT AS A FUNCTION OF FUSED GLASS THICKNESS.

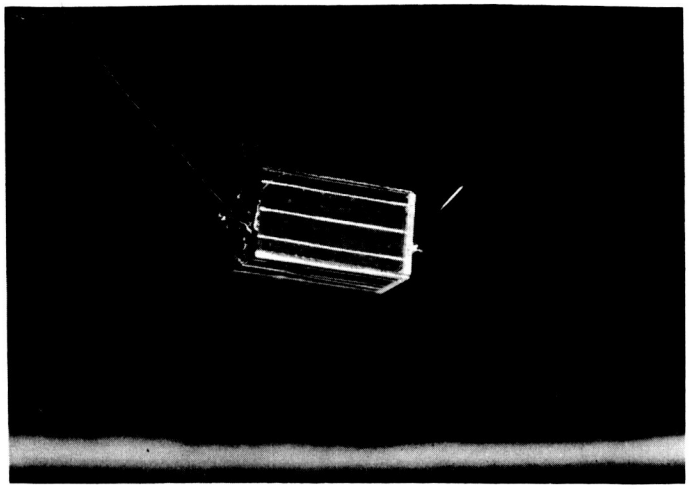

(a) SAMPLE

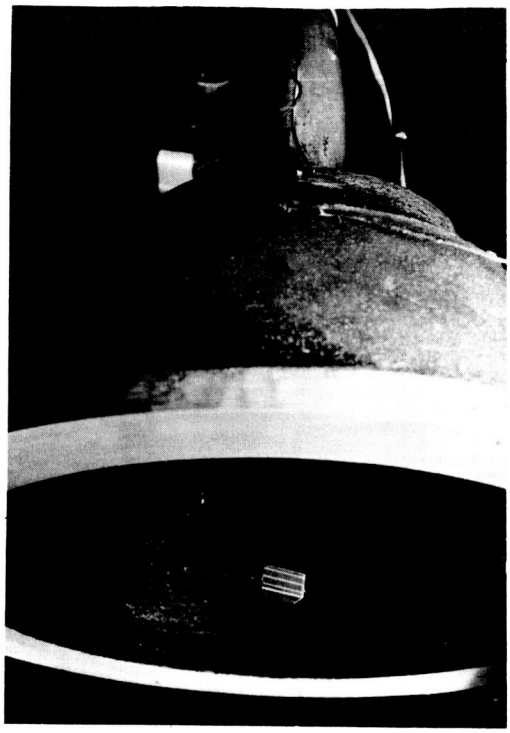

(b) SAMPLE SUSPENDED

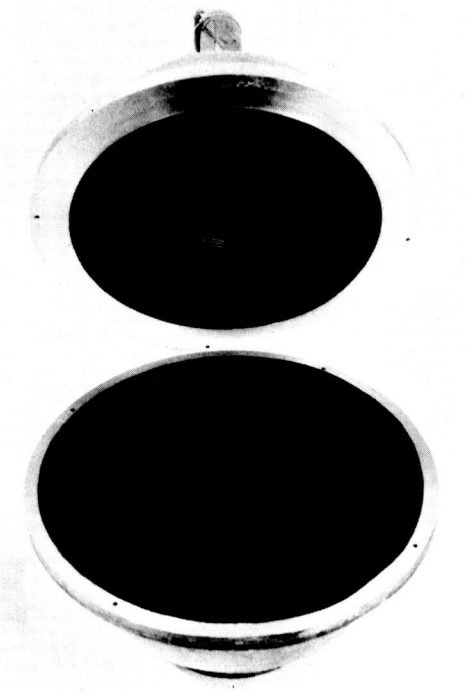

(c) SPHERE OPEN

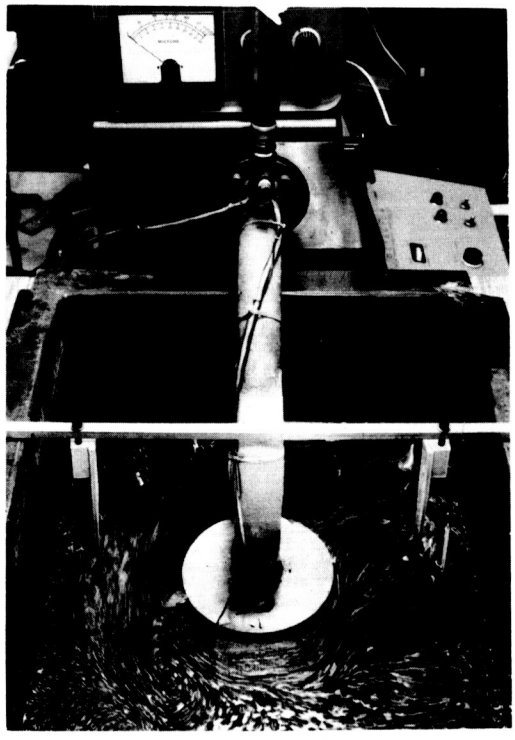

(d) SPHERE IMMERSED

FIGURE 8 - VIEWS OF THERMAL EMITTANCE SAMPLE AND EQUIPMENT

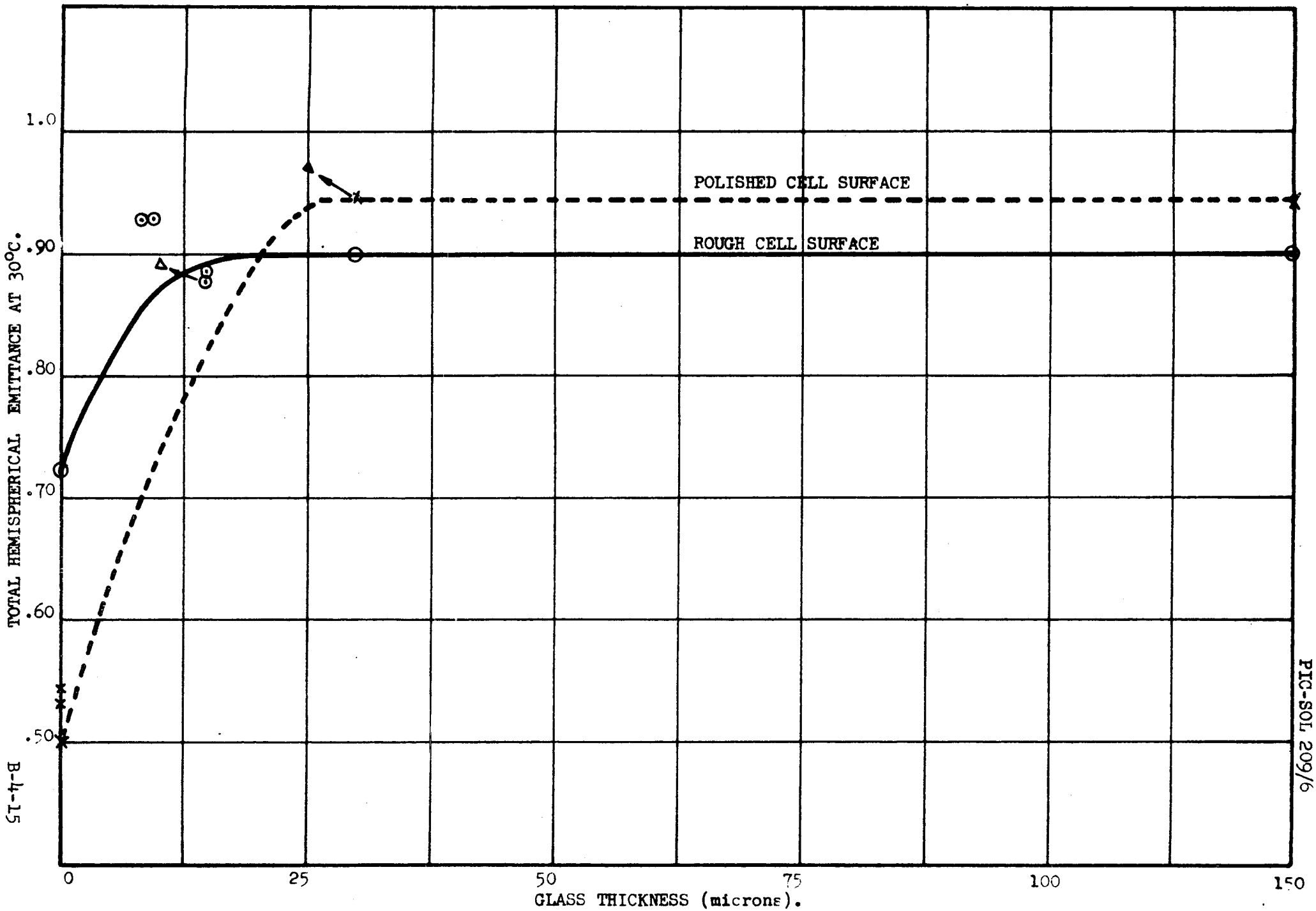

FIGURE 9. TOTAL HEMISPHERICAL EMITTANCE AT 30°C AS A FUNCTION OF GLASS COVER THICKNESS.

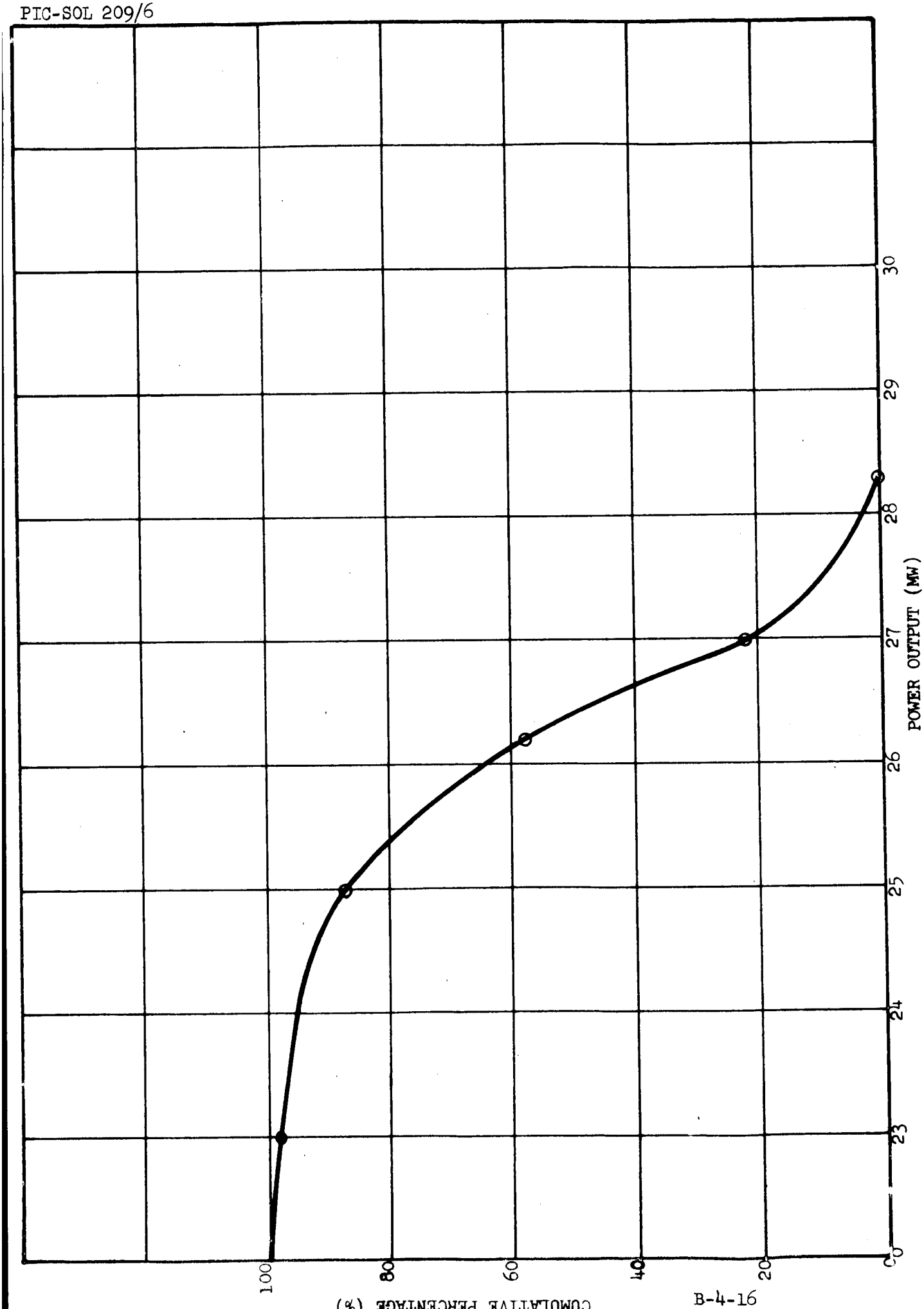

FIGURE 10. CUMULATIVE OUTPUT FOR 2 cm^2 CELLS WITH 1 MIL INTEGRAL GLASS.

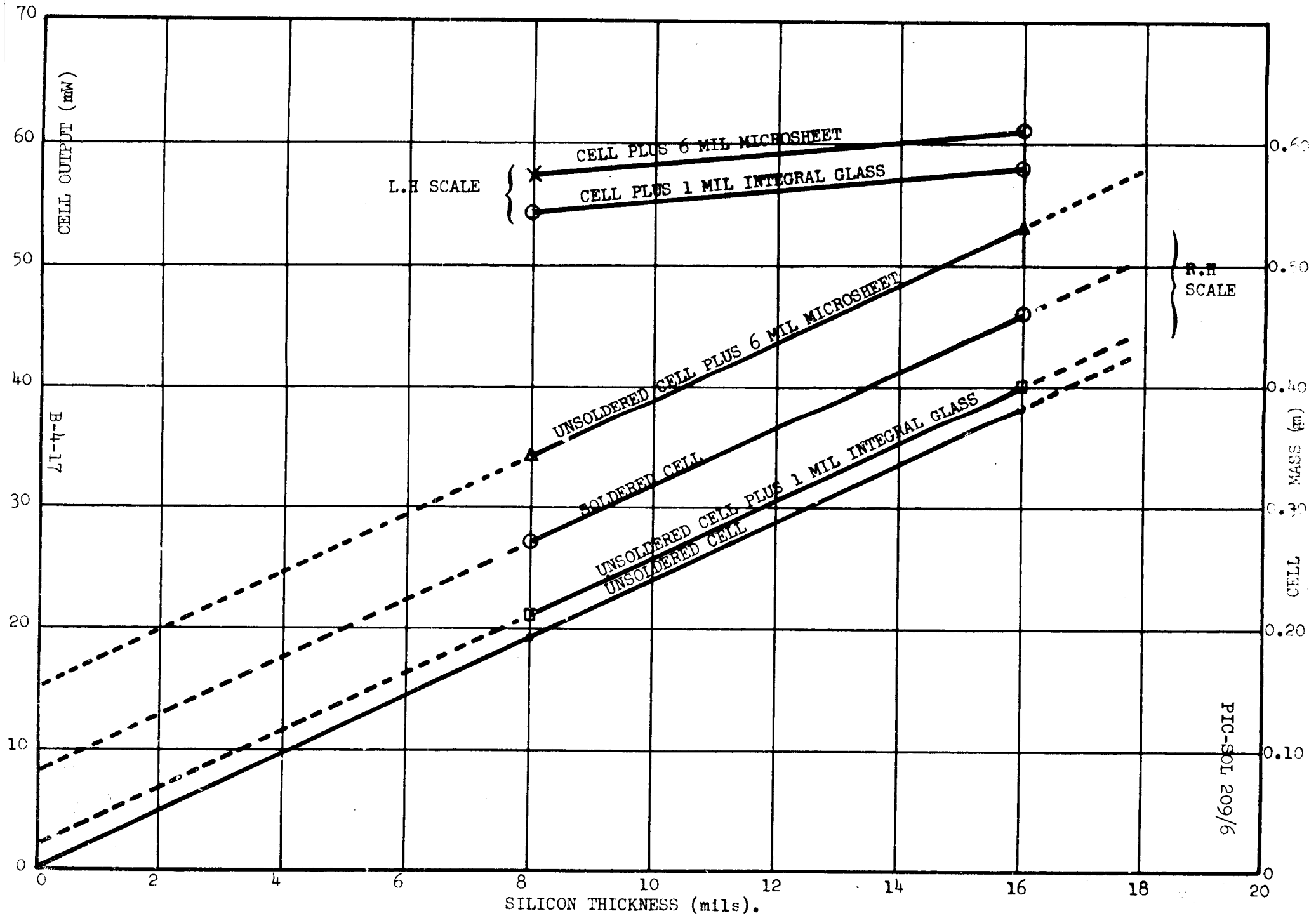

FIGURE 11. MASS AND OUTPUT OF 4 CM^2 CELLS VERSUS SLICE THICKNESS.

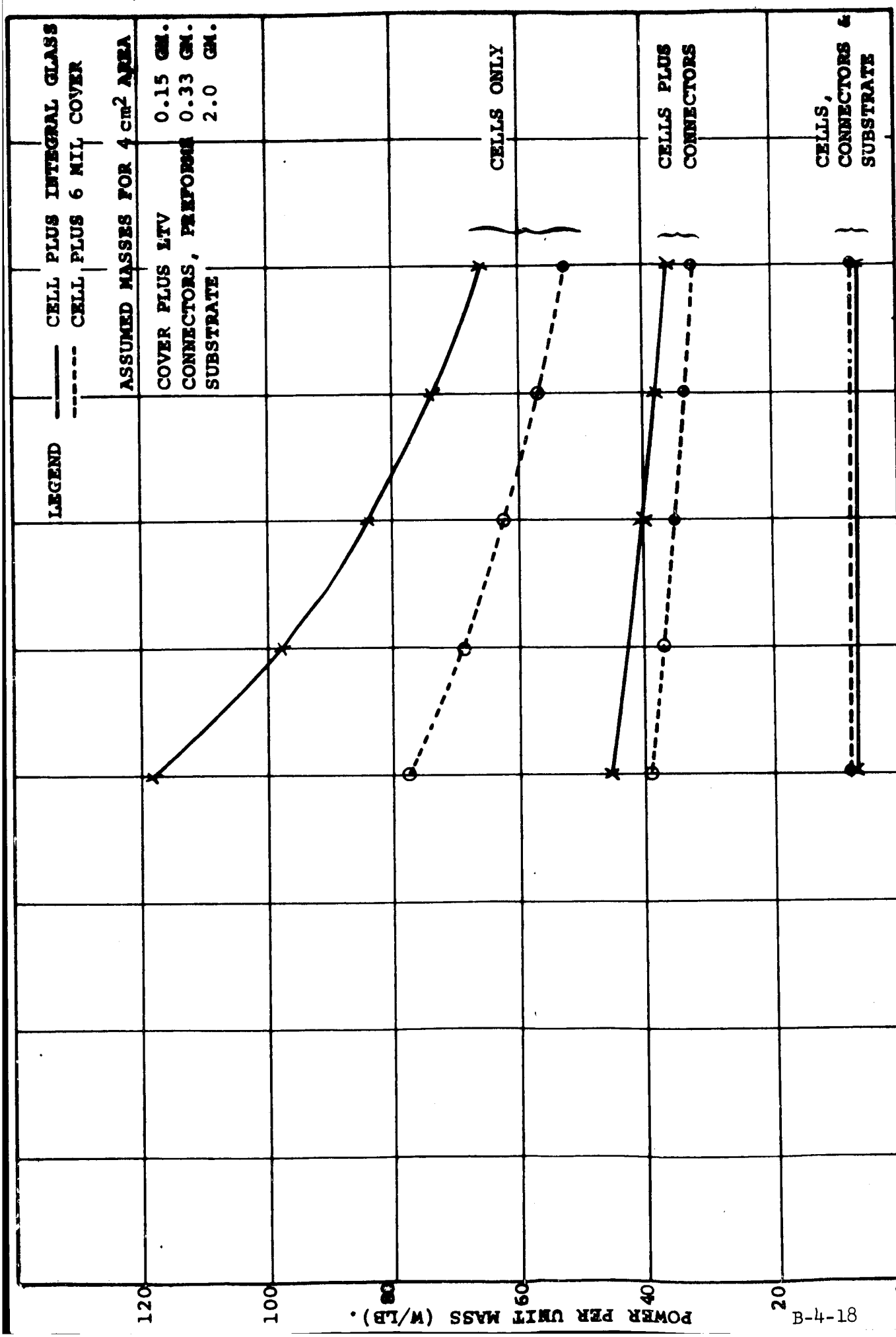

FIGURE 12. WATTS PER. POUND VERSUS SLICE THICKNESS

Discussion

Oman: Thank you, Mr. Iles. Are there questions or comments?

Ratcheson, Boeing: On your systems curves where you plotted relative watts per pound, what thickness of cells were these plotted against - were these 12 mil or 8 mil cells?

Iles: They ranged from 16 mils down to 8 mils.

Ratcheson: I see. Have you been able to successfully apply thicker coatings than 1 mil or has this been your outside limit?

Iles: Yes, we've applied up to 6 mils in integrally fused layers. We have applied 20 mil slides of prefabricated glass directly to the cell, using a fused layer as the adhesive bond. I forgot to mention that the output for these thick slides was about 5% lower than we would have expected from the fused layer alone, showing that the interaction of a thick slide and the fused layer did give us some added losses in transparency.

Ratcheson: Well, what about layers in the area of 3 or 4 mils thick?

Iles: I showed a curve of short circuit current and the current at 430 millivolts for layers up to 3 mils thick. Would you like to see that again?

Ratcheson: If it's handy, yes.

Iles: Could we see slide 7, please? Maybe we can take another question while we're waiting.

Don Ritchie, JPL: You made a statement: "reasonable production rates." What is your opinion of a reasonable production rate?

Iles: Five hundred a week is reasonable for a new process... This is the curve I mentioned. These are the measured values for the short circuit current and the current at 430 millivolts for layers 3 mils thick.

Mann - Spectrolab: On your curves of emissivity versus thickness, you showed values after a mil or so of 0.9 to 0.97, which would appear to be rather high. Would you perhaps clarify what experimental errors you anticipated - or perhaps could you indicate the emissivity that you would obtain by your technique with, say, a conventional glass?

Iles: Yes, I indicated the conventional glass slide emissivity was either 0.9 or 0.94 depending on the surface finish of the cell. Those were measured values using the same equipment.

Mann: That value is some 5 to 8% above what is normally obtained with other kinds of equipment for measuring emissivity, though.

Iles: OK. Well, this is a self-consistent set of comparison values.

Author's note: The quoted emittance values were for the glass layers only. Experimental corrections were made for the other exposed areas on the cells.

PIC-SOL 209/6
Section B-5

SOLAR CELL COATINGS

Presented by

B. S. Marks

Lockheed Missiles & Space Co.

Research Laboratories

Palo Alto, California

18 October 1965

Abstract

17318

A new semiorganic resin was synthesized and developed for solar cell surface protection. The coatings are spray applied and applicable to individual solar cells or to large arrays. The coatings have been tested on solar cells for emissivity, light transmission, as well as for environmental space effects, including ultraviolet, vacuum, electron irradiation, and temperature extremes. The effects of these tests on the performance of the solar cells were monitored and are included in this paper. Comparisons of these tests with similar tests on conventionally protected solar cells are made and discussed.

Author

SOLAR CELL COATINGS

B. S. Marks
Lockheed Missiles and Space Co.
Research Laboratories
Palo Alto, California

Introduction

At present cover slides are used to protect solar cells for three main reasons:

1. Increase emissivity of the solar cell to provide a lower operating temperature, subsequently raising the electric power output of the solar cell.

2. To protect the solar cell from radiation damage by attenuating electrons and protons in the space environment.

3. As a substrate for blue (UV) and red (IR) reflection filters, to decrease the operating temperature, and to ensure higher solar cell efficiency.

An adhesive is required to fasten the cover glass to the solar cell; however, the adhesive used must be protected from UV radiation to prevent its degradation, with resulting discoloration and some loss in transmission of light.

Feasibility of Integral Cell Covers

An integral protective shield might be desired to replace the coverglass and adhesive sandwich for the following reasons:

- Material Costs: The cover glass or slide is generally microsheet glass or fused silica. It generally has a dual coating system; namely, 1) an antireflective inorganic salt coating on one side, and 2) a UV reflective diffraction coating for the protection of the adhesive on the opposite side. The latter coating is particularly expensive in that it is a multicoated system, with exacting thickness requirements laid down by vacuum deposition techniques.

- Labor Costs: The job of placing the slides and adhering them individually to each solar cell requires infinite care and precaution resulting in high labor costs. Furthermore, breakage, particularly of the thinner cover glasses, can add to the cost.

- o Emissivity: The emissivity of the cover glass coated with the antireflective inorganic salt is usually about 0.8, which is high compared to the uncovered solar cell, but still not as high as could be obtained.

- o Weight Factors: For many missions, thick cover slides are required for radiation protection, but, for others, thinner ones are sufficient. Due to the fragility of the slides, 6 mils thick cover slides appear to have been chosen as the minimum thickness. A thickness of 1/2 of this or less with its weight advantage would often otherwise suffice.

- o New Solar Cell Types: Cover glasses may or may not be readily usable for new solar cell types. In particular, the use of cover slides is not easily adaptable to thin film or dendritic types of solar cells.

Thus, the principal advantage to be gained through integral solar cell covers is the elimination of the need for the complex, costly slide/adhesive approach.

Coatings as Integral Cover Materials

It was felt that an integral protective shield could take the form of a coating to obviate the deficiencies enumerated above. Such a coating would have the following characteristics:

- o Inexpensive materialwise in comparison to the cover glass assembly as it could be prepared and formulated as a solution ready for application.

- o Inexpensive laborwise, since a coating can be applied via spray, brush, or roll-coating technique with spray being preferred for this task. Furthermore, a solar cell panel could be sprayed after it is assembled, obviating special handling.

- o Coating materials which have higher emissivity (in the order of 0.9) could be chosen.

- o The weight factor for a solar cell coating can be decided definitively. Given thicknesses of coating can be spray-applied to give exactly what is desired for a particular mission. Furthermore, areas which are not to be sprayed can be taped or masked before spraying and subsequently removed.

- o New solar cell types, in particular the thin film, dendritic growth, and wrap-around solar cells are admirably suited for coating protection.

Based on the preceding reasoning, the next logical question is what type of materials does one choose to perform this coating task? In essence, as part of our synthetic materials effort in certain new and novel semiorganic polymers, it was noted that certain of these polymers gave better than 97% light transmission in the range of 4000 - 12,000 Å. Based on this optical clarity, further investigation of these materials for solar cell coatings or shielding materials was carried out.

Methods of crosslinking the resins and formulating to obtain desired coating properties were found. Coating systems which gave fairly interesting overall balance of properties when coated on solar cells were subsequently obtained.

Description of the LMSC Solar Cell Coating

Application of the coating to solar cell is fairly straightforward. The formulated coating is placed in solution prior to use and is spray-applied to the preheated (200°F) solar cell or solar cell panel, followed by oven cure at 250°F for 1.5 hours. By small changes in the relative amount of curing agent, the coating surface can be modified from a smooth bright shiny finish all the way to matte finish.

The properties obtained with the smooth shiny finish are summarized in Table 1, where they are compared with the conventionally used Corning 7940 (blue filter, 20-mil fused silica) cover slide.

As shown with the Lion Optical Surface Comparator at room temperature, the coating has a greater emissivity than the fused silica cover slide (0.9 vs 0.8), which will in itself give, based on the lower surface temperature, an increase in power output of about 4%. The blue filter used on the cover slide approach, however, reflects the ultraviolet solar radiation, also resulting in a lower solar cell surface temperature. Thus, from the standpoint of equilibrium temperature, both approaches are roughly equivalent.

Optical methods of measurement of covers and coatings were considered secondary to direct measurement of coated solar cells. The comparative measurements reported herein were all carried out in the form of current-voltage (I-V). An Optical Coating Laboratory Model 31 Solar Simulator was used as the solar simulator light source for all I-V measurements.

As shown in Table I, a 2-mil LMSC coating results in a loss of 2.3% in the solar cells output as measured by short circuit current, compared to as much as a 6.0% loss by covering the solar cell with a Corning 7940 fused silica cover slide adhered to the solar cell with LTV-602 adhesive. The I-V curves for two 1 by 2 cm solar cells before and after coating are shown in Figure 1 (before) and Figure 2 (after). Little difference can be noted in the two curves.

Environmental Testing

Coated solar cells were subjected to vacuum at 2×10^{-6} torr and ultraviolet radiation of 700 sun hours. They showed a loss of 7.3% in short circuit current as compared to a 1% loss for the conventional blue filtered Corning 7940 covered solar cell. The ultraviolet radiation source used was an argon filled A-H6 high pressure mercury arc lamp. The lamp was mounted in the vacuum equipment shown in Figure 3 and the coated or covered solar cells mounted at 1, 2, and 6 sun position, as shown in Figure 4.

Using a 2 Mev Van de Graaff accelerator conventionally covered, LMSC coated, and bare solar cells were subjected to electron irradiation of 10^{16} e/cm^2 at 1.5 Mev. This resulted in negligible coating damage (~0.5% Isc). Solar cells protected by a 20-mil thick, blue filter, fused silica cover slide showed a loss in excess of 3% Isc due to the cover slide.

Table II summarizes the electron damage results of a more recent irradiation using 1 Mev electrons and total flux of 9×10^{15} e/cm^2. The energy of electrons reaching the solar cell is diminished by traversing the protective shielding as shown in line 1(1,2).

This results in reduced damage to the solar cell because of the energy dependence for electron damage. The resultant calculated loss in short circuit current is shown in the second line. Since the 2-mil Lockheed coating is relatively thin, electron energy attenuation is small and therefore damage to the solar cell by the 1 Mev electron beam is approximately equal to that for the uncovered solar cell. However, if one examines the fourth horizontal line showing the observed loss of short circuit current after irradiation one finds that the loss of output of the 2-mil coated cell equals the loss of the conventional 20-mil fused silica blue filtered covered cell. The only explanation for this apparent inconsistency is summarized in line 3; namely, degradation changes in the protective cover assembly, which would appear to be tied to loss of light transmission.

In the case of the blue filtered fused silica cover slide, the loss in transmission amounts to 4%, without the blue filter the loss is only 2%, and in the case of the Lockheed coating, the loss is ~1%. Consequently, after 1 Mev electron irradiation, the resultant output of solar cells with the 2-mil coating is equivalent to those with the 20-mil fused silica blue filter conventional cover slide.

The total loss of short circuit current due to covering or coating, UV damage, electron damage, as stipulated, is shown in Table 1 as 10.6% for solar cells protected with the 2-mil Lockheed coating as compared to 11% for those protected with the blue filter, 20-mil fused silica cover slide.

As part of the space environment requirements studies, solar cells with the 2-mil Lockheed coating were subjected to a 24 hour soak at -260°F. Thermal cycling was performed between -225°F and 176°F. No discernible change in short circuit current was evident in either test.

The estimated relative cost included in Table 1, although not of scientific interest, may be of interest to round out the comparative story.

Fluorescent Properties

Some of the new polymers synthesized, when formulated and coated on solar cells, resulted in little or no loss of short-circuit current as compared to the uncoated solar cell. In an attempt to explain this phenomenon, the following possible causes were investigated:

1. A possible photoelectric effect in the coating was ruled out.

2. Possible current resistance of the silicon surface decreased by the coating. Electrical resistance $>10^{11}$ ohm/sq at 1.5-100 volts showed the coating to be a good insulator and hence of no aid in carrying current.

3. Reflectivity of coating compared to that for the uncovered solar cell was also investigated. Reflectivity measurement of an uncoated solar cell and LMSC-coated solar cell showed that, from 5000-8000 Å, the coated solar cell gave more reflection than the uncoated (Fig. 5). This possibility was thus ruled out.

4. Under black light (ultraviolet >3100 Å) the coating on a glass slide was noted to fluoresce in the yellow green (5400-5500 Å). The coating also demonstrated this effect on solar cells.

It was interesting to note that a theoretical study of the possible increase of efficiency of solar cells by the use of directed fluorescent coatings has been made [3]. In their analysis [3] they assume that the fluorescent coating absorbs a large fraction of activating wavelengths and reflects away from the rest which are unused. They[3] also assume fluorescnece at wavelengths most sensitive for solar cell absorption.

The difference in energy between the absorbed wavelength and the fluorescing wavelength is given off as heat, which results in less efficiency of the solar cell. This heat was also included in the overall calculation to detract from the cell's power output.

In actuality, the LMSC coatings do not reflect the ultraviolet and hence any fluorescnece obtained is a gain in output. In any case, after integrating all the factors based on the above assumptions they[3] obtain the following equation:

$$\text{Fractional Improvement in Output of Solar Cell Due to Fluorescent Coating} = aA_c + bB_c - 1$$

wherein:

a = probability a photon will be absorbed by the coating, will be remitted by fluorescence, and absorbed by solar cell

b = transparency of fluorescent coating

A_c and B_c contain factors such as solar cell response, incident solar energy, etc.

Due to geometry of a coating on one surface, the probability "a" >0.5 is limited, and the authors also indicate that "b" = 0.9 is not too likely. This, however, is not the case with our coating; transmission of ~ 97 percent was noted. Their calculations showed that wherein "a" = 0.50 and b = 0.95 their increased output ranges from 4.7 to 5 percent. The big rise in fractional improvement lies wherein "a" becomes larger than 0.5, which is difficult to obtain in that it is to a large extent a fixed parameter. In any case, these values include the heat produced by fluorescence as a loss in solar cell efficiency, considering all unabsorbed ultraviolet as reflected; wherein, as stated earlier, the LMSC solar cell coating does not reflect the ultraviolet (no blue filter) and hence any fluorescence obtained is a gain in output.

A desired fluorescent coating should strongly absorb ultraviolet wavelengths and fluoresce the preferred wavelengths which most activate solar cells. This usually is in the red end of the visible spectrum. By necessity, the coating should also have the good properties enumerated in Table 1.

Conclusion

In conclusion, the Lockheed solar cell coating presents an attractive solution to the many problems posed by the cover slide/filter/adhesive system. Thermal incompatibilities are eliminated. Application cost is drastically reduced. Solar cell performance is comparable to that for conventionally covered solar cells, and is not in any way compromised by adverse environmental effects.

Future activity includes flight testing of the material as it is presently developed. Further development is possible and encouraged in the areas of: 1) reduction of ultraviolet darkening; 2) building up of thicker coats; and, 3) optimization of fluorescent output enhancement. The specific adaptation of the coating to the newer types of solar cells should also be pursued.

References

1. D. L. Reynard, "Proton and Electron Irradiation of N/P Silicon Solar Cells", LMSC Report No. 3-56-65-4, Palo Alto, California, 12 April 1965.

2. "Energy Loss and Range of Electrons and Protons", U. S. Dept. Commerce, W.B.S. Circ. 577, March 1962.

3. J. K. Baker, "Temperature Control Techniques for Solar Energy Converters", NSD-TR-61-689, February 1962, pp. 76-80.

TABLE 1

SOLAR CELL SHIELDING

Property	LMSC Semi-Organic Coating	Corning 7940 Fused-Silica Cover Slide
1. Emissivity (Lion Optical Surface Comparator) Flat Emission	0.9 (room temp.) (Lion O.S.C.)	0.8 (room temp.) (Lion O.S.C.)
2. Loss Isc (Short Circuit Current) caused by covering solar cell with coating or cover	-2.3%, 2 mil	-6% with blue filter, 20 mil
3. Ultraviolet Damage; Loss Isc after 700 sun hours at 2×10^{-6} torr. Loss Isc due to coating	-7.3%	-1% with LTV 602 adhesive
4. Electron Damage (1.5 Mev, 10^{16} e/cm^2). Loss Isc due to coating	-1%	-4%
5. Loss Isc, total of 2, 3,4, above	-10.6%	-11%
6. Thermal Shock to -260°F	Passes	Passes
7. Cost	$0.125/solar cell	$1.25/solar cell, 1 x 2 cm

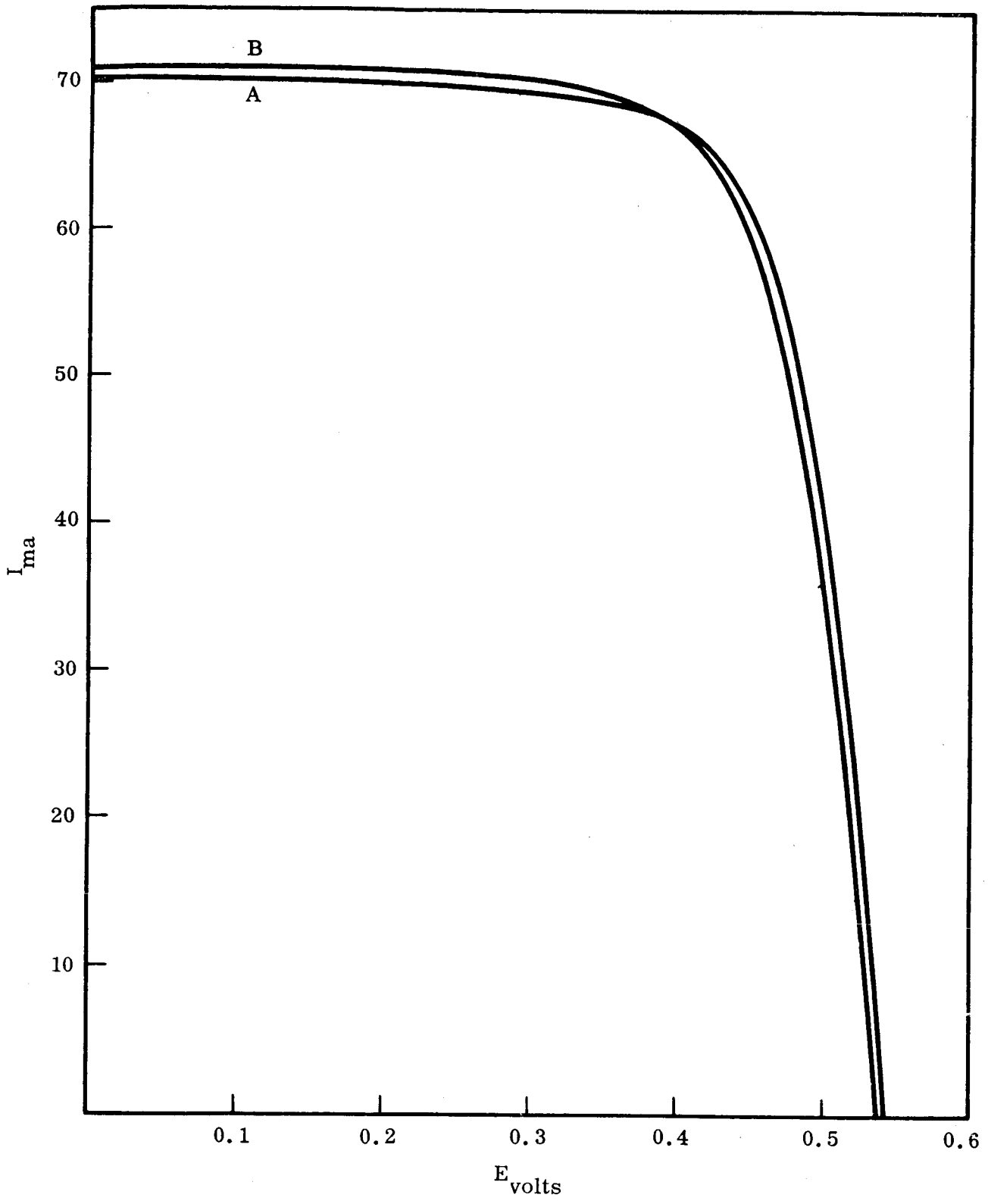

Fig. 1 UNCOATED 1 × 2 CM SOLAR CELLS A AND B

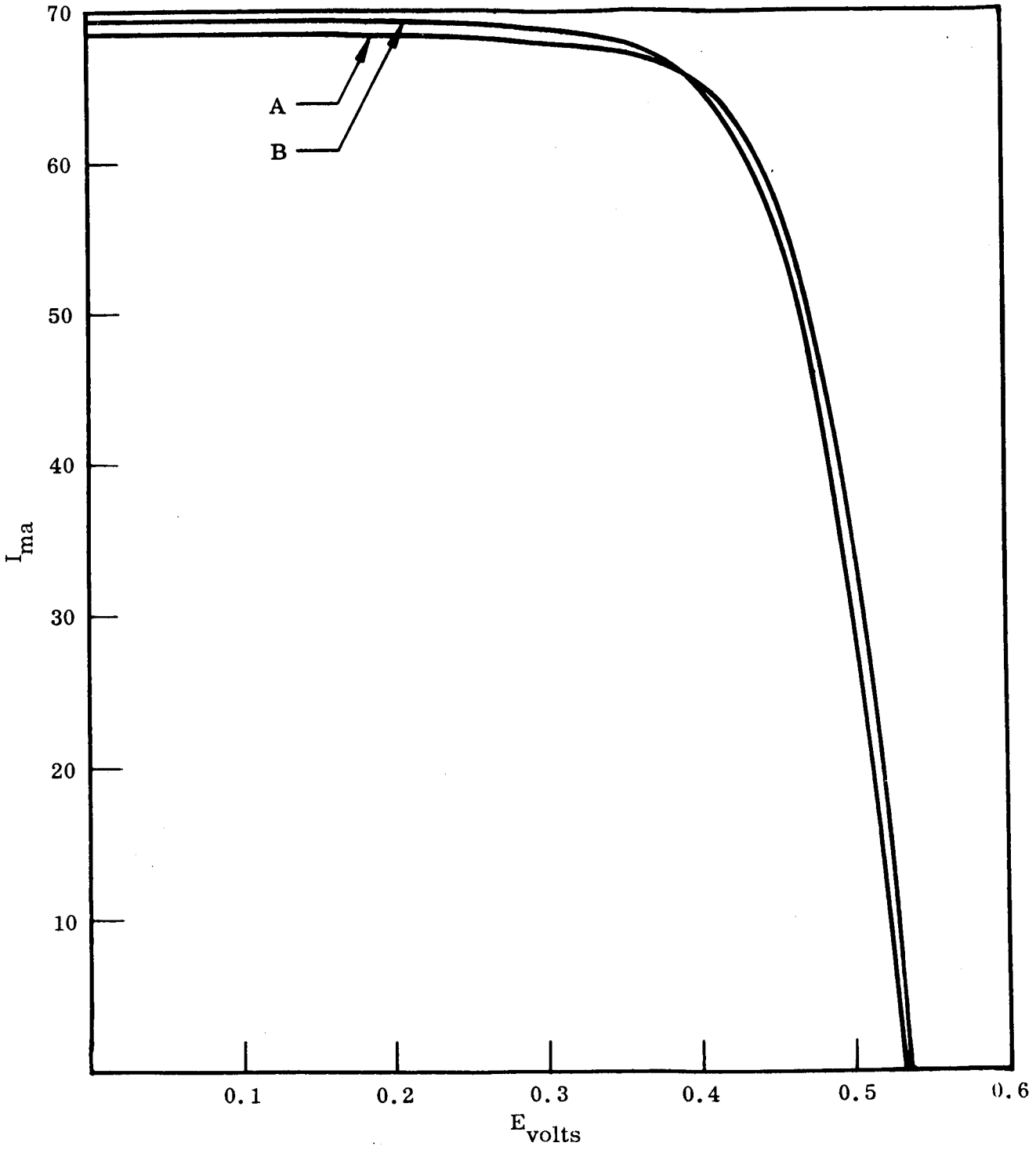

Fig. 2 2 MIL LMSC COATED 1 × 2 CM SOLAR CELLS A AND B

TABLE 2

Protection for Solar Cell	No Protection	B + Blue Filter	B	2-mil LMSC Coating
1. Electron Energy at Solar Cell	1 Mev	0.85 Mev	0.85 Mev	0.98 Mev
2. Electron Damage to Solar Cell Isc Loss	0.26	0.23 calc	0.23 calc	0.26
3. Electron Damage to Cover or Coating Isc Loss	0	~ 0.04	~ 0.02	~ 0.01
4. Total Isc Loss Observed	0.26	0.27	0.25	0.27

B = 20 mil fused silica cover slide adhered with LTV-602 to the solar cell.

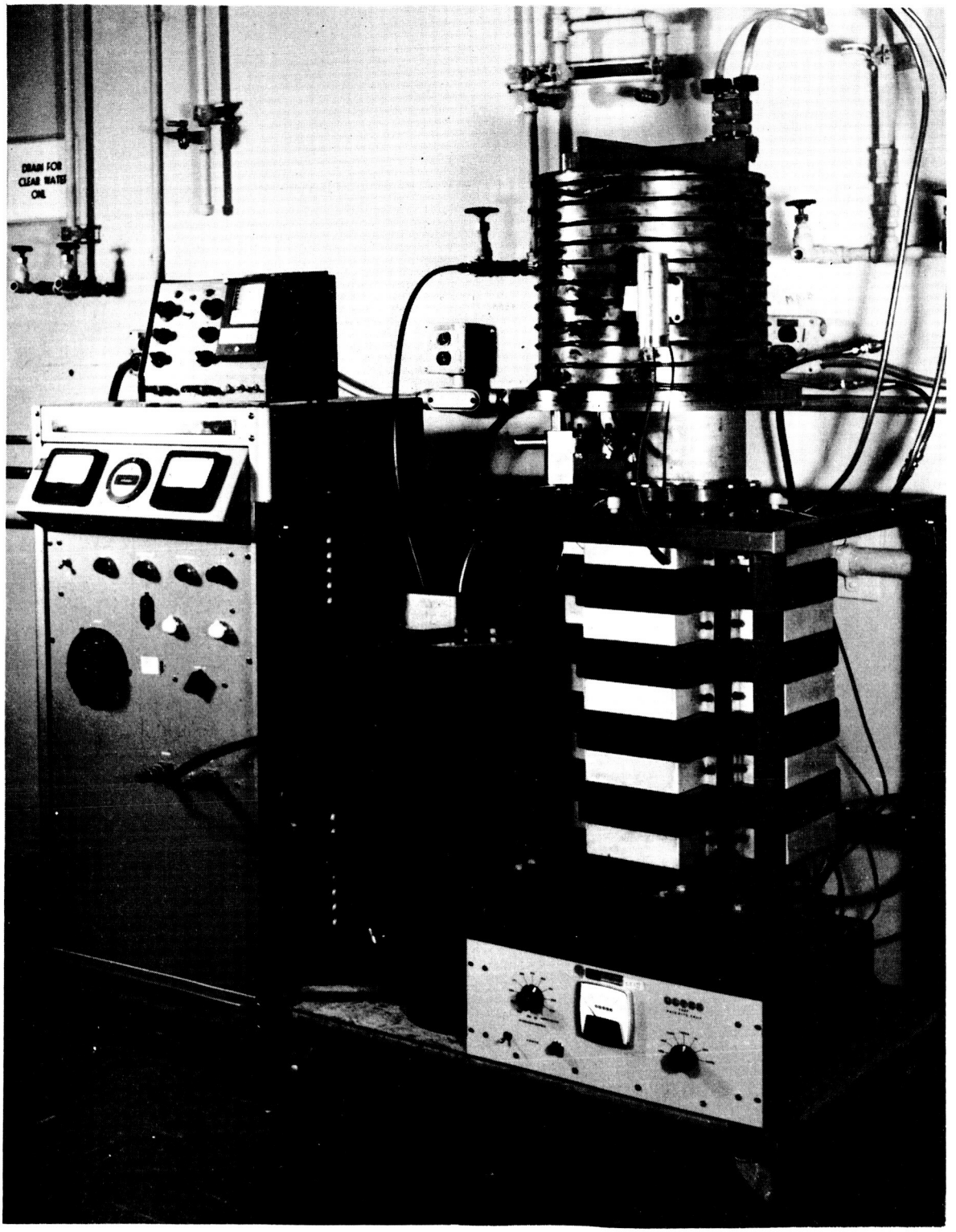

Fig. 3 ULTRAVIOLET-VACUUM SIMULATION EQUIPMENT

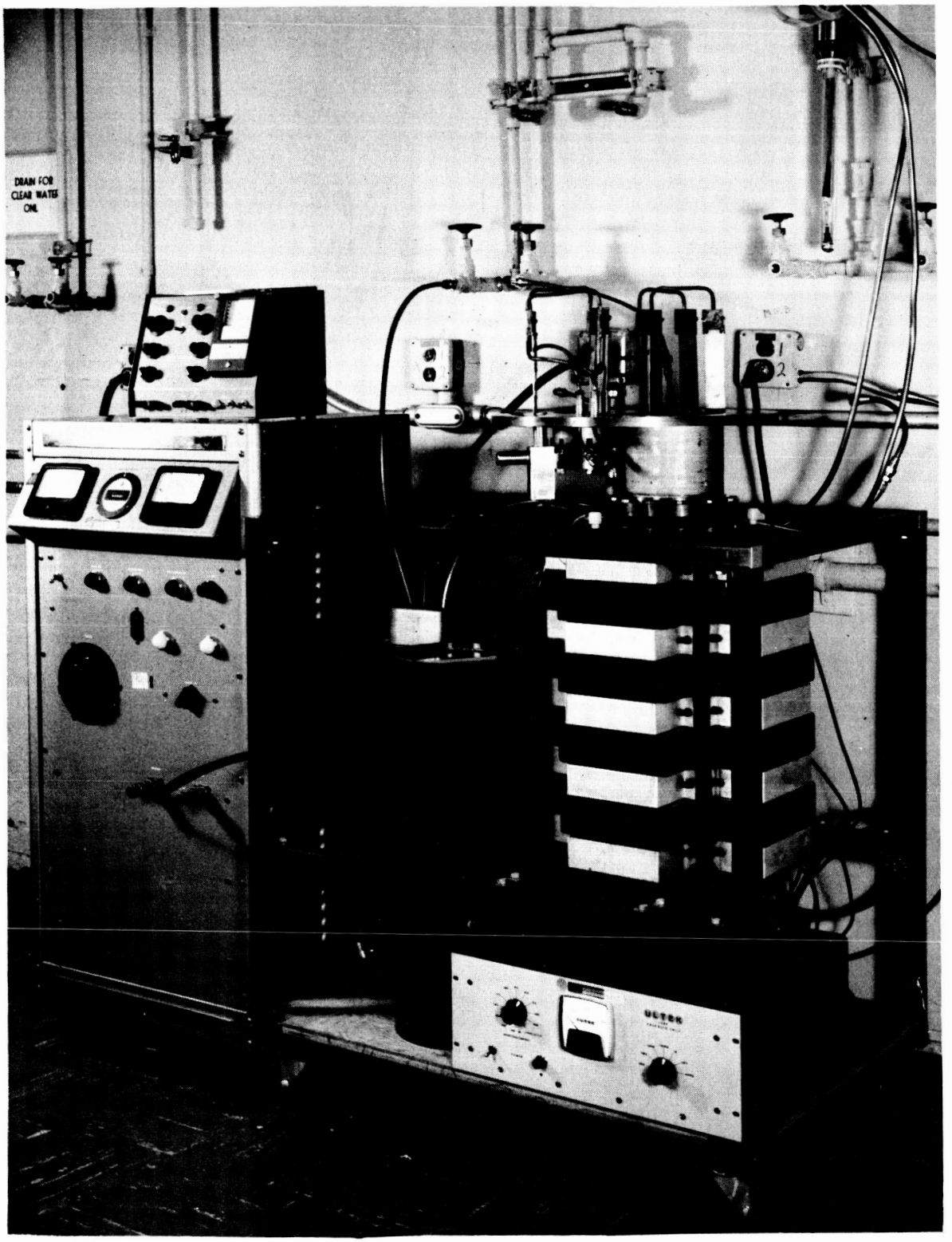

Fig. 4 ENVIRONMENTAL TEST EQUIPMENT

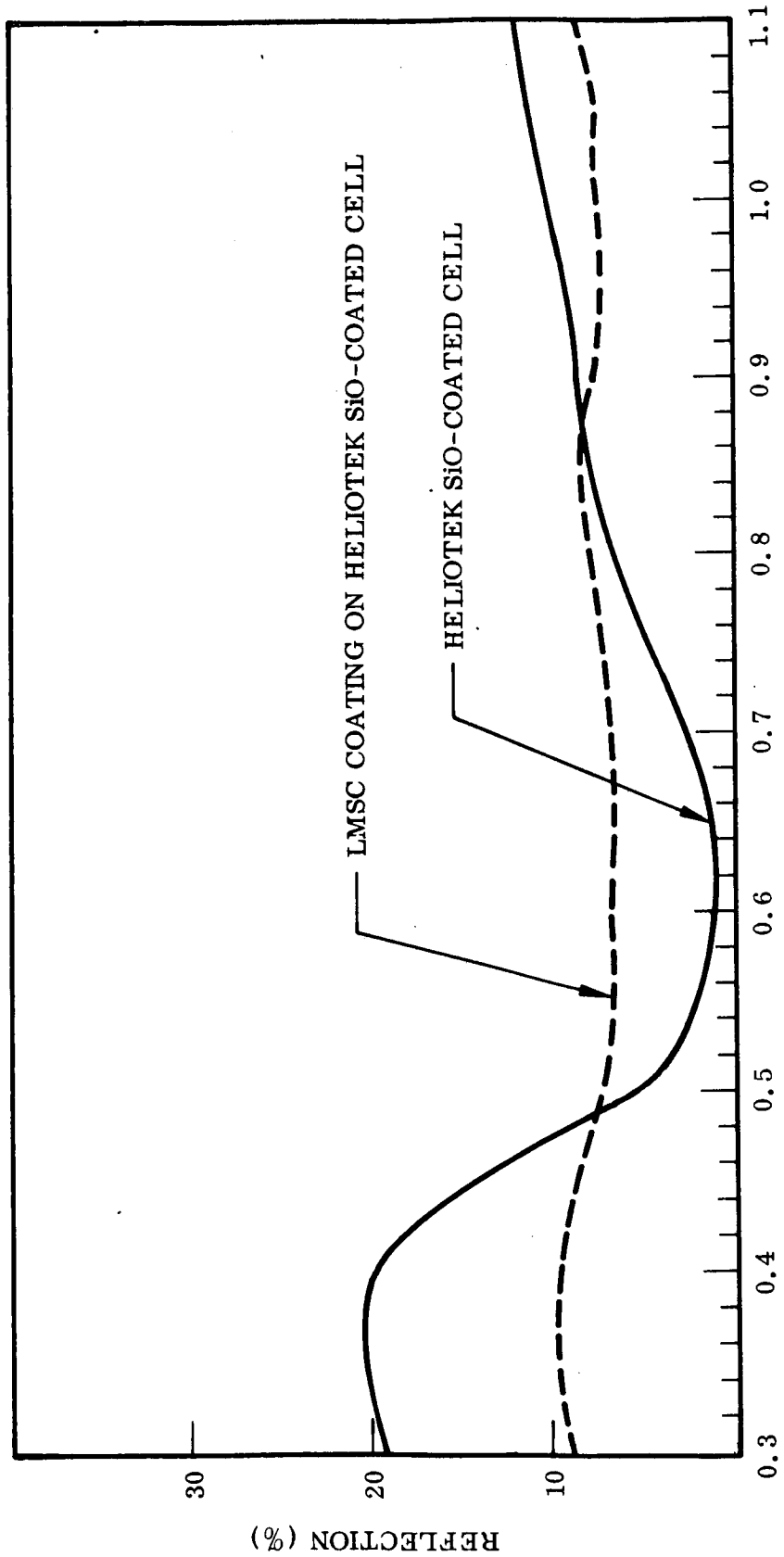

Fig. 5 REFLECTIVITY OF SiO-COATED VS. LMSC-COATED SOLAR CELLS

Discussion

Oman: Thank you very much, Dr. Marks. I feel that I have heard a truly revolutionary paper. Not only is there a breakthrough in the state of the art indicated here, and also we have made a step toward - at the end of the day - achieving the goal which was outlined to us the first thing in the morning about getting 3 or 4 times more efficiency; but we have a speaker that talks dollars and cents and he talks dollars and cents in the quantities that I can understand. So we now will hear a discussion.

Loferski - Brown: In discussing the relative results for different kinds of covers in radiation damage experiments, you showed figures such as 26% degradation, 27% and so on. Isn't the scatter in the experiments of such an order that really drawing any kind of conclusions from a difference between 26 and 27% is a little bit questionable.

Marks: There is a fair scatter; however, quite a number of cells have been done and they all fit, within the range that we consider to be valid for these numbers.

Oman: Now, we'll hear from a technologically unemployed manufacturer of solar cell covers, Al Mann. (laughter)

Mann: Now that I'm unemployed, I'd like to ask several questions. One, related to the question that Joe just asked, if you will recall the slide in which you showed the various degradations . . .

Marks: The electron damage?

Mann: The electron damage, yes. The experiment was done with 1-1.5 Mev electrons which penetrate all of the coatings, and if you will note, the unprotected cell itself would indicate that it was probably the best choice under that environment.

Marks: No, you have to remember one thing. This is just one, and I stress one, Mev electrons. This is one of the shortcomings of our (collectively) measurements.

Mann: I'm saying that that's not the case that you have in space, that you have a spectrum of particles, and that I don't think that you can draw any conclusions from that specific slide in that regard. The second point is that...

Marks: I didn't draw any conclusions. I just stated the facts of what our measurements were.

Mann: No, but you stated some conclusions at the end, saying - trying to point to the fact that this coating was therefore comparable to the thicker coating as far as degradation is concerned...

Marks: To 1-1.5 Mev electrons....

Mann: 1-1.5 Mev electrons.

Marks: Period.

Mann: OK. But not in space.

Marks: All right.

Mann: Second point is that the ultraviolet degradation was based upon 700 hours, which is a little over 29 days in space or, in an eclipsed orbit, maybe 40 days in space. Of course, some of the missions which you fly are very short and perhaps that's sufficient, but in general it is not. Now, related to that question, what is the cause of the 7.3% degradation? Is it an absorption which is essentially complete over a certain band - spectral band - or is it general? What is the spectral distribution of absorption?

Marks: As I stated earlier, we had no interest in any optical measurements. It was strictly short current measurements, and hence I am unable to answer your question.

Mann: Then what happens after 7000 hours?

Marks: We do not know. The original desire was to simulate a mission of one of the satellites that we have flying and the mission test time required was 700 hours, and so we did this testing. Unfortunately, we didn't go any further than that. I will state, however, that we ran our tests at 1, 2, and 6 suns, as I indicated, and there is a tendency for the damage to asymptote off. It could continue this way and asymptote off fully, or it could conceivably go upward again with increased test time.

Mann: The measurements were made, I take it, with a mercury lamp?

Marks: Yes, an AH-6.

Mann: Yes - which may not be accurate as far as the ultraviolet damage is concerned. It may not provide accurate data as to ultraviolet degradation in space. The next point is that - since I'm unemployed - (laughter) - the index of refraction of your material is approximately what?

Marks: Fairly close to glass.

Mann: Fairly close to glass?

Marks: Yes.

Mann: Well, the reflections which you indicate would - which you claim would indicate an index refraction substantially below 1.3, and although that's not impossible, it's very unlikely.

Marks: I have no good data on that and I would not like to comment on it....

Haynos - GSFC: Many extensive tests have been performed on electron degradation, particularly on the cover slides and these do not indicate that we have a 25% loss in transmission due to the blue filter.

Marks: No. We claim that there's a 2% loss in transmission due to degradation to the blue filter of the cover glass itself. However, the total degradation that the solar cell sees - with the cover slide on, is 27%.

Haynos: Then that does conform.

Marks: I'm sorry, if that was not clear.

Prince - EOS: This coating sounds fabulous. I'd like to know what it is and how do we get hold of it?

Marks: Well, I'm theoretically not allowed to talk about it at the present time. (laughter) In fact, I have clearance only on information presented in this paper. I will say, however, that the material is new and novel and has an organometallic structure. I'm sorry, no further information can be given at this time.

Schach - GSFC: Have you exposed the coating to irradiation whose total path length would be within the film itself - not into the cell; in other words, say with electrons of the order of perhaps 100 Kev or protons about the same order?

Marks: No exposure with particles of those energies were carried out. However, this is something we would like to do in the future.

Schach: My guess is that you might get more damage with low energy particles than with 1 Mev electrons. It would be interesting to see if this is the case.

Massie - Aero Propulsion Lab: Have you compared the moisture permeability of this coating to, say, H film or mylar? and if so, what were your results?

Marks: We do not have any information on the coating's permeability. This material is not a film in the same sense as H film or mylar; it is instead a protective coating.

Potter - NASA-Lewis: How hot do you have to heat the cells when you apply this coating?

Marks: 200°F. This is done to flash off the solvent in which the coating is dissolved.

Rappaport - RCA: I'm wondering whether it is possible that the increase in current that you are seeing with this coating is due to the improvement of the surface recombination velocity of the silicon. There are materials known - and one organic material I know of is pyrogallic acid, I believe, and potassium dichromate, which, when applied to a surface of silicon, decreases the surface recombination velocity, so the electron - the carriers in the film are reflected back into the semiconductor. If this is an organic film, it is possible that the small - 5% or what improvement you see could be due to this reduction of surface recombination velocity. It would be worth measuring.

Marks: You have to remember, however, that there is a silicon monoxide coating between the silicon and this coating.

Rappaport: It is probably worth forgetting about my original remark. (laughter)

Oman: Any more questions: Well, we will give Al Mann one more opportunity then. (laughter) This will be the last question.

Mann: As far as the increase that you get...First, a comment about that fluorescence work. That fluorescence work was done a few years ago to show what we concluded to be the infeasibility of using fluorescents as a means of gaining output and efficiency of solar cells. I do not believe it was written to try to show that it was a feasible technique. Furthermore, it is our experience that the cells which you are using were terminated optically by the coating in such a way that as soon as you put any termination on it such as a conventional slip with adhesive - that the short circuit current increased by several percent. I do not think this had to do with fluorescence.

Marks: This could very well be, although I do not see how. The only thing we have seen is the fluorescence of the coating material that we are talking about here. This fluoresced in the yellow-green at about 5400 to 5500 Å. Another coating fluoresced in the red over 6000Å and there we saw the actual current enhancement above and beyond what the solar cell would do bare, as much as 1%. This is what caused our interest.

Voice: It would be easy to check by using an ultraviolet source.

Marks: This will have to be done. If this is negative, it may be something that we just do not understand at the present time. I am just reporting what was found and your helpful comments are appreciated.

Oman: Thank you very much, Dr. Marks, for a very interesting and outstanding paper. (applause)

****